THE EFFECT OF MICROWAVES ON ION EXCHANGE IN ZEOLITES

A Thesis Submitted to
the Graduate School of Engineering and Sciences of
İzmir Institute of Technology
in Partial Fulfillment of the Requirements for the Degree of

DOCTOR OF PHILOSOPHY

in Chemical Engineering

by
Yelda AKDENİZ

June 2009
İZMİR

We approve the thesis of **Yelda AKDENİZ**

_____
Prof. Dr. Semra ÜLKÜ
Supervisor

_____
Prof. Dr. Devrim BALKÖSE
Committee Member

_____
Prof. Dr. Ahmet EROĞLU
Committee Member

_____
Prof.Dr. Hayrettin YÜCEL
Committee Member

_____
Doç. Dr. Fehime ÖZKAN
Committee Member

30 June 2009

_____
Prof. Dr. Devrim BALKÖSE
Head of the Chemical Engineering Department

_____
Prof. Dr. Hasan BÖKE
Dean of the Graduate School of Engineering and Sciences

dedicated to

my family

ACKNOWLEDGEMENT

Sincere gratitude is expressed to my advisor, Prof. Dr. Semra Ülkü, for providing the opportunity to research on zeolite world, and her inexhaustible effort in advising, ideas and the guidance in the preparation of this manuscript. I would like to acknowledge the Head of Chemical Engineering Department, Prof. Dr. Devrim Balköse for her support, stimulating suggestions and encouragement during my PhD education. I would like to express my appreciation to Prof. Dr. Muhsin Çiftçioğlu for his great help and also my thanks for his generosity for letting me use his graduate laboratories anytime.

Special thanks to my colleagues and roommates Özlem Duvarcı, Filiz Ömürlü and Berna Topuz for their interest, contributions, and sincere friendship. Without them, I'm sure my thesis would not have been completed in such an enjoyable or efficient manner. My absolute thanks to Nesrin Gaffaroğulları for her friendship, support and patience during long ICP analysis sessions. I ought to thank to Mert Tunçer for his precious help, guidance and advices through the antibacterial tests. I would like to thank to Gökhan Erdoğan and the MAM team for their precious contributions during SEM and XRD analysis of the samples.

I would like to express my gratitude to all members of my family, for their patient devotion, understanding, and support all throughout the study.

ABSTRACT

THE EFFECT OF MICROWAVES ON ION EXCHANGE IN ZEOLITES

Recent innovations of microwave field lead many scientists to focus on this phenomenon and it has been begun to be applied in different fields of zeolite applications.

The purpose of this study is to determine the effect of microwave irradiation on ion exchange degree and on the structure of natural zeolite. The clinoptilolite rich mineral from Western Anatolia was used throughout the experiments. The ion exchange experiments were performed using $AgNO_3$, $Co{\cdot}(NO_3)_2{\cdot}6H_2O$ and $Cu{\cdot}(NO_3)_2{\cdot}5/2H_2O$ within 0.01M - 1M and 40 ^oC - 80 ^oC concentration and temperature range in conventional waterbath and microwave. Different solid and solution conditions on ion exchange degree were determined, as well. Metal exchanged minerals were characterized by using instrumental techniques. Antibacterial activity of the Ag-exchanged clinoptilolite against *E. coli* was determined by Kirby–Bauer method.

The Ag^+, Co^{2+} and Cu^{2+} amounts within the mineral increased with decreasing S/L while increased with increasing temperature and time. For some utilized parameters microwave treatment was effective however on the whole it did not significantly improved the degree of ion exchange compared to waterbath treatment. The inspection of XRD patterns and FTIR spectra of metal exchanged minerals confirmed that no transition of clinoptilolite phase and no shifts in peak positions occurred with exchange methods applied. The sorption processes are controlled mainly by external-phase mass transfer. Ag^+, Co^{2+} and Cu^{2+} sorptions on NaCLI exhibited a good fit to Freundlich model and Langmuir models. All metal exchanged minerals showed considerable superiority against E.Coli.

ÖZET

MİKRODALGANIN ZEOLİTLERDE İYON DEĞİŞİMİNE ETKİSİ

Mikrodalga alanında yapılan son zamanlardaki yenilikler bilim adamlarının konuya yönelmesini sağlamış ve mikrodalga zeolitin farklı dallarındaki kullanım alanlarında yerini almıştır.

Bu çalışmada, mikrodalga kullanımının diğer yöntemlere kıyasla malzemelerin yapılarında birtakım değişiklikler meydana getirebileceği göz önünde bulundurularak mikrodalga kullanımının iyon değişim mekanizması ve zeolitlerin yapısına etkileri incelenmiştir. Batı Anadolu'nun Manisa,Gördes yöresinden temin edilen klinoptilolit mineralince zengin zeolit minerali deneysel çalışmada kullanılmıştır. Klinoptolit mineralinin $AgNO_3$, $Co(NO_3)_2 \cdot 6H_2O$ ve $Cu(NO_3)_2 \cdot 5/2H_2O$ çözeltileriyle 0.01 M - 1M ve 40^oC -80^oC derişim ve sıcaklık aralığında su banyosu ve mikrodalga yöntemleri kullanılarak iyon değişim deneyleri gerçekleştirilmiştir. Zeolit/çözelti oranının, sıcaklığının ve uygulanan metodun iyon değişimine etkisi incelenmiştir. Metal yüklenmiş mineraller farklı analiz yöntemleri ile karakterize edilmiştir. Ag^+, Co^{2+} ve Cu^{2+} yüklenmiş minerallerin E.Coli bakterisine karşı anti bakteriyel etkisi Kirby-Bauer yöntemiyle belirlenmiştir.

Her iki iyon değişim yöntemi için, klinoptolit mineralinin içinde bulunan Ag^+, Co^{2+} ve Cu^{2+} miktarlarının azalan klinoptolit /çözelti oranı, artan çözelti sıcaklığı ve zamanla arttığı saptanmıştır. Mikrodalga yönteminin bazı parametrelerde daha etkili olmuştur fakat genel olarak söz edilen katyonlar için iyon değişim derecesini önemli ölçüde arttırmadığı gözlemiştir. XRD, ve FTIR sonuçlarına göre, Ag^+, Co^{2+} ve Cu^{2+} yüklemesinin klinoptolit mineralince yapısında herhangi bir değişikliğe neden olmadığı tespit edilmiştir. Sorpsiyon proseslerini, film fazındaki kütle transferi kontrol etmektedir. Ag^+, Co^{2+} ve Cu^+ klinoptolit mineralinin adsorpsiyon denge izotermleri Freundlich ve Langmuir Modeline uygunluk göstermiştir. Ag^+, Co^{2+} ve Cu^{2+} yüklenmiş klinoptolit minerali E.Coli bakterisine karşı direnç göstermiştir.

TABLE OF CONTENTS

LIST OF TABLES

LIST OF FIGURES

CHAPTER 1

INTRODUCTION

Porous materials have attracted the engineers' attention due to their commercial applications in chemical separations and heterogeneous catalysis as well as the scientific interest came in sight by their synthesis, processing, and characterization. Zeolite minerals have been known since the eighteenth century but they remained a curiosity for scientists until their unique physical and chemical properties haven't been attracted the attention of many researches. These minerals are recognized as some of the most important silicates in volcanic rocks. These are mostly formed by reaction of pore-waters with volcanic glass and also by alteration of pre-existing feldspars, feldspathoids, poorly crystalline clays and biogenic silica (Palaban, 1987). They are porous crystalline, hydrated alumina silicates of group I and II elements in particular with sodium, potassium, calcium, magnesium, and barium. The zeolite framework structurally consists of an assemblage of SiO_4 and AlO_4 tetrahedra, joined together in various regular arrangements through shared oxygen atoms, to form an open crystal lattice containing pores of molecular dimensions into which quest molecules can penetrate. Since the positive charge of a silicon atom is higher than an aluminum atom, the net charge on each site of an aluminum tetrahedron is negative and it is balanced by one of the exchangeable cations present in the framework.

Clinoptilolite is a member of heulandite group of natural zeolites which belongs to structural group 7 and have a monoclinic symmetry and a Si /Al ratio between 4.25 and 5.25 (Gottardi and Galli, 1985). The structure of clinoptilolite consists of a three dimensional system of the three types of channels. Two parallel channels, channel A (10 member ring) and channel B (8 member ring), are perpendicularly intersected by channel C (8 member ring) with sizes 0.44*0.72 nm, 0.41*0.47 nm and 0.40*0.54 nm, respectively (Tsitsishvilli et al., 1992). The main exchangeable cations located within the cationic sites of clinoptilolite are Na, Ca, K, Mg and Ba.

Zeolites have a number of characteristic properties and are important for commercial applications. They are summarized as; they have high degree of hydration and ease of dehydration, stable crystal structure, low density and large void volume when dehydrated, cation exchange property, uniform molecular sized channels, high thermal and hydrothermal stability, high internal surface area, catalytic property with H-exchanged forms, special electrical properties and can adsorb gases and vapors. These properties of zeolites are strongly influenced by their chemical composition; framework composition and extra-framework composition such as the number, type and location of the exchangeable cations which strongly affect the ion exchange performance of zeolites. The ion exchange, adsorption and catalytic properties of zeolites as well as large deposits existing in different parts of the world lead many researchers to focus on their different applications. Zeolites are being widely used in many applications such as fertilizer in the agricultural and horticultural field, as catalyst in petroleum refining industry, as filler in paper industry, as adsorbents in the removal of organic contaminants, as fertilizer in the agricultural and horticultural field, as animal feed supply, and etc but they are often limited to countries having their own deposits. However, natural zeolites haven't had the commercial success of synthetic zeolites, partly because synthetics were developed and used extensively before the existence of large deposits of natural zeolites was known. Additional to the uses of zeolite in many industrial applications, in recent years these exciting minerals are being used in biomedical applications due to their good biological properties which are extremely important for industry. The synthetic zeolites are now doing the bulk of the work but natural zeolites are cheaper and more accessible though no less effective alternatives in biomedical area.

The recent use of microwaves in various fields of science makes it an interesting topic for the last few years especially in chemistry and chemical engineering. Microwave is a kind of electromagnetic radiation with a high frequency between 0.3 and 300 GHz. In microwaves a form of radio waves pass through the material instead of direct heating. The energy transformation may occur through different mechanisms; the most frequent among them are ionic conduction and dipole rotation (Bekkum et al., 1991). The heating and processing of materials with microwave is getting increasingly popular for many industrial applications. It is used in many kinds of fields such as, biology, medicine, chemistry and chemical engineering, because it has been claimed by many researchers that microwave irradiation on heating and other processes have many

advantages. For example, it enhances the reaction speed, supplies uniform and direct heating, produces high efficiency in energy and high heating temperature, and reduces the reaction temperatures of some processes but also the cost and time of the process applied. After 1980s interdisciplinary phenomena which called microwave chemistry was introduced into the science world. At the beginning of 1990s, microwave technique began to be applied in the synthesis of zeolite and in the following years it has been started to be used in many researches. If microwave radiation is use as heat source for ion exchange process, rapid, uniform and direct heat without any problems of heat transfer through walls of container is achieved (Romero et al., 2004). The microwave heating to higher temperature studies showed that there are several factors which affect the heating. Hydrated zeolites absorb microwave energy more efficiently than dry zeolites, H-form of zeolites interacts little with microwaves and degree of interaction strongly depends on the chemical composition and structure (Ohgushi et al., 2001). Energy adsorption in zeolites is a complex process and was considered that it is strongly affected by the presence of metal ions. The Na^+ ions within the large cavity in zeolite structure act as strong microwave absorbers. Both ionic conduction by Na^+, K^+, and other ions, and dipole rotation by water molecules can take place (Pilter et al., 2000). Besides, the synthesis of zeolitic materials in a microwave environment has been successfully achieved in many cases with shortened nucleation and crystal growth periods. Interesting results were obtained by microwave activation of zeolitic catalyst.

In the past few years, heating of materials, driving chemical reactions by microwave energy has been a popular theme in the scientific community. This non-classical heating technique is slowly moving from a laboratory curiosity to an established technique heavily used in both academia and industry since it has many advantages on heating and on other processes. The ion exchange in the presence of microwave irradiation is a recent topic and it has many scientific vacancies. Because the mechanisms of microwave which assist reactions and processes are unclear deeper investigation is essential for wider and efficient application of microwave in many fields of science. Despite the fact that the mechanism of interaction of microwave radiation with a material has not been completely understood, it is comprehensible that a microwave treated material may present some different properties when compared to conventional treatment.

The cation exchange process as a whole and the effect of microwave treatment method and parameters influence on ion exchange process are the subject of this PhD

study which covers the theoretical background of zeolites, sorption and ion exchange processes and microwaves. In the experimental part, the ion exchange with natural zeolite, clinoptilolite, will be performed with Ag^{+}, Co^{2+} and Cu^{2+} in their appropriate nitrate solutions. The Ag^{+}, Co^{2+} and Cu^{2+} exchanged minerals will be characterized using different characterization techniques that are available to describe the cation exchange mechanism and structural changes occurred within the mineral. The preference of Ag^{+}, Co^{2+} and Cu^{2+} exchange on clinoptilolite is due to the potential use of its Ag^{+}, Co^{2+} and Cu^{2+} exchanged forms in the antimicrobial material production such as antibacterial materials for medical applications and antimicrobial ceramics. The wide abundance of clinoptilolite in Turkey created an economical potential for the country besides the use of microwave irradiation in the process of ion exchange will be determined.

CHAPTER 2

INTRODUCTION TO ZEOLITES

2.1. Zeolites

The history of zeolites began with the discovery of first zeolite mineral stilbite, by the Swedish mineralogist, Axel Fredrik Cronsdent in 1756. He recognized zeolites as a new class of mineral consisting of hydrated aluminosilicate of the alkali and alkaline earths. The history was followed the discovery of important properties of zeolite. By the mid-1930's the literature described the ion-exchange, adsorption, molecular sieve properties of zeolite minerals (Mumpton, 1997). From the mid to late 1940's zeolite both the natural and the synthetic forms started to be used in industry. R. Milton and co-worker D.W. Breck discovered a number of commercially significant zeolites, type A, X and Y (Bekkum et al., 1991). In the 1980's there has been extensive work carried out on the synthesis and applications of zeolites of both types.

2.1.1. Structure and Properties of Zeolites

Zeolites are porous crystalline, hydrated alumina silicates of group I and II elements in particular with sodium, potassium, magnesium, calcium, barium and strontium. The zeolite structurally framework consists of an assemblage of SiO_4 and AlO_4 tetrahedra, joined together in various regular arrangements through shared oxygen atoms, to form an open crystal lattice containing pores of molecular dimensions into which quest molecules can penetrate. The zeolite framework is open; contains channels and cavities in which the exchangeable cations and the water molecules exist. The

cations often have a high degree of mobility giving rise to facile ion exchange and water molecules which are readily lost and regained. It should be noted that the sites of all adsorption, catalytic and ion exchange reactions of both synthetic and natural zeolites are basically within the crystal structure. The isomorphic substitution of Si by Al causes a negative charge in the zeolite structure and it is balanced by introducing exchanged monovalent, divalent, or trivalent cations in the structural sites of the zeolite The mobile non-framework cations are located in cavities in the channel walls and coordinated with the water molecules within the channel. The structural formula of a zeolite is best expressed for the crystallographic unit cell as: $(M^{+}, M^{2+}).\ ((AlO_2)_x\ (SiO_2)y).\ wH2O$ **;** where (M^{+} is usually Na^{+} or K^{+}, M^{2+} is Mg^{2+}, Ca^{2+} or Fe^{2+}, rarely Ba^{2+}, Li^{2+}), w is the number of water molecules and the ratio y/x is Si/Al ratio (Breck,1974).

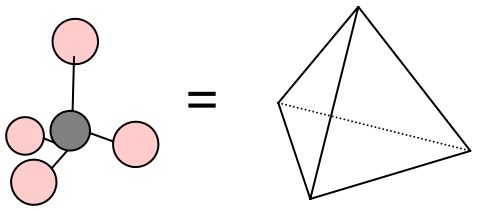

Figure 2.1. Representation of SiO_4^{4-} or AlO_4^{5-}.

The extent and location of water molecules incorporation depends either on the size, shape of the cavities and channels present or the number and the nature of the cations in the structure. Water molecules greatly influence the position of exchangeable cations and regulate their mobility within the structure. If the framework cations hydrated, they are reluctant to exchange sites but required to give off their coordinated water molecules (Higgins et al., 2001).

Zeolites have a number of characteristic properties and are important for commercial applications which make zeolites a promising material for various applications which are summarized as follows; they have microporous character with uniform pore dimensions, they allow certain molecules to enter the crystals while rejecting others based on their size and shape, they have ability to develop an internal acidity which makes them interesting materials for catalyzing organic reactions, have high thermal stability. These properties of zeolites make them a reliable material compared to other crystalline inorganic oxide materials (Bekkum et al., 1991).

There are more than 50 types of zeolite which occur in nature; however only mordenite, clinoptilolite, ferrierite, chabazite, erionite, philipsite and analcime have a remarkable value as mineral resources. Among these naturally occurring zeolite minerals, clinoptilolite is the most abundant and well known zeolite and occurs in large mineable deposits of relatively high purity in many parts of the world, including Turkey with a uniform and regular pore sizes. The composition, purity and property show change among the deposits. Clinoptilolite is a member of a heulandite group of natural zeolite and is iso-structural with the zeolite heulandite. The difference between clinoptilolite and heulandite is that, with heating at 450 ^{o}C clinoptilolite survives its crystal structure whereas heulandite does not (Gottardi and Galli, 1985). Si/Al ratio of clinoptilolite is in the range of 4.25- 5.25 whereas heulandite has Si/Al ratio below 4.00. Clinoptilolite has sheet like structure and is connected to each other by a few bonds. These sheets contain open and these rings stack together from sheet to sheet to form channels throughout the crystal structure. The size of these channels controls the size of the molecules or ions that can pass through them and therefore a zeolite like clinoptilolite can act as a molecular sieve.

Structure of clinoptilolite consists of a two dimensional system of the three types of channels; two parallel channels, channel A (10 member ring) and channel B (8 member ring), are perpendicularly intersected by channel C (8 member ring) with sizes 0.44*0.72 nm, 0.41*0.47 nm and 0.40*0.54 nm, respectively. In these channels there are four main sites namely M1, M2, M3 and M4. The Figure 2.2 shows the clinoptilolite structure and the main cation positions in the structure (Arcoya et al, 1996).

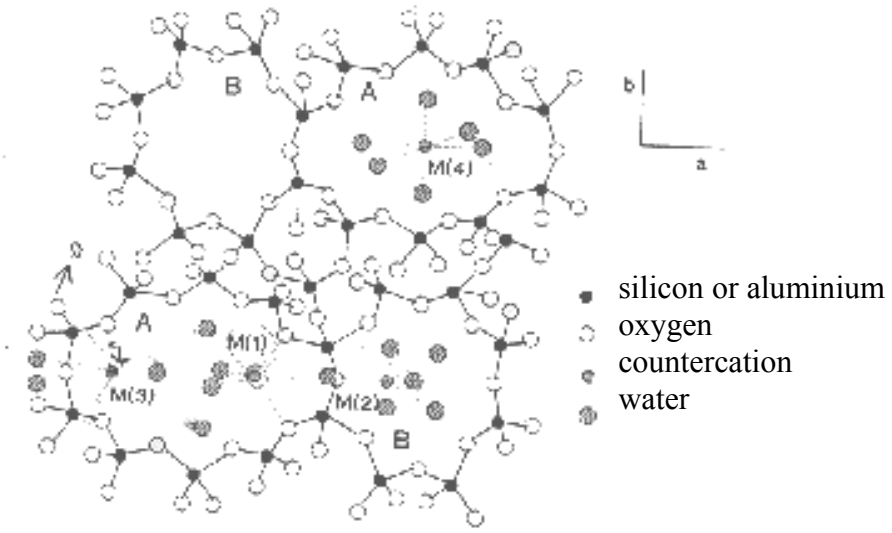

Figure 2.2. The main cation positions in clinoptilolite.
(Source: Arcoya et al, 1996).

M1 is located in channel A, coordinated with two framework oxygen atoms, five water molecules and is occupied by Ca^{2+} and preferably Na^{+}. M2 is situated in channel B, coordinated with three framework oxygen atoms and five water molecules. It is occupied by Na^{+} and preferably by Ca^{2+}. M3, in channel C, coordinated by six framework oxygen atoms and three water molecules. This site is occupied by K^{+} and preferably by Ba^{2+}. Because this position is very close to M1 which a simultaneous occupancy of both sites is not possible. M4 is located in channel A like M1, but a center of inversion. Its octahedral coordination is achieved by six water molecules. The occupancy of this position is low, and corresponds to Mg^{2+} (Arcoya et al, 1996).

2.1.2 Application and Uses of Zeolites

After zeolites were introduced as a new class of commercial adsorbent and mineral molecular sieve, they created a new branch of chemical technology and had considerable place in the industry. The applications of both zeolites in general are based on their unique adsorption, cation-exchange, dehydration–rehydration, and catalytic properties.

Zeolites are extremely used as catalysts in several important reactions involving organic molecules since they have the ability to act as catalysts for chemical reactions which take place within the internal cavities. The main industrial application areas of zeolites as catalyst are: petroleum refining, synfuels production, petrochemical production, cracking, isomerization and hydrocarbon synthesis. Today, zeolites are used commercially for enhanced hydrocarbon oxidation in conventional diesel engines and NO_x reduction. Zeolites serve as oxidation or reduction catalysts; have often been introduced into the framework after metal. The most promising results were obtained with the studies done by using metal-exchanged (Cu, Fe, Co, Pt, Rh, and Ni) zeolites such as ZSM-5, mordenite, zeolite Y (Moreno et al., 2004). Additionally, in the production of high-value chemicals such as pharmaceuticals and cosmetics zeolite catalysis were taking the high portion in industry.

The adsorption property is one of the most important characteristics of zeolites which strongly depend on the framework compositions. The ability to preferentially adsorb certain molecules, while excluding others, has opened up a wide range of molecular sieving applications. This includes applications in drying, purification, and separation. For example, they are being used as adsorbents in the removal of organic contaminants, such as phenol and aniline, the removal of water from organic solvents, the removal of organics from water, nitrogen and phosphorus removal from wastewater. The other important applications of adsorption of zeolites are the control of "greenhouse" gases (CO, CH_4, N_2O), the utilization of CH_4, and the flue gas treatment (SOx, NOx) . Narin (2001) chromatographically studied the carbon monoxide adsorption in clinoptilolite which was conducted in the range of 60-120 ^oC. The equilibrium constants (Henry's law constants, K) were in good agreement with the

results in the literature and mesopore diffusion resistance was found to be the controlling mechanism in CO diffusion in clinoptilolite.

Natural and synthetic zeolites were introduced as ion exchangers after soils and clays and are being extensively used in that respect since the hydrated cations within the zeolite pores are loosely bound to the zeolite framework, and can readily exchange with other cations when in aqueous media. For example, clinoptilolite currently is used to remove Sr and Cs from low-level effluents from a nuclear power plant before they are released to sea. Several zeolite processes have been developed to counteract the fallout from the 1986 Chernobyl disaster. They are added to soils reduced the uptake of ^{137}Cs by pasture plants in the vicinity of Chernobyl. Additionally, they are being used for extracting NH_4^+ from municipal and agricultural waste streams. Zeolite A, X, Y, Z and clinoptilolite supporting metal ions (Ag, Cu, Zn, Hg, Sn, Pb, Bi, Cd, Cr, Ti) are used as bactericides for water disinfection (Rivera-Garza, 2000). Türkmen. (2001) studied the removal of heavy metals (Pb^{2+}, Cu^{2+}, Zn^{2+}) from wastewaters by use of natural zeolite from Western Anatolia and concluded that it is an efficient ion exchanger and can be used for wastewater treatment. Cansever (2003) studied NH_4^+ removal from wastewater effluent by means of natural zeolite from Gördes, Turkey and investigated the effect of experimental conditions on the exchange performance. The highest amount of NH_4^+ removal per gram zeolite was found in the solution having 1% solid to liquid ratio. The exchange capacity was independent of the particle size and initial concentration of NH_4^+ has an effect on the exchange degree. The competing cation namely K^+ and Ca^{2+} have affected the exchange degree while Mg^{2+} ion has been found to have no effect.

Zeolites are being used in the agricultural and horticultural field due to their ability to slow-release fertilization or combination of ion exchange and mineral dissolution reactions. Mainly K^+ and NH_4^+ saturated clinoptilolite are used for this purpose for producing fruits and vegetables without a need of fertilization.

Natural zeolites also are used as dietary supplements. The animals fed with clinoptilolite added fodder generally grew faster and gained beneficial weight with simultaneous decrease in the amount and cost of the feed. Mineral adsorbent based on natural zeolite prevents mycotoxins from being poisoned. The apparent ability of clinoptilolite and other zeolites to absorb aflatoxins that contaminate animal feeds has resulted in measurable improvements in the health of swine, sheep, and chickens. Due to uptake of NH_4^+ by the zeolite, animals' excrement was less odoriferous and zeolite-filled air scrubbers were being used to improve poultry-house environments by

extracting NH_3 from the air. Additionally, the removal of ammonium from hatchery and aquarium waters and generation of oxygen for aeration systems in aquaria and transport are done by zeolitic materials**.**

The bulk of synthetic zeolites produced are used as detergent builders in order to reduce the effect of hard water ions. After the EPA regulations concerning water pollution, the use of phosphates in detergents was banned and synthetic zeolite has replaced in many formulations.

Perlite and volcanic glasses were being used as lightweight aggregate in concrete; recently zeolitic tuffs were used in that field. Predicting the thermal behavior of natural and cation-exchanged forms of clinoptilolites can provide useful information such as for thermal transformation into ceramics or lightweight aggregates. The heating temperatures for zeolite case are somewhat higher than those needed to expand perlite, but the products are much stronger. Çağlar et al. (2007) investigated the effect of heat treatment on zeolitic tuff from Turkey. The heat treatment conditions for maximum density and hardness were determined. Zeolitic tuff mainly containing clinoptilolite might be used in the production of lightweight aggregates and concrete bricks and also as an alternative source of substitute material in ceramic industry considering both its low cost and simple processing. Langella et al. (2003) investigated the thermal behavior of two clinoptilolites from an epiclastic and a pyroclastic deposit of Sardinia and of their exchanged forms (Li, Na, K, Cs, Mg, Ca, Sr and ammonium) by differential thermal analysis and thermogravimetry up to 1000ºC. The presence of cations such as Cs or K, which have low surface or volume charge densities, was found to increase the thermal resistance. In particular, the crystallinity of Cs- and K-exchanged forms of both clinoptilolites was not affected by thermal treatment at 450ºC and was just slightly reduced by thermal treatment at 600ºC.

Additional to the zeolite uses in many industrial applications, in recent years these exciting materials are increasingly being used in biomedical applications. Due to their known biological properties with long term chemical and biological stability, their reversible binding ability small molecules, their size and shape selectivity, immune system regulation ability. Natural zeolites mainly clinoptilolite is being used for this purpose; however it is very important to investigate them properly due to eliminate their side effects. For example, the lead content in some zeolite and clays should be reduced to ppb levels to eliminate the toxicity problems. Purified natural clinoptilolite has been developed as a non-toxic pharmaceutical and an active material in the therapy of acute

diarrheic diseases (Rodriguez-Fuentes et al., 1997). In ruminants clinoptilolite alters rumen fermentation; thereby modify volatile fatty acid production by rumen microbes and changing milk and body fat. Pigs, chicken, and turkeys are protected from mycotoxins in contaminated grains. Aflatoxins include a group of widespread, naturally occurring, fungal poisons which have been seen in animal diseases and aflatoxin B1 (AFB1) is the most toxic and cancerogenic of the aflatoxins. Hydration of the exchangeable cations creates a hydrophilic environment on the surface of zeolites and is important for the adsorption of different organic molecules, including mycotoxins on zeolites. A proposed mechanism of aflatoxin chemisorption by mineral adsorbents involves the rapid formation of a complex between a ligand and the mineral. The affinity of different cation-exchanged forms of clinoptilolite for aflatoxin B1 *in vitro* was studied by Tomasevic et al. (2001) and showed that the different exchanged forms of clinoptilolites adsorbed substantial amount of aflatoxin B1. Grce and Pevelic (2004) studied the antiviral properties of fine powder clinoptilolite. They treated different viral suspensions and concluded that, an antiviral property of clinoptilolite opens a possibility of therapeutical application of clinoptilolite either locally against herpesvirus infection or orally in case of adenovirus or enterovirus infections. Tomasevic-Canavic (2005) investigated the extraction efficiency of lead present as impurities in clinoptilolite using EDTA. They concluded that, this way of clinoptilolite purification is possible and can be used for medical application.

Aspirin causes gastrointestinal side effects in many patients. Some studies suggest that the absorption of aspirin from buffered products can be decreased, while the others do not cause any change. Since the aspirin is administered in the form of solid dosage, it must first be dissolved by gastrointestinal fluids before it can be absorbed. In order to investigate the aspirin-zeolite combination product Lam et al. (1998) studied theoretically the physical adsorption of aspirin on the natural clinoptilolite. Since dimensions of the clinoptilolite channels are smaller compared to aspirin external surface interaction was only possible. They concluded that compared to Na zeolite aspirin molecule adsorbed in acidic zeolite better.

The finely ground clinoptilolite is a potential adjuvant in anticancer and tumor therapy. Clinoptilolite treatment of mice and dogs suffering from a variety of tumor types led to improvement in the overall health status, prolongation of life-span, and decrease in the size of tumors. Local application of clinoptilolite to skin cancers of dogs effectively reduced tumor formation and growth. In vitro tissue culture studies showed

that finely ground clinoptilolite inhibits protein B, induces expression of different tumor suppressor proteins, and blocks cell growth in several cancer cell lines. These results indicate that clinoptilolite treatment might affect cancer growth by attenuating survival signals and inducing tumor suppressor genes in treated cells (Pavelic et al., 2001; Tomasevic-Canovic, 2005). Doretea and Pivac (2003) studied the ex vivo effect of clinoptilolite on the serotonergic receptors (binding of ^{3}H-8-OH-DPAT to 5-HT_{1A} and ^{3}H-5-HT to 5-HT_{1B}) in the brain of mice non-tumourous and mammary carcinoma suffering female mice. The reduction in binding of ^{3}H-8-OH-DPAT to 5-HT_{1A} in mammary carcinoma bearing mice when compared to control mice fed with standard food was observed. The addition of clinoptilolite to the feed of mice stopped the decrease in 5-HT_{1A} receptors binding; a possible beneficial effect of clinoptilolite was accomplished.

Papaioannou et al. (2004) studied the use of clinoptilolite-rich tuff, alone or in combination with certain antimicrobials on the health status and performance of pigs and its compatibility during simultaneous oral administration of antimicrobials such as enrofloxain or salinomycin. The performances and health of pigs were tested with respect to their feed configuration; with and without the clinoptilolite and/or antimicrobials. The clinical test showed that the dietary use of clinoptilolite does not cause any worse effect to pigs than weaning to slaughter or any incompatibility with in-feed of antimicrobials. Clinoptilolite addition to feeds was also supportive for antimicrobial medication.

The antimicrobial effects of natural zeolites namely clinoptilolite and its certain metal-exchanged forms are well known. They controlled the release of agents against microbial pollution and exhibit good antibacterial and antifungal activity. Rivera-Garza et al. (2000) investigated the antimicrobial effect of the Mexican zeolitic mineral from Taxco, Guerrero exchanged with silver ions. Escherichia coli and Streptococcus faecalis as indicators of fecal contamination of water were chosen to determine the antibacterial effect of the silver zeolitic mineral. Silver clinoptilolite mineral removed the pathogenic microorganisms E. coli and S. faecalis from water. Farias et al. (2003) studied the interaction between the natural zeolite and its metal exchanged forms (Ca-zeolite and Na-zeolite) and two drugs namely metronidazole and sulfamethoxazole. Zeolitic materials and drugs could be simultaneously administrated to a patient without any loss of the individual pharmaceutical effect of each product. Top and Ülkü (2004) studied the silver, zinc and copper exchange in a Na-clinoptilolite mineral from Gördes, Turkey

and resulting effect on antibacterial activity toward *Pseudomonas aeruginosa and Escherichia coli*. The equilibrium studies were performed at 25 ^{0}C, 0.1N total normality. The results showed that Na-clinoptilolite was selective for silver ions over a wide concentration range, but unselective for zinc and copper ions except in low concentration range. The increase of metal loading to the clinoptilolite rich sample did not always yield increase in antimicrobial activity but reached certain limits. Finally, they concluded that Ag-clinoptilolite can be proposed as low cost antimicrobial material.

As a conclusion, many benefits achieved from the properties and applications of zeolites which became the milestone of the basic investments from decades to the present in many areas. However, each property does not have the same value for every application; thus characterization related to specific application is a need. For that purpose, before using zeolite for certain application it is important to see if it has the desired properties for specific application otherwise zeolite has to be modified to meet specifications.

2.1.3 Characterization Methods for Zeolite

X-ray diffraction (XRD) technique is the best way to check the structure of the crystalline materials. Not only zeolite phase is quantitatively identified but also information on the adsorbent structure and microstructure is obtained by this technique. It is well known that the size and the charge of the exchangeable cations affect the framework of zeolite during the exchange process. A change of the peak intensities is due to a change of some atomic positions within the unit cell or to an atomic density change (Cullity, 1979). Arcoya et al. (1996) studied the role of counteractions on the molecular sieve properties of a clinoptilolite. Thermal and structural stability of the cation enriched forms of clinoptilolite activated at different temperatures studied by XRD showed that cation exchange did not modify the X-Ray diffraction pattern of the minerals however, heating above 700K reflected as changes in peaks intensities at 9.92^{o,} 22.43^o and 30.50^o 2θ. Korkuna et al. (2005) investigated the structural properties of original, acid treated and Pd exchanged clinoptilolite. The decrease in peak intensities

after treatment and disappearance of some peaks after exchange was observed. Castaldi et al. (2008) doping this natural zeolite with Pb^{2+}, Cd^{2+} and Zn^{2+} cations seems to change significantly the monoclinic structure of clinoptilolite but not the lattice parameters. The addition of Pb^{2+} cations, most intense (0 2 0) line around 9.6 in the 2θ degree is lowered with respect to the not polluted zeolite. Benaliouche et al. (2008) investigated the Ag-and Cu-exchanged X zeolites using XRD. They concluded that no shifts in the peak positions and no significant diffraction lines corresponding to formation of new phases were observed which are indicating well dispersion of these metals in zeolite framework. The decrease in peak intensity with the increasing exchange degree correspond a loss of crystallinity.

Porous materials are generally defined in terms of their adsorption properties. In principle, volumetric and gravimetric systems are used for determination of adsorption related properties of zeolitc materials. The sorption on zeolitic particles is a complex process because of their porous structure, inner and outer charged surfaces, mineralogical heterogeneity, existence of crystal edges, broken bonds, and other imperfections on the surface (Perić et al., 2004).

Erdem et al. (2004), studied adsorption behavior of natural (clinoptilolite) zeolites with respect to Co^{2+}, Cu^{2+}, Zn^{2+}, and Mn^{2+}. The sorption data have been subjected to different sorption isotherms, namely, Langmuir, Freundlich, and Dubinin–Kaganer–Radushkevich (DKR) and concluded that DKR and Langmuir equations describe the sorption isotherms of single-solute systems. Adsorption phenomena depend on charge density and hydrated ion diameter. Korkuna et al. (2005) investigated sorption properties of Transcarpathian zeolites namely clinoptilolite and mordenite and they showed Type IV sorption characteristic for mesoporous structures. Akdeniz and Ülkü (2005) investigated the adsorption-related properties of (K-Ca rich) clinoptilolite rich mineral by volumetric system using N_2 and Ar as adsorptive gas. BET and Langmuir Surface Areas were found as 22.65 g/cm^2, 27.96 g/cm^2 for N_2 adsorption and 17.25 g/cm^2, 22.45 g/cm^2 for Ar adsorption, respectively. The minerals showed bi-porous structure with sizes of 9 Å and 18 Å (Akdeniz and Ülkü, 2005). Castro et al. (2008) studied the micro and mesoporosity of natural and ion-exchanged [Cu (II), Zn (II) and Ag (I)] mordenites from Palmarito ore (Cuba) by adsorption of N_2 at 77 K, H_2O at 300 K and CO_2 at 273 K and concluded that Palmarito ore possesses a high concentration of mordenite and a more open porosity than other naturally found

mordenites. The ion-exchange processes modify the micro and mesoporosity of the zeolite, resulting in more accessibility to N_2 adsorption.

Inductively coupled plasma spectrometer (ICP) can provide elemental and isotopic information for a wide field of applications in the environmental and earth sciences. Top and Ülkü (2004) determined the chemical composition original and Na-clinoptilolite rich mineral from Gördes region, Anatolia by means of ICP analysis and based on 72 oxygen atoms in the unit cell they determined the formulas of the minerals as follows; $(Na_{0.816}\ K_{2.070})\ (Ca_{1.060}\ Mg_{0.264})\ (Al_{5.653}\ Fe_{0.390})\ (Si_{30.084})\ O_{72}.\ 20.023\ H_2O$, and$(Na_{4.763}\ K_{1.057})\ (Ca_{0.076}\ Mg_{0.094})\ (Al_{5.843}\ Fe_{0.221})\ (Si_{29.911})\ O_{72}.17.049\ H_2O$. Akdeniz and Ülkü (2005) determined the chemical composition of clinoptilolite rich mineral from Bigadiç region, Anatolia in a same manner. The mineral was called K-Ca rich due to the highest amount for K and Ca determined as 2.23 and 2.29 w/w%, respectively. The other exchangeable cations within the mineral as Fe, Na and Mg were present in ppm levels while trace elements were found in ppb levels. The Si/Al ratio of the mineral was 6.60 supporting the literature.

Thermal analyses techniques such as; Thermogravimetric Analysis (TGA), Differential Thermal Analysis (DTA), are good and straightforward methods are used to determine the thermal stability of the zeolitic minerals. Aliberti et al. (1975) investigated the thermal behavior of clinoptilolite by means of DTA and derivative thermogravimetry DTG. They reported that the clinoptilolite exhibited strong dehydration effect centered on 130 ^oC and the weaker dehydration effect at about 400 ^oC. Bish (1978) studied the thermal behavior of zeolites and reported that in the determination of thermal stability of zeolites, the amount and type of extra framework cations, Al/Si ratio, presence or absence of water, time, temperature and heating rate are important parameters. Ca-clinoptilolite gives endotherm at lower temperatures than Na-clinoptilolite. The endotherm at 230 ^oC was related to cationic ratio (Na+K/Ca+Mg) of clinoptilolite and only occurred on clinoptilolite DSC curve. (Esenli and Kumbasar, 1994). Afzal et al. (2000) studied on the thermal behavior of Co^{2+}, Cu^{2+} and Ni^{2+} exchanged zeolite 4A. The mass loss for the metal-exchanged zeolite was found greater than that for the pure zeolite. The DTA peak maximum for the metal-exchanged zeolite (except for Cu) was shifted towards lower temperature and as the metal concentration was increased, the water content also increased. The water-cation, water-water and water-oxygen atom interactions differ for the zeolites having different cation content. Joshi et al. (2002) studied the influence of the size of the extra framework monovalnet

cations in X-type zeolite on their thermal behavior. They synthesized the NaX zeolite and followed the conventional ion exchange to obtain K^+, Rb^+, and Cs^+ exchanged forms of NaX zeolite with the appropriate chloride solutions and characterized. They observed no changes in the framework composition, phase purity, crystallinity and crystallite size of the exchanged and parent minerals. The thermodynamically observed results showed that the temperature required for complete desorption of water decreases with the increase in the size of non-framework cations. Vujakoviæ et al. (2001) studied the surfactant and anion adsorption of clinoptilolite in different forms (Ca^{++}, Na^+, Ca^{++}/H^+ and H^+) and surface modified clinoptilolite (SCM). SCM is greatly influenced by cationic and structural form of clinoptilolite and metal forms did not go under structural deformation with heating upto 700 ^oC.

Thermal stability of zeolites are also described in terms Si/(Si+Al) ratio. Zeolites with high silica content having Si/(Si+Al) ratio higher than 0.79 (Si/Al ≥ 3.80) and zeolites with low silica having Si/(Si+Al) ratio lower than 0.56 (Si/Al ≤ 1.28) exhibit a large and poor thermal stability, respectively. The intermediate Si/(Si+Al) ratio in between the region 0.6-0.8 comprises zeolites with thermal stability ranging from a very low to a very high degree which indicates that in the latter region Si/(Si+Al) ratio can not be used alone to predict the thermal stability of zeolites. In addition to that, zeolites containing monovalent alkali cations (e.g. K^+, Na^+) are said to be more stable than those containing divalent cations (e.g. Ca^{2+}). Larger cations (e.g. K^+) prevent the zeolite structure from collapse while smaller cations (e.g. Na^+, Ca^{2+}) do not (Cruciani G., 2006).

Upon modification by ion exchange changes occurred within the minerals. The zeolitic water loss in the monovalent and bivalent cations decreased with increased size in the size of non-framework cations. Thermal stability of zeolites increased due to the presence of larger and less electronegative non-framework cations (Castaldi et. al, 2005). Castaldi et al. (2004) characterized the natural zeolite exchanged with different cations by thermal analysis. Misshra D. (2004) studied the structural and thermal stability of zeolite-13X and its Mn(II) and Zn(II) exchange forms up to 900°C and concluded that a little change in d-spacing occurred and peak intensities were reduced after exchange with Mn(II) and Zn(II) ions but the structure remained crystalline. Concepcion et al. (2005) studied the thermal behavior of Ag-exchanged natural and synthetic zeolites and they concluded that Ag-natural clinoptilolite samples were less thermally stable. Akdeniz and Ülkü (2005) studied the dehydration behavior

clinoptilolite rich mineral from Bigadiç and concluded that the mineral has good thermal stability. The phase transition started after 600 ^{o}C and decomposed after 850 ^{o}C. Çağlar et al. (2006) studied thermal behavior of zeolitic tuff from Gördes-Manisa in the temperature range of 200–1200 °C. They concluded that heating the tuff up to 600 °C did not cause any structural change detectable by X-Ray powder diffraction and thermal characterization methods with regard to the original sample, while further increase in the temperature caused structural breakdown of zeolitic tuff.

Fourier transform infra-red spectroscopy (FTIR) is a measurement technique where most chemical compounds exhibit characteristic infrared spectra, depending on their molecular symmetry, atomic weights and bond strength. The intense and adsorption characteristic for clinoptilolite is given in Table 2.1. (Breck, 1974).

Table 2.1. The IR Assignments of Clinoptilolite.

CLASS	**VIBRATION**	
Internal Tetrahedra	Asymmetry Stretch O-Si(Al)- O	1250 cm^{-1} – 950 cm^{-1}
	Symmetry Stretch	750 cm^{-1} – 650 cm^{-1}
	T-O Double Ring	500 cm^{-1} – 420 cm^{-1}
External Linkages	Pore Openning	420cm^{-1} – 300 cm^{-1}
	T-O Double Ring	650 cm^{-1} – 500 cm^{-1}
	Symmetry Stretch	750 cm^{-1} – 820 cm^{-1}
	Asymmetry Stretch	1150 cm^{-1} – 1050 cm^{-}
Additional	H bonded H_2O, H-O stretching	3400cm^{-1}
	Isolated OH Stretching	3700cm^{-1}

According to Breck, IR spectra of zeolites are divided into two classes. The first class of vibrations arises due to internal vibrations of the TO_4 tetrahedron, which is a primary unit structure, and is not sensitive to the other structural units. The second class of vibrations is related to the linkages between the tetrahedral. The introducing the non-tetrahedral cations in the alumino-silicate framework can change the IR spectra in the pseudo lattice vibration range. These changes more often characterized by the shifts in the bands of the framework (Korkuna et al., 2005).

Rodriguez-Fuentes et al. (1998) had studied thermal and cation influence on IR vibrations of modified natural clinoptilolite. They observed small differences in the absorbance values for the minerals treated with sodium and silver and concluded that the difference is due to the nature of the ions in the zeolite network, because the position of a cation in the clinoptilolite structure is influenced by its ionic potential. FTIR spectra of hydrated exchanged zeolites do not change with introducing different cations such as Zn, Cd and Pb into framework however, for the samples dehydrated at 245 ^{o}C the changes were observed in the spectra region corresponding to pseudo-lattice vibrations (500- 700 cm^{-1}). The shift of these band positions were not evident for exchanged zeolites but their peak intensity at 615 cm^{-1} was increased following the order Zn> Cd> Pb indicating that these cations were absorbed by zeolites (Castaldi et al., 2005; Mozgowa et al., 2000). In some cases, the presence of some exchangeable cations can cause change in IR spectra in the range of pseudo-lattice and lattice vibrations below 400 cm^{-1} such as Pd can cause shifts in the bands related to Brϕnsted acidic sites that interact with Pd (Korkuna et al., 2005). Çağlar et al. (2006) had studied thermal behavior of zeolitic tuff from Gördes-Manisa in the temperature range of 200–1200 °C. They observed the peaks related with isolated and H-bonded O–H stretching at 3700 and 3400 cm^{-1}, respectively, and H2O bending at 1620 cm^{-1}, T–Ostretching at 1060 cm^{-1}, external T–O at 790 cm^{-1}, external and internal double-ring vibrations at 609 cm^{-1} for the zeolitic tuff at room temperature. The appearance of these characteristic peaks in the the IRspectrum of zeolitic tuff until heat to 600 ^{o}C were lost with further heating, the absorbance at 609 cm^{-1} is the characteristic peak related with the amount of clinoptilolite structure present in the zeolitic tuff was decreased and disappeared at 800 ^{o}C regarding to structural deformation.

The scanning electron microscope (SEM) is a type of electron microscope identifies and quantifies the element constituents of the sample. Rivera et al. (2000) investigated the antibacterial effect of silver supported natural Mexican Zeolite and used electron microscope for the microanalyses and silver particles were detected as white in the SEM micrographs. They have observed the similar crystal morphology as Mumpton and Ormsby reported for zeolites in 1976. Çağlar et al. (2006) studied thermal behavior of zeolitic tuff from Gördes-Manisa in the temperature range of 200–1200 °C and SEM micrographs of the minerals were taken before and after the heat treatment. They observed that the zeolite crystals were still present in the samples heated until 1000 ^{o}C but they were not exactly in the same form seen in the original rock sample.

CHAPTER 3

ADSORPTION AND ION EXCHANGE

3.1. Adsorption

The types of sorption classified according to the types of bonding involved which are namely physical sorption, chemical sorption and electrostatic sorption (ion exchange). In physical sorption, there is no exchange of electrons, rather intermolecular attractions occur between 'valence free' sites which are independent of the electronic properties. The heat of adsorption, or activation energy, is low and therefore this type of adsorption is stable only at temperatures below about 150 °C. Chemical adsorption, or chemisorption, involves an exchange of electrons between specific surface sites and solute molecules, which results in the formation of a chemical bond. Chemisorption is presented by much stronger adsorption energy than physical adsorption and it is more stable at higher temperatures. The last type of sorption is electrostatic sorption named also as ion exchange and involves coulombic attractive forces between ions and charged functional groups.

The term adsorption includes the uptake of gaseous or liquid components of mixtures on the external and/or internal surface of porous solids. In chemical engineering, adsorption is called the separation process during which specific components of one phase of a fluid are transferred onto the surface of a solid adsorbent. The adsorption of various substances on solids increases free surface energy of the solids due to their extensive surface area. According to the second law of thermodynamics, this energy has to be reduced and it is achieved by reducing the surface tension by the capture of external substances. Two competitive types of influence occur; repulsion between the cloud of electrons in the atoms and Van der Waals nuclear attraction force and as a result of the balance of these two forces, in the potential energy curve at a short distance from the surface there is a hollow as shown in

Figure 3.1. Molecules or atoms that reach this hollow are adsorbed by this potential energy and cannot be rescued unless they obtain enough kinetic energy to be desorbed.

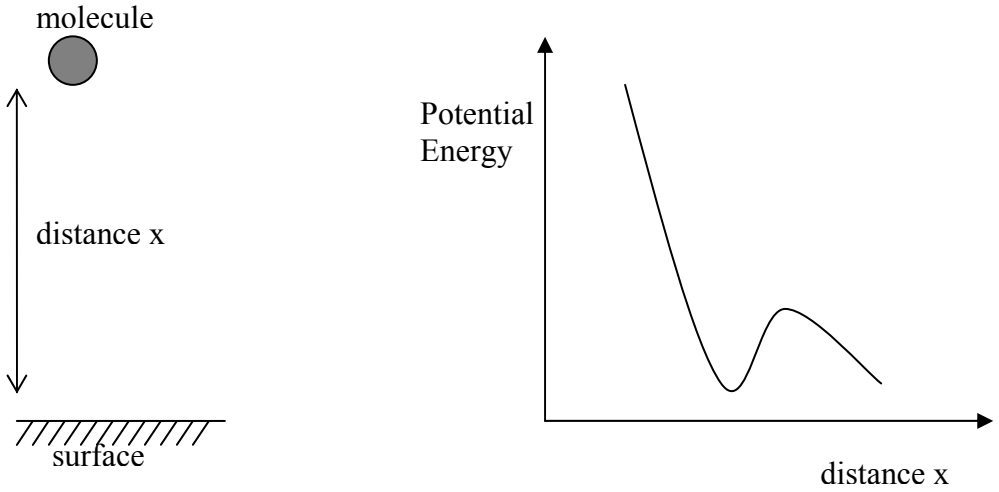

Figure 3.1. Potential Energy versus distance.

The number of pores, their shape, and size determine the adsorption capacity and adsorption rate of the adsorbent material. According to IUPAC, pores are classified as macro-, meso- or micropores for the pore diameters (nm) $d_p > 50$, $2 \leq d_p \leq 50$ and $d_p < 2$, respectively. Adsorptive molecules transport through macropores to the mesopores and finally to the micropores. The micropores are the largest portion of the internal surface and make the most to the total pore volume and attractive forces are stronger in the microporosity. The total pore volume and the pore size distribution determine the adsorption capacity.

3.2. Ion Exchange

Ion exchange takes the charged ions from a solution and releases an equivalent amount of other ions into the solution. The ability to exchange ions is due to the properties of the structure of the materials. The exchanger consists of positive and/or negative excess charge which is in specific locations in the solid structure or in functional groups. The charge is compensated by the counter ions, which can move within the structure and can be replaced by other ions of equal charge sign. Although

ion exchange is similar to sorption but there is a characteristic difference between them: ion exchange is a stoichiometric process in contrast to sorption. In ion-exchange process, for every ion that is removed, another ion of the same sign is released into the solution while in sorption, no replacement of the solute takes place. In principle, ion exchange is redistribution of ions between two phases by diffusion and chemical factors are less trivial, even absent. It involves coulombic attractive forces between ions and charged functional groups. Ion exchange by solids sometimes involves more phenomena; much seen as inorganic natural materials the ion uptake is attributed to ion exchange and adsorption mechanisms, to even internal precipitation mechanisms (Inglezakis et al., 2004). It is dependent on chemical structure, size, and charge of ions. Some ions that can bind to ion exchangers are summarized as follows; H^+ (proton) and OH^- (hydroxyl); single charged monoatomic ions like Na^+, K^+, or Cl^-; double charged monoatomic ions like Ca^{2+} or Mg^{2+}; polyatomic inorganic ions like SO_4^{2-} or PO_4^{3-}; organic bases, molecules containing the amino functional group; organic acids, molecules containing carboxylic acid functional group; bio-molecules, etc.

Ion exchange capacity is the total available exchange capacity of an ion exchanger described by the number of functional groups on it. This value is constant for a given ion exchange material and is generally given as milliequivalents per gram (meq/g) and/or milliequivalents per millilitre (meq/mL), based on the dry weight of material. The exchange capacity depends on the number of functional group per gram of exchanger. The extent of the use of the total exchange capacity depends on the level of ionization of the functional groups of the exchanger and on the chemical and physical conditions of the process.

The ion exchange reaction occurring between the particle and the solution will involve the steps as;

i. Diffusion of the ions through the bulk solution in order to reach the ion exchanger particle.
ii. Diffusion of the ion through the film surrounding the particle.
iii. Diffusion of the ion across the film–particle interface.
iv. Diffusion of the ion through the particle
v. Actual chemical reaction involving the exchange of ions.

Steps (i), (iii) and (v) are generally fast and do not determine the rate of the reaction whereas step (ii) or (iv) controls the kinetics of the overall process

3.3. Ion Exchange Materials

The ion exchange materials are available in a variety of forms which have different chemical and physical properties and can be naturally occurring or synthetic.

3.3.1. Naturally Occurring Ion Exchangers

Most common natural inorganic ion exchangers are clays and natural zeolites. Natural zeolites were the first materials to be used in ion exchange processes and clay materials are often used as backfill or buffer materials for radioactive waste disposal sites because of their low permeability and easy workability. The main disadvantages of natural inorganic ion exchangers are; their relatively low exchange capacities; their relatively low abrasion resistance and mechanical durability; their non-controllable pore size; zeolites are difficult to size mechanically; they can be partially decomposed in acids or alkalis; their limited chemical stability in many solutions, especially those with a very low salt content, they sometimes need a chemical or thermal pretreatment.

A large number of organic materials such as polysaccharides, proteins and carbonaceous materials exhibit ion exchange properties. They exhibit a very low ion exchange capacity compared with synthetics but they are widely available at a very low cost. They are normally used as sorbents, with their ion exchange properties being a secondary consideration. The main limitations of natural organic ion exchangers are; their low exchange capacity compared with other materials; their excessive swelling and tendency to peptize; limited radiation stability of cellulosic and protein materials; their weak physical structures; their non-uniform physical properties; their being non-selective and they are unstable outside a moderately neutral pH range.

3.3.2. Synthetic Ion Exchangers

Synthetic ion exchangers are produced by creating chemical compounds with the desired physical and chemical properties. They can either be inorganic (mineral) or organic (generally polymer) based. The largest group of ion exchangers available today is synthetic organic ion exchangers in a powdered or bead form. The framework of them is a flexible random network of hydrocarbon chains which carry fixed ionic charges at various locations. The main advantages of synthetic organic ion exchangers are their high capacity, wide applicability, wide versatility and low cost relative to some synthetic inorganic media. However, their use is limited by their poor radiation and thermal stabilities and they exhibit a reduction in their ion exchange capacity, owing to physical degradation at both the molecular and macroscopic level.

Synthetic zeolites were the first inorganic materials to be used for the large scale removal of radionuclides from nuclear waste effluents. They are used extensively in the cleanup of large volumes of contaminated water and many other applications but have limitations. A relatively high cost compared with natural zeolites; they have a limited chemical stability at extreme pH ranges; their ion specificity is susceptible to interference from similar sized ions; the materials tend to be brittle, which limit their mechanical stability.

3.4. Possible Mechanisms in Zeolite-Solution System

Adsorption, ion exchange, surface precipitation and dissolution are possible mechanisms in zeolite– metal solution interaction. Investigation of these interactions is important to understand the mechanism throughout the process and for selection of appropriate application.

3.4.1. Adsorption

Adsorption is one of the most important chemical processes in soils, clays, minerals. The adsorption may be controlled by weak forces as physical, Van der Waals and electrostatic outer-sphere complexes or by stronger forces as chemical interactions and inner-sphere complexes. In general, the process of adsorption begins as soon as outer-sphere complexes are formed on external surface sites of the adsorbent. The outer-sphere mechanism in zeolite metal system is shown in the following reaction (Doula and Ioannou, 2003).

$$(S\text{-}O^-)_2 + M^{2+} \rightleftharpoons (S\text{-}O)_2 \cdots\cdots M^{2+}$$

where S corresponds to either surface central Si or Al and M^{2+} for metal cation.

The outer-sphere complexation involves the ion-exchange reactions between metal ions and surface counterbalance cations. There is a strong dependence on ionic strength for an outer-sphere complex and it involves electrostatic bonding mechanisms. They are usually rapid and reversible which make them less stable compared to inner-sphere surface complexes (Stumm, 1990).

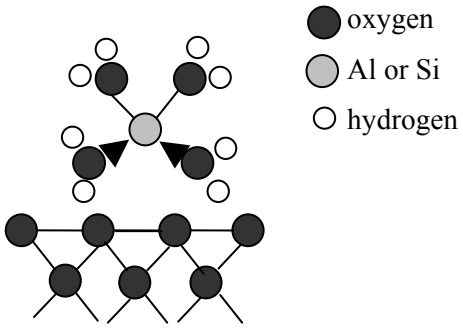

Figure 3.2. Schematic presentation of outer-sphere complex formation in zeolite.

The increase in metal concentration forces metal ions into internal surface sites cause formation of inner-sphere complexes. The inner-sphere mechanism in zeolite metal system is shown in the following reaction.

$$\equiv S\text{-}OH + M^{2+} \rightleftharpoons S\text{-}OM^{+} + H^{+}$$

$$2\equiv S\text{-}OH + M^{2+} \rightleftharpoons (\equiv S\text{-}O)_2\, M + 2H^{+}$$

where S corresponds to either surface central Si or Al and M^{2+} for metal cation.

Inner-sphere complexation involves covalent bonding and makes more stable surface groups. Inner-sphere complexation is slower and irreversible in contrast to outer-sphere complexation. H^{+} ions are released as products of these complex formations and the process causes a total decrease in solution pH.

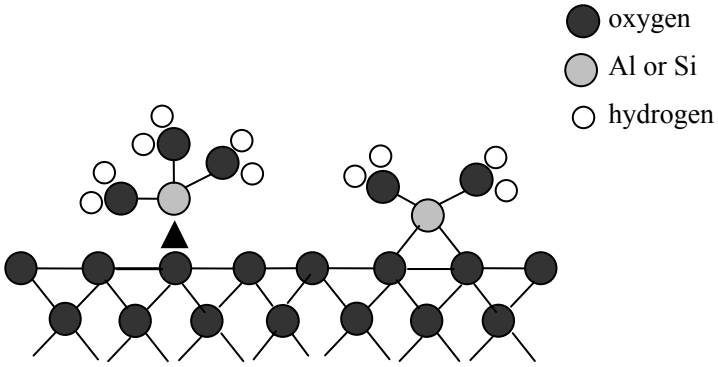

Figure 3.3. Schematic presentation of inner-sphere complex formation in zeolite.

Outer and inner sphere complexes are formed soon after the metal is adsorbed by a surface. During metal adsorption, metals are in the form complexes with inorganic or organic ligands. These complexing ligands have a significant effect on metal ion behavior. The metal– ligand interaction with a solid is described by the following reactions (Stumm and James, 1990).

$$\equiv S\text{-}OH + L^{-} + M^{+z} \rightleftharpoons S\text{-}L\text{-}M^{+} + OH^{-}$$

$$\equiv S\text{-}OH + L^{-} + M^{+z} \rightleftharpoons \equiv S\text{-}OM\text{-}L^{(z-2)} + H^{+}$$

The metal–ligand complexes may form in solution and adsorb weakly. They compete with surface complex formation reactions resulting with adsorption decrease compared to the ligand-free system. The metal–ligand complexes may also interact indirectly at the surface, by altering the surface electrical properties or they may adsorb

strongly and enhance the removal of metal or ligand, or both from solution compared to the case where either one is present alone (Stumm and James, 1990).

Šljivić et al (2008) studied the adsorption of a zeolite, clay and diatomite from Serbia toward aqueous Cu^{2+} ions at different pH. The adsorbents were characterized with respect to phase composition, specific surface area and point of zero charge. The amounts of Cu^{2+} removed from the solution, increased with increasing initial pH, at pH=7, regardless of the adsorbent type and metal concentration, due to precipitation of Cu $(OH)_2$. The maximum adsorption capacities decreased zeolite, clay and diatomite respectively where the Langmuir equation was most suitable for data fitting. The proportion of Cu^{2+} desorbed in acidic media decreased with the increase of previously adsorbed amounts by zeolite and clay while the opposite was true for diatomite. Ion exchange of exchangeable cations and protons were identified as main adsorption mechanisms.

3.4.2. Ion Exchange

Clay minerals because of their two-dimensional framework structure may undergo swelling or shrinking with ion exchange process while zeolites do not undergo any appreciable dimensional change since they have three dimensional structures. Together with their considerable ability to cation exchange, they are preferred by other organic exchangers. The ion exchange behavior of the zeolite mineral depends upon; the nature of the cation species, the cation size both anhydrous and hydrated and the cation valance, the exchange temperature, the concentration of the cation species in solution, the anion species associated with the cation in the solution, the solvent, the structural characteristics of the particular zeolite (Breck,1974). The ion exchange process may be represented as follows.

$$z_B A^{ZA} + z_B \overline{B^{ZB}} \rightleftharpoons z_B \overline{A^{ZB}} + z_A B^{ZB}$$

where; z_A & z_B are the valances of the ions; A^{ZA} initially in the solution; B^{ZB} initially in the zeolite and characters with a bar related to a cation inside the zeolite crystal. The followings are simple examples of ion exchange in zeolites.

$$\overline{Na}^{+} + K^{+} \rightleftharpoons Na^{+} + \overline{K}^{+} \quad \text{for uni-univalent exchange}$$

$$2\,\overline{Na}^{+} + Ca^{2+} \rightleftharpoons 2\,Na^{+} + \overline{Ca}^{2+} \quad \text{for uni-divalent exchange}$$

The exchangeable cations are located in the framework channel, coordinated with defined number of water molecules affect their mobility within the structure. The ion exchangeability depends primarily on the charge of the ion, the ionic radius and the degree of hydration, as well (Trgo et al., 2006). The larger the charge on the ion the greater is the force with which it is attracted by the functional groups of opposite charge on the ion exchanger; hence, the larger is its exchange capacity, and it's more difficult to remove during the exchanger. There is also a relation between ionic charge and hydration enthalpy. Table 3.1 represents ionic radii, hydrated ionic radii and free energies of hydration for certain ions.

Table 3.1. The properties of exchangeable cations.

Cation	Ionic Radius‡ (Å)	Hydrated Radius‡ (Å)	Heats of Hydration* (kcal/mol)
Na^{+}	0.95	3.58	97
K^{+}	1.33	3.31	79
Mg^{2+}	0.65	4.28	450
Ca^{2+}	0.99	4.12	373
Fe^{3+}	0.75	4.28	1057
Ag^{+}	1.28	3.43	162
Cu^{2+}	0.82	4.19	536
Co^{2+}	0.95	4.18	504

*Woods and Gunter, 2001
‡ Semmens et al., 1975

The higher charge shows the higher enthalpy. The large ion charge/size ratio results in an increase in the hydration energy and an increase in the ionic radius results by a decrease in the hydration enthalpy. If an ionic radius is compared with the free dimensions of the clinoptilolite channels (4.0x5.5-4.4x7.2 A), it is apparent that all of

the anhydrous ions can pass readily through the channels, but since the hydrated ions are approximately the same size as the channel dimensions, they may exchange only with difficulty (Semmens et al., 1974). Additionally, if the volume of the ion is greater the electric field in the solution will be weaker, thus, the smaller is its degree of hydration. The so-called hydrodynamic radii of ions decrease with increasing atomic weight; hence, their exchange energy is that the ion is transported from the solution to the ion exchanger. Erdem et al. (2004) studied the removal of heavy metal cations by natural zeolites taken from Enli Mining Company from Manisa Gördes in Western Anatolian Region. They studied the adsorption behavior of natural zeolites namely clinoptilolite with respect to $Co^{2+,}$ Cu^{2+}, Zn^{2+}, and Mn^{2+} with the aim of considering its application to purity metal finishing wastewaters. According to the equilibrium studies, the selectivity sequence can be given as $Co^{2+} > Cu^{2+} > Zn^{2+} > Mn^{2+}$. They concluded that, an adsorption phenomenon depends on charge density and hydrated ion diameter and natural zeolites have great potential to remove cationic heavy metal species from industrial wastewater.

The Eisenman's model says that the selectivity of exchange cations is accounted for only in terms of their hydration free energies and their energies of electrostatic interaction with the zeolite fixed anions. The free energy of ion exchange reaction could be considered in two parts. The first part may represent the difference between the free energy of the ions in zeolite while the second part may represent the free energy differences of hydration of the ions in the solution. If the electrostatic fields in zeolite are strong, then the first part dominates and small ions are preferred. Strong electrostatic fields occur in zeolites with a high framework charge and correspondingly low Si/Al ratio. However, if these electrostatic fields are weak (as in zeolites with a high Si/Al ratio), the hydration free energy becomes more important. So, weakly hydrated cations are preferred. The low Si/Al ratio provides a weak anionic field within the zeolite. Consideration of Eisenman's model in the case of exchange on zeolite in the presence of weakly anionic field indicates that selectivity is predominantly determined by the free energies of hydration of the competing cations. According to the theory, the free energies of hydration listed in Table 3.1 indicate that copper with the largest hydration energy, prefers the solution phase where it may satisfy its hydration requirements, and barium, with least hydration energy, prefers the zeolite phase**.**

Cation exchange in zeolites leads to alteration of stability, adsorption behaviour, and selectivity, catalytic activity and other important physical properties. Ion exchange

is also considered as a modification process as well as a direct application. As mentioned above, ion exchange depends as much on the properties of the exchanger as on the properties of the ions undergoing exchange. Woods and Gunter (2001) studied the Na-and Cs-exchange in a clinoptilolite-rich rock. They analyzed the outgoing cations which are Na and Cs, the batch experiments performed with 1/25 of solid/solution ratio. They found that for the Na and Cs exchanged samples the concentration of the outgoing divalent cations increased with time and temperature. They also concluded the different and unpredictable behavior of monovalent cations.

For several ion exchange and equilibrium studies, researchers have been reported different contact times range from a several minutes to even weeks in the literature. The adsorption and/or ion exchange sites on the clays i.e. clinoptilolite, are covered by the metal ions and the rate processes become dependent on the rate at which the adsorptive is transported from the bulk liquid phase to the actual adsorption sites. Bektaş and Kara (2004) investigated the removal of Pb from aqueous solution by means of clinoptilolite revealed that approximately 120 minutes of contact time is sufficient for the system to reach equilibrium. Trgo et al. (2006) studied the ion exchange kinetics of Zn and Pb modified clinoptilolite and they concluded that ion exchange of Zn is rapid at initial times with extended and slower uptake until equilibrium whereas ion exchange of Pb is more rapid and the equilibrium is accomplished in 20 min. Another recent study has been conducted by Sarı et al. (2007) on the similar topic and they concluded that maximum adsorption amount of Pb (II) onto clinoptilolite was obtained in 30min and no significant difference in adsorption amount occurred afterward. For their further adsorption study they used 30min for contact time. The difference of equilibrium times are basically related to the nature of exchanging cation and absorbent however influence of the dust produced during the grinding process on ion exchange kinetics is essential. Clinoptilolite surface and pore openings are partially covered by dust produced during grinding and results in pore clogging which was reduced on a great degree by washing . For example, smaller unwashed particles exhibit slower kinetics (Inglezakis et al., 1999).

At equilibrium amount of metal ions sorbed (q_e) by the adsorbent is determined by the mass balance given in Equation3.1.

$$q_e = V(C_i - C_e)/M \qquad (3.1)$$

where; V is the solution volume (mL), M is the amount of adsorbent (g) and C_i and C_e (mg/L) are the initial and equilibrium metal concentrations, respectively.

Analysis of adsorption isotherms is a extremely important in describing the adsorbate and adsorbent interaction. Equilibrium studies determine the capacity of the adsorbent and are described by adsorption isotherms and constant which express the surface properties and affinity of the adsorbent toward the selected adsorbate. The Langmuir and Freundlich equations are mostly used to describe the sorption equilibrium isotherms and given in Equation 3.2 and Equation 3.3 respectively.

$$qe = Q_o \bullet b \bullet C_e /(1 + b \bullet C_e) \tag{3.2}$$

$$qe = K_f \bullet C_e^{\,1/n} \tag{3.3}$$

where, qe (mg metal ion/g adsorbent), C_e is the equilibrium metal ion concentration in solution, Q_o (mg metal ion/g zeolite) and b (L/mg metal ion) are Langmuir isotherm constants. Kf (mg metal ion/gr zeolite) and n (gr zeolite/L) are Freundlich isotherm constant.

Freundlich model is based on sorption on a heterogonous surface. K_F is indicative of the adsorption capacity of the adsorbent, the greater the K_F value the greater the adsorption. The other constant for this model is n which is used to verify the type of adsorption. If n is equal to unity the adsorption process is linear while if it is below unity it indicated that adsorption is a chemical process; whereas n above unity associated with a favorable adsorption and physical process (Vimonses et al., 2008). Langmuir based on the assumption that uptake occurs on homogenous surface by monolayer sorption without interaction between sorbed molecules. The characteristic of Langmuir isotherm is expressed in terms of dimensionless constant, separation factor or equilibrium parameter, R_L, and it is defined by Equation 3.4.

$$R_L = 1/ (1 + b\ C_i) \tag{3.4}$$

where Ci is the initial metal ion concentration (mg/L) . Depending on the value of the constant, R_L, there are four possibilities describing the adsorption character. Favorable adsorption for R_L values determined between 0 and 1, unfavorable adsorption for R_L>1,

linear adsorption for R_L=1 and suggesting irreversible adsorption for R_L=0 (Wang *et.al,* 2007).

The Langmuir constant *b* is related to the free energy change of sorption (ΔG, J/mol) according to the following formula given in Equation 3.5.

$$\Delta G = -RT \ln b \tag{3.5}$$

where *R* is the gas constant (8.314 J/(mol K)) and *T* is the temperature (K). The Gibbs free energy indicates the degree of spontaneity of the sorption process, negative values reflecting a more energetically favorable sorption process.

Thermodynamic reaction of adsorption process can be determined via thermodynamic parameters, such as the changes in the standard free energy (ΔG°), the enthalpy (ΔH°) and entropy (ΔS°) associated with the adsorption process, using the following Equation 3.6 and Equation3.7.

$$(\Delta G^\circ) = (\Delta H^\circ) - T\,(\Delta S^\circ) \tag{3.6}$$

$$(\Delta G^\circ) = -\,R\,T \ln (1000\,b) \tag{3.7}$$

where *b* is the langmuir isotherm, *R* is the ideal gas constant (8.314 J/ mol K) and *T* is the adsorption temperature in Kelvin. Values of (ΔG°) (kJ /mol) at different temperatures were evaluated from equations above. Plot of ln *b* versus *1/T* should give a linear line, where values of (ΔH°) (kJ/mol) and (ΔS°) (J/mol K) can be calculated from the slope and intercept of van't Hoff plots.

Chemical kinetics is an informative way of describing the reaction pathways and time needed to reach equilibrium. The dependence of sorption kinetics on the physical and chemical characteristics of the adsorbent is obvious and influences the mechanism. The ion exchange process in most clay systems are fast and rate is limited only by the rate at which ions can diffuse in and out of the exchanger structure. Sorption kinetics of clinoptilolite systems for understanding the reaction pathways and mechanisms of the process kinetic models, namely, the first order, pseudo-first order, pseudo-second order and intra-particle diffusion models generally used.

First order kinetic model based on a reversible reaction with equilibrium state being established between two phases. It is expressed as given in Equation 3.8.

$$dC_B/dt = -dC_A/dt = k_1 \bullet C_A - k_2 \bullet C_B$$

$$= k_1(C_{A0} - X_A \bullet C_{A0}) - k_1 (C_{B0} - X_A \bullet C_{A0}) \quad (3.8)$$

where C_A (mg/l) is the concentration of solute on the adsorbent and C_B (mg/l) is the concentration of solute in solution at time t, C_{A0} *and* C_{B0} are the initial concentrations of solute on adsorbent and solution, respectively. X_A is the conversion of solute; k_1 and k_2 are the first order rate constants. At equilibrium the relation is given in Equation 3.9.

$$dC_B/dt = -dC_A/dt = 0 \quad (3.9)$$

Boundary conditions:

t=0 Ct=0

$t = t$ $Ct = Ct$

The equilibrium constant, K_c, is defined as the ration of k_1 *to* k_2. Finally, it becomes in the form given as in Equation 3.10 and Equation 3.11.

$$ln[(Ct-Ce)/(Co-Ce)] = -k' \bullet t \quad (3.10)$$

$$k' = k_1(1 + 1/K_c) = k_1 + k_2. \quad (3.11)$$

Fist order kinetic model follows the plot *of* $ln[(Ct-Ce)/(Co-Ce)]$ versus *time*, and the slope will give k'.

Pseudo-first order kinetic model is the first defined equation for the sorption of liquid/solid system based on the solid capacity. This kinetic is based on the assumption that the rate of change of solute uptake with time is directly proportional to the difference in saturation concentration and the amount of solid uptake with time (Vimonses, 2008). Mostly, this equation does not will well through the whole range of contact time. It is represented by Equation 3.12.

$$dqt/dt = k_2 (qe-qt) \quad (3.12)$$

Boundary conditions:

t=0 qt=0

$t = t$ qt = qt.

$$ln[qe\text{-}qt] = k_2 \bullet t \quad (3.13)$$

where qe (mg/g) and qt (mg/g) are the amounts of solute on the surface of the adsorbent at equilibrium and at any time t, respectively and k_2 is the pseudo-first order rate constant (1/min). Plot of $ln[qe\text{-}qt]$ versus *time* gives the slope of k_2.

Pseudo-second order kinetic model is based on the sorption equilibrium capacity and it is expressed in the form of as given in Equation 3.14.

$$dq/q_t = k_2'(q_e - qt)^2 \quad (3.14)$$

Boundary conditions:

t=0 qt=0

$t = t$ qt = qt.

$$t/q_t = 1/k_2' \bullet q_e^2 + 1/q_e \bullet t \quad (3.15)$$

where q_e (mg/g) amount of solute sorbed at equilibrium and k_2' (g/mg) min is the equilibrium rate constant of pseudo-second order model. Plot of $1/q_t$ against *time* gives the k_2'.

The sorption process, for example a batch adsorber in which zeolite particles are brought into contact with a fluid phase, is expressed with either one or more of the following steps.

(i) Solute transfer from the bulk fluid surrounding the zeolite particle to the stagnant layer, of thickness δ_f, surrounding the zeolite particle.

(ii) Solute transport from the boundary film to the zeolite's surface, macropores.

(iii) Solute transfer from the surface to active pores of zeolite's.

(iv) Solute molecules diffuse into the internal surfaces of the adsorbent.

It is generally known that a typical liquid/solid sorption process was mainly described by two mechanisms which are external fluid film diffusion and/or internal-micropore diffusion. The slowest step of the sorption process controls the speed of the process and called the rate-limiting step.

The biporous zeolite consists of small microporous crystals formed in macroporous structure. For biporous adsorbents like zeolites at least two and possibly three resistances exist; the diffusional resistance of the micropores within the micro particles and the diffusional resistance of the meso and macropores. If the adsorption occurs from a binary or multi-component fluid phase, diffusion through the laminar fluid film surrounding the particle is the external fluid film or surface resistance.

In liquid/solid systems, if the diffusion within the adsorbent particle is rapid sorption occurs on the external surface where the rate of solute accumulation in the solid phase is equal to the solute transfer across the liquid film. Considering the system linear, isothermal and there is no concentration gradient through the particle and adsorbate as well. The driving force in this case is the difference across the boundary layer and sorption rate is then given as;

$$dC_t / dt = -k_f S_s (C_t - C_s) \qquad (3.16)$$

$$S_S = 6 \cdot m_s / d_p . \rho_p (1-\varepsilon_p) \qquad (3.17)$$

$$m_s = W / V \qquad (3.18)$$

where W is the mass of adsorbent, V is volume of particle free fluid, d_p is mean particle diameter, ρ_p is particle density, C is the concentration in liquid phase and ε_p is particle voidage. The differential mass balance of the solute within the particle as $C_t = C_s$ at t=0 becomes;

$$\ln (C_t / C_o) = -k_f S_s \, dt \qquad (3.19)$$

The plot of $ln\ (C_t / C_o)$ versus *time* will yield a slope of $-k_f S_s$ from which external fluid film diffusion coefficient can be determined.

The sorption process may also be controlled by diffusion within the zeolite particles. Microporous diffusion is the diffusion of solutes within the zeolite intracrystallines. Macropore diffusion expresses the diffusion of solutes in fluid-filled surface and pores.

In case of diffusion within the microparticle is the rate controlling the uptake rate for uniform spherical zeolite particle is expressed by the following equations by assuming that diffusion occurs in only radial direction and system is isothermal.

$$\frac{\partial q}{\partial t} = \frac{1}{r^2}\frac{\partial}{\partial R}\left(r^2 D_c \frac{\partial q}{\partial r}\right) \tag{3.20}$$

$$\frac{\partial q}{\partial t} = D_c\left(\frac{\partial^2 q}{\partial r^2} + \frac{2}{r}\frac{\partial q}{\partial r}\right) \tag{3.21}$$

Boundary conditions:

$t<0$	$C=C_o$	$q=q_o$
$t\geq 0$	$C=C_x$	$q(r_c, t) \rightarrow q_x$
$t\rightarrow\infty$	$C=C_x$	$q(r, t) \rightarrow q_x$

$\left.\frac{\partial q}{\partial t}\right|_{r=0} = 0$ for all t

$$\frac{m_t}{m_x} = \frac{q-q_o}{q_x-q_0} = 1 - \frac{6}{\pi^2}\sum_{n=1}^{\infty}\frac{1}{n^2}\exp\left(-\frac{n^2\pi^2 D_c t}{r_c^{\,2}}\right) \tag{3.22}$$

For the long term region and short term regions, further simplifications the final form of the equations are defined by Equation 3.22 and Equation.3.23, respectively. The slopes of the plots $\ln\left[1-\frac{m_t}{m_\infty}\right]$ versus t for long term region and $\frac{m_t}{m_\infty}$ versus $\sqrt{t}$ for short term region micropore diffusion coefficient are to be calculated.

$$\frac{m_t}{m_x} = \frac{6}{\sqrt{\pi}}\sqrt{\frac{D_c t}{r_c^{\,2}}} \tag{3.23}$$

$$\frac{m_t}{m_x} = 1 - \frac{6}{\pi^2}\exp\left[\frac{-\pi^2 D_c t}{r_c^{\,2}}\right] \tag{3.24}$$

If the micropore diffusion is rapid, there will be uniform concentration profile through a microparticle then diffusion through the macropores is the rate controlling the uptake rate for uniform spherical zeolite particle and is expressed by the following equation by assuming diffusion occurs in only radial direction, system is isothermal and pore diffusivity is independent of concentration.

$$(1-\varepsilon_p)\frac{\partial q}{\partial t}+\varepsilon_p\frac{\partial C}{\partial t}=\varepsilon_p D_p\left(\frac{\partial^2 C}{\partial R^2}+\frac{2}{R}\frac{\partial C}{\partial R}\right) \tag{3.25}$$

$$\frac{\partial C}{\partial t}=\frac{\varepsilon_p D_p}{\varepsilon_p+(1-\varepsilon_p)K}\left(\frac{\partial^2 C}{\partial R^2}+\frac{2}{R}\frac{\partial C}{\partial R}\right) \tag{3.26}$$

Boundary conditions:

$C(R,0) = C_{o,}$ $\quad q(R,0) = q_{o,}$

$C(R_p,t) = C_{x,}$ $\quad q(R_p,t) = q_x$

$$\left.\frac{\partial C}{\partial R}\right|_{R=0}=\left.\frac{\partial q}{\partial R}\right|_{R=0}=0$$

Effective macropore diffusivity is defined as,

$$D_e=\frac{\varepsilon_p D_p}{\varepsilon_p+(1-\varepsilon_p)K} \tag{3.27}$$

The solution of the uptake curve is identical to Equation 3.22 with D_c/ r_c^2 replaced by $(D_p/ R_p^2)/ [1+ K (1-\varepsilon_p) /\varepsilon_p]$ and solution is obtained by Equation 3.23 and Equation 3.24.

As mentioned earlier, external film diffusion is a measure of the resistance to the transport of ions from bulk solution through the zeolite particle which depends mainly on the particle size, solution concentration and film thickness. Internal diffusion depends on the structure of zeolite particle and since they are bi-dispersed sorbents, both surface or pore diffusions may dominate different regions. In micropores, surface

diffusion may be dominant, while pore diffusion may be dominant in macropores thus, the use of lumped parameter D_e as effective parameter is recommended. Biot number is the ratio of the external-phase mass-transfer rate to pore- phase mass-transfer rate.

$$\mathrm{Bi} = r_p \, k_f / \mathrm{D_e} \qquad (3.28)$$

indicating which diffusion stage controls the adsorption rate. The value of Biot number generally over the 10-30 range, the pore-phase mass transfer rate is reduced and controls the overall exchange rate, while for a smaller Biot number signals an external (film) mass transfer rate controlled process (Paoli et al., 1996 and Chiang et al., 2002).

3.4.3. Surface Precipitation

Surface precipitation form due to the increase in metal cation or anion sorbed on a surface to higher surface coverage. There is a strong and continuous relation between surface complexation and precipitation. At low surface coverage, complexation is the dominating mechanism while with the increase of surface coverage nucleation occurs and aggregates on the surface start forming. Surface precipitation becomes the only controlling mechanism in metal-zeolite system with further increase in surface coverage. Precipitation in the system depends on the solubility product, alkalinity of the exchanger and acidity of the metal solution. The controlling the pH of metal-zeolite solution is important in order to prevent significant precipitation during ion exchange (Doula and Ioannou, 2003). In some cases, as metal ions exchanged in the mineral and solid species might grow on the surface, as precipitates and may clog the part of the pores and decrease the uptake of the metal. For example in the case of Cu^{2+} exchange, atacamite $CuCl_2.2Cu(OH)_2$ grew on the surface of clinoptilolite and decreased the Cu^{2+} uptake by the mineral (Inglezakis et.al, 2005).

3.4.4. Dissolution

In addition to ion exchange, adsorption and surface precipitation, dissolution also occurs in zeolite-solution system. The collision of metal ions and ligands on surface sites cause dissolution of Al^{3+} and/or Si^{+4}. The type of the surface species strongly affects the dissolution process such as an inner-sphere complex with a ligand such as Cl- which makes the detachment of a central metal ion easier thus, dissolution increases. Shift of electron density from ligands toward the central metal ion at the surface is responsible for this case. Surface protonation also tends to increase the dissolution, because bonds in the surface central ions are polarized and cationic surface group becomes easily broken (Doula and Ioannou, 2003; Doule et al., 2002). The dissolution of clinoptilolite framework is affected by the presence of exchangeable cations in the solution phase. Si and Al from the framework possibly move toward solution phase which is called as dissolution. It is mainly depends on the solution pH, but also on the surface protonation and nature of solution ions. The strong relation between ionic strength and pH of the solution with Si or Al dissolution in zeolites are in relation. Si dissolution increases with decreasing ionic strength and increasing solution pH while for the Al dissolution case visa versa situation is valid. At acidic and neutral pH values the dissolution of Al represented by the following reaction;

$$\equiv Al\text{-}OH + H^+ \rightleftharpoons \equiv Al - OH_2^+ \rightleftharpoons Al^{3+} + H_2O$$

As mentioned earlier, formation of surface complexes increases Al dissolution, and the related mechanism is given in the following reaction;

$$\equiv Al^{3+} + OH^- \rightleftharpoons Al(OH)^{2+} + H^+$$
$$Al(OH)^{2+} + OH^- \rightleftharpoons Al(OH)_2^+ + H^+$$
$$Al(OH)^{2+} + OH^- \rightleftharpoons Al(OH)_3 + H^+$$

Si dissolution is independent of H^+ and OH^- ions but dependent on pH which is high at high pH. Si dissolution is represented by the following reaction;

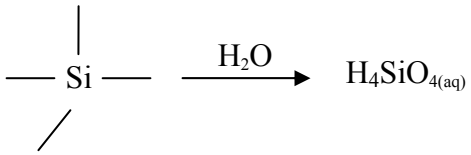

At high pH values, Si-O bonds are polarized and weakened at basic condition by the presence of charged Si-O species; thus detachment Si atom becomes easier resulting in higher Si dissolution in the system. The minimum Si dissolution occurs at pH equal to pH_{pzc}.

As a conclusion, pH is an important and common parameter for the zeolite-metal interactions. It influences character of the exchanging ions and character of the zeolite itself. Possible mechanisms responsible for pH change in zeolite-metal solution can finally be summarized as:

i. H^+ in the solution exchanges with the extra framework cations in the zeolite (Na^+,K^+,Ca^{2+} and Mg^{2+}) form outer and/or inner complexes in acid to neutral pH range. H^+ competes with metal cations result in the metal uptake decreases. As a result, solution pH increases.

ii. H^+ in surface hydroxyl groups (Si-OH and Al-OH) behaves as an exchangeable cation at acidic and neutral pH range which causes a decrease in solution pH.

iii. Protonation of neutral and negative surface hydroxyl groups by H^+ at acidic to neutral pH range causes an increase in solution pH.

iv. At higher pH, OH^- ions may react with clinoptilolite surface and cause a decrease in solution pH.

v. Formation of metal-hydroxyl complexes cause decrease in solution pH (Doula et al., 2002; Ersoy and Çelik, 2002; Trgo and Peric, 2003).

CHAPTER 4

MICROWAVES

In the past few years, heating of materials, driving chemical reactions by microwave energy has been a popular theme in the scientific community. This non-classical heating technique is gradually moving from a laboratory curiosity to an established technique heavily used in both academia and industry.

Microwaves are a form of electromagnetic radiation with frequencies ranging from several hundred MHz to several hundred GHz and wavelengths ranging approximately from 1 to 20 centimeters. In the electromagnetic spectrum, the microwave radiation region is located between infrared radiations and radiowave. Microwave frequency includes three bands; the ultra high frequency in the range 300MHz to 3 GHz, the super-high frequency in the range 3GHz to 30 GHz and extremely high frequency in the range 30GHz to 300 GHz. Virtually all domestic and commercial equipment today uses a frequency of 2.45 GHz with wavelength of 12.2 cm for operation. The high frequency of microwaves bring advantage of being able to carry more information than ordinary radiowaves and their use in some areas was replaced by microwaves in the recent years. Microwave energy is being used in many applications. In the early 1950s, the microwave energy primarily started to be used our home microwave ovens and cell phones. In the following years it took its place in the areas categorized; communication and information transfer; processing and manufacturing; diagnostic and analyses; weapons; and medical treatment.

The microwave system is made up of four basic components: power supply, magnetron, and applicator such as, oven for the heating of the target material and waveguide for transporting microwaves from the generator to the applicator. The microwave power is supplied from a self-contained microwave power supply unit that contains a magnetron tube, transformer, relay, choke and controls. The microwave energy is directed to the applicator by a waveguide (Hoque, 1999).

4.1 Microwave Heating

In the microwave systems, the energy transfer does not occur by conduction or convection as in conventional heating, but by dielectric loss. Materials dissipate microwave energy by two main mechanisms: dipole rotation and ionic conduction. When molecules with a permanent dipole are submitted to an electric field, they become aligned. If this field oscillates, the orientation changes with each alternation. The strong agitation, provided by the reorientation of molecules, in phase with the electrical field excitation, causes an intense internal heating. During ionic conduction, as the dissolved charged particles usually ions in a sample oscillate back and forth under the influence of the micro-wave field, they collide with their neighboring molecules or atoms. This collision causes agitation or motion, creating heat. Figure 4.1 shows the mechanism of microwave heating (Wathey et al., 2002).

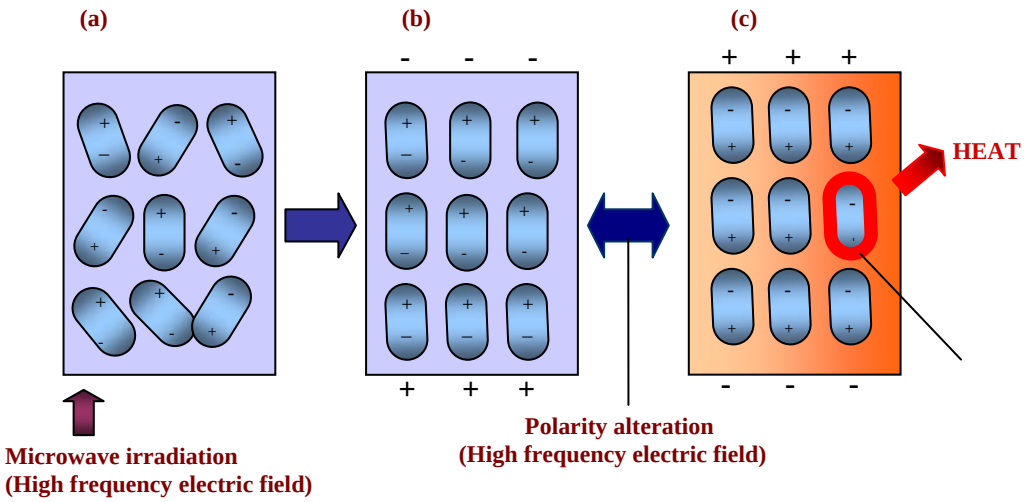

Figure 4.1. Mechanism of Microwave Heating.

Dipoles within the substance to be heated are irregularly arranged, as shown above in part a, but, when irradiated with microwaves, they arrange themselves in a regular pattern, as in part b and c. As the positive and negative poles alternate with each other at high frequencies, the phenomena between in the parts b to c and c to b are repeated. The repeating event produces heat from the friction of the oscillating and rotating dipoles. In short, the heat generation in the microwave technology is dependent on the nature of the dipole and the frequency of the applied radiation. If the frequency

of the radiation is too high, the dipole does not have time to align itself with the field before the field changes its direction again. In these circumstances, no motion and consequently no heating occurs if the dipole align itself perfectly with the alternating electric field and, therefore follows the field fluctuations. However, if the applied field is in the intermediate frequency region, a phenomenon occurs that lies between these two extremes. In this situation, the dipole does not follow it perfectly. This results in the generation of heat (Wathey, 2002).

4.2. Interaction of Microwaves with Material

The amount of microwave energy absorbed by materials depends on many factors and their behavior in the microwave field can be measured by some physical properties. The size of the load, its orientation with respect to the waves, and the dielectric and thermal properties of the material are important factors but the most critical parameters that the microwave radiation depends on are dielectric constant, ε', and dielectric loss factor, ε''. The dielectric constant describes the case with which a material is polarized by an electric field while dielectric loss factor measures the efficiency of conversion of the electromagnetic radiation to heat. Both,ε' and ε'' vary with the frequency and their ratio gives the dielectric loss tangent. It defines the ability of a material to convert electromagnetic energy into thermal energy at temperature and frequency applied and is defined by Equation 4.1.

$$\text{tan loss} = \tan\delta = \varepsilon'' / \varepsilon' \qquad (4.1)$$

The dielectric properties of a material are dependent on its atomic/molecular geometry. Therefore, any thermally induced changes causing molecular or structural rearrangement will affect tan loss factor. Microwave interaction with matter is also characterized by a penetration depth, Dp, may also be the limiting factor and is defined in Equation 4.2.

$$D_p \approx \frac{\lambda_o \sqrt{\varepsilon'}}{2\pi\varepsilon''} \tag{4.2}$$

where, λ_o is wavelength of the microwave radiation.

Generally stated, the depth of penetration is smaller for microwaves because the frequency is many times higher than the radio frequency installations. Not only is the penetration depth a function of the frequency of the microwaves and the material composition, but also a function of dielectric properties of the material. When electromagnetic radiation strikes a material, part of radiation will be reflected. The remaining part penetrates into the material and is gradually absorbed. Thus, microwaves can penetrate only a certain distance into a bulk material as shown in Figure 4.2.

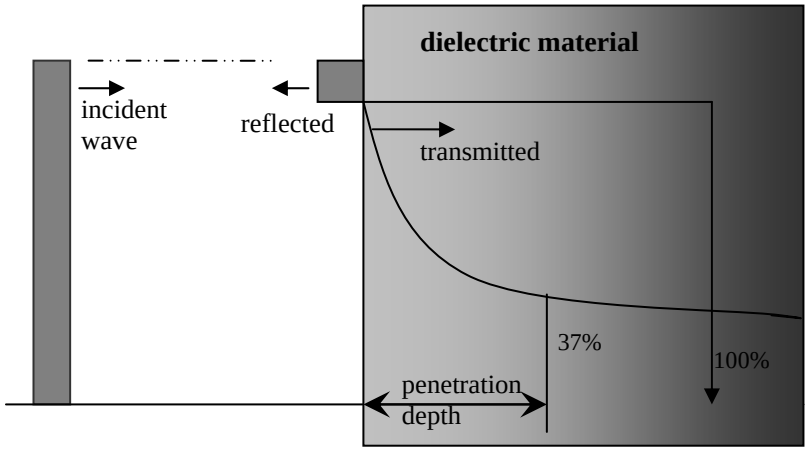

Figure 4.2. Flow electromagnetic wave into dielectric material.

Microwaves may be reflected, passed through, or absorbed by the materials depending on the material type. Metals in general have high conductivity and are classed as conductors. They reflect microwaves and that is why the walls of a microwave oven are generally made of metal confining the microwaves inside the cavity. The see-through panel in the microwave oven door contains a metal screen which reflects the microwaves but the microwaves cannot penetrate this screen, because the holes in the screen are much smaller than the microwaves. Materials which are transparent to microwaves are classed as insulators such as some glass, pottery, paper and most plastics allow the waves to pass through. Insulators are often used in microwave ovens to support the material to be heated. These materials do not take up

microwave energy but allow the solutions inside to absorb the microwaves. Materials which are excellent absorbers of microwave energy are easily heated and are classed as dielectrics.

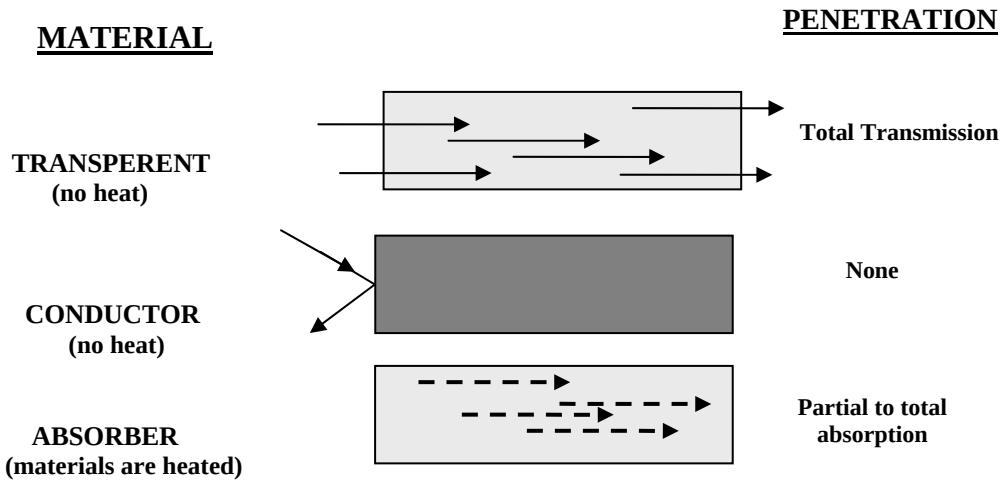

Figure 4.3. Interaction Microwave with Materials

In literature, many materials were investigated in order to determine their interaction with microwaves. Microwave heating behaviour of several metal oxides was investigated and they were classified according to heating rate into hyperactive, active, difficult to heat and inactive. The highest temperatures were obtained with carbon and most of the metals oxides such as; NiO, MnO , FeO , CoO , CuO and WO. In the beginning of 1990s heating of around 40 minerals was done in order to investigate if the microwave energy could be effective in the heating of minerals and inorganic compounds. The mineral samples were characterized before and after microwave heating and minerals were divided into two groups. In the first group samples, no or very little heat was generated and the mineral properties remained essentially unchanged. In the second group samples, heat was generated and the minerals were either thermally stable or decomposed reacted rapidly into a different product. The test results indicated that most silicates, carbonates, sulphates, some oxides and sulphides fall in the first group. Both synthetic and natural jarosite, some metal oxides such as hematite, magnetite and cassiterite are heated easily and fall in the second group (Wathey et al., 2002).

As previously discussed, there are two specific mechanisms of interaction between materials and microwaves; dipole interactions and ionic conduction. Dipole

interactions occur with polar molecules. The polar ends of a molecule tend to align themselves and oscillate in step with the oscillating electrical field of the microwaves. Collisions and friction between the moving molecules result in heating. Consequently, the more polar a molecule is the more effectively it will be influenced by the microwave field. Ionic conduction different from dipole interactions do not have a dipole moment. They are charged species that are distributed and can couple with the oscillating electrical field of the microwaves. The effectiveness or rate of microwave heating of an ionic solution is a function of the concentration of ions in solution. The chemical composition of the material, as well as the physical size and shape, will affect how it behaves in a microwave field. The movements of the ions in the matrix by the interaction with microwave radiation are a much stronger heat generation than the corresponding motion of dipoles. Therefore, the ionic species heat up extremely rapidly when exposed to microwave irradiation. The property of ionic species can be used to improve the heating ability of non-polar solvents upon exposure to microwave radiation. For example when Fe is substituted instead for Zn in sphalerite, the resulting Fe sphalerite becomes microwave responsive. It was also found that, dark-colored compounds heated rapidly to high temperature and heating rates of dark colored compounds were much higher than those of light colored materials (Haque, 1999). In order to allow efficient heating by microwave radiation of poor dielectric samples, the addition of small amounts of additives like ionic salts that have large loss tangent values enable adequate heating of the mixture. This is often provides an efficient way of using non-polar solvents for microwave radiation. Moreover, ionic liquids dissolved to appreciable extent in a wider range in organic solvents than water and alcohols in which they interact more efficiently. Thus, they can be used in non-polar organic solvents highly efficient additives to increase microwave absorption (Wathey et al., 2002; Haque, 1999).

4.3. Microwave Heating System versus Conventional Heating System

Microwave heating occurs somehow differently from conventional heating. In conventional heating systems, the mixture must be in physical contact with a surface

that is at a higher temperature than the rest of the mixture where energy is transferred from a surface to the bulk mixture by means of thermal conduction. The energy is supplied by the use of a heating mantle, oil bath, steam bath, or even an immersion heater. The energy can either make the reaction thermodynamically allowed or it can increase the reaction kinetics. On the contrary, in microwave systems the energy transfer does occur by dielectric loss. In other words, in conventional heating heat transfer occurs from the heating device to the medium, while in microwave heating heat is dissipated inside the irradiated medium. Additionally, in all conventional heating of open reaction vessels, the highest temperature that can be achieved is limited by the boiling point of the particular mixture. In order to reach a higher temperature in the open vessel, a higher-boiling solvent must be used. Figure 4.4 shows the comparison of the mechanisms of conventional and microwave heating systems.

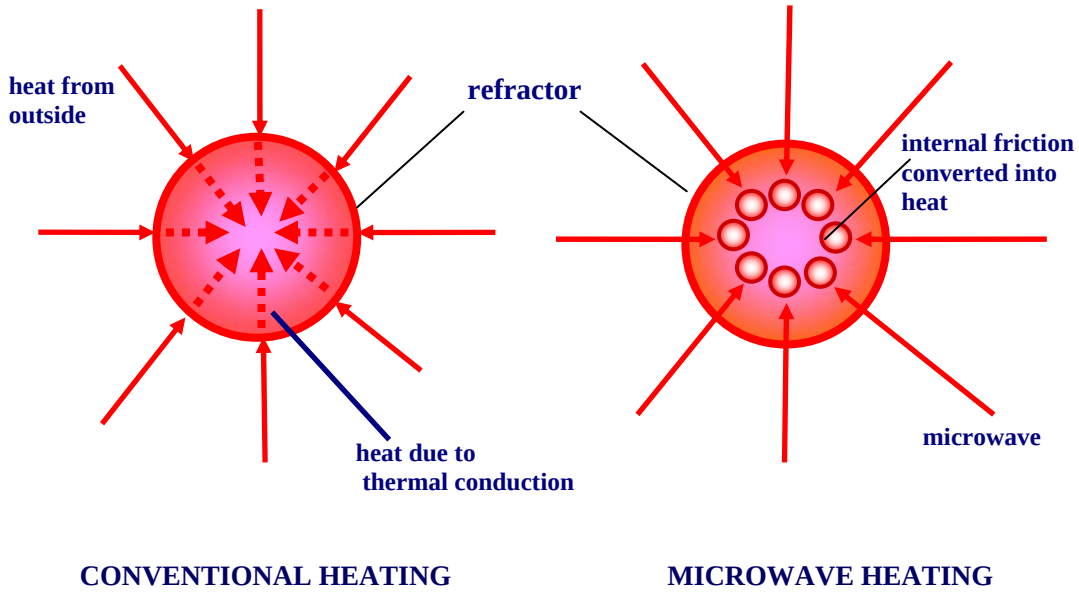

Figure 4.4. Conventional Heating System versus Microwave Heating System.

Figure 4.4 clearly explains the differences between two mechanisms. In the conventional heating system, heat is transmitted from the exterior of a substance to its interior whereas in the microwave heating system, microwaves penetrate into the core of a substance to directly heat the inside.

In contrast with conventional heating, microwave heat transfer is not limited by thermal conduction or convection currents. This means that a much faster temperature increase can be obtained. Furthermore, the maximum temperature of the material heated

by microwaves is only dependent on the rate of heat loss and the power applied. Although microwaves create volumetric heating, it is well known that the field distribution is uneven in the irradiated material, and therefore the energy is not homogeneously dissipated.

As a general conclusion, advantages of microwave heating over conventional heating can be summarized as follows;

1. Microwave has non-contact heating.
2. Microwave heating is an energy transfer, not heat transfer.
3. Microwave heating is more rapid.
4. Selective heating of material is possible.
5. Microwave is easy method with quick start-up and stop.
6. No temperature gradient occurs.
7. Microwave has higher level of safety and automation. (Haque, 1999)

To understand how microwave heating can have effects that are different from conventional heating techniques, thing that is absorbing the microwave energy in the reaction mixture should be determined. It is due to the fact that materials or components of a reaction mixture can differ in their ability to absorb microwaves.

4.3.1. Case 1: Solvent and Reactants Absorb Microwaves Equally

If the bulk solvent and reactants absorb microwaves equally, the energy transfer and heating will occur to the allowed depth of penetration into the bulk mixture. Homogeneous reaction conditions can be established thorough mixing, and at equilibrium, the temperature of the reactants will be the same as that of the bulk solvent. In this case, reaction rates can be increased by increasing the temperature of the reaction mixture. The case is achieved using closed-vessel microwave techniques, and also using the same reaction chemistry and solvent. Alternatively, using conventional heating techniques, higher reaction temperatures can be achieved in a closed reactor system, or by using a higher-boiling solvent in an open vessel.

4.3.2. Case 2: Solvent Absorbs Microwaves

Microwaves are absorbed by bulk solvent not by the reactants so, the solvent energy transfer and heating of the solvent will occur to the allowed depth of penetration. Then bulk solvent in turn will heat the reactants by conduction. Homogeneous reaction conditions can be established with thorough mixing, and at equilibrium the temperature of the reactants will be the same as that of the bulk solvent. The ability of solvents to interact with microwave radiation can be classified into two important cases that have to be considered. The first one is the solvent's ability to absorb microwave energy and the second one is its ability to convert the absorbed energy into heat. The interaction of a solvent with the microwave irradiation is really complex phenomena.

4.3.3. Case 3: Reactants Absorb Microwaves, Solvent Much Less

If the bulk solvent does not absorb microwaves, but the reactants do, direct energy transfer and heating of the reactant molecules will occur to the allowed depth of penetration just as in case 2. The same situation is applicable for this case but just in visa versa reactant to solvent relation is valid.

This case is significantly different from conventional heating techniques. Reaction rates can be increased by increasing the temperature of the reactants, delivering microwave energy faster than the heat that can be transferred to the bulk solvent and radiated to the environment

4.3.4. Case 4: Catalyst on Absorbing Microwaves

Some unusual reaction conditions can be created in a microwave field when catalysts are present in the mixture, particularly when the catalyst is deposited on a microwave-absorbing material. For example, palladium on carbon is a common catalyst

in some reaction mechanisms. Carbon or graphite is an excellent absorber of microwave energy, with a dissipation factor significantly higher than most solvents. An unexpected effect of the microwave field is that it can directly heat some catalyst supports, and create a condition where the catalyst is at a substantially higher temperature than the rest of the bulk mixture. The catalyst support will transfer heat to the bulk mixture by conduction.

4.4. Microwave in Zeolite Scientific Community

The recent innovations of microwaves in various fields of science lead many researchers to focus on this phenomenon. After 1980s a new interdisciplinary of microwave chemistry was performed and at the beginning of 1990s, microwave technique began to be applied in the synthesis and other applications related to zeolites. Han et al.(1999) and Xrachum et al. (2000) studied the molecular sieve membrane of Na-A zeolite crystals on α-Al_2O_3 substrate and it has been successfully synthesized by means of microwave. They concluded that by microwave synthesis the reaction time reduced and more stable and dense membranes were obtained.

There microwave irradiation on heating and other processes have many advantages compared to conventional methods as discussed in pervious pages. Katsuki et al. (1999) studied the microwave hydrothermal (MH) versus conventional hydrothermal (CH) synthesis of NaY Zeolite. They focused on the synthesis of NaY zeolite crystals from colloidal silica, sodium aluminate, and sodium hydroxide and deionized water at 100 ^{o}C-120 ^{o}C and concluded that NaY zeolite crystallization was enhanced by 3 to 4 times with MH process compared to CH. Stout and Komerneni., 2002 studied microwave-assisted method for the rapid removal of K from Phlogopite. They investigated the ability to remove K rapidly with a solution containing sodium tetraphenylborate (NaTPB) from the interlayer of naturally occurring phlogopite using microwave and conventional heating treatments. They concluded that microwave assisted treatment considerably decreased the exchange time compared to continuous treatments. Chitrakar et al. (2002) had studied the synthesis of o-$LiMnO_2$ by microwave They synthesized o-$LiMnO_2$ with different routes including hydrothermal, reflux or

microwave irradiation They showed that with all synthesis is possible however, formation of semi-crystalline o-$LiMnO_2$ was achieved by the interaction of microwave irradiation with suspension of γ-MnOOH in a 4M LiOH solution in a very short time when compared to conventional methods.

If the microwave radiation is used as heat source to ion exchange process, the rapid, uniform and direct heat is achieved. The basicity on the framework of zeolites is linked to the partial negative charge on the oxygen atoms and can be increased by the ion exchange of the cation that counter balances the negative charges by a less electronegative cation. Yin and Yin, 1998 studied the dispersion and solid-state ion exchange of $ZnCl_2$ onto the surface of NaY zeolite using microwave irradiation and resulting product was characterized by X-Ray diffraction and Infrared Spectrometer (IR) techniques. $ZnCl_2$ was dispersed on the surface of NaY under microwave irradiation and increased with increasing $ZnCl_2$ loadings. The appearance of a new band at 809 cm^{-1} in the framework IR spectra of the coordination of $ZnCl_2$/NaY sample is considered due to the coordination of $ZnCl_2$ with oxygen from the NaY zeolite lattice. Romero et al. (2004) studied potassium exchange in NaX zeolite by employing microwave radiation. The reaction was found very rapid even the volume of the exchange was reduced to conditions close to incipient wetness without the protonation of zeolite; thus, microwave reduced the time and volume required for the ion exchange process (Romera et al., 2004)

Because of the unique heating mechanism of microwave irradiation it has a specific effect on ion exchange behavior of zeolite molecular sieve. Compared to the ion-exchange conducted in commercial waterbath method, microwave irradiation conducted ion exchange has many advantages for rare earth ions such as; Ce^{3+}, Eu^{2+} and Sm^{2+} without structural changes observed for the exchanged zeolite. The movement of water molecules and rare earth ions is much higher in microwave heating compared to that commercial waterbath heating. This movement of water molecules results in rare earth ions entering into the c-direction channel, which is normally not accessible to rare earth ions in commercial waterbath ion exchange. Additionally, the degree of ion exchange is not affected by the ion concentration of the solution in commercial waterbath method. However, in microwave driven ion exchange, the concentration of the rare earth ion solution has a significant effect on the extent of ion exchange. Higher rare earth ion concentrations of solution will lead to a higher degree of ion exchange. Compared to the commercial waterbath ion exchange method the exchange time in

microwave driven ion exchange with fixed rare earth ion concentration and microwave power level will affect the luminescence intensity of the exchanged product. The start quenching time of Ce^{3+} luminescence is 8min in microwave driven ion exchange while it takes about 8hours in commercial waterbath ion exchange method. Therefore, the ion exchange conducted in microwave is feasible, convenient and fast compared to commercial ion exchange methods (Xu et al., 2007)

The microwave heating to higher temperature studies showed that there are several factors affect the heating. Hydrated zeolites absorb microwave energy more efficiently than dry zeolites, H-form of zeolites interacts little with microwaves and degree of interaction strongly depends on the chemical composition and structure (Ohgushi et al., 2001). The Na^+ ions within the large cavity in zeolite structure act as strong microwave absorbers. This agrees with the MacDowell's suggestion that is the sodium ions "rattling in the cavities" absorbs microwave (Whittington and Milestone, 1992).

Energy adsorption in zeolites is a complex process and it was thought that it is strongly affected by the presence of metal ions, first of all the Na^+. Both ionic conduction by Na^+, K^+, and other ions, and dipole rotation by water molecules can take place. (Pilter et al., 2000). Ohgushi and Numata (2003) studied the importance of Site III cation of zeolite A in microwave Heating. They studied the properties of dehydrated $Na_{12-2x}Ca_x$-A zeolites, x is in the range of 0.1 to 4, in microwave heating and calculated the microwave absorption efficiencies of the zeolites as function of temperature by using their dielectric properties. They have found that $Na_{12}A$ is easily heated to higher temperature while $Na_{12}Ca_4A$ is not so heated and final heating temperature of $Na_{12}Ca_1A$ is much closer to that of $Na_{12}Ca_4A$ than $Na_{12}A$. The change in the cation compositions did also cause changes in absorption efficiency. The cation distribution in zeolite A denotes Na^+ ion on the site III is the most weakly bound cation and has larger contribution towards microwave heating while Na^+ is in site I/II and Ca^{2+} in site site has small contribution.

Structural changes such as phase transition, amorphization might be observed during conventional heating of crystalline materials. Recently, the use of microwaves for heating and processing of materials in many areas of chemistry increased and it is important to determine if structural changes occurred within the material during microwave irradiation. For example; in steel making industry in order to modify the physical characteristics of iron and to recover iron from the slag, microwave heating

tests 1000 W, 2450 MHz are being used. In research and development laboratories, the heating behavior of the steel making slag was investigated with and without the addition of carbon or magnetite. Test results demonstrated that both carbon and magnetite addition increased the heating rate of the slag; 1000 ^{o}C with carbon, 800 ^{o}C with magnetite, compared to 650 ^{o}C without any addition and the amount of iron recovered increased with heating time. Microwave heating altered the physical and chemical properties of the slag (Hoque, 1999). Pilter et al. (2000) investigated the effect of microwave irradiation on zeolite Na-A in comparison with classical heat treatment. The classical heated and/or microwave heated samples were investigated by XRD and compared with respect to original using the intensities and the d values of the characteristic (0 0 2) refection of zeolite Na-A, which is the most intense peak of the original zeolite. The intensity of the (0 0 2) peak decreased significantly during the microwave treatment while it slightly changed upon conventional heating (Pilter et al., 2000).

Microwaves can cause different biological effects depending upon field strength, frequency of microwave, modulation and duration of the irradiation. The factors other than thermal effects might be involved in the effects of microwave irradiation on microorganisms. Microwave is used for food pack sterilization leading to the cell deaths by the heat and electric field produced. Compared to conventional heat sterilization the death rates of *Eschorichia Coli* were higher with microwave irradiation at 45-50 ^{o}C. Microwave affects all biological levels, from microbial cells to animals, as well as humans (Banik et al., 2003).

CHAPTER 5

MATERIALS AND METHOD

The experimental section of this study is outlined as three parts. In the first part, zeolitic mineral to be used was characterized by different instrumental techniques. Following the characterization section the ion exchange experiments were conducted in constant temperature waterbath with orbital shaking and microwave. Finally, the characterization of the exchanged samples was performed and antibacterial tests were done. From this point forward, the zeolitic mineral used in the text will called as CLI.

5.1. Characterization of Zeolitic Tuff

CLI was supplied from Gördes Region, Western Anatolia of Turkey. Initially the mineral was prepared since the preparation step is important for obtaining representative samples prior to the experiments and is given as follows;

1. The clinoptilolite rich mineral taken from deposit was crushed in Fritsch jaw crusher and sieved into different particle size ranges as given in Table 5.1.

Table 5.1. Particle Size ranges.

Size Range
>1.7 mm
850-500 μm
500-250 μm
250-150 μm
150-75 μm
<75 μm

2. The wet sieving was done in each particle size range order to remove soluble impurities. The remaining slurry having CLI with particle size of <25 micron was left in basket for 2 week. The clear solution of the suspension in basket was centrifuged in Sigma Laboratory Centrifuges 6K15 with 9000 rpm for an hour.

3. The wet sieved clinoptilolite rich mineral was dried overnight at 65 ^{o}C and then kept in constant 75% RH for at least one week in order to obtain same condition before analysis.

The characterization techniques and conditions set for each technique were as follows;

X-Ray Diffraction (XRD); To obtain the crystal structure and structural properties X-Ray patterns of the zeolitic tuff were determined. The X-Ray powder diffraction measurements were carried out using Philips X/Pert X-Ray diffractometer with Ni filtered CuK_{α} radiation in the range of 5 to 40 ^{o}2Theta.

The zeolitic minerals from different part of Turkey were investigated under the Governmental Projects which were held in İzmir Institute of Technology, Chemical Engineering Department. Reference Intensity Ratio (RIR) method was used and it was found that it was mainly clinoptilolite (%60-65) and additionally, quartz, analcime and mordenite was found in the structure.

*Inductively Coupled Plasma- Atomic Emission and Mass Spectrometry (ICP-AES & ICP-MS); C*hemical analyses of the zeolitic minerals were realized by Inductively Coupled Plasma Atomic Emission Spectrometry (ICP-AES,Varian). The lithium borate fusion method used in the determination of the major elements within the zeolitic minerals such as sodium, calcium, magnesium, potassium, barium, iron, aluminum, and silicon. The wavelengths of the elements were chosen for the experimental conditions and are as follows; Ag (328.068 nm), Al (396.152 nm), Ca (317.933 nm), Co (238.892 nm), Cu (324.754 nm), Fe (259.754 nm), K (769.896 nm), Mg (279.553 nm), Na (589.592 nm) and Si (251.611 nm). First 0.1 g. sample was mixed thoroughly with 1g. lithuim tetraborate and metaborate and mixed thoroughly until homogeneity was obtained. Then it was placed in 1000 ^{o}C furnace for about 50 to 60 min. The glass bead formed was dissolved in ≈70ml 1.6 M HNO_3 and the volume was completed to 250 ml with de-ionized water. If necessary the solutions were diluted prior to ICP-AES analysis.

The chemical analysis of trace elements in the zeolitic minerals used in Part I experiments were determined by Inductively Coupled Plasma Mass Spectrometry

(7500CE-Octopole Reaction System, Agilent). The acid digestion method was used to determine the chemical compositions of minor elements such as titanium, cadmium, chromium, silver, zinc, lead, lithium, nickel, copper and they were analyzed using ICP-MS. First 0.2 g. sample was taken into a teflon beaker. Then, 4ml. HNO_3, 5ml. HF and 3ml. $HClO_3$ was added onto sample and was mixed thoroughly. The solution was put on 180 ^oC hot plate until all liquid part was evaporated. The residual was then dissolved in 5ml. HNO_3 (%65 w/w) and 5ml H_2O and completed to 100 ml with de-ionized water.

Three repetitions of the solid and liquid phase analyses of the ion exchanged minerals were done and all were given in Appendix. In the thesis, average values of three measurements were used for discussion.

Volumetric N_2 Adsorption; The N_2 adsorption analyses of the zeolitic minerals were done by means of volumetric method. The samples were first degassed at 350 ^oC for 24 hours. The analysis was carried out with liquid N_2 at its normal boiling temperatures of 77K.

Scanning Electron Microscopy (SEM); The morphology of the zeolitic minerals was determined by scanning electron microscope. The SEM micrographs were obtained on a Philips XL 305 SEM. EDX (Energy Dispersive X-Ray) analysis was performed to determine the chemical compositions of the cations within the mineral by using EDAX-EDS connected to SEM Philips XL 30S FEG and results were compared with ICP data.

Fourier Transform Infra-red (FTIR) Spectrometry; The Infrared spectra of all the samples were taken by Fourier Transform Infrared Spectrometer, Shimadzu (FTIR-Shimadzu 8601) using KBr pellet technique. Powdered mineral particles are mixed with KBr and compressed into 1cm diameter pellets under 8 ton force. Typical pellet contains 1-2 wt% samples in KBr.

Thermal Analysis (TGA, DSC, and DTA): In order to obtain thermal behaviour of zeolitic minerals, Thermogravimetric Analyzer (TGA-51/51H, Shimadzu), Differential Scanning Calorimetry (DSC-50, Shimadzu) and Differential Thermal Analysis (DTA-50, Shimadzu) were used. The samples were heated up to 1000 ^oC for DTA and TGA and upto 500 ^oC for DSC analysis with a heating rate of 10 ^oC/min under 40 ml/min N_2 atmosphere.

The dielectric constant of the NaCLI mineral was determined from the Capacitance (F) data. The powder mineral was first compressed into pellet having 10mm diameter and 0.5mm thickness under 8ton forces. Electric contacts were taken on pellet's surface using silver using film thermal evaporation technique. The capacitance

of the pellet was measured in the frequency range of $2*10^3$-$4*10^3$ Hz at room temperature using Keithley 2420 Analyzer.

5.2. Ion Exchange

5.2.1. Chemicals

Chemicals and their specifications used in the experimental study are given as follows:

1. Sodium Chloride -NaCl; Panreac QuimicaSa, 99.5%, Mw=58.44 g/mol.
2. Silver Nitrate- Ag $(NO)_3$; Fluka, 99.5%, Mw=169.88 g/mol.
3. Copper (II) Nitrate pentahemihydrate– Cu $(NO_3)_2 5/2H_2O$; Aldrich 99.99 %, Mw= 232.59 g/mol.
4. Cobalt II Nitrate Hexahydrate- Co $(NO3)_2.6H_2O$; Sigma 98%, Mw: 291.03 g/mol.
5. Lithium metaborate anhydrous – $LiBO_2$; Fluka 98%, Molar Ratio= B_2O_3/ LiO_2= 0.95-1.05; Mw= 49.75 g/mol.
6. Lithium tetraborate - $B_4Li_2O_7$; Fluka 99%, Mw=169.12 g/mol.
7. Muller-Hinton Agar-Agar; granulated, purified and free from inhibitors for microbiology, Merck**.**
8. Muller-Hinton broth; Merck

The ion exchange experiments were performed using 150 –250 μm particle sized CLI. The exchange processes were carried out in a constant-temperature waterbath (GLC Model-1084) and microwave irradiation (Mars-CEM Digestion/Extraction & CEM Focused Microwave™ Synthesis System) methods for Ag^+, Co^{2+} and Cu^{2+} ions in their appropriate nitrate solutions. The effect of solution temperature, Solid/Solution ratio and contact time on ion exchange was determined.

Before the ion exchange experiments were performed, near homoionic form of CLI was prepared as follows; 125 g mineral was treated with 1250 ml of 1 N NaCl solution in a constant-temperature waterbath maintained at 80 ^oC for 10 days. NaCl

solution was replaced in every three days. After the exchange was completed, mineral was washed with de-ionized water until all Cl^- was removed and dried overnight at 65 ^oC. The Na-form of CLI will be called NaCLI from this point forward.

5.2.2. Ion Exchange in Conventional Waterbath

The conventional exchange was conducted using constant-temperature waterbath with orbital shaker at 180 rpm, GLC Model-1084.

Ag^+ exchange; NaCLI was put in 0.01 M $AgNO_3$ solution in constant temperature waterbath maintained at 40 ^oC, 60 ^oC or 80 ^oC. Solid/Solution ratios were chosen as; 1/20, 1/50 and 1/100. At first, the exchange was conducted for 30 min, 1hr 24hrs, 48 hrs and 72 hrs. Additional of 0.1 M $AgNO_3$ of exchange was conducted at 80 ^oC for S/L=1/100, 1hr and 24hrs. 1M $AgNO_3$ of exchange was conducted also at 80 ^oC for S/L=1/100, 10 min and 30 min in order to comparable with microwave treatment. Three parallel runs were performed for each condition. pH changes during the ion exchange process at 60 and 80 ^oC was measured for all S/L ratios. For Ag^+ exchange case; the minerals were covered with aluminum foil and kept at dark place for further analysis.

Co^{2+} & Cu^{2+} exchange; NaCLI was put in 0.01 M $Co{\cdot}(NO_3)_2{\cdot}6H_2O$ and $Cu{\cdot}(NO_3)_2{\cdot}5/2H_2O$ solution in constant temperature waterbath maintained at 80 ^oC for 1hr and 24 hrs.. Elimination of 48 hrs and 72 hrs of exchange time was decided after kinetic study was performed for each cation. Elimination of the exchange conducted at 40 ^oC and 60 ^oC was due to the evaluation of first sight ICP-AES results of Ag^+ exchange. Solid/Solution ratios were chosen as; 1/20, 1/50 and 1/100. Three parallel runs were performed for each condition. pH change during ion exchange process conducted at 80 ^oC was measured for all S/L ratios. Additional of 0.1 M $Co{\cdot}(NO_3)_2{\cdot}6H_2O$ of exchange was conducted at 80 ^oC for S/L=1/100, 1hr and 24hrs. 1M $Co{\cdot}(NO_3)_2{\cdot}6H_2O$ of exchange was conducted at 80 ^oC for S/L=1/100, 10 min and 30 min.

After the exchange was completed in constant temperature waterbath, minerals were washed with de-ionized water and dried overnight at 65 ^oC.

5.2.2. Ion Exchange in Microwave

Exchange by microwave irradiation was conducted using Mars 5-CEM, Digestion and Extraction laboratory microwave oven system and CEM Focused Microwave™ Synthesis System. In Mars 5-CEM, Digestion and Extraction laboratory microwave oven system, the solutions were placed in a specially made Teflon-lined polyamide vessel through which microwave radiation in which temperature and pressure can be controlled within the vessels. The frequency of the microwave radiation was 2.450 GHz. Microwave power was manually set to appropriate watts depending on the number of the vessels used for the run in progress. However microwave power regulates itself in order to keep the temperature at the set value therefore alternating microwave power was applied throughout the runs. In CEM Focused Microwave™ Synthesis System, Discovery microwave system, fixed power control option offers the application of desired power from the beginning till the end of the reaction since there is a cooling feature in the system. It directs a gas source onto the outside wall of the reaction vessel which provides the ability to rapidly cool (quench) a reaction at the same time and/or after the application of microwave energy. It is the most direct method to energize reaction system and applies a specified amount of energy for a specified amount of time. For the exchange conditions considered in this study, the continuous microwave power of 50 watts used. After the exchange was completed in microwave oven, minerals were washed with de-ionized and dried overnight at 65 ^{o}C.

Ag^{+} exchange; NaCLI was put in 0.01 M $AgNO_3$ solution placed in a specially made Teflon-lined polyamide vessel. The exchange was conducted at 40 ^{o}C, 60 ^{o}C and 80 ^{o}C for 30 min and 1hr. Solid/Solution ratios were chosen as; 1/20, 1/50 and 1/100. Three parallel runs were performed for each condition. Additional of 0.1 M $AgNO_3$ of exchange was conducted at 80 ^{o}C for S/L=1/100, 10 min., 30 min. and 1hr. 1M $AgNO_3$ of exchange was conducted at 80 ^{o}C for S/L=1/100, 10 min and 30 min.

Co^{2+} & Cu^{2+} exchange; NaCLI was put in 0.01 M $Co(NO_3)_2 \cdot 6H_2O$ or $Cu(NO_3)_2 \cdot 5/2H_2O$ solution placed in a specially made Teflon-lined polyamide vessels. The exchange was conducted at 80 ^{o}C for 30 min and 1hr. Solid/Solution ratios were chosen as; 1/20, 1/50 and 1/100. It has been determined from first evaluated ICP-AES results of Ag^{+} exchange that temperature did not have significant influence on exchange

degree therefore the exchanges at 40 °C and 60 °C were eliminated. Three parallel runs were performed for each condition. Additional of 0.1 M $Co(NO_3)_2 \cdot 6H_2O$ of exchange was conducted at 80 °C for S/L=1/100, 10 min., 30 min. and 1hr. 1M $Co(NO_3)_2 \cdot 6H_2O$ of exchange was conducted at 80 °C for S/L=1/100, 10 min and 30 min.

5.3. Characterization of Metal Exchanged Minerals and Antibacterial Test

The Na- CLI and Ag^+, Co^{2+} and Cu^{2+} exchanged forms of the mineral were characterized by the techniques namely TGA, DTA, DSC, FTIR, XRD, Volumetric N_2 adsorption, ICP-AES and SEM.

Antibacterial activity of the exchanged clinoptilolite rich minerals against *E. coli* was determined by the disk diffusion (Kirby–Bauer) method. First, agar – broth for the growth media was prepared by mixing 1 liters of deionized water with 20 g of agar and 21 g of broth. Prepared solution was put into 121 °C autoclave for 15 minutes. Equal amounts of sterilized solution were poured into Petri dishes and they were left for drying and solidification of the growth media. Then, *E.coli* bacteria taken from the stock was taken on the Petri dishes by the help of a needle holder. Bacterial cultures grown on Mueller–Hinton agar medium were incubated at 37 °C for 24 hrs. One of the colonies was dissolved in 4 ml of distilled water; and its turbidity was adjusted to McFarland no. 0.5 for the preparation of bacterial suspension. After placing a sterile cotton swab in the bacterial suspension, the swab was streaked in at least two directions over the surface of the Mueller–Hinton agar to obtain uniform growth. (Ag^+, Co^{2+} and Cu^{2+}) exchanged minerals, ≈ 0.15g, in the form of pellets with 8 mm in diameter were placed into the Petri dishes. They were incubated at 37 °C for one day and finally, the width of inhibition zone of each sample in the plates was measured after 24hours.

CHAPTER 6

RESULTS AND DISCUSSION

6.1. Characterization of Zeolitic Tuff

The X-Ray diffraction pattern and SEM micrograph of the zeolitic tuff namely CLI are presented in Figures 6.1 and 6.2, respectively.

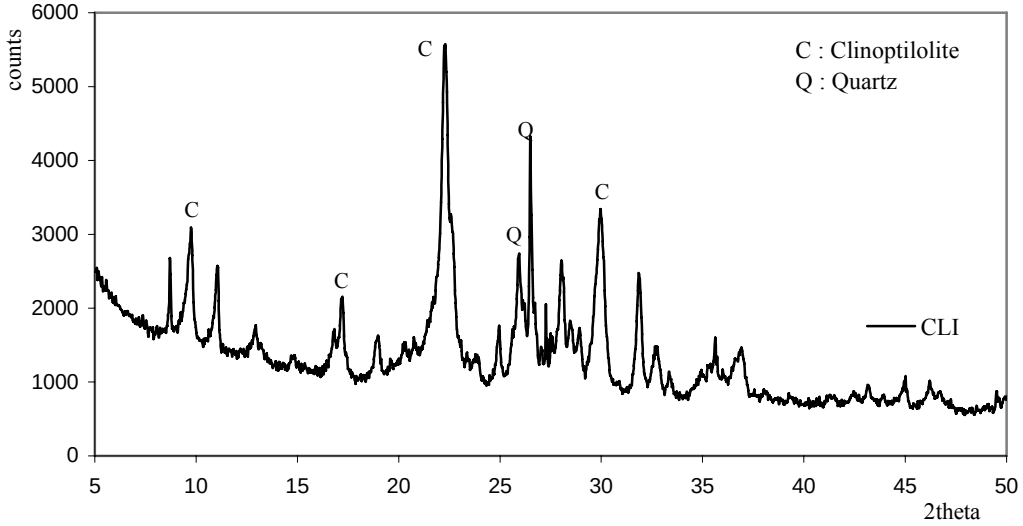

Figure 6.1. X-Ray diffraction pattern of CLI.

The X-Ray peaks of CLI were examined by software in X-Ray diffractometer called SMSP. The main peaks matched with the clinoptilolite (monoclinic; a=17.66 b=17.91 c=7.41 β= 116.40) and heulandite (monoclinic; a=17.69 Å b=17.92 Å c=7.42 Å β= 116.47^{o}) mineral characteristic peaks found in the SMSP library belonging to JSPDS card 83-1261 and JSPDS card 80-0465, respectively. CLI was identified as clinoptilolite rich mineral with 50 %-60 % purity having quartz (JSPDS card 83-0539 & 78-1252) as a main impurity.

Scanning electron micrograph of CLI is given in Figure 6.2 that shows typical hexagonal plate like clinoptilolite crystals.

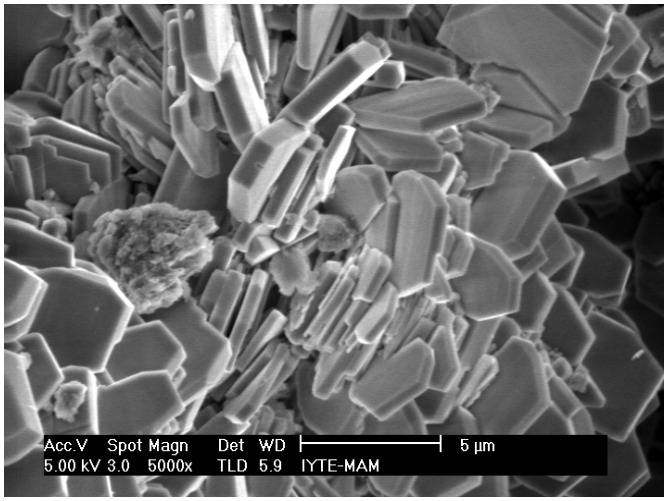

Figure 6.2. SEM micrograph of CLI.

Chemical compositions of major and trace elements of CLI are given in Table 6.1a and 6.1b, respectively.

Table 6.1. Chemical Composition of CLI.

a) Major Elements in Oxide Forms

OXIDES	**CLI** w/w %
SiO_2	69.89
Al_2O_3	11.21
Fe_2O_3	1.15
K_2O	5.48
CaO	1.89
Na_2O	1.56
MgO	0.22
CEC(meq/g) $\Sigma(Ca^{2+}+Na^{+}+K^{+}+Mg^{2+})$	**2.45**

b) Trace Elements

ELEMENTS	**CLI-ppb**
Ag	<30
Ba	154
Cd	<10
Co	<30
Cr	<10
Cu	150
Zn	60.12
Ni	<5
Pb	48.72

CLI is defined as K-rich mineral due to its highest K^+ content. Trace elements within the mineral were found at ppb levels in which Ba^{2+} has the highest amount as

indicated in Table 6.1.b., hence their effect on metal ion exchange processes is considered to be negligible. Therefore, in this study the change in the chemical composition of major elements during ion exchange has been considered.

The structural information of CLI was also determined by the FTIR technique and its spectrum is given in Figure 6.3.

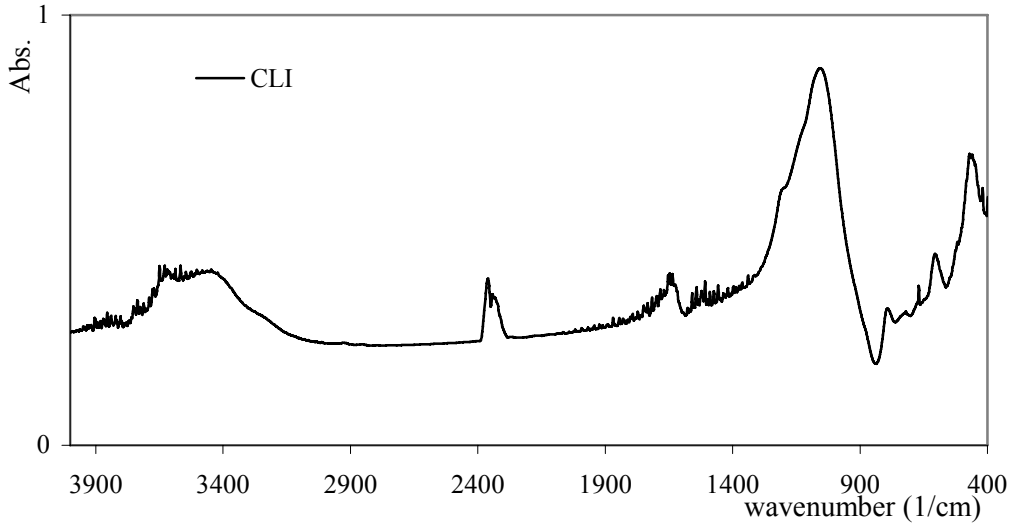

Figure 6.3. FTIR spectrum of CLI.

The characteristic bands of clinoptilolite were at 1060 cm^{-1}, 790 cm^{-1} and 609 cm^{-1} due to asymmetry stretch O-Si(Al)-O, symmetry stretch and Si(Al)-O double ring, respectively (Breck, 1974). Peaks related with isolated OH stretching at 3700 cm^{-1}, H-bonded O–H stretching at 3400 cm^{-1} and H_2O bending at 1620 cm^{-1} were detected on FTIR spectrum of CLI, as well.

Table 6.2 and Figure 6.4 summarize the thermal and adsorption related properties of CLI.

Table 6.2. Properties of CLI.

Water Content –TGA	12.50 %	
Dehydration behaviour –DTA	Endotherm at 53.73 ^oC	Exotherm starts ~ 800 ^oC
Surface Area (N_2 Adsorption)	BET Model (m^2/g)	Langmuir Model (m^2/g)
	45.8	65.4

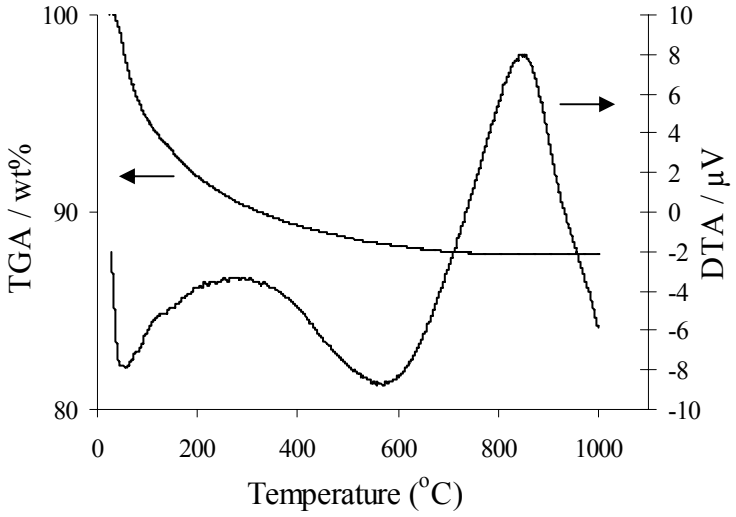

Figure 6.4. TGA and DTA curves of CLI.

CLI was thermally stable up to 800 °C, and further increase in temperature causes structural changes due to conversion of its structure to another crystal or amorphous phase. The N_2 volume adsorbed at highest P/P_o for NaCLI is found as 42.1 cm^3/gr STP. Surface areas were found as 45.8 m^2/gr and 65.4 m^2/gr from BET and Langmuir models, respectively.

6.2. Ag^+, Co^{2+} and Cu^{2+} Exchange on NaCLI

Since Na^+ is the most weakly bound ion in clinoptilolite and it is easily exchanged with cations within the solution, Na-forms are preferred as a starting material for the ion exchange processes using zeolitic minerals. Therefore, before ion exchange experiments CLI was converted into Na-form (near homoionic) by treating the mineral with 1N NaCl at 80 °C for 10 days. Chemical compositions of NaCLI in the form of w/w% are tabulated in Table 6.3. Na^+ amount in NaCLI was increased almost four times after the treatment.

Table 6.3. Chemical Composition of NaCLI.

oxides	**NaCLI** w/w %
SiO_2	69.14
Al_2O_3	11.54
Fe_2O_3	1.16
K_2O	3.92
CaO	0.88
Na_2O	5.61
MgO	0.18
Si/Al	***5.60***
CEC(meq/g) $\sum(Ca^{2+}+Na^{+}+K^{+}+Mg^{2+})$	***2.45***

The exchange degree of Ag^{+}, Co^{2+} and Cu^{2+} on NaCLI for different S/L ratio, time and temperature was determined in waterbath and with the microwave irradiation. Since the solid phase and liquid phase analysis is very important for defining the mechanism which describes the solid-solution interaction, both phases were analyzed for all set of exchange. The chemical compositions of solid phase raw data for all ion exchange processes were given from the average of three runs within 0.05 confidence interval.

For the utilized conditions, w/w% of 0.01 M Ag (NO_3) exchanged NaCLI in waterbath and with microwave irradiation is tabulated in Table 6.4 and Table 6.5, respectively which are being representative to whole Ag^{+} exchange on NaCLI.

Table 6.4. Average chemical composition against time in solid phase (w/w %) (0.01M $AgNO_3$, 80 ^oC, waterbath).

		S/L=1/20		S/L=1/50		S/L=1/100	
	NaCLI	**1 hour**	**24 hours**	**1 hour**	**24 hours**	**1 hour**	**24 hours**
Al_2O_3	11.54	11.89	11.34	11.76	10.91	11.11	10.74
SiO_2	69.14	64.92	66.24	66.25	65.45	63.90	65.04
CaO	0.87	0.50	0.39	0.55	0.34	0.50	0.33
Fe_2O_3	1.16	1.59	1.18	1.40	1.26	1.70	1.18
K_2O	3.92	3.09	4.59	2.73	4.02	2.95	3.91
MgO	0.18	0.22	0.17	0.14	0.17	0.16	0.15
Na_2O	5.60	5.11	4.68	2.92	2.25	3.15	2.39
Ag_2O	0.001	1.54	2.16	5.17	4.35	7.90	7.41

Table 6.5. Average chemical composition against time in solid phase (w/w %) (0.01M $AgNO_3$, 80 ^oC, microwave irradiation).

		S/L=1/20		S/L=1/50		S/L=1/100	
	NaCLI	**30 min**	**1 hour**	**30 min**	**1 hour**	**30 min**	**1 hour**
Al_2O_3	11.543	12.08	11.42	11.02	11.53	11.43	11.26
SiO_2	69.143	67.77	66.71	66.02	66.05	65.60	66.71
CaO	0.877	0.46	0.59	0.48	0.48	0.54	0.59
Fe_2O_3	1.162	1.40	1.40	1.45	1.45	1.66	1.61
K_2O	3.921	3.37	3.22	3.58	3.58	2.97	2.96
MgO	0.186	0.18	0.18	0.18	0.18	0.18	0.16
Na_2O	5.606	4.37	4.20	3.90	3.90	3.16	3.47
AgO	0.001	1.58	1.78	5.21	5.23	6.55	7.90

As indicated in Table 6.4 and Table 6.5, after the exchange with Ag^+ no considerable changes were observed for the major cations within the mineral except Ca^{2+} and Na^+. The higher exchange level of these cations could be explained by their structural location in the mineral. In the clinoptilolite structure Na^+-Ca^{2+}, K^+-Ba^{2+} and Mg^{2+} are located in channel A at site Ml-M2, in channel C at site M3 and in channel A

at site M4, respectively. The strong bonding of K^+ may affect its exchange capability since six framework oxygen atoms and three water molecules coordinate K^+ at site M3. The higher exchange level of Na^+ compared to other cations is not only due to its structural location but also due to its weak bound strength in clinoptilolite.

The hydrated ionic radii of the cations affect their degree of exchange. The hydrated radii of the cations with nearly the same size of the channel dimensions results in difficulty of exchange. The ease of Na^+ exchange with Ag^+ is due to its lower hydrated radii compared to other cations. Mg^{2+} and Fe^{3+} having high hydrated radii cannot move easily out of the channels (Dyer and White, 1999) therefore their exchange with Ag^+ is low. As well as the hydrated radii, heats of hydration of the exchangeable cations have also effect on the exchange process. Monovalent cations bond to their waters of hydration with much less energy than do divalent cations. Cation exchange in zeolites actually occurs in association with water molecules and in the presence of more water molecules, bonding is tighter to the smaller highly charged cation. Therefore the lack of exchange noted for Mg^{2+} comes from the inability of the charge on the clinoptilolite framework to remove the waters of hydration from the Mg^{2+} ions. The chemical compositions of solid phase raw data for all sets of Ag^+ exchange NaCLI were plotted from the average of three runs within 0.05 confidence interval and are given in Appendix A between Figure A.1 and Figure A.12.

Any adsorbent was positively charged at the pH lower than pH_{pzc} and negatively charged at pH higher than pH_{pzc} therefore adjusting the solution pH is important. Zeta potential measurement for the NaCLI system is given in Figure 6.5 in order to determine the pH_{pzc}[1] for this specific mineral.

[1] pH_{pzc} : pH for which the charge of particles is zero.

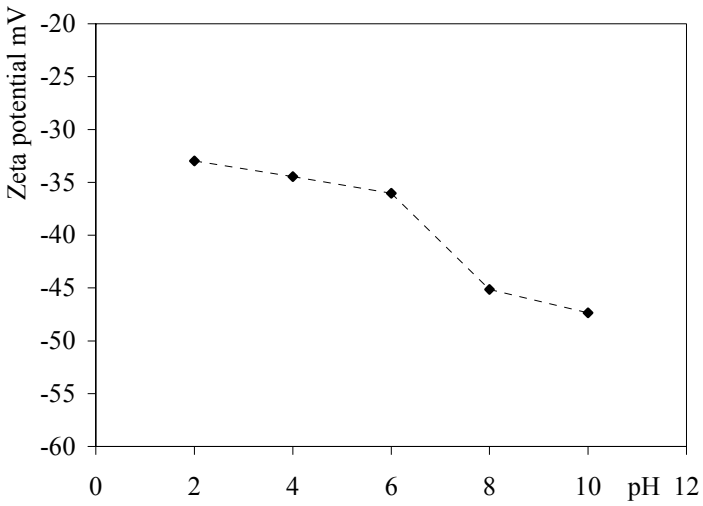

Figure 6.5. The relation between zeta potential and pH (ultra pure water –NaCLI system).

The pH is an important parameter for preferential sorption of cations or anions. As it was discussed in theoretical part, in addition to ion exchange and adsorption surface precipitation may also occur in zeolite-solution system. The pH control of zeolite-solution system is important in order to prevent significant precipitation during ion exchange. Additionally, depending on the solution pH, Si and Al from the framework possibly move toward solution phase which is called as dissolution (Doula and Ioannou, 2003). Therefore in the first place, the change in pH with time and liquid phase chemical compositions for ultrapure water–NaCLI system was determined. The presence of surface imperfections and mineralogical heterogeneity (soluble impurity) promote the solubility of the amorphous aluminosilicate surface layers besides detachment of framework ions. The data obtained may also help to distinguish the mechanism of zeolite-solution interaction. The pH versus time graphs and liquid phase chemical compositions for ultrapure water-NaCLI system at 80 ^{o}C are given in Figure 6.6 and Table 6.6, respectively.

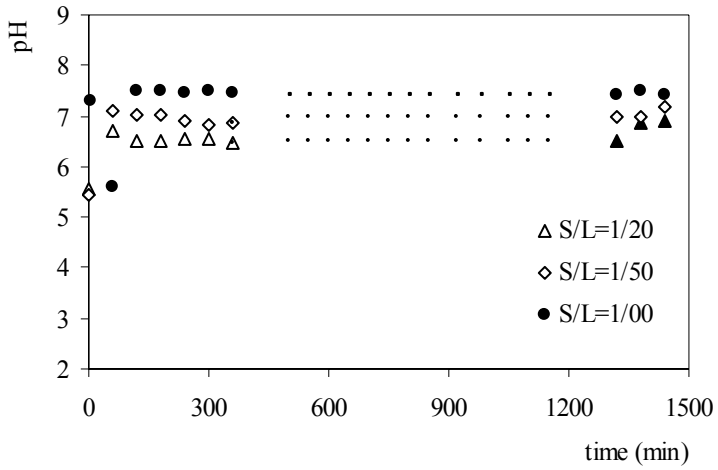

Figure 6.6. pH versus time (ultrapure water–NaCLI , 80 ^{o}C, waterbath).

Table 6.6. Solution phase chemical compositions (ultrapure water–NaCLI, 80 ^{o}C, waterbath).

Elements	S/L=1/20	S/L=1/50	S/L=1/100
	(mg cation/gr zeolite)		
Al	0.06	0.06	0.15
Si	0.80	1.69	2.47
Ca	0.00	0.01	0.04
Fe	0.04	0.06	0.04
K	0.06	0.10	0.00
Mg	0.00	0.00	0.21
Na	1.75	3.78	1.93
Ag	0.00	0.01	0.04

As indicated from data, cations exist in trace amounts while some do not even exist in the solutions which might be the soluble impurities within the mineral rather than strongly bound framework cations. Therefore, detection of exchangeable cations in trace amounts together with slight pH change of the solution is the indication of limited dissolution of the framework cations. The pH versus time graphs for ultrapure water-NaCLI system at 60 ^{o}C is given in Appendix D.

The change in pH for Ag $(NO)_3$-NaCLI system can be explained by different events. For example, if H^+ in the solution exchanges with exchangeable cations on

outer/inner surface of clinoptilolite or H^+ in surface hydroxyl groups of Si-OH and Al-OH behaves as an exchangeable cation, solution pH increases. Contrarily, due to the formation of metal-hydroxyl complexes pH of the solution decreases. Thus pH change with time for Ag^+ exchange on NaCLI at 60 ^oC and 80 ^oC was monitored. pH versus time for 0.01 M $Ag(NO)_3$ – NaCLI system at 80 ^oC is given in Figure 6.7.

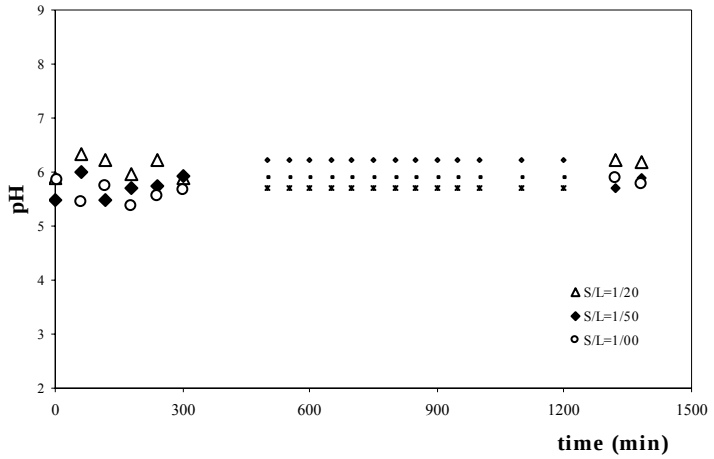

Figure 6.7. pH versus time (Ag^+ -NaCLI ,80 ^oC , waterbath).

Slight changes of pH were detected throughout the exchange process for all the S/L ratios. Similar to the ultrapure water-NaCLI system, the exchangeable cations exist in trace amounts while some even do not exist in the solution phase for $Ag(NO)_3$-NaCLI exchange. The total amount of H^+ ion change is much lower than those for exchangeable cation (Appendix B) which is the indication of limited dissolution of the framework cations and protonation of surface hydroxyl groups by H^+. The pH versus time for 0.01 M $Ag(NO)_3$ – NaCLI system at 60 ^oC is given in Appendix D.

Either the liquid cases or the solid cases were examined and reported widely in literature. However, chemical compositions of the cations in both phases have great importance in describing the mechanisms for metal solution-clinoptilolite interaction. The solid and liquid phase compositions of 0.01 M Ag $(NO)_3$ exchanged NaCLI for S/L=1/20 for 1hr in waterbath and for S/L=1/100 for 30 min in microwave are given in Table 6.7 and Table 6.8.

Table 6.7. Solid and liquid phase compositions (0.01 M $Ag(NO)_3$, 80 ^oC, S/L=1/100, 1hr, waterbath.)

	SOLID (meq/gr zeolite)		LIQUID (meq/gr zeolite)	
Elements	Initial	Final	Initial	Final
Ca	0.31	0.15	0	0.003
Fe	0.44	0.72	0	0.003
K	0.83	0.70	0	0.008
Mg	0.09	0.10	0	0.000
Na	1.81	0.96	0	0.365
Ag	0.00	0.68	1.000	0.124
(meq/gr zeolite)	$\sum(Ca^{2+}+Na^{+}+K^{+}+Mg^{2+})$		Ag^{+}	
	1.15		*0.88*	

Table 6.8. Solid and liquid phase compositions (0.01 M $Ag(NO)_3$, 80 ^oC, S/L=1/100, 1hr, microwave irradiation).

	SOLID (meq/gr zeolite)		LIQUID (meq/gr zeolite)	
Elements	Initial	Final	Initial	Final
Ca	0.31	0.21	0	0.02
Fe	0.44	0.60	0	0.00
K	0.83	0.63	0	0.01
Mg	0.09	0.08	0	0.00
Na	1.81	1.12	0	0.71
Ag	0.00	0.68	0.500	0.38
(meq/gr zeolite)	$\sum(Ca^{2+}+Na^{+}+K^{+}+Mg^{2+})$		Ag^{+}	
	1.01		*0.62*	

There is a non-stoichiometry between the amount of Ag^{+} uptake and total amount of exchangeable cations release as indicated in Table 6.7 and 6.8 for waterbath and microwave irradiated exchanges, respectively. Total amount of exchangeable cations [$\sum(Ca^{2+}+Na^{+}+K^{+}+Mg^{2+})$] release is higher than metal uptake for both exchanges. This may be due to the lack of the detection of change in the amounts of exchangeable cations in liquid phase where metal cation hydrolysis reaction might have occurred (inner-sphere complex formation). The exchangeable cations hydrolyzed with -OH

groups in the solution and form metal-hyroxyl complexes which are not detected by ICP-AES however due to the slight increase in solution pH (5.46-5.76) negligible formation of metal hydroxyl species was expected.

Theoretical exchange capacity (TEC) of NaCLI was calculated as 2.75 meq/gr zeolite as given in Table 6.2. For the utilized conditions, experimental exchange capacities (CEC) of Ag^+ exchanged NaCLI in waterbath and microwave were found 1.01 meq/gr zeolite and 1.15 meq/gr zeolite as given in Table 6.7 and Table 6.8, respectively. The lower experimental CEC of the Ag^+ exchanged NaCLI might be due to pretreatment of mineral which resulted with formation of incomplete homoionic form. Besides, some cations cannot be easily removed from the NaCLI structure due to their low mobility and strong bonding forces within the mineral. Additionally, impurities such as feldspar, quartz and salts within the structure do not allow the mineral exchange to a degree level of TEC.

The chemical compositions of liquid phase raw data for all other sets of Ag^+ exchanged NaCLI were plotted from the average of three runs within 0.05 confidence interval and are given in Appendix B between Figure B.1 and Figure B.12. The liquid phase and solid phase compositions of Ag^+ exchanged NaCLI for all other sets are given in Appendix C between Table C1 and C57.

The effect of S/L ratio and time on the exchange degree of Ag^+ for the 0.01 M Ag $(NO)_3$ exchanged NaCLI at 80 ^oC in waterbath and with microwave irradiation in Figure 6.8 and Figure 6.9, respectively.

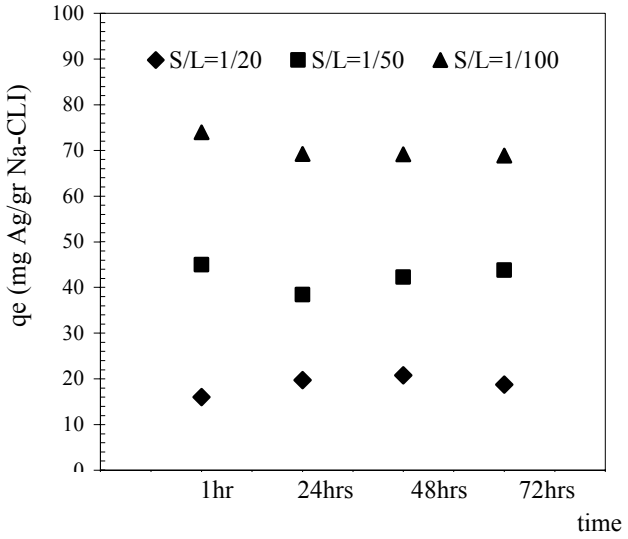

Figure 6.8. Effect of S/L ratio and time on Ag^{+} exchange (NaCLI, 80 ^{o}C, waterbath).

As concluded from Figure 6.8, amount of Ag^{+} exchanged on NaCLI increased with decreasing S/L ratio. As the S/L ratio decreased from 1/20 to 1/100, Ag^{+} amount increased five percent by weight. However, Ag^{+} amount within the mineral did not change with time therefore it is not necessary to continue the exchange after 1 hr.

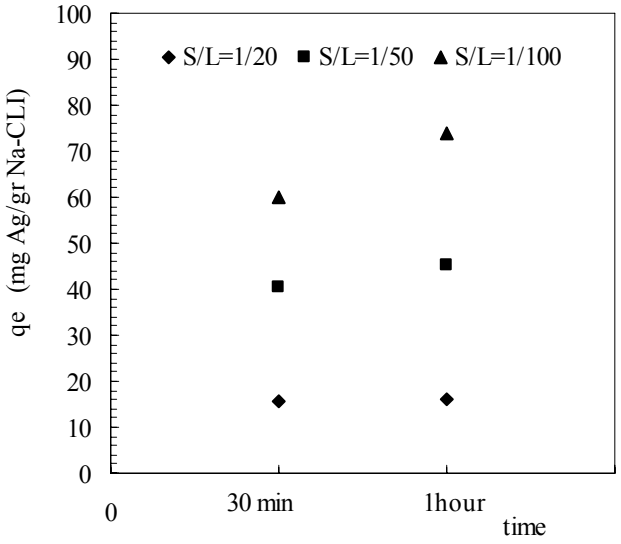

Figure 6.9. Effect of S/L ratio and time on Ag^{+} exchange (80 ^{o}C, microwave irradiation).

The amount of 0.01 M Ag $(NO)_3$ exchanged against S/L ratio and time in waterbath at 40 ^oC and 60 ^oC were given in Appendix D.

For microwave irradiated exchange, the Ag^+ amount exchanged on NaCLI also increased with decreasing S/L ratio as indicated from Figure 6.9. As the time of treatment increased, the Ag^+ amount did not increased as expected even slight decrease was observed for the run in which S/L ratio equals to 1/100. This might be due to the reason that during the total exchange period no continuous microwave energy was applied. Because in principal, as long as the system reaches to the set point temperature it stops the microwave energy and starts immediately after if a decrease in temperature occurs. Thus, due to the working principle of microwave system (EDMS) there is no continuous microwave supply through the total time of exchange. Total irradiation time for 10 min, 30 min and 1 hr of microwave processing was clocked and detected as 6 min, 18 min and 42 min, respectively. Therefore, total microwave irradiation time used is not equal to the total exchange time. Additionally, as mentioned in Chapter 5, microwave power was adjusted to appropriate watts depending on the number of the vessels used for the run in progress. For example, if 1 to 4 vessels used microwave power is adjusted to 300watts or for 4 to 8 vessel it is adjusted to 600watts and for maximum capacity of 8 to 12 vessels microwave power was adjusted to 1200 watts. However, while ramping and keeping the temperature at "set value" the used microwave power changes with time. For example, for ion exchange in progress with 5 vessels at 80 ^oC, microwave oven uses 70% of 600 watts initially with the preceding time it uses 20% of 600 watts. Besides the non-continuous microwave power used for any exchange process, microwave power was not used with 100% continuous power efficiency. Therefore, the exchange degree for Ag^+ did not increase for microwave irradiated exchange compared to waterbath exchange as expected. For the microwave irradiated exchanges at 40 ^oC and 60 ^oC were given in Appendix D.

The effect of temperature at constant S/L ratio and time was investigated for 0.01 M Ag $(NO)_3$ exchanged NaCLI in waterbath and with microwave irradiation. The effect of increase in temperature for waterbath (24hrs) and microwave (1hr) treatments with different S/L ratios is given in Figure 6.10 and Figure 6.11, respectively.

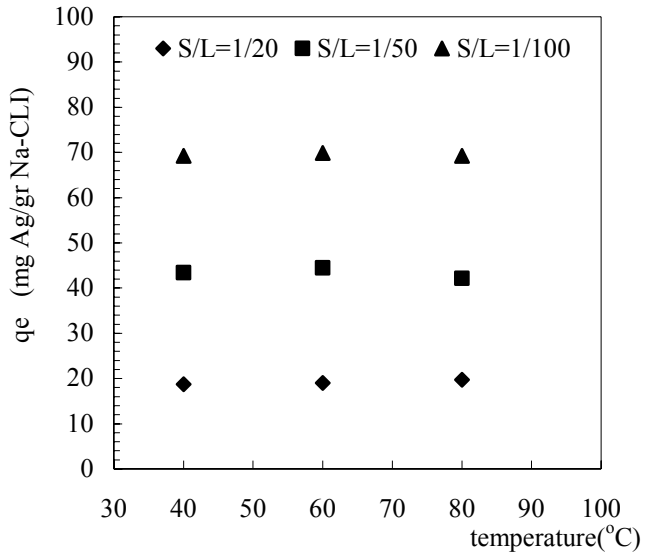

Figure 6.10. Effect of S/L ratio temperature on Ag^+ exchange (waterbath).

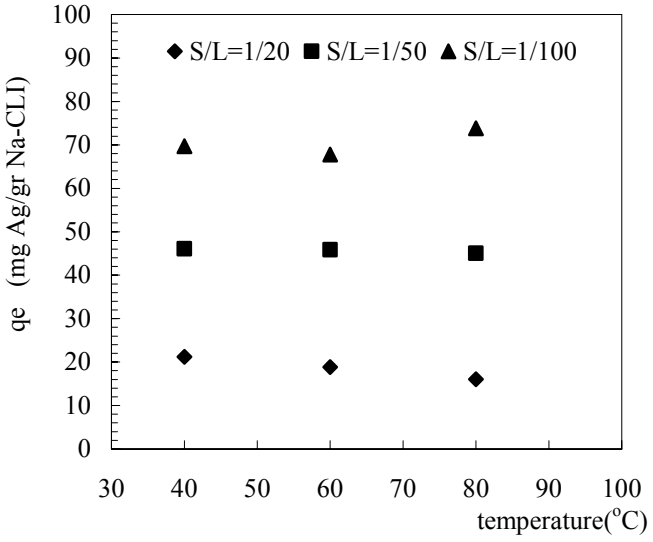

Figure 6.11. Effect of S/L ratio temperature on Ag^+ exchange (microwave irradiation).

As the temperature increased from 40 °C to 80 °C, the Ag^+ amount in the NaCLI increased slightly for every S/L both in waterbath and with microwave irradiation. Besides, Ag^+ amount increased more significantly with decreasing S/L ratio at constant temperature. Therefore S/L ratio has higher effect on the exchange degree while temperature has less prominent effect.

In the same manner, the exchange degree of Co^{2+} in waterbath and with microwave irradiation for different S/L ratio, time and temperature was investigated. The chemical compositions (w/w %) of 0.01M $Co(NO3)_2.6H_2O$ exchanged NaCLI for the utilized conditions in waterbath and with microwave irradiation are tabulated in Table 6.9 and Table 6.10, respectively which are representing whole Co^{2+} exchange on NaCLI in waterbath and with microwave irradiation.

Table 6.9. Average chemical composition against time in solid phase (w/w %). (0.01M $Co(NO_3)_2.6H_2O$, NaCLI 80 ^oC,waterbath).

		S/L=1/20		**S/L=1/50**		**S/L=1/100**	
	NaCLI	**1hour**	**24 hours**	**1hour**	**24 hours**	**1hour**	**24 hours**
Al_2O_3	11.54	11.90	11.01	11.79	11.72	12.07	11.41
SiO_2	69.14	67.15	63.66	68.72	65.29	69.78	65.82
CaO	0.87	0.36	0.35	0.53	0.39	0.38	0.40
Fe_2O_3	1.16	1.28	1.46	1.32	1.43	1.36	1.45
K_2O	3.92	3.22	2.85	3.03	2.91	3.12	2.95
MgO	0.18	0.15	0.17	0.15	0.18	0.15	0.18
Na_2O	5.60	3.92	3.57	2.84	2.61	2.27	2.15
CoO	0.001	1.34	1.31	2.72	2.62	3.24	3.15

Table 6.10. Average chemical composition against time in solid phase (w/w %). (0.01M $Co(NO_3)_2.6H_2O$, NaCLI 80 ^oC,microwave irradiation).

		S/L=1/20		S/L=1/50		S/L=1/100	
	NaCLI	**30 min**	**1 hour**	**30 min**	**1 hour**	**30 min**	**1 hour**
Al_2O_3	11.543	10.74	11.84	11.32	11.95	11.55	12.02
SiO_2	69.143	63.35	65.01	63.92	64.45	63.70	64.53
CaO	0.877	0.38	0.36	0.34	0.41	0.41	0.39
Fe_2O_3	1.162	1.34	1.30	1.56	1.62	1.30	1.28
K_2O	3.921	3.37	3.22	3.29	3.13	3.24	3.30
MgO	0.186	0.17	0.17	0.14	0.16	0.15	0.16
Na_2O	5.606	3.46	3.30	2.19	2.61	2.66	2.69
CoO	0.001	1.29	1.34	2.38	2.66	3.27	3.34

The behaviors of major exchangeable cations within the NaCLI during Co^{2+} exchanges in waterbath and with microwave irradiation were very much alike to Ag^+ exchange studies. As indicated in Table 6.9 and Table 6.10, no considerable changes were observed for the major cations except Ca^{2+} and Na^+ due to same reasons discussed for Ag^+ exchange experiments. The chemical compositions of solid phase raw data for all other sets of Co^+ exchanged NaCLI were plotted from the average of three runs within 0.05 confidence interval and are given in Appendix A in Figure A.13 and Figure A.14.

Solid and liquid phase compositions of 0.01M Co $(NO3)_2.6H_2O$ exchanged NaCLI with S/L=1/100 for 1hr in waterbath and with S/L=1/50 for 1hr with microwave irradiation are given and discussed in Table 6.11 and Table 6.12, respectively as being a representative case to whole.

Table 6.11. Solid and liquid phase compositions (0.01 M $Co(NO_3)_2.6H_2O$, 80 ^oC, S/L=1/100, 1hr, waterbath.)

	SOLID (meq/gr zeolite)		LIQUID (meq/gr zeolite)	
Elements	Initial	Final	Initial	Final
Ca	0.09	0.07	0	**0.00**
Fe	0.31	0.26	0	0.00
K	0.36	0.33	0	0.01
Mg	0.04	0.04	0	0.00
Na	0.92	0.37	0	0.31
Co	0.01	0.43	1.000	0.43
(meq/gr zeolite)	$\sum(Ca^{2+}+Na^{+}+K^{+}+Mg^{2+})$		Co^{2+}	
	0.61		*0.57*	

Table 6.12. Solid and liquid phase compositions (0.01 M Co $(NO_3)_2.6H_2O$, 80 ^oC, S/L=1/50, 1hr, microwave irradiation.)

	SOLID (meq/gr zeolite)		LIQUID (meq/gr zeolite)	
Elements	Initial	Final	Initial	Final
Ca	0.09	**0.07**	0	0.00
Fe	0.31	**0.30**	0	0.00
K	0.36	0.33	0	0.01
Mg	0.04	**0.04**	0	0.00
Na	0.92	**0.42**	0	0.26
Co	0.01	**0.36**	0.500	0.09
(meq/gr zeolite)	$\sum(Ca^{2+}+Na^{+}+K^{+}+Mg^{2+})$		Co^{2+}	
	0.55		*0.41*	

As indicated in Table 6.11 and 6.12, total amount of exchangeable cations [$\sum(Ca^{2+}+Na^{+}+K^{+}+Mg^{2+})$] release is a little bit higher than Co^{2+} uptake which may be due to experimental and/or instrumental error since slight change of pH (5.50-5.86) was during the exchange was indicating negligible formation metal-hyroxyl complexes in liquid phase.

The experimental exchange capacity (CEC) for the given Co^{2+} exchanges is approximately 0.65 meq/gr zeolite which lower compared to TEC of NaCLI (2.75 meq/gr zeolite) since all the exchangeable cations in different sites could not be replaced by Co^{2+} ions. Thus, in no case all Na^{+} and other exchangeable ions were replaced by Co^{2+} in all cases and H^{+} competes for the ionic exchange sites of the lattice with Co^{2+}. Besides, cations cannot be easily removed from the NaCLI and impurities such as feldspar, quartz and salts within the structure do not allow the mineral to exchange up to a degree level of TEC. The pretreatment of the mineral might have an effect on CEC, as well.

The chemical compositions of liquid phase raw data for all other sets of Co^{2+} exchange NaCLI were plotted from the average of three runs within 0.05 confidence interval and are given in Appendix B between Figure B.13 and Figure B.14. The liquid phase and solid phase compositions of Co^{2+} exchanged NaCLI for all other sets are given in Appendix C between Table C.58 and C.71.

The effect of S/L ratio and time on the exchange degree is summarized for 0.01M Co $(NO3)_2.6H_2O$ exchanged NaCLI at 80 ^{o}C in waterbath and with microwave irradiaiton in Figure 6.12 and Figure 6.13, respectively.

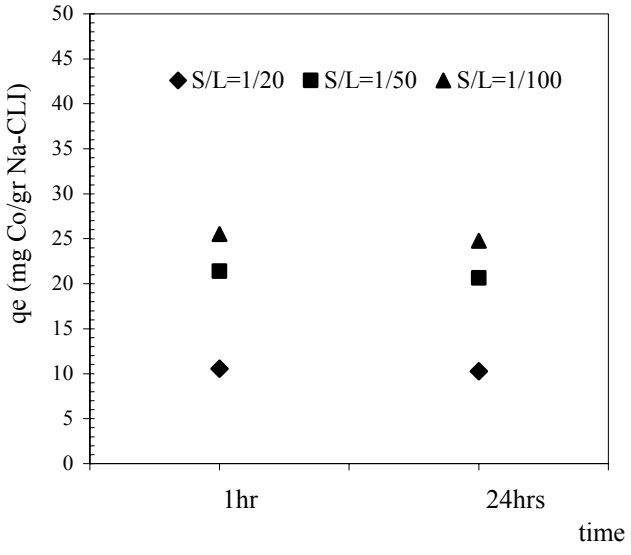

Figure 6.12. Effect of S/L ratio and time on Co^{2+} exchange (80 ^{o}C, waterbath).

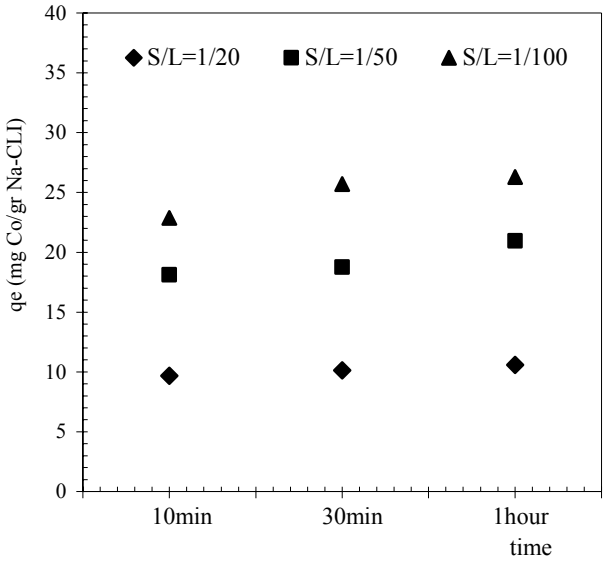

Figure 6.13. Effect of S/L ratio and time on Co^{2+} exchange (80 ^{o}C, microwave irradiation).

As indicated from Figure 6.12, the amount of 0.01M $Co(NO3)_2.6H_2O$ exchanged on NaCLI increased with decreasing S/L ratio in the case of waterbath treatment. As the S/L ratio decreased from 1/20 to 1/100 Co^{2+} amount increased almost three percent by weight but did not change after 1hr. For microwave irradiated exchange shown in Figure 6.13, the Co^{2+} amount exchange on NaCLI also increased with decreasing S/L. As the time of treatment increased, Co^{2+} amount did not increase due to same reasons discussed for Ag^{+} exchange case.

The exchange degree of Cu^{2+} in waterbath and with microwave irradiation for different S/L ratio, time and temperature was investigated in terms of major exchangeable cation compositions. Representing the whole, the chemical compositions (w/w %) of 0.01M $Cu(NO_3)_25/2H_2O$ exchanged NaCLI for the utilized conditions in waterbath and with microwave irradiation are tabulated in Table 6.13 and Table 6.14, respectively.

Table 6.13. Average chemical composition against time in solid phase (w/w %). (0.01M Cu $(NO_3)_2 5/2H_2O$, NaCLI 80 ^oC,waterbath).

		S/L=1/20		S/L=1/50		S/L=1/100	
	NaCLI	**1hour**	**24 hours**	**1hour**	**24 hours**	**1hour**	**24 hours**
Al_2O_3	11.54	11.51	11.62	11.43	11.46	11.90	11.62
SiO_2	69.14	66.35	65.34	66.67	64.42	67.67	64.95
CaO	0.87	0.26	0.39	0.44	0.30	0.41	0.26
Fe_2O_3	1.16	1.53	1.42	1.47	1.36	1.34	1.39
K_2O	3.92	2.98	3.03	3.11	2.94	3.45	2.89
MgO	0.18	0.13	0.17	0.14	0.18	0.14	0.18
Na_2O	5.60	4.07	3.74	2.90	2.46	1.89	1.65
CuO	0.001	1.51	1.59	3.00	3.16	3.93	3.98

Table 6.14. Average chemical composition against time in solid phase (w/w %). (0.01M Cu $(NO_3)_2 5/2H_2O$, NaCLI 80 ^oC,microwave irradiation).

		S/L=1/20		S/L=1/50		S/L=1/100	
	NaCLI	**30 min**	**1 hour**	**30 min**	**1 hour**	**30 min**	**1 hour**
Al_2O_3	11.543	11.60	11.49	11.51	11.31	11.49	11.56
SiO_2	69.143	64.08	63.19	63.56	63.14	63.65	64.23
CaO	0.877	0.53	0.39	0.47	0.44	0.38	0.39
Fe_2O_3	1.162	1.84	1.36	1.64	1.80	2.04	1.48
K_2O	3.921	3.27	3.65	3.28	3.23	3.24	3.13
MgO	0.186	0.17	0.16	0.17	0.16	0.16	0.16
Na_2O	5.606	4.70	4.23	3.07	2.91	2.12	1.99
CuO	0.001	1.52	2.16	3.02	3.07	3.77	4.31

As indicated in Table 6.13 and Table 6.14, the behaviors of major exchangeable cations within NaCLI for Cu^{2+} exchange were very much alike to Ag^{+} and Co^{2+} exchange. Considerable changes were observed for the major cations, Ca^{2+} and Na^{+}, for Cu^{2+} exchange on NaCLI. The chemical compositions of solid phase raw data for all

other sets of Cu^{+} exchange NaCLI were plotted from the average of three runs within 0.05 confidence interval and are given in Appendix A in Figure A.15 and Figure A.16.

Solid and liquid phase compositions of 0.01M $Cu(NO_3)_25/2H_2O$ exchanged NaCLI with S/L=1/50 for 1hr in waterbath and with S/L=1/100 for 30 min with microwave irradiation are given and discussed in Table 6.15 and Table 6.16.

Table 6.15. Solid and liquid phase compositions (0.01 M $Cu(NO_3)_25/2H_2O$, 80 ^{o}C, S/L=1/50, 1hr, waterbath.)

	SOLID (meq/gr zeolite)		LIQUID (meq/gr zeolite)	
Elements	Initial	Final	Initial	Final
Ca	0.09	0.08	0	**0.003**
Fe	0.31	0.28	0	0.000
K	0.36	0.33	0	0.006
Mg	0.04	0.03	0	0.001
Na	0.92	0.47	0	0.311
Cu	0.01	0.38	0.500	0.103
(meq/gr zeolite)	$\sum(Ca^{2+}+Na^{+}+K^{+}+Mg^{2+})$		Cu^{2+}	
	0.50		*0.40*	

Table 6.16. Solid and liquid phase compositions (0.01 M $Cu(NO_3)_25/2H_2O$, 80 ^{o}C, S/L=1/100, 30 min, microwave irradiation).

	SOLID (meq/gr zeolite)		LIQUID (meq/gr zeolite)	
Elements	Initial	Final	Initial	Final
Ca	0.09	0.07	0	0.00
Fe	0.31	0.38	0	0.00
K	0.36	0.34	0	0.01
Mg	0.04	0.04	0	0.00
Na	0.92	0.34	0	0.36
Cu	0.01	0.47	1.000	0.49
(meq/gr zeolite)	$\sum(Ca^{2+}+Na^{+}+K^{+}+Mg^{2+})$		Cu^{2+}	
	0.62		*0.51*	

Total amount of exchangeable cations [$\sum(Ca^{2+}+Na^{+}+K^{+}+Mg^{2+})$] release is a little higher than Cu^{2+} uptake as indicated in Table 6.15 and 6.16. Alike the Ag^{+} and Co^{2+} exchange cases, the change in the amounts of exchangeable cations in liquid phase is lower compared to solid case might be explained by hydrolysis of the exchangeable cation with -OH groups in the solution and form metal-hydroxyl complexes. However, alike the Ag^{+} and Co^{2+} exchange cases negligible formation of metal hydroxyl species was expected due to slight increase in pH (4.20-4.37) therefore difference may be due to experimental and/or instrumental error.

Theoretical exchange capacity, of NaCLI, 2.45 meq/gr zeolite is again higher than experimental exchange capacity (CEC) which was calculated around 0.60 meq/gr zeolite for the given Cu^{2+} exchange conditions. The lack of the replacement of all exchangeable cations available in different sites by Cu^{2+} results in lower CEC. H^{+} competes for the ionic exchange sites of the lattice with Co^{2+}, as well.

The chemical compositions of liquid phase raw data for all other sets of Cu^{2+} exchange NaCLI were plotted from the average of three runs within 0.05 confidence interval and are given in Appendix B between Figure B.15 and Figure B.16. The liquid solid and liquid phase compositions of Cu $(NO_3)_25/2H_2O$ exchanged NaCLI for all other sets are given in Appendix C between Table C.72 and C.83.

The effect of S/L ratio and time on the exchange degree is summarized for 0.01M $Cu(NO_3)_25/2H_2O$ exchanged NaCLI at 80 ^oC in waterbath and with microwave irradiation in Figure 6.14 and Figure 6.15, respectively.

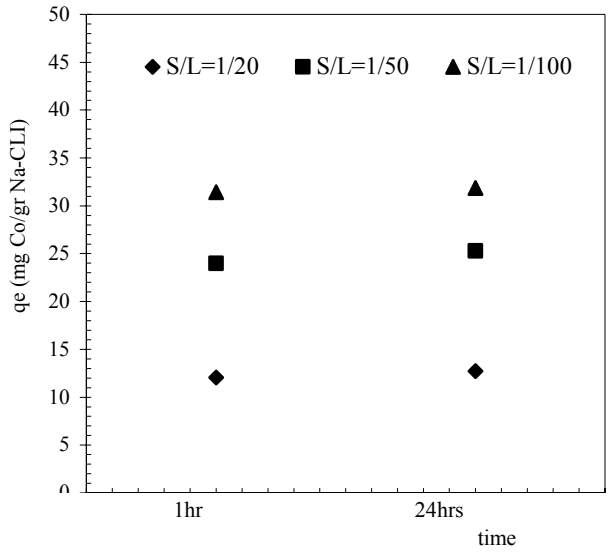

Figure 6.14. Effect of S/L ratio and time on Cu^{2+} exchange (80 ^oC, waterbath).

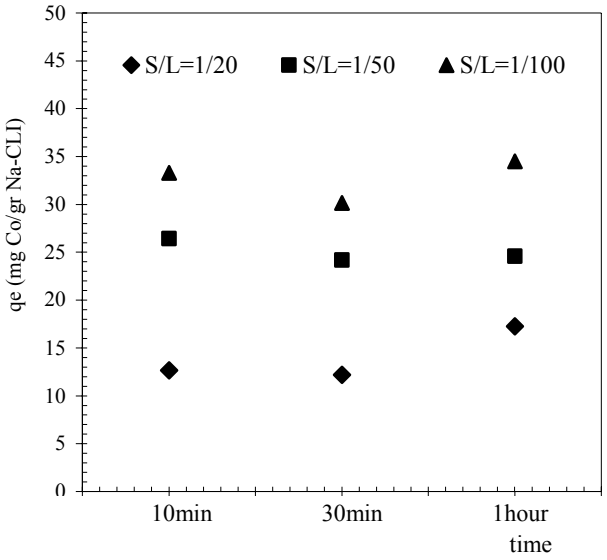

Figure 6.15. Effect of S/L ratio and time on Cu^{2+} exchange (80 ^{o}C, microwave irradiation).

As indicated in Figure 6.14, the amount of Cu^{2+} exchanged on NaCLI increased with decreasing S/L ratio for exchange conducted in waterbath. Microwave irradiated exchange as shown in Figure 6.15, the Cu^{2+} amount exchange on NaCLI also increased with decreasing S/L. As the time of treatment increased the Cu^{2+} amount did not increased alike to Ag^{+} and Co^{2+} exchange cases.

The Ag^{+}, Co^{2+} and Cu^{2+} exchange behaviors were investigated within each other in accordance with the amount in the solid phase. The exchange degree of Ag^{+}, Co^{2+} and Cu^{2+} on NaCLI starting with 0.01M metal ion concentration are given in Figure 6.16 and Figure 6.17 for waterbath and microwave treatments, respectively.

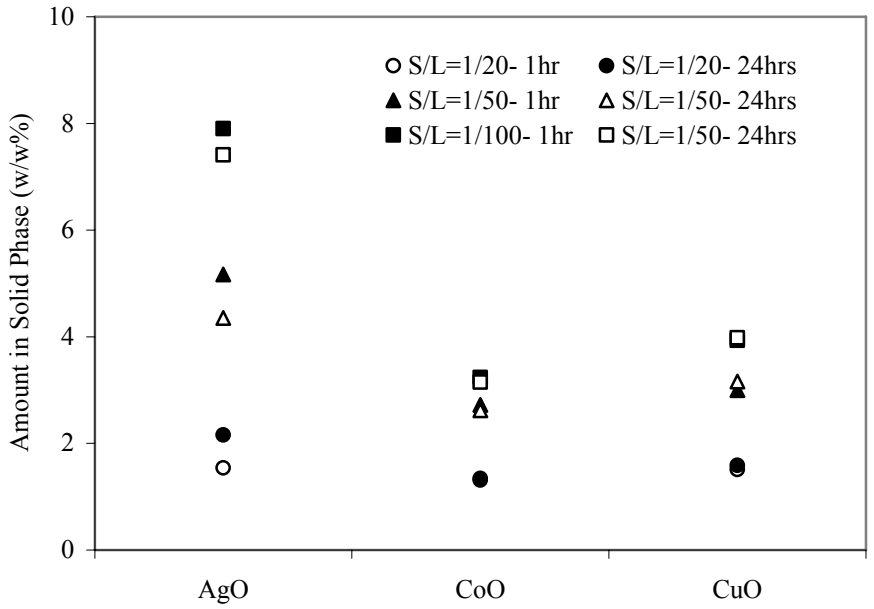

Figure 6.16. Ag^{+}, Co^{2+} and Cu^{2+} on NaCLI (80 ^{o}C, waterbath).

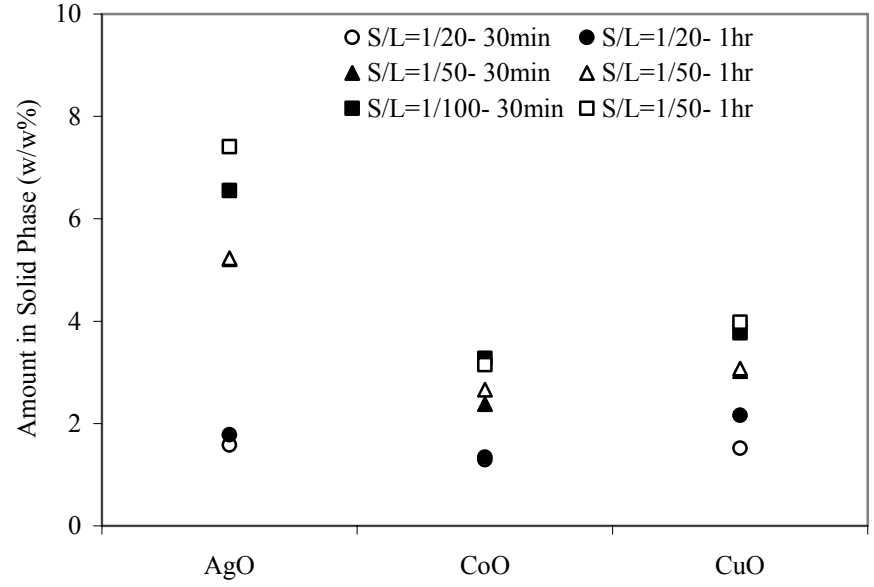

Figure 6.17. Ag^{+}, Co^{2+} and Cu^{2+} on NaCLI (80 ^{o}C, microwave irradiation).

The exchange degree of Ag^{+}, Co^{2+} and Cu^{2+} in waterbath and microwave are compared for 80 ^{o}C for different times and data are represented in Appendix D. Figure 6.18 shows the 0.01M of Ag $(NO)_3$, $Co(NO_3)_26H_2O$ and $Cu(NO_3)_25/2\ H_2O$ exchange for common time of 1hr at 80 ^{o}C for waterbath and microwave treatments.

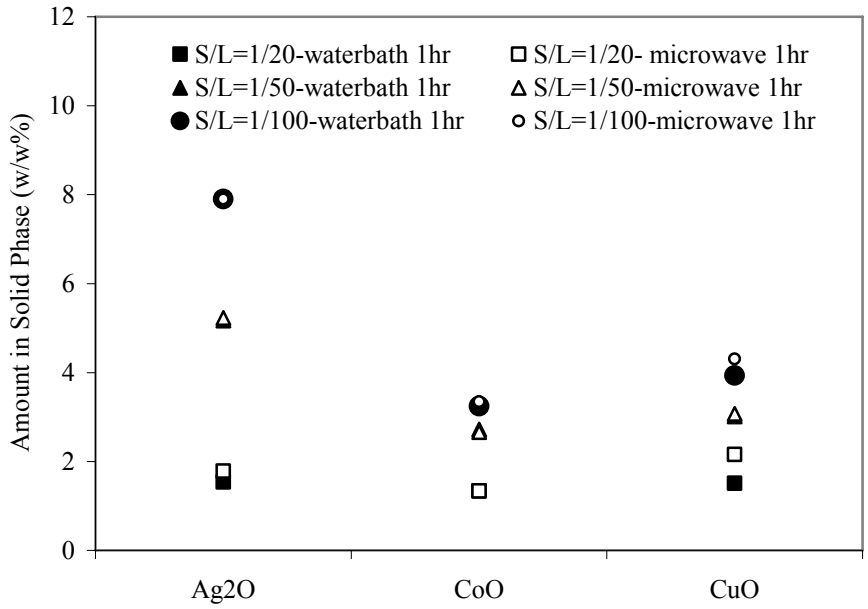

Figure 6.18. Ag^{+}, Co^{2+} and Cu^{2+} exchange on NaCLI at 80 ^{o}C

As indicated between Figure 6.16 and 6.18, the higher rate of Ag^{+} exchange both for the waterbath and microwave treatments as compared to Co^{2+} and Cu^{2+} exchange rates is possibly related to the higher hydrated radii and heats of hydration of Cu^{2+} and Co^{2+} compared to Ag^{+}.

Finally, ion exchange was predominating mechanism whereas limited inner-sphere complex formation, dissolution and surface precipitation might exist for Ag^{+}, Co^{2+} and Cu^{2+} exchanges on NaCLI. S/L ratio has the highest effect on the exchange degree compared to temperature and time. The microwave has equal and in some cases higher exchange degrees for each cation compared to waterbath. The efficiency of microwave irradiation on the exchange degree of Ag^{+}, Co^{2+} and Cu^{2+} on NaCLI might be due its homoionic form (Na-form). Na^{+} ion is the most weakly bound cation and has larger contribution towards microwave irradiation (Whittington and Milestone, 1992; Akdeniz. and Ülkü, 2007). The depth of penetration and dielectric properties of the metal solution-NaCLI system might have an influence on the exchange degree, as well. The dielectric constant of the NaCLI was determined as 13 however metal solution-NaCLI system probably have different dielectric constants and they needed to be determined for better analyze. Therefore, deeper investigation is needed in that respect.

Microwave interaction with matter is characterized by a penetration depth, DP, which possibly changes the ion exchange degree as discussed in Chapter 4. For this

purpose, the solid and solution amounts were altered for the 30 min microwave treatment at 80 ^{o}C for Ag^{+}, Co^{2+} and Cu^{2+} exchange on NaCLI starting with 0.01M metal solutions. The effect of DP on exchange degree is shown in Figure 6.19.

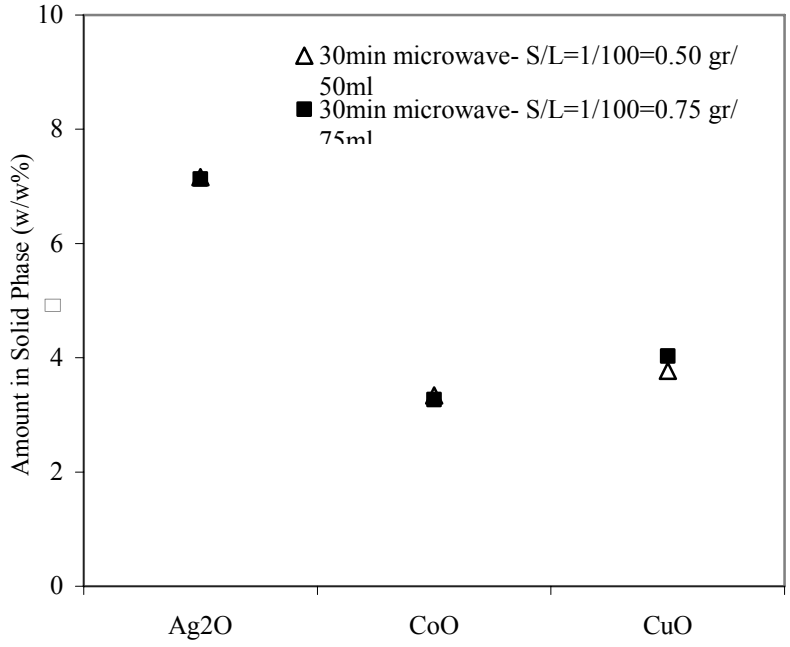

Figure 6.19. Depth of penetration effect on exchange degree.

The difference in the solid content of $AgNO_3$ Co (NO_3) $6H_2O$, Cu (NO_3) $5/2H_2O$ and NaCLI systems run under microwave irradiation did not significantly change the metal amounts sorbed on NaCLI. However, variations of solid and solution amounts thus the dielectric properties of the system should be considered in order to see the effect of DP on exchange degree.

The concentration of the cation solutions might have significant effect on the extent of ion exchange. The higher ion concentrations of solution might lead to a higher degree of ion exchange with time in microwave compared to the commercial waterbath method (Xu et al., 2007). Therefore, ion exchange of Ag^{+}, Co^{2+} and Cu^{2+} exchange on NaCLI with higher concentration of the cation solutions in waterbath and with microwave irradiation were considered. Solid phase chemical compositions conditions (w/w %) of 0.1 M Ag (NO_3), 0.1 M $Co(NO_3)6H_2O$ and 0.1M $Cu(NO_3)5/2H_2O$ exchanged NaCLI in waterbath and microwave are tabulated in Table 6.17 through Table 6.19.

Table 6.17. Average chemical composition against time in solid phase (w/w %) (0.1M $AgNO_3$, 80 ^oC, waterbath and microwave irradiation).

		Waterbath		**microwave**		
	NaCLI	**1 hour**	**24 hours**	**10min**	**30min**	**1hour**
Al_2O_3	11.99	11.02	10.70	10.49	10.77	10.66
SiO_2	72.33	69.88	67.25	68.07	68.44	69.40
CaO	0.29	0.19	0.23	0.29	0.25	0.25
Fe_2O_3	1.39	1.42	1.30	1.62	1.35	1.30
K_2O	2.77	2.12	1.98	1.96	2.08	2.09
MgO	0.18	0.15	0.14	0.15	0.15	0.13
Na_2O	5.17	0.98	0.78	0.89	0.83	0.91
Ag_2O	0.22	14.30	14.38	13.71	13.45	13.41

Table 6.18. Average chemical composition against time in solid phase (w/w %). (0.1M $Co(NO_3)_2.6H_2O$, 80 ^oC, waterbath and microwave irradiation).

		Waterbath		**microwave**		
	NaCLI	**1 hour**	**24 hours**	**10min**	**30min**	**1hour**
Al_2O_3	11.99	11.45	11.69	11.30	11.30	11.38
SiO_2	72.33	71.66	67.71	72.88	73.10	72.98
CaO	0.29	0.24	0.25	0.21	0.22	0.21
Fe_2O_3	1.39	1.22	1.23	1.44	1.44	1.12
K_2O	2.77	2.27	2.37	2.43	2.43	2.35
MgO	0.18	0.16	0.20	0.15	0.14	0.14
Na_2O	5.17	1.80	2.05	1.95	1.87	1.74
CoO	0.22	4.00	4.05	3.33	3.38	3.62

Table 6.19. Average chemical composition against time in solid phase, (w/w %). (0.1M $Cu(NO_3)_2.5/2H_2O$, 80 ^oC, waterbath and microwave irradiation).

		Waterbath		**Microwave**		
	NaCLI	**1 hour**	**24 hours**	**10min**	**30min**	**1hour**
Al_2O_3	11.99	11.42	11.53	11.93	11.84	11.55
SiO_2	72.33	72.16	72.32	73.96	74.15	73.29
CaO	0.29	0.31	0.16	0.33	0.25	0.45
Fe_2O_3	1.39	1.89	1.15	1.99	1.53	2.09
K_2O	2.77	2.24	2.18	2.42	2.46	2.30
MgO	0.18	0.16	0.15	0.16	0.15	0.15
Na_2O	5.17	1.25	1.22	1.16	1.40	1.46
CuO	0.22	4.95	5.12	5.02	4.72	4.84

As indicated in Table 6.17 through Table 6.19, increasing the metal solution concentration to 0.1M did not significantly increase the amount of Ag^+, Co^{2+} and Cu^{2+} adsorbed on NaCLI for microwave irradiated ion exchange compared to ion exchange conducted in commercial waterbath as expected. The chemical compositions of solid phase raw data for other sets of Ag^+, Co^{2+} and Cu^{2+} exchange NaCLI were plotted from the average of three runs within 0.05 confidence interval and are given in Appendix A in Figure A.17 through Figure A.19.

The liquid phase and solid phase compositions of 0.1 M Ag $(NO)_3$, 0.1 M $Co(NO_3)6H_2O$ –NaCLI and exchanged NaCLI for utilized condition in waterbath and microwave are given in Table 6.20 through Table 6.25.

Table 6.20. Solid and liquid phase compositions (0.1 M $Ag(NO)_3$, 80 ^oC, S/L=1/100, 24hrs, waterbath

	SOLID (meq/gr zeolite)		LIQUID (meq/gr zeolite)	
Elements	Initial	Final	Initial	Final
Ca	0.10	0.08	0	7.031
Fe	0.52	0.49	0	0.084
K	0.58	0.42	0	0.068
Mg	0.09	0.07	0	0.905
Na	1.66	0.25	0	2.627
Ag	0.00	1.25	10.000	8.457
(meq/gr zeolite)	$\sum(Ca^{2+}+Na^{+}+K^{+}+Mg^{2+})$		Ag^{+}	
	1.60		*1.54*	

Table 6.21. Solid and liquid phase compositions (0.1 M $Ag(NO)_3$, 80 ^oC, S/L=1/100, 1hr, microwave irradiation).

	SOLID (meq/gr zeolite)		LIQUID (meq/gr zeolite)	
Elements	Initial	Final	Initial	Final
Ca	0.10	0.09	0	-0.414
Fe	0.52	0.48	0	0.003
K	0.58	0.44	0	0.049
Mg	0.09	0.06	0	0.002
Na	1.66	0.29	0	0.787
Ag	0.00	1.16	10.000	8.688
(meq/gr zeolite)	$\sum(Ca^{2+}+Na^{+}+K^{+}+Mg^{2+})$		Ag^{+}	
	1.54		*1.31*	

Table 6.22. Solid and liquid phase compositions (0.1M $Co(NO_3)6H_2O$, 80°C, S/L=1/100, 1hr, waterbath).

	SOLID (meq/gr zeolite)		LIQUID (meq/gr zeolite)	
Elements	Initial	Final	Initial	Final
Ca	0.05	0.04	0	**0.331**
Fe	0.26	0.23	0	0.048
K	0.29	0.24	0	0.021
Mg	0.04	0.04	0	0.298
Na	0.83	0.27	0	1.318
Co	0.00	0.53	10.340	9.743
(meq/gr zeolite)	$\sum(Ca^{2+}+Na^{+}+K^{+}+Mg^{2+})$		Co^{2+}	
	0.62		*0.60*	

Table 6.23. Solid and liquid phase compositions (0.1M $Co(NO_3)6H_2O$, 80°C, S/L=1/100, 1hr, microwave irradiation).

	SOLID (meq/gr zeolite)		LIQUID (meq/gr zeolite)	
Elements	Initial	Final	Initial	Final
Ca	0.05	0.04	0	-0.030
Fe	0.26	0.59	0	0.002
K	0.29	0.25	0	0.010
Mg	0.04	0.03	0	0.005
Na	0.83	0.27	0	0.306
Co	0.00	0.48	10.870	10.321
(meq/gr zeolite)	$\sum(Ca^{2+}+Na^{+}+K^{+}+Mg^{2+})$		Co^{2+}	
	0.60		*0.54*	

Table 6.24. Solid and liquid phase compositions (0.1M $Cu(NO_3)_2.5/2H_2O$, 80°C, S/L=1/100, 1hr, waterbath).

	SOLID (meq/gr zeolite)		LIQUID (meq/gr zeolite)	
Elements	Initial	Final	Initial	Final
Ca	0.05	0.05	0	**4.052**
Fe	0.26	0.36	0	0.046
K	0.29	0.24	0	0.035
Mg	0.04	0.04	0	0.547
Na	0.83	0.20	0	1.694
Cu	0.00	0.68	11.673	10.906
(meq/gr zeolite)	$\sum(Ca^{2+}+Na^{+}+K^{+}+Mg^{2+})$		Cu^{2+}	
	0.70		*0.76*	

Table 6.25. Solid and liquid phase compositions (0.1M $Cu(NO_3)_2.5/2H_2O$, 80°C, S/L=1/100, 1hr, microwave irradiation).

	SOLID (meq/gr zeolite)		LIQUID (meq/gr zeolite)	
Elements	Initial	Final	Initial	Final
Ca	0.05	0.07	0	-0.052
Fe	0.26	0.46	0	0.004
K	0.29	0.24	0	0.016
Mg	0.04	0.04	0	0.002
Na	0.83	0.25	0	0.382
Cu	0.00	0.64	10.650	10.128
(meq/gr zeolite)	$\sum(Ca^{2+}+Na^{+}+K^{+}+Mg^{2+})$		Cu^{2+}	
	0.65		*0.53*	

There non-stoichiometry between the amount of Ag^{+}, Co^{2+} and Cu^{2+} uptake and total amount of exchangeable cations release for waterbath and microwave irradiated exchange which was due to hydrolysis of the exchangeable cation with -OH groups in the solution and formation metal-hydroxyl complexes. The experimental and/or instrumental error results with non-stoichiometry between the releasing and uptake of

the cations from the structure, as well. Ion exchange was considered as the predominant uptake mechanism for the processes conducted with higher metal concentration. The chemical compositions of liquid phase raw data for all other sets of Ag^{+}, Co^{2+} and Cu^{2+} exchanged NaCLI were plotted from the average of three runs within 0.05 confidence interval and are given in Appendix B, Figure B.15 and Figure B.16. The liquid phase and solid phase compositions of Ag^{+}, Co^{2+} and Cu^{2+} exchanged NaCLI for all other sets are given in Appendix C between Table C 93 and Table C108.

The exchange degree of Ag^{+}, Co^{2+} and Cu^{2+} on NaCLI were investigated within each other in accordance with the amount in the solid phase. The Ag^{+}, Co^{2+} and Cu^{2+} amounts (w/w%) starting with 0.1M initial metal ion concentration are given in Figure 6.20 through 6.22 for waterbath and microwave treatments.

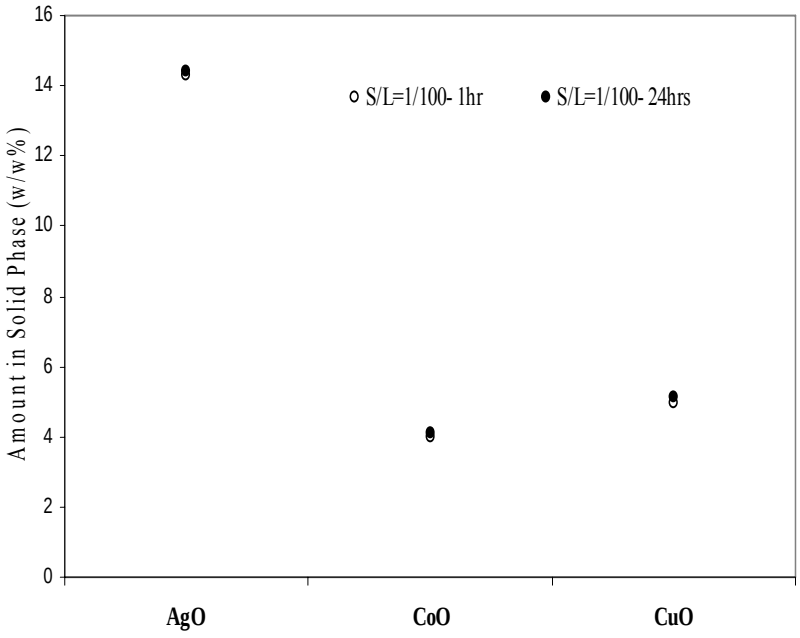

Figure 6.20. Ag^{+}, Co^{2+} and Cu^{2+} exchange on NaCLI (80 ^{o}C, waterbath).

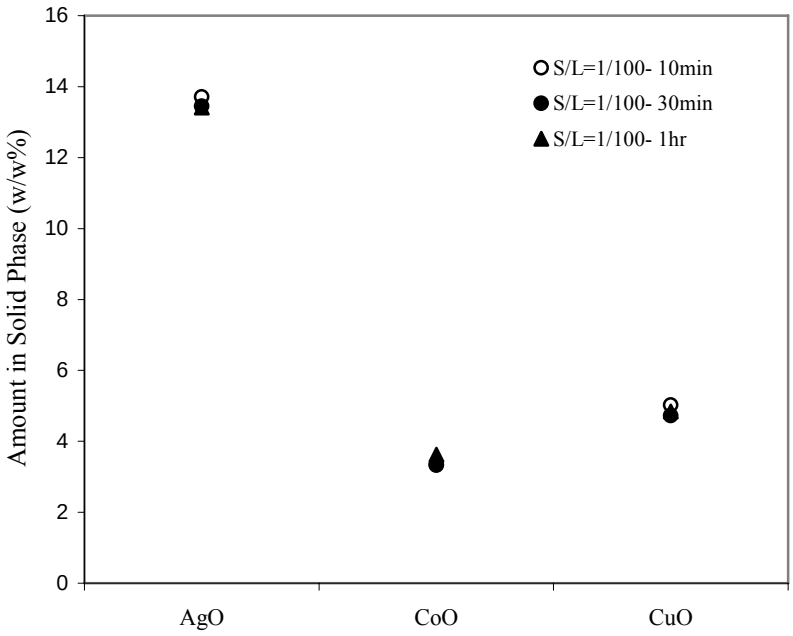

Figure 6.21. Ag^{+}, Co^{2+} and Cu^{2+} exchange on NaCLI (80 ^{o}C, microwave irradiaiton).

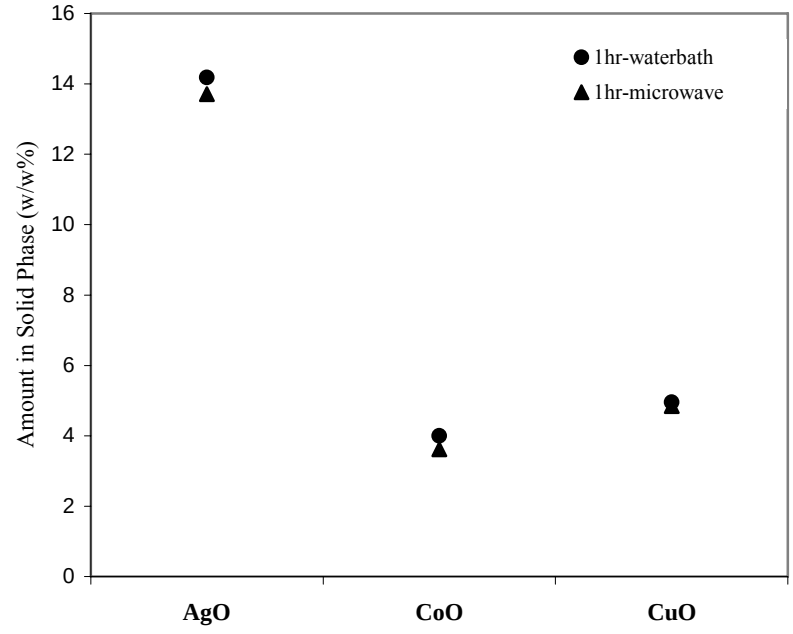

Figure 6.22. Ag^{+}, Co^{2+} and Cu^{2+} exchange on NaCLI (1hr, 80 ^{o}C).

Almost the same exchange degrees for Ag^{+}, Co^{2+} and Cu^{2} were observed as initial metal concentration was increased from 0.01 M to 0.1M for imicrowave and waterbath conducted exchanges.

Further increase in initial concentration of the cation solution (1M) for Ag^{+}, Co^{2+} and Cu^{2+} exchange on NaCLI in waterbath and with microwave irradiation were determined. Solid phase chemical compositions conditions (w/w%) of 1 M $Ag(NO_3)$, 1M $Co(NO)_36H_2O$ and 1M $Co(NO)_35/2H_2O$ exchanged NaCLI in waterbath and microwave are tabulated in Figure 6.23, Figure 6.24 and Figure 6.25, respectively.

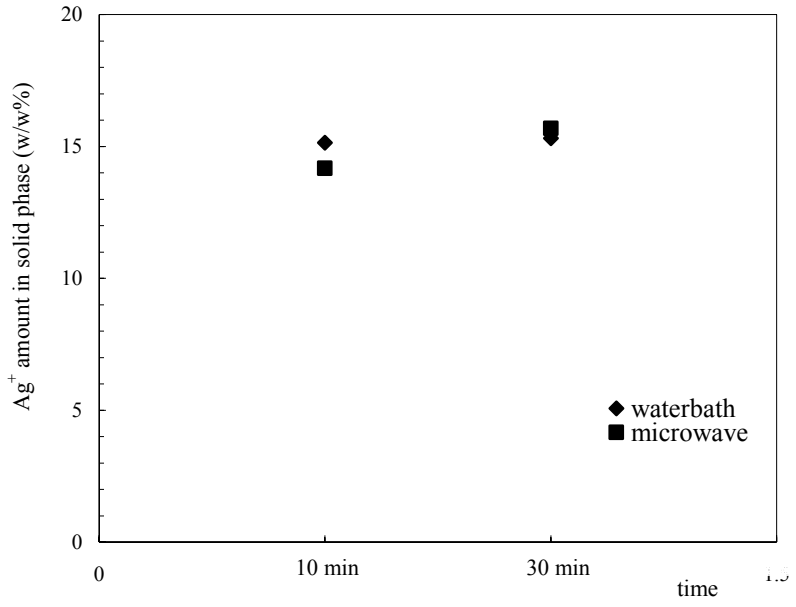

Figure 6.23. Ag^{+} exchange on NaCLI against time (80 ^{o}C ,S/L=1/100).

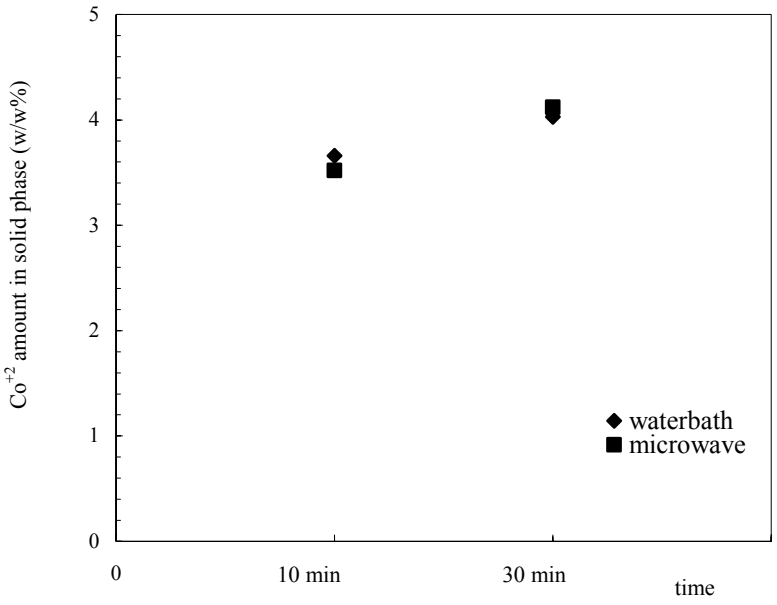

Figure 6.24. Co^{2+} exchange on NaCLI against time (80 ^{o}C, S/L=1/100).

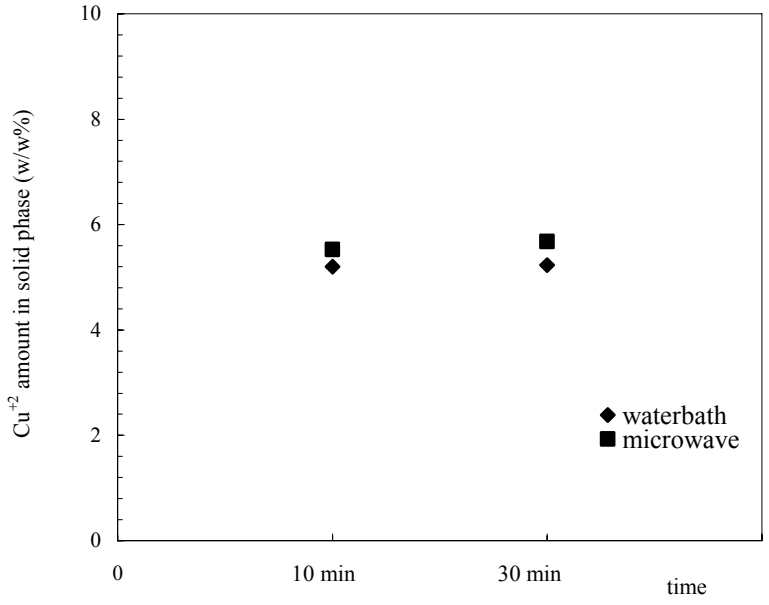

Figure 6.25. Cu^{2+} exchange on NaCLI against time (80 ^{o}C, S/L=1/100).

Starting from the fact that higher ion concentrations of solution might lead higher degree of ion exchange with time in microwave driven ion exchange compared to the waterbath exchange. However, the exchange degree for Ag^{+}, Co^{2+} and Cu^{2+}

starting with 0.01M, 0.1M and 1M metal ion concentration did not increase the exchange degree for Ag^{+}, Co^{2+} and Cu^{2+} in microwave as expected. The highest degree of exchange was observed for the Ag^{+} exchange compared to Co^{2+} and Cu^{2+} in both treatments for all cases. As well as the hydrated radii and hydration energies of ions, dielectric properties of system might have an influence on exchange degree therefore deeper investigation is needed in that respect.

In addition to microwave conducted exchanges in Mars 5-CEM Digestion and Extraction laboratory microwave oven system (EDMS), the ion exchange of Ag^{+}, Co^{2+} and Cu^{2+} exchange on NaCLI was conducted in Discovery-CEM microwave system (DMS) in which microwave power was continuous through the total time of exchange. The microwave conducted exchanges in EDMS and DMS were determined and considered. Solid phase chemical compositions conditions (w/w%) of 0.1 M and 1M $Ag(NO_3)$, $Co(NO)_36H_2O$ and $Cu(NO)_35/2H_2O$ exchanged NaCLI for 10 minutes in both microwave systems are tabulated in Figure 6.26.

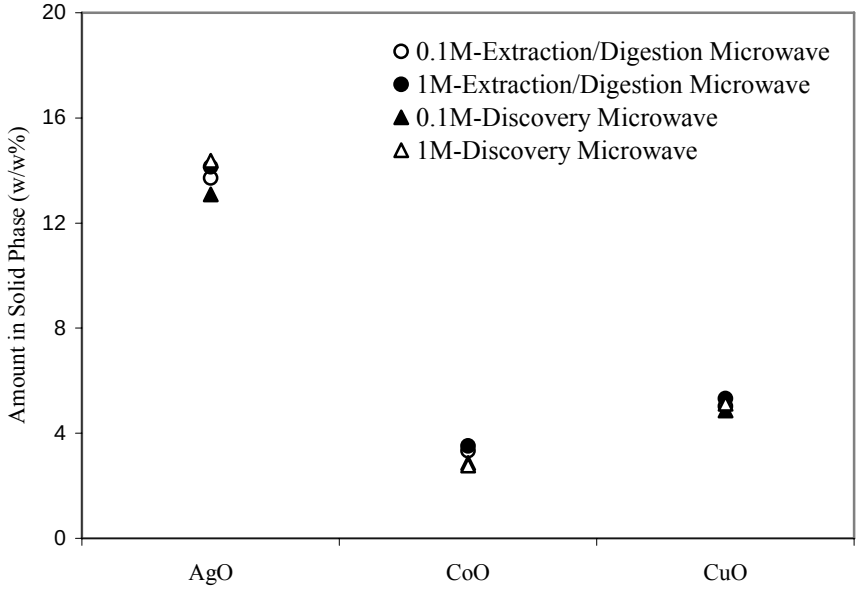

Figure 6.26. Ag^{+}, Co^{2+} and Cu^{2+} exchange on NaCLI (10min, 80 ^{o}C , S/L=1/100).

The DMS system uses 300 watts microwave power in principle. However for the above exchanges considered, 50 watts of continuous microwave energy was applied. Because, temperature of the system increases very much without control if 300 watts microwave power is being used. After several trials, the system temperature was kept at

80 ^{o}C for 10 minutes if 50 watts of continuous microwave power was applied. As indicated in Figure 6.26, the exchange degree for Ag^{+}, Co^{2+} and Cu^{2+} starting with 0.1M and 1M metal ion concentration did not increase the exchange degree for Ag^{+}, Co^{2+} and Cu^{2+} in DMS as expected. Because, the microwave power used was not sufficient enough to obtain higher exchange degrees compared to EDMS even if it was continuous.

Thus, two different microwave instruments with different working principles were used for ion exchange both having disadvantages. In EDMS, microwave power was not continuous and it was not used with 100% continuous efficiency through the total exchange time. Although microwave power was continuous in DMS it was insufficient for exchange systems considered here. As a suggestion, in order to work with higher microwave power, the cooling system around the vessel could be modified in DMS system. For example instead of air, liquid nitrogen could be used which might keep the system at 80 ^{o}C with the application of 300 watt microwave power. The ion exchange conducted with high and continuous microwave power, the higher exchange rates of different cations on clinoptilolite rich mineral could be obtained.

6.3. X-Ray Analyses of Ag^{+}, Co^{2+} and Cu^{2+} Exchanged NaCLI

Ag^{+}, Co^{2+} and Cu^{2+} exchanged NaCLI samples were investigated by powder XRD. The patterns were examined using intensities which were outlined by Arcoya *et. al,* 1999. Additionally, the peaks of were examined by SMSP attached to X-Ray diffractometer and presence of extra peaks were examined in the same manner. The XRD patterns of Ag^{+}, Co^{2+} and Cu^{2+} exchanged NaCLI for 24 hrs in waterbath and for 1hr with microwave irradiaiton in comparison to NaCLI are given in between Figures 6.27 and 6.29. X-Ray patterns of Ag^{+}, Co^{2+} and Cu^{2+} exchanged NaCLI for the all utilized parameters for waterbath and with microwave irradiation are given in Appendix E.

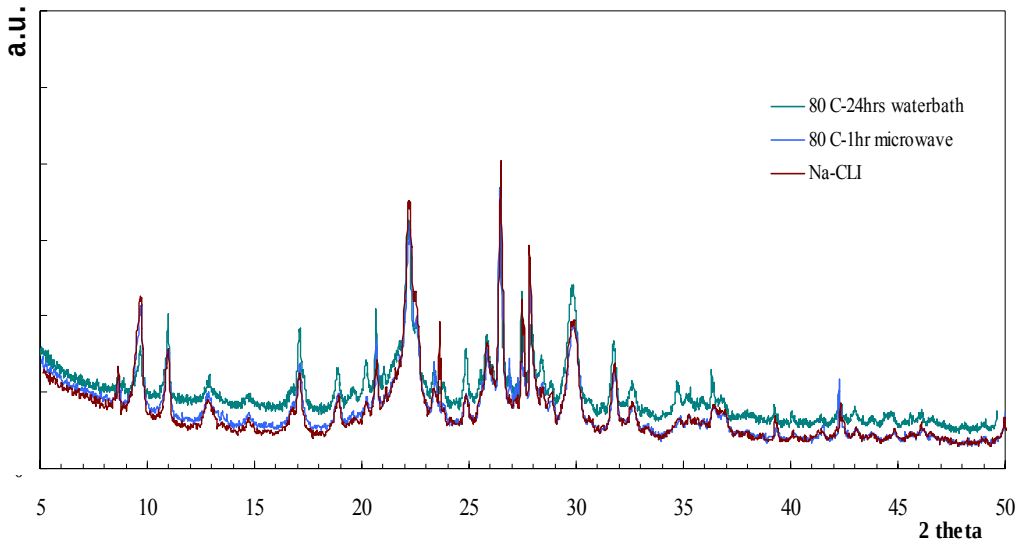

Figure 6.27. XRD pattern of Ag^{+} exchanged NaCLI (80 ^{o}C, waterbath and microwave irradiation).

The main peaks of Ag^{+} exchanged NaCLI in waterbath were overlapped with the archived data of clinoptilolite mineral peaks in the SMSP library belonging to JSPDS 22-1235 card and main impurity was identified as quartz belonging to JSPDS 83-0335 card. For the microwave case, main peaks were overlapped mainly with the clinoptilolite and heulandite mineral peaks belonging to JSPDS 39-1383 and JSPDS 82-1229 card, respectively. Again the main impurity was quartz identified with JSPDS 86-1630 card.

The characteristic peak intensities at 9.92 and 30.05^{o} 2theta relative to most intense peak at 22.40 ^{o} 2theta of Ag^{+} exchanged minerals were examined in comparison to NaCLI peak intensity ratios. The decrease on the peak ratio at 9.92^{o} 2theta which is attributed to framework cations probably caused by the compositional change within the mineral after the exchange. The change in peak ratio at 30.05^{o} 2theta was small compared to change in peak ratio at 9.92^{o} 2theta. The comparative analysis showed that small peak appeared at around 42.5^{o} 2theta Ag^{+} exchanged NaCLI for 1hr microwave.

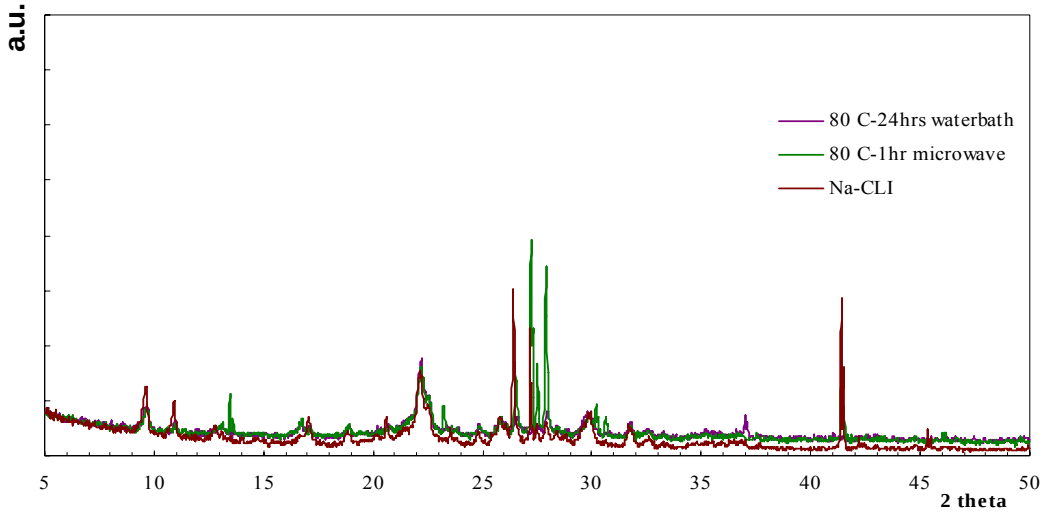

Figure 6.28. XRD pattern of Co^{2+} exchanged NaCLI (80 ^{o}C ,waterbath and microwave irradiation).

The main peaks of Co^{2+} exchanged NaCLI in waterbath were overlapped with the K-heulandite and clinoptilolite mineral peaks in the SMSP library belonging to JSPDS 76-2213 and JSPDS 25-1349 card, respectively. Main impurity was identified as quartz belonging to JSPDS 85-0335 card. For the microwave case, main peaks were overlapped mainly with heulandite mineral peaks belonging to JSPDS 82-1228 card. The main impurity was α-quartz identified with JSPDS 75-0443 card. The peaks appeared at around 13.60, 27.30 and 46.21^{o} 2theta are attributed to Co oxide identified by the archived data found in SMSP library belonging to JSPDS 27-0516 card.

For Co^{2+} exchanged NaCLI, peak intensities at around 9.92 and 30.05^{o} 2theta relative to most intense peak at around 22.40 ^{o} 2theta were examined in comparison to NaCLI. The alteration of peak ratios at 30.05^{o} 2theta and 9.92^{o} 2theta are not significant but higher for 30.05^{o} 2theta case. The intense peak at 41.4 ^{o} 2theta might depend on the nature of NaCLI mineral which is being K-rich (SMSP)

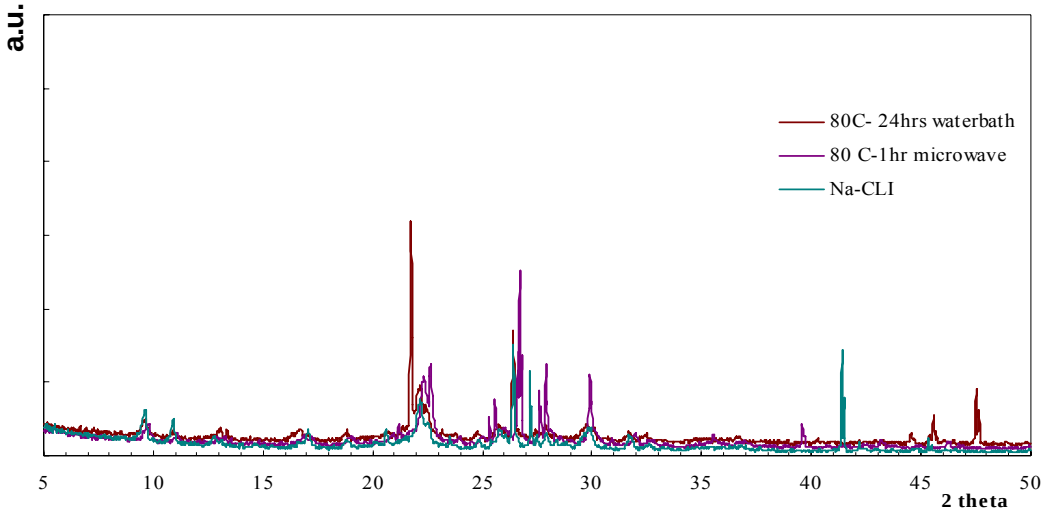

Figure 6.29. XRD pattern of Cu^{2+} exchanged NaCLI (80 ^{o}C, waterbath and microwave irradiation).

The main peaks of Cu^{2+} exchanged NaCLI in waterbath were overlapped with the Na-K-Ca clinoptilolite mineral peaks in the SMSP library belonging to JSPDS 39-1383 and the additional peaks are between 44 and 46 ^{o}2theta are attributed to this match. Main impurity was identified as quartz belonging to JSPDS 85-0335 card. The comparative analysis showed that peaks appeared between 44- 45^{o} 2theta is attributed to Cu^{2+}. For the microwave case, main peaks were overlapped mainly with Ca-clinoptilolite and heulandite mineral peaks in the SMSP library belonging to JSPDS 25-1349 and JSPDS 77-0334 card, respectively. The main impurity was α-quartz identified with JSPDS 75-0443 card.

Peak intensity ratios were examined for Cu^{2+} exchanged NaCLI in comparison to NaCLI both for waterbath and microwave exchanges. The alteration of peak ratios at 30.05^{o} 2theta and 9.92^{o} 2theta are not significant. The intense peak at 41.4 ^{o} 2theta probably depends on nature of NaCLI mineral which is being K-rich (SMSP).

The overall X-Ray examination of Ag^{+}, Co^{2+} and Cu^{2+} exchanged NaCLI showed that modification of NaCLI with ion exchange in waterbath and microwave showed that did not lead significant structural changes. No shifts in peak positions of characteristic peaks of clinoptilolite and insignificant decrease in characteristic peak intensities relative to most intense peak of clinoptilolite on XRD patterns of all samples is an indication of no crystallinity loss of NaCLI in its metal exchanged forms (Benaliouche et al., 2008).

6.4. FTIR Analyses of Ag^{+}, Co^{2+} and Cu^{2+} Exchanged NaCLI

The FTIR of Ag^{+}, Co^{2+} and Cu^{2+} exchanged NaCLI samples in comparison to NaCLI with S/L=1/100 for 24 hrs. in waterbath and 1hr in microwave are given in Figure 6.30 and Figure 6.31, respectively.

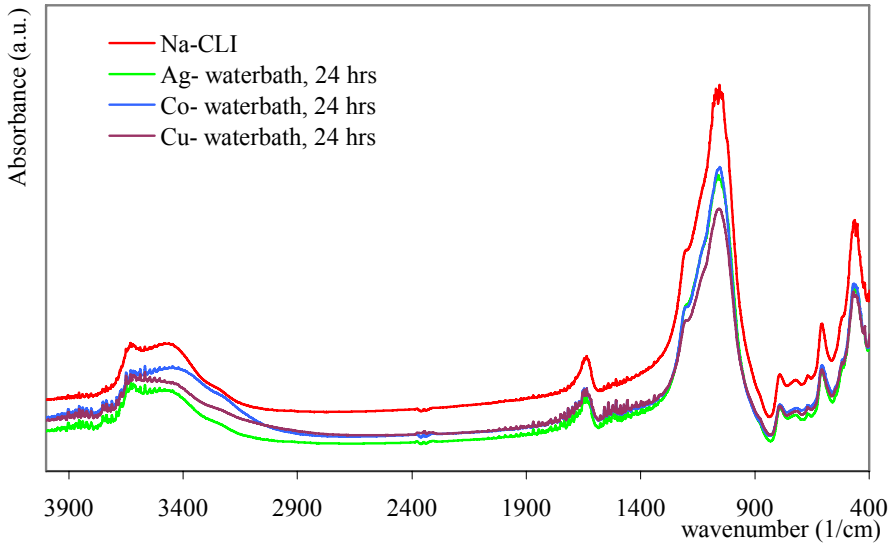

Figure 6.30. FTIR Spectra of Ag^{+}, Co^{2+} and Cu^{2+} exchanged NaCLI (80^{o}C, waterbath).

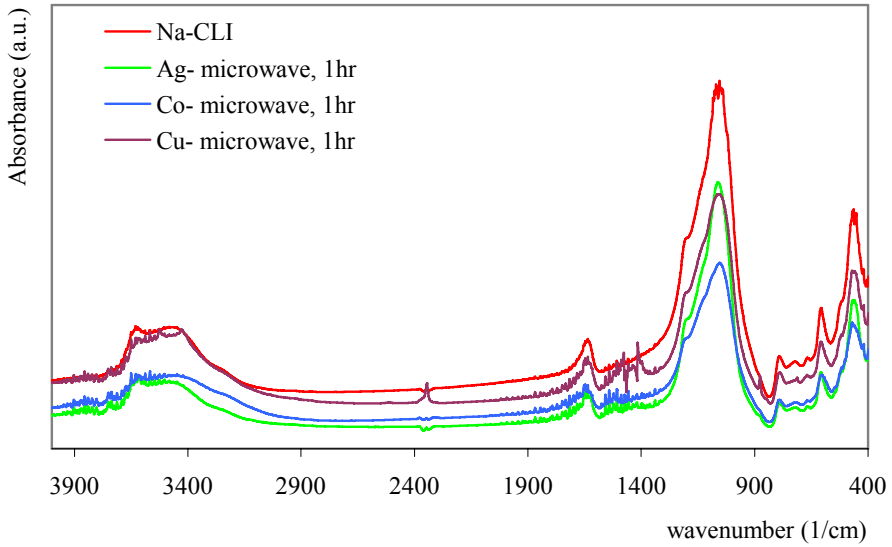

Figure 6.31. FTIR Spectra of Ag^{+}, Co^{2+} and Cu^{2+} exchanged NaCLI (80 ^{o}C, microwave irradiaiton).

FTIR spectra are very useful in getting structural information, cation substitutions and channel sizes hence metal exchanged NaCLI samples were examined by FTIR. Following the Figures 6.30 and 6.31, major bands attributed to characteristic of clinoptilolite at 1060, 790 cm^{-1} and 609 cm^{-1} and related with isolated OH stretching at 3700 cm^{-1}, H-bonded O–H stretching at 3400 cm^{-1} and H_2O bending at 1620 cm^{-1} were observed for Ag^{+}, Co^{2+} and Cu^{2+} exchanged NaCLI both in waterbath and microwave (Breck, 1974). The unchanged position of the main band at 1060 cm^{-1} due to Si-O(Si) and Si-O(Al) vibrations showed that no framework dealumination within the NaCLI with Ag^{+}, Co^{2+} and Cu^{2+} metal exchanges.

However, it is not appropriate to examine the FTIR spectra on the region based between 400- 4000 cm^{-1} because getting right information is not possible through on that basis. Introducing the non-tetrahedral cations into the alumino-silicate framework change the IR spectra in the range of pseudo lattice vibrations at 500-700 cm^{-1} which are characterized by shifts and intensity changes in the bands (Korkuna et al., 2005).

The FTIR spectrum in the extended region from 500 to 750 cm^{-1} for Ag^{+}, Co^{2+} and Cu^{2+} exchanged NaCLI samples with S/L= 1/100 at 80°C in waterbath and microwave are given in Figure 6.32 and Figure 6.33, respectively The peak intensity ratio at 609 cm^{-1} relative to the main band intensity at 1060 cm^{-1} were examined and are given in Table 6.26.

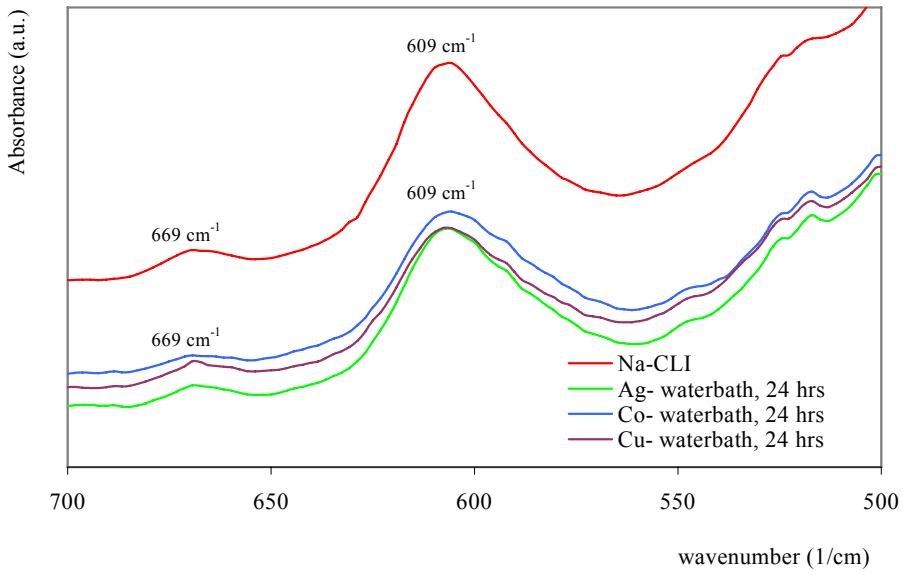

Figure 6.32. FTIR spectra in the 500-700 cm^{-1} region for Ag^{+}, Co^{2+} and Cu^{2+} exchanged NaCLI (80°C, waterbath).

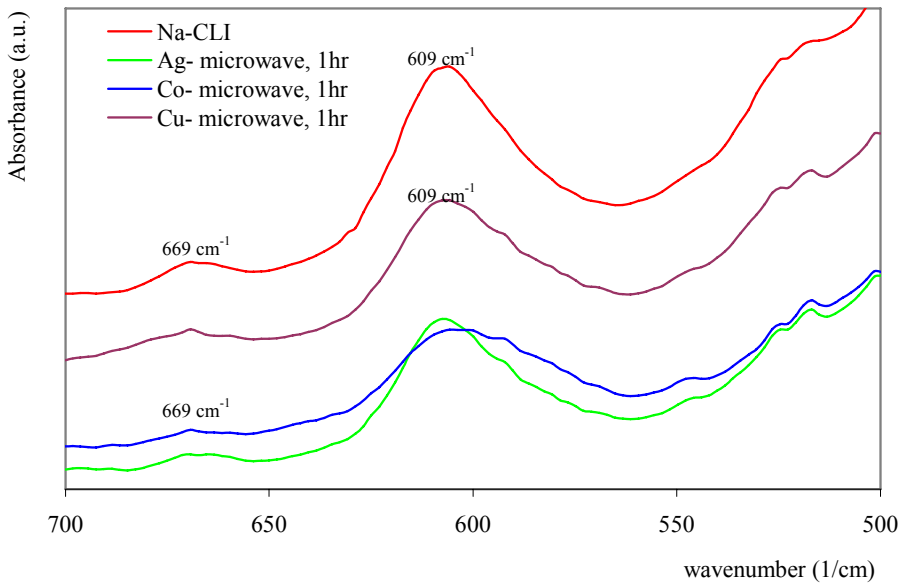

Figure 6.33. FTIR spectra in the 500-700 cm^{-1} region for Ag^{+}, Co^{2+} and Cu^{2+} exchanged NaCLI (80^{o}C , microwave irradiation).

Table 6.26. The 609 cm^{-1} to 1060 cm^{-1} peak intensity ratio for Ag^{+}, Co^{2+} and Cu^{2+} exchanged NaCLI (80^{o}C, waterbath (wb) and microwave (mw)).

Peak Intensity Ratio	NaCLI	S/L=1/20		S/L=1/50		S/L=1/100	
		Wb	**mw**	**Wb**	**mw**	**wb**	**mw**
Ag^{+}	**0.18**	0.17	0.16	0.18	0.15	0.19	0.17
Co^{2+}		0.22	0.21	0.21	0.23	0.22	0.22
Cu^{2+}		0.21	0.20	0.22	0.21	0.19	0.23

The embedding the Ag^{+}, Co^{2+} and Cu^{2+} cations into the structure of NaCLI do not result in the prominent shifts of the band positions as seen in Figure 6.32 and Figure 6.33. As indicated in Table 6.26, introducing the cations into the structure did not distinctly change the peak intensities at 609 cm^{-1} whereas slight changes might due to the nature of the mineral, NaCLI.

The FTIR spectrum exhibits three major hydroxyl bands attributed to. (a) SiOH groups terminating the crystal structure (3740 -3730 cm^{-1}), (b) AlOH gropus (3680-3670 cm^{-1}), and (c) OH groups in the supercage (3644-3628 cm^{-1}) (Benaliouche et al.,

2008). Therefore peaks due to formation hydroxyl species were examined in the range 3600- 3750 cm^{-1}.

The FTIR spectrum of Ag^{+}, Co^{2+} and Cu^{2+} exchanged NaCLI samples examined in the extended region from 3600 to 3750 cm^{-1}, as well. The spectrum of metal exchanged forms of NaCLI with S/L=1/100 at 80°C in waterbath and microwave are given Figure 6.34 and Figure 6.35, respectively.

The isolated OH^{-} stretching vibrations at 3628 cm^{-1} are attributed to interaction between the water hydroxyl and also the cations present. The peak intensity ratio at 3680 cm^{-1} relative to the main band at 1060 cm^{-1} were examined and given in Table 6.27.

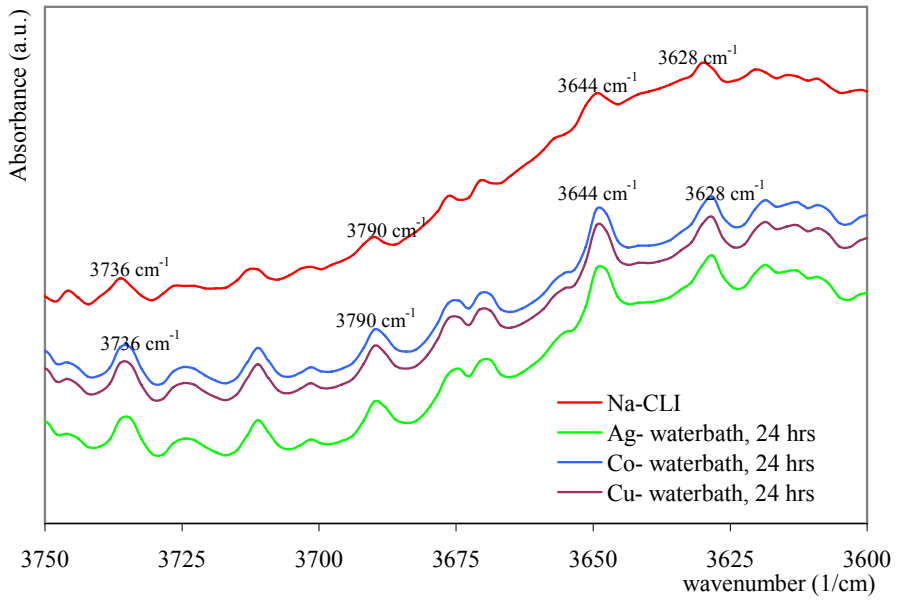

Figure 6.34. FTIR spectra in the 3400 cm^{-1} region for Ag^{+}, Co^{2+} and Cu^{2+} exchanged NaCLI (80°C, waterbath)

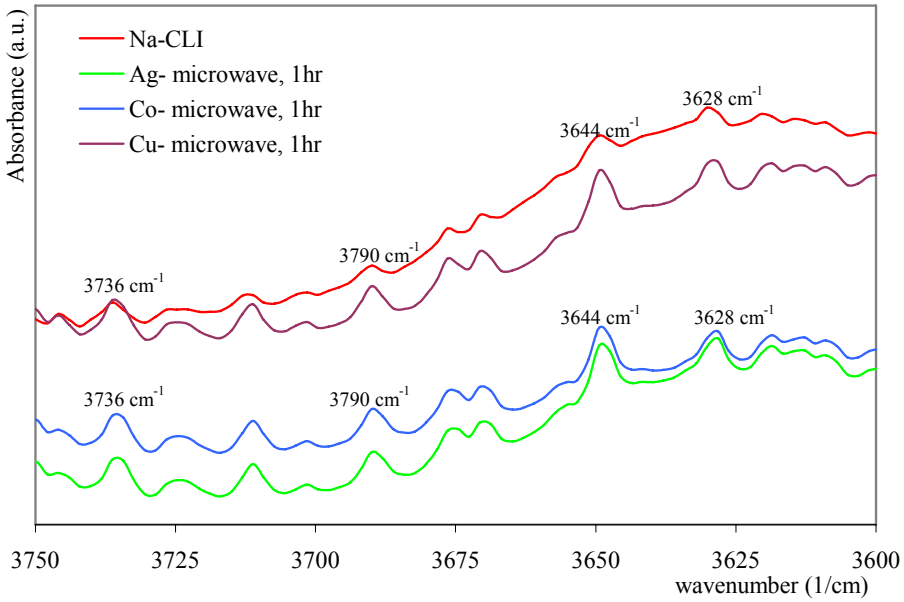

Figure 6.35. FTIR spectra in the 3400 cm^{-1} region for Ag^{+}, Co^{2+} and Cu^{2+} exchanged NaCLI (80°C, microwave irradiation).

Table 6.27. The 3628 cm^{-1} to 1060 cm^{-1} peak intensity ratio for Ag^{+}, Co^{2+} and Cu^{2+} exchanged NaCLI (80°C, waterbath (wb) and microwave (mw)).

Peak Intensity Ratio	NaCLI	S/L=1/20		S/L=1/50		S/L=1/100	
		wb	**mw**	**wb**	**mw**	**wb**	**mw**
Ag^{+}	**0.14**	0.14	0.14	0.15	0.13	0.16	0.14
Co^{2+}		0.14	0.13	0.14	0.14	0.13	0.14
Cu^{2+}		0.14	0.14	0.19	0.15	0.16	0.15

As seen in Figure 6.34 and Figure 6.35, the intensity increased in the hydroxyl group in the supercages at 3644 cm^{-1}, 3790 cm^{-1} and 3736 cm^{-1} indicating the association of OH groups with exchanged cations (Benaliouche et al., 2008). In addition, no shifts in the position of bands were observed. As indicated in Table 6.27, introducing the cations into the structure did not distinctly change the peak intensities of the NaCLI at 3628 cm^{-1}.

FTIR patterns of Ag^{+}, Co^{2+} and Cu^{2+} exchanged NaCLI for the all utilized parameters for waterbath and microwaves are given in Appendix F.

6.5. SEM Analyses of Ag^{+}, Co^{2+} and Cu^{2+} Exchange NaCLI

The micrographs of Ag^{+} exchanged NaCLIs were taken by using BSE back scattered electron (BSE) detector since elements with higher atomic number were seen brighter on BSE detector used micrographs. Therefore better clear identification of Ag^{+} ions within the mineral is possible. The SEM micrograph Ag^{+} exchanged NaCLI in waterbath and microwave are given in Figure 6.36 and 6.37, respectively

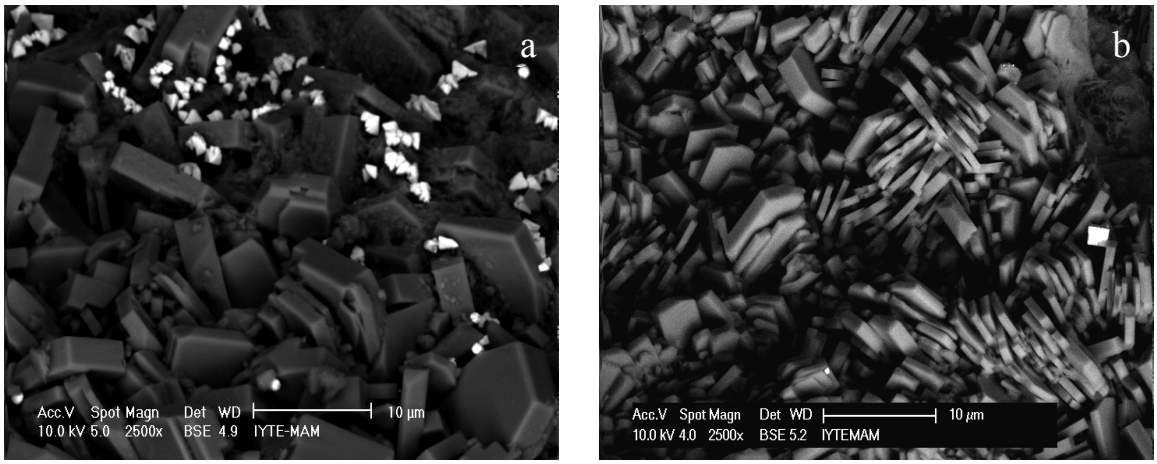

Figure 6.36. SEM micrograph of Ag^{+} exchanged NaCLI in waterbath a) S/L=1/50 at 40 ^{o}C for 3days b) S/L=1/100 at 80 ^{o}C for 1hour.

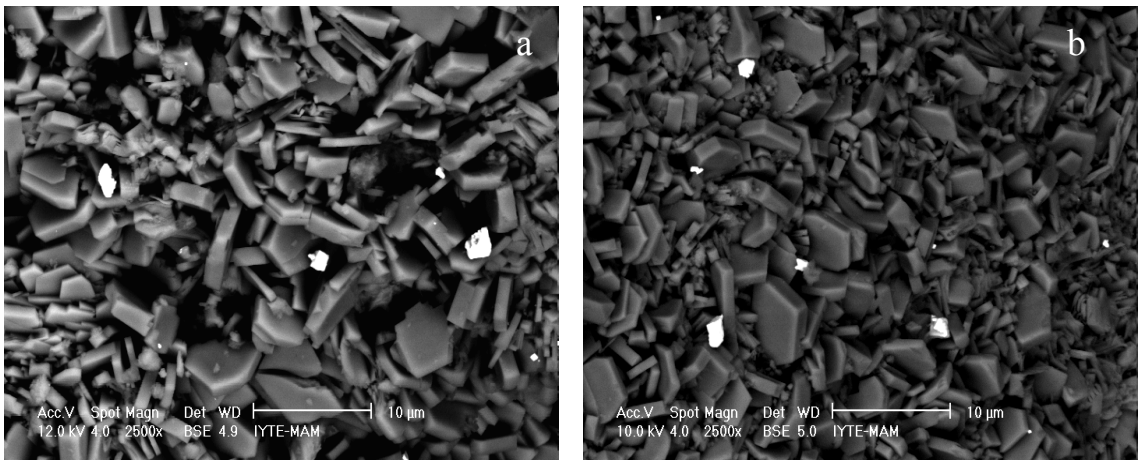

Figure 6.37. SEM micrograph of Ag^{+} exchanged NaCLI with microwave irradiation a) S/L=1/100 at 80 ^{o}C for 30minute b) S/L=1/100 at 80 ^{o}C for 1hour.

In the above micrographs, white particles were corresponding to Ag^+ ions and observed for all the exchange runs in waterbath and microwave which were given in Appendix G. In order to make clear that the white particles in micrographs are Ag^+, EDX analysis was done directly onto the white particle on randomly selected run and it is given in Figure 6.38.

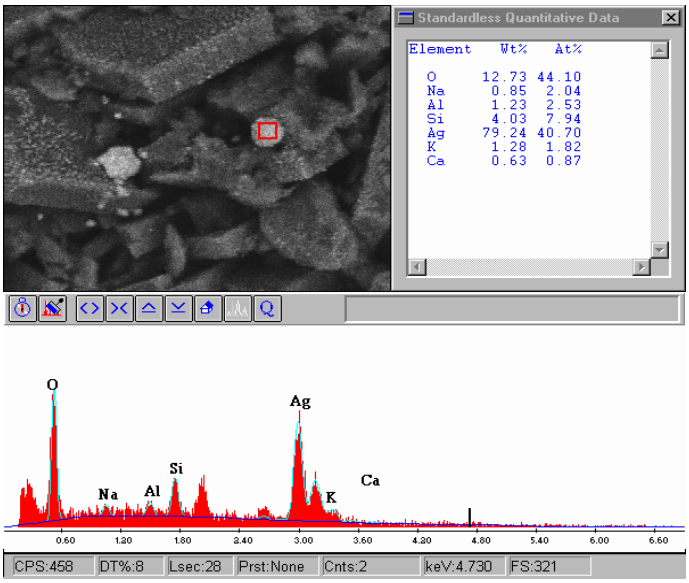

Figure 6.38. EDX analysis of Ag^+ exchanged NaCLI (S/L=1/100, 1day, 80 ^oC, waterbath).

It is agreed from the EDX analysis that those white particles were corresponding to Ag^+ ions. Rivera-Garza, 2000, had studied the antibacterial activity of Ag-exchanged Mexican zeolite and observed similar white particles on the surface of the zeolitic material. They analyzed those particles showed that they have high concentration of Ag.

As indicated from the micrographs, the distribution the Ag^+ ions were not homogenous and in all exchanged NaCLI. This doesn't mean those minerals have no or smaller Ag^+ content compared to the ones that have white particles were seen on their SEM micrograph. The EDX analysis done on the Ag^+ exchanged NaCLI with S/L=1/100 at 60 ^oC for 24hrs in waterbath and given in Figure 6.39. The element wt% shows that even the absence of the white particles the Ag^+ amount within the mineral is quite high.

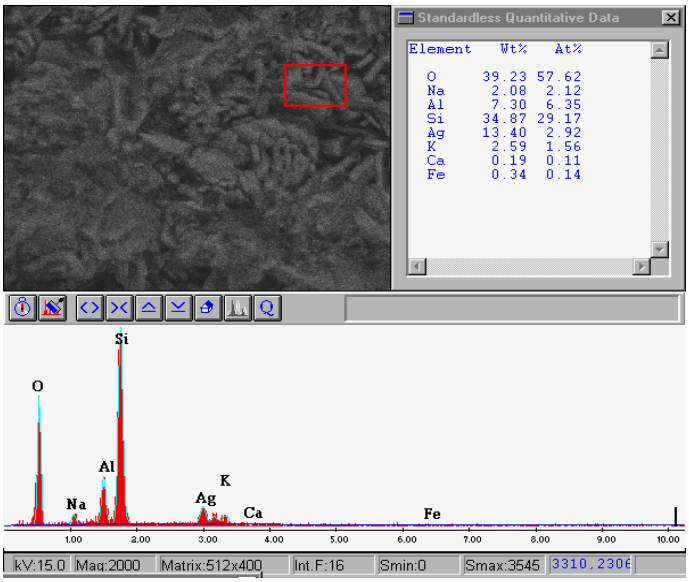

Figure 6.39. EDX analysis of Ag^{+} exchanged NaCLI (S/L=1/100, 24hrs, 60 ^{o}C, waterbath)

The exchanged the minerals were washed several times after the exchange completed, dried and kept for various analyses and during washing, Ag^{+} particles on the surface of the minerals might sweep away. This may cause non-homogenous distribution of Ag^{+} ions detected on SEM micrograph. The mapping result for the same experimental set is given in Figure 6.40.

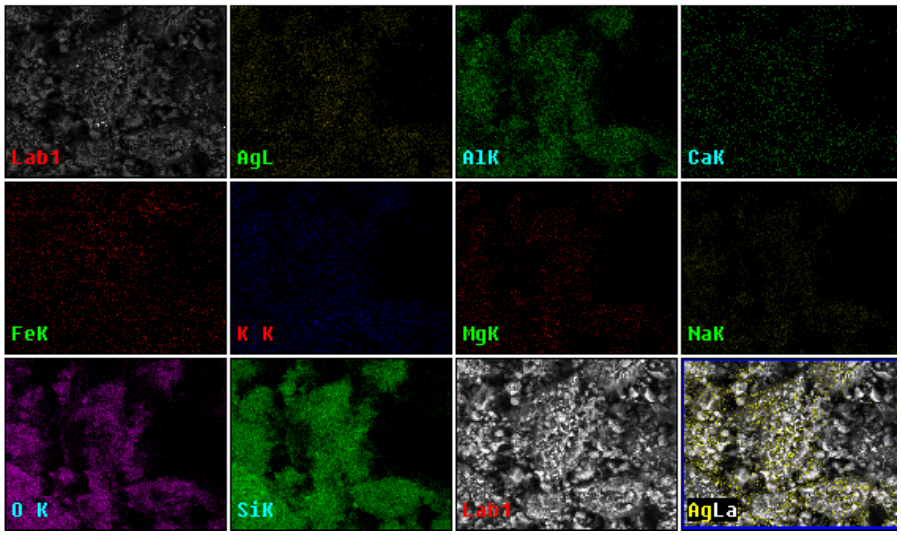

Figure 6.40. SEM Mapping for Ag^{+} exchanged NaCLI (S/L=1/100, 60 ^{o}C 24hrs, waterbath).

The micrographs of Co^{2+} and Cu^{2+} exchanged NaCLIs were taken by using secondary electron (SE) detector and are given in Figure 6.41 and 6.42 for waterbath and microwave treatments, respectively.

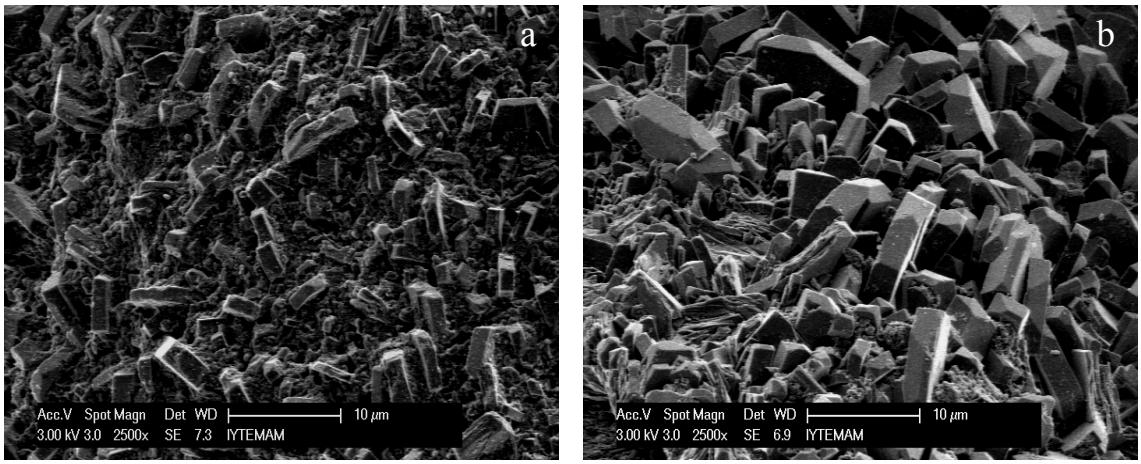

Figure 6.41. SEM micrograph of Co^{2+} exchanged NaCLI at 80 ^{o}C a) S/L=1/50 for 24hrs, in waterbath b) S/L=1/20 for 1hour with microwave irradiation.

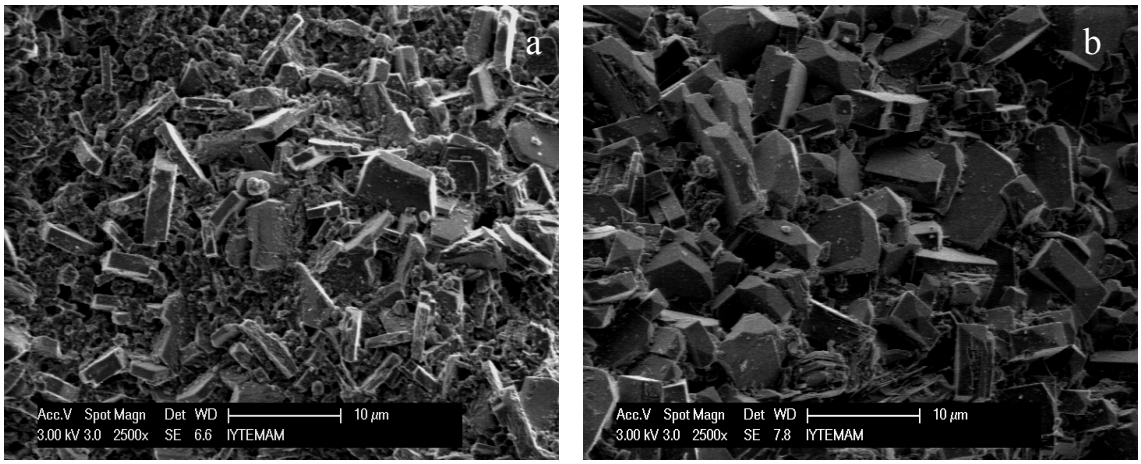

Figure 6.42. SEM micrograph of Cu^{2+} exchanged NaCLI at 80 ^{o}C a) S/L=1/20 for 24hrs, in waterbath b) S/L=1/100 for 1hour with microwave irradiation.

The EDX analysis done on Co^{2+} and Cu^{2+} exchanged NaCLI were done for the runs which are selected randomly are given in Figure 6.43 and 6.44, respectively.

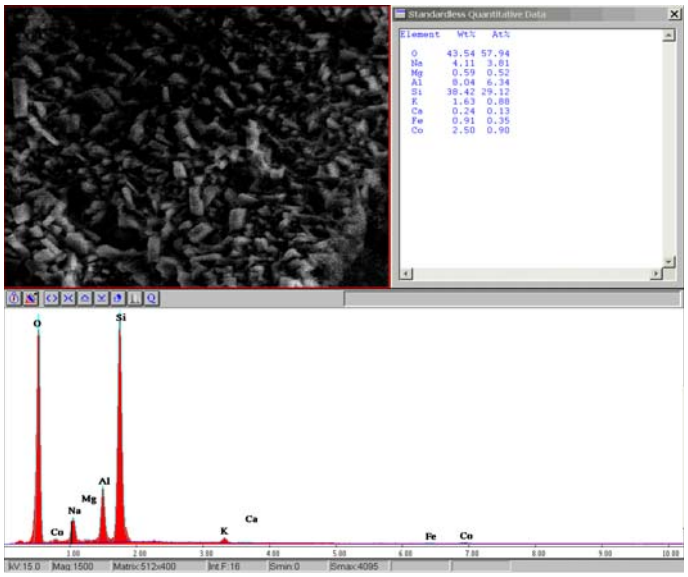

Figure 6.43. EDX analysis of Co^{2+} exchanged NaCLI (S/L=1/100, 80 ^{o}C, 24 hrs, waterbath).

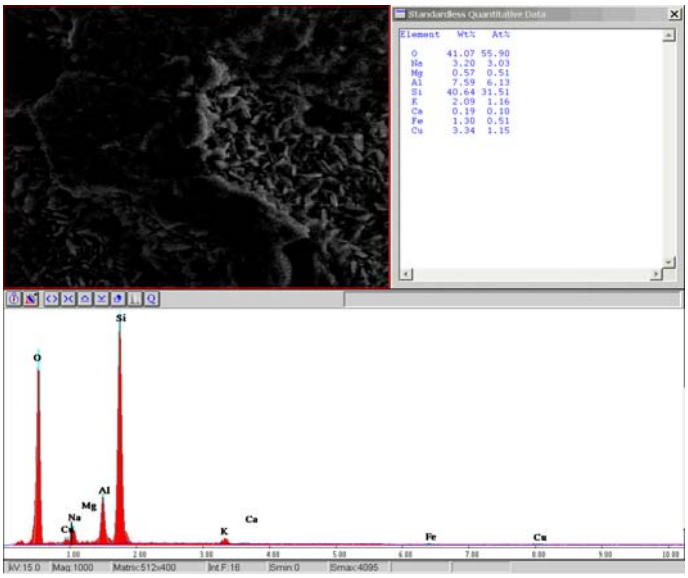

Figure 6.44. EDX analysis of Cu^{2+} exchanged NaCLI (S/L=1/20, 80 ^{o}C, 1hr microwave irradiation).

Co^{2+} and Cu^{2+} exchanged NaCLI did not show any structural changes with waterbath and microwave treatments. Typical clinoptilolite crystals were clearly observed in all SEM micrograph. Co^{2+} and Cu^{2+} exchange degrees on NaCLI

determined from EDX analysis are in good agreement and compatible with ICP data. SEM micrographs of some selected Ag^{+} Co^{2+} and Cu^{2+} exchanged NaCLI for the utilized parameters for waterbath and microwave irradiated exchange are given in Appendix G.

6.6. N_2 Adsorption Isotherms of Ag^{+}, Co^{2+} and Cu^{2+} Exchanged NaCLI

The adsorption-desorption isotherms for Ag^{+}, Co^{2+} and Cu^{2+} exchanged NaCLI for 24hrs in waterbath and 1hr in microwave are shown in Figure 6.45a and Figure 6.45b, respectively. The full fill symbols are corresponding to adsorption whereas empty symbols are corresponding desorption. The S/L ratio parameter for these experimental sets was 1/100.

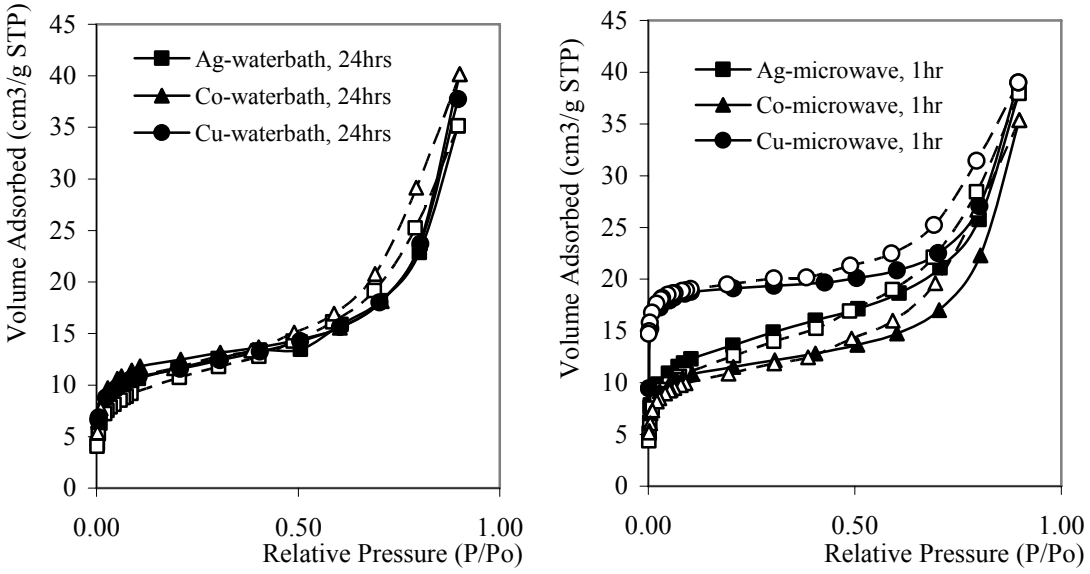

Figure 6.45. Sorption Isotherms of Ag^{+}, Co^{2+}, Cu^{2+} treated NaCLI.

Based on the IUPAC classification of sorption isotherms all the Ag^{+}, Co^{2+}, Cu^{2+} treated NaCLI showed Type 4 isotherm and hysteresis loops of the isotherms are typical for mesoporous materials. In addition, the presence of impurities within the mineral and the exchangeable cations located in NaCLI channels are generating a kind of barrier for N_2 molecules and their diffusion becomes hard (Korkuna et. al, 2005). The volume adsorbed for the Ag^{+}, Co^{2+} and Cu^{2+} exchanged NaCLI in waterbath are found as 35.13

cm^3/gr STP, 40.16 cm^3/gr STP and 37.75 cm^3/gr STP, respectively. For the microwave case, volume adsorbed are found as 37.94 cm^3/gr STP, 35.37 cm^3/gr STP and 39.01 cm^3/gr STP for the Ag^+, Co^{2+} and Cu^{2+} exchanged NaCLI, respectively. The volume adsorbed at highest P/P_o for NaCLI is found 42.14 cm^3/gr STP. The volume adsorbed decrease for Ag^+, Co^{2+} and Cu^{2+} exchanged NaCLI was likely due to impurities and framework cations present within the structure. In the case microwave irradiation, Cu^{2+} exchanged NaCLI has different sorption isotherm which shows it has more microporous structure compared to Ag^+ and Co^{2+} exchanged NaCLI. The external surface areas for Ag^+, Co^{2+} and Cu^{2+} exchanged NaCLI were found as 31.48 m^2/gr, 17.90 m^2/gr and 9.25 m^2/gr, respectively. Because, formation of surface complexes and precipitations were higher in the case of Ag^+ and Co^{2+} exchanged NaCLI which are supported by SEM and ICP. The sorption of N_2 is lower in the case of Ag^+ and Co^{2+} exchanged NaCLI compared to Cu^{2+} exchanged NaCLI due to the blockage of the precipitates and formations on the surface of NaCLI. All other sorption of Ag^+, Co^{2+} and Cu^{2+} exchanged NaCLI for the utilized parameters for waterbath and microwaves are given in Appendix H.

6.7. Thermal Analysis Results of Ag^+, Co^{2+} and Cu^{2+} Exchanged NaCLI

Thermal analysis techniques are important in evaluating the thermal behavior of zeolitic material which is directly dependent on type and population of cations within the structure (Perraki and Orfanoudaki et al., 2004). TGA curves of Ag^+, Co^{2+} and Cu^{2+} exchanged NaCLI with S/L=1/200 at 80 ^oC in waterbath for 24hrs and in microwave for 1hr are given in Figure 6.46.a and Figure 6.46.b, respectively.

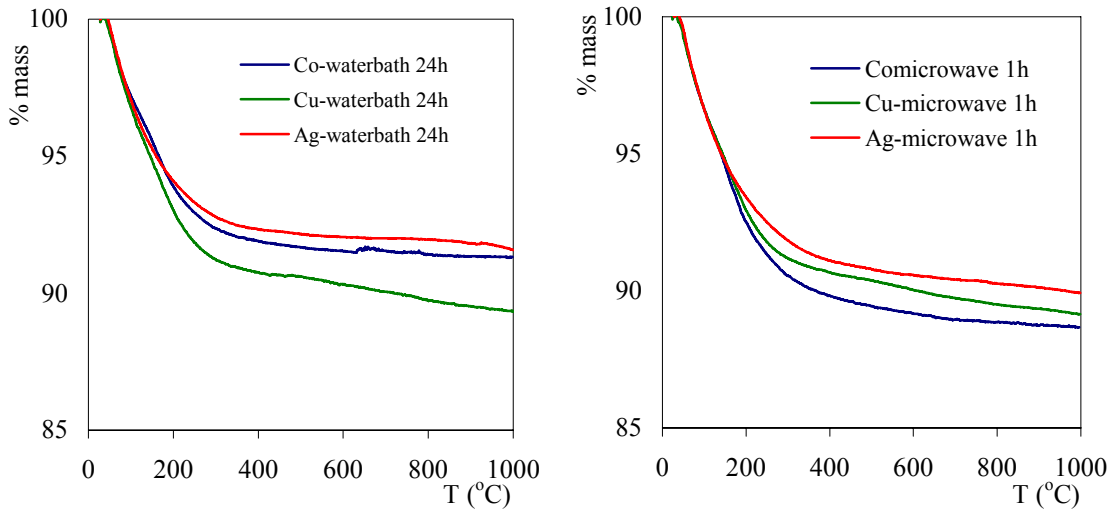

Figure 6.46. TGA curve of Ag^{+}, Co^{2+} and Cu^{2+} exchanged NaCLI.

Zeolites exchanged with monovalent cations have lower loss of zeolitic water compared to zeolites exchanged with bivalent cations. The quantity of of weakly bound water is dependent on the size of the cations (Castaldi et al, 2005). TGA curves indicating smooth mass loss without any evident steps. Conspicuously, desorption of water starts at around the same temperature but completed at different temperatures due to the different cation content of different metal exchanged forms of NaCLI. It can be seen from Figure 6.46.a, the dehydration of Cu^{2+} exchanged NaCLI was completed at higher temperatures and its zeolitic water is high compared to Ag^{+} and Co^{2+} exchanged NaCLI in waterbath treatment. The temperature needed for complete dehydration of water decreases with increasing size of the non-framework cations (Korkuna et al, 2005).

DTA curves of Ag^{+}, Co^{2+} and Cu^{2+} exchanged NaCLI with S/L=1/200 at 80 ^{o}C in waterbath for 24hrs and in microwave for 1hr are given in Figure 6.47 and Figure 6.48, respectively.

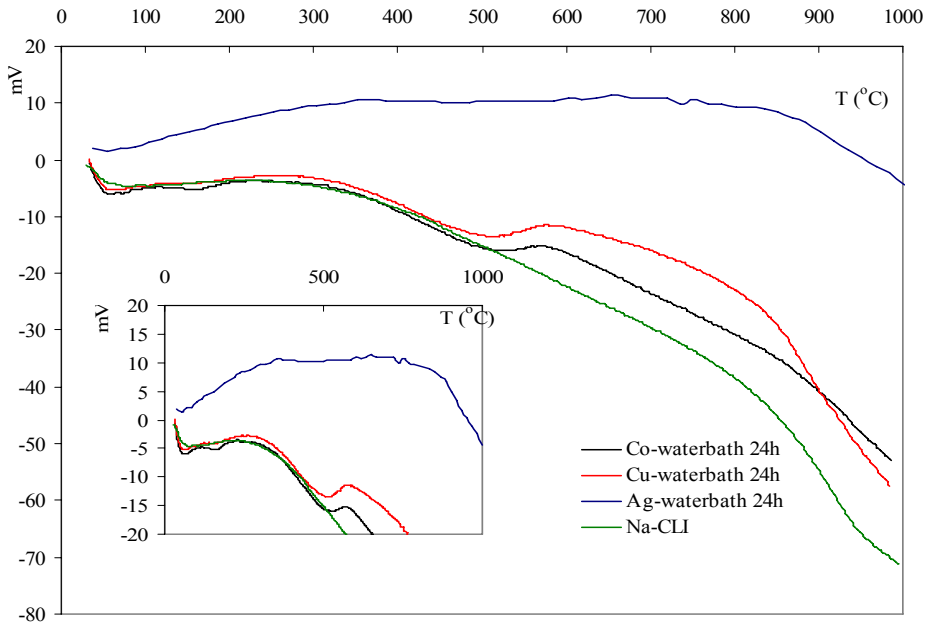

Figure 6.47. DTA curve of Ag^{+}, Co^{2+} and Cu^{2+} exchanged NaCLI.

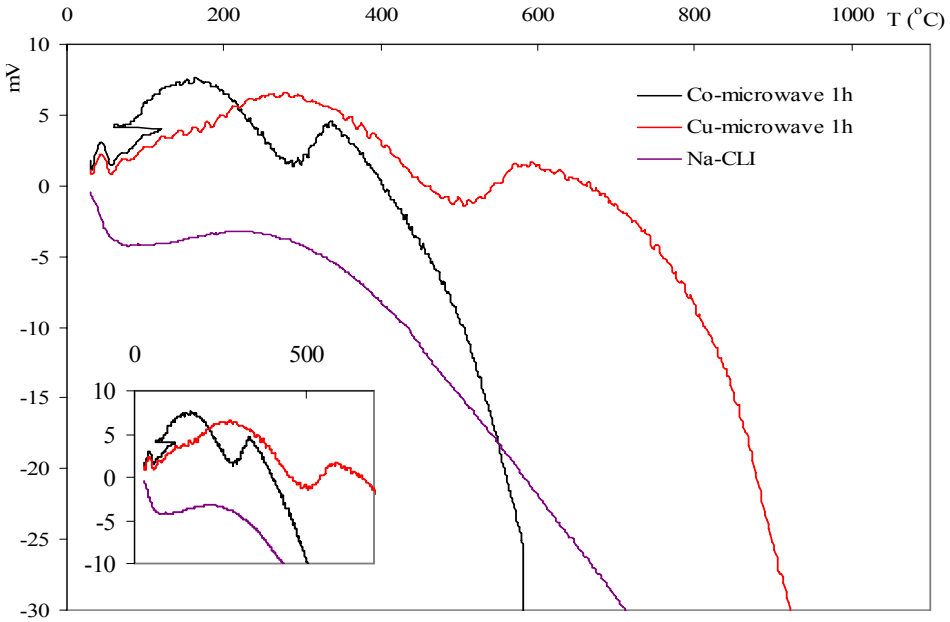

Figure 6.48. DTA curve of Ag^{+}, Co^{2+} and Cu^{2+} exchanged NaCLI .

As seen in DTA curves of Ag^{+}, Co^{2+} and Cu^{2+} exchanged NaCLI low temperature endotherm peaks existed between 25-125 °C in accordance with the

dehydration of physically adsorbed water. The desorption of zeolitic water which is tightly bound to structure is responsible for the major mass loss observed between 200-400 ^{o}C.

Following the DTA figures above, thermal behavior of Co^{2+} and Cu^{2+} exchanged NaCLI did not change as compared to NaCLI. However, due to possible oxidation reaction occurrence in the case of Ag^{+} exchanged NaCLI resulted in exothermic reaction in waterbath treatment case. Si/Al ratio of Ag^{+}, Co^{2+} and Cu^{2+} exchanged NaCLI samples discussed in Figure 6.47 and Figure 6.48 were found higher than 3.80 and may be called thermally stable.

6.8. Kinetic Study of Ag^{+}, Co^{2+} and Cu^{2+} exchange NaCLI

The amount Ag^{+}, Co^{2+} and Cu^{2+} adsorbed (q_t) on NaCLI with time were determined. The sorption kinetics suggested that quite short times are sufficient to achieve equilibrium in all cases as indicated in Figure 6.49. Almost within an hour system reaches to equilibrium therefore further progress to exchanges are not necessary. It has been determined that Ag^{+}, Co^{2+} and Cu^{2+} adsorbed (q_t) on NaCLI with time increased with the decrease of S/L ratio due to increase in solute–solution interaction.

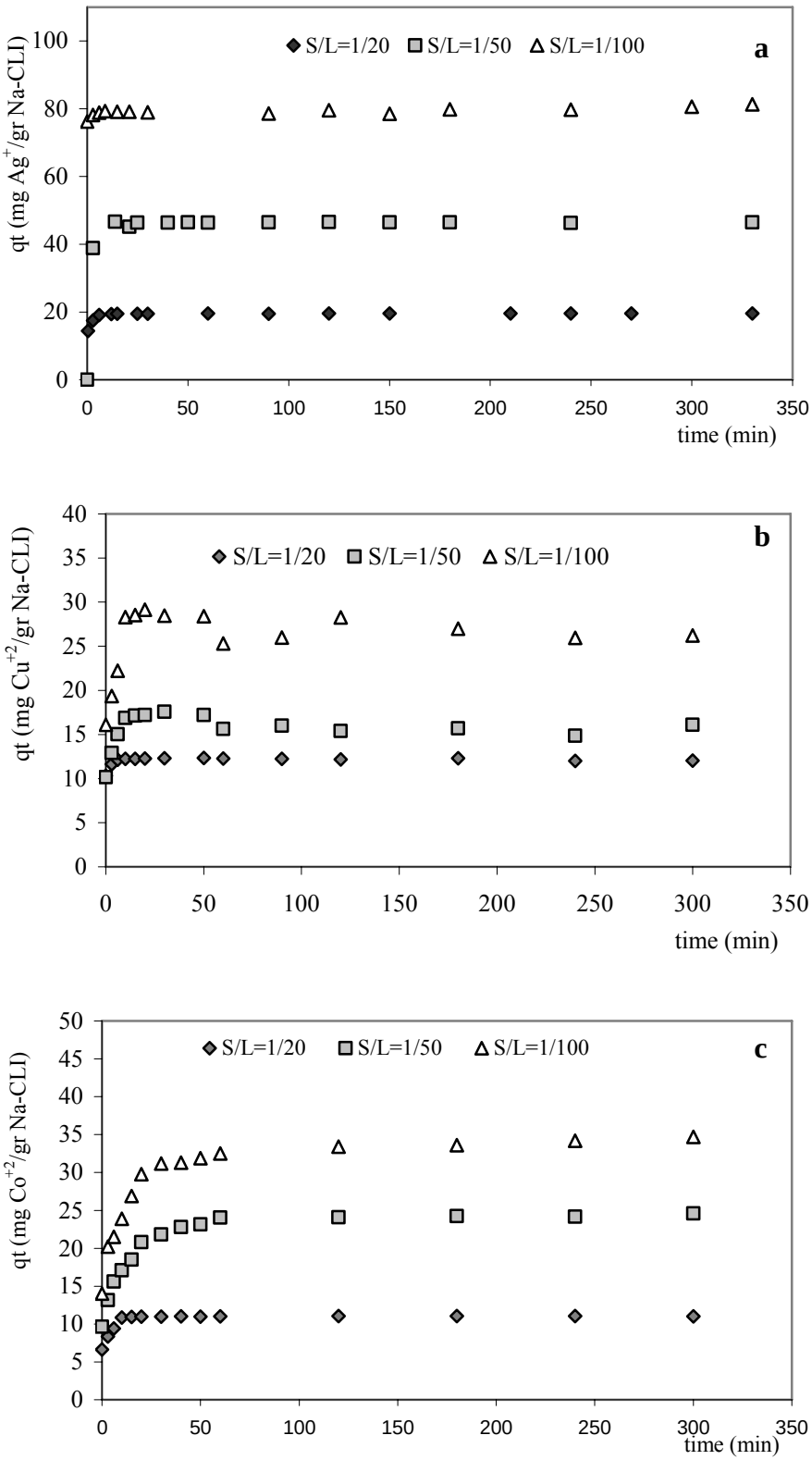

Figure 6.49. Amount adsorbed (q_t) a) Ag^+ b) Cu^{2+} c) Co^{2+} on NaCLI against time.

The rate laws describing the metal ion sorption from batch with different kinetic models, namely, first order, pseudo-first and pseudo-second order are given in between Figures 6.50 and 6.52.

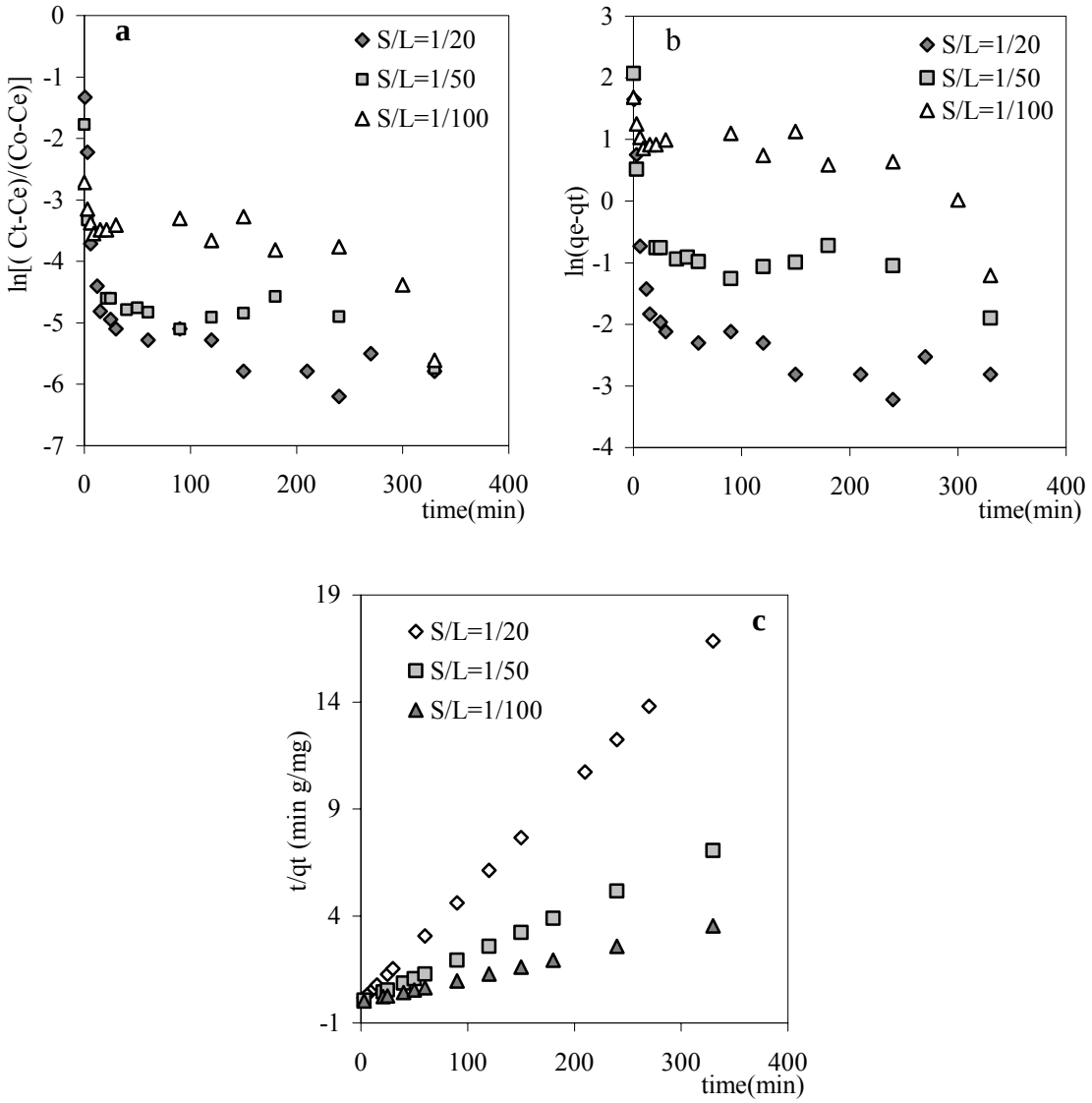

Figure 6.50. a) First order model b) Pseudo-first order model c) Pseudo-second order model for Ag^{+} sorption on NaCLI at 80 ^{o}C.

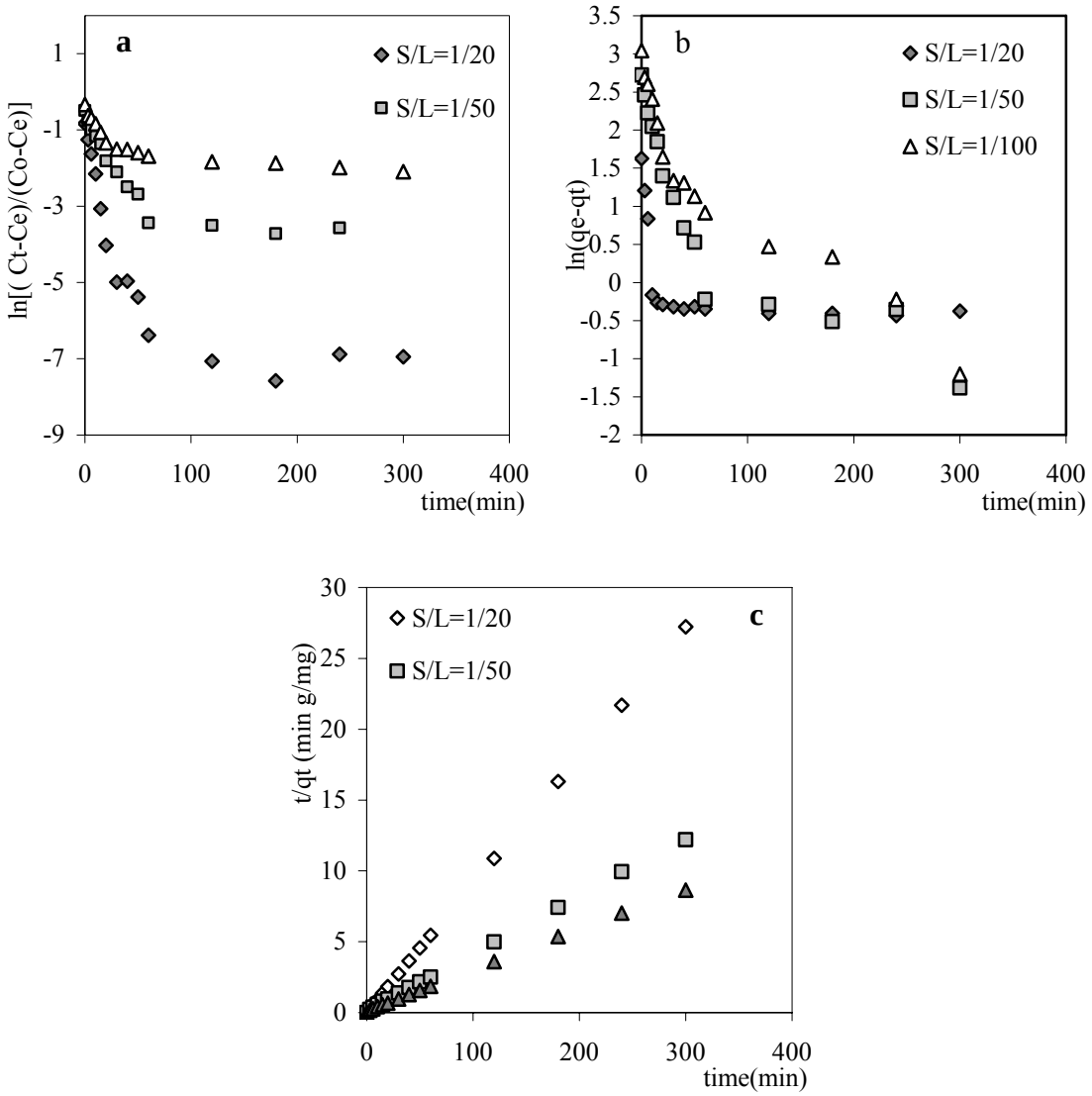

Figure 6.51. a) First order model b) Pseudo-first order model c) Pseudo-second order model for Co^{2+} sorption on NaCLI at 80 ^{o}C.

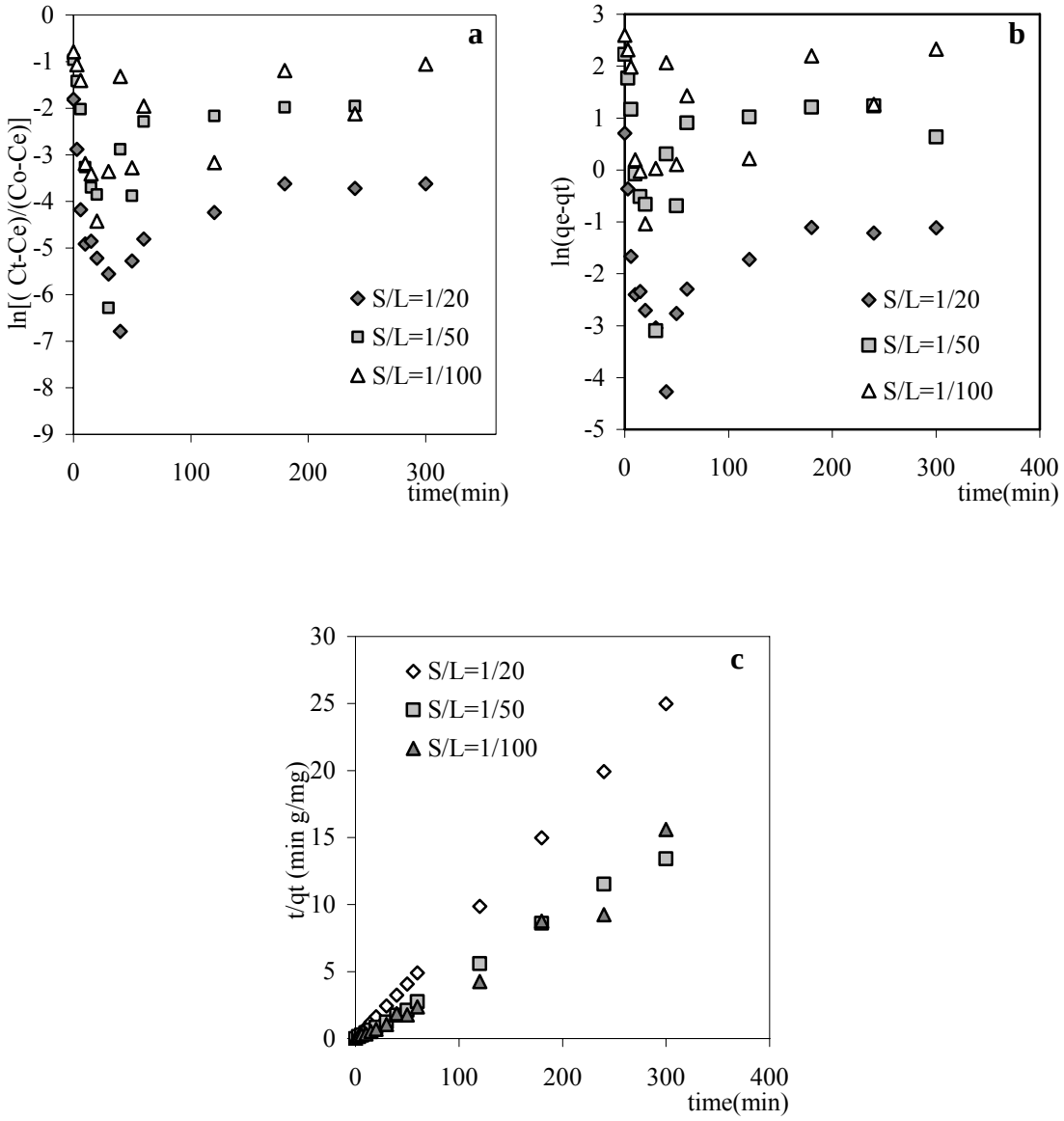

Figure 6.52. a) First order model b) Pseudo-first order model c) Pseudo-second order model for Cu^{2+} sorption on NaCLI at 80 ^{o}C.

Several other studies on the sorption of divalent metals on heterogeneous sorbents show that the kinetics generally follows a pseudo-second order rate law (Jha et al., 2008).The calculated kinetic parameters are given in Table 6.28.

Table 6.28. Kinetic parameters for models.

Parameters	First Order					Pseudo-First Order		Pseudo-Second Order	
	K_C	$k'*10^3$	k_1*10^3	k_1*10^3	R^2	k_1*10^3	R^2	k_2	R^2
Ag^+									
S/L=1/20	0.47	8.10	2.57	5.53	0.43	8.10	0.43	0.30	1
S/L=1/50	0.48	5.70	1.84	3.86	0.35	5.70	0.35	0.09	1
S/L=1/100	0.28	4.70	1.02	3.68	0.66	4.70	0.66	0.04	1
Co^{2+}									
S/L=1/20	0.81	1.87	8.37	10.33	0.58	3.30	0.22	0.27	0.97
S/L=1/50	0.08	1.32	0.99	12.21	0.79	11.5	0.74	0.01	0.98
S/L=1/100	0.04	4.5	0.17	0.43	0.62	11.6	0.85	0.008	1
Cu^{2+}									
S/L=1/20	0.48	0.27	0.88	1.82	<0.10	2.70	<0.10	0.41	1
S/L=1/50	0.06	0.28	0.17	2.63	<0.10	2.80	<0.10	0.56	0.99
S/L=1/100	0.02	0.02	0.08	3.20	<0.10	3.30	<0.10	0.02	0.97

The kinetic experiments for all cases were carried out in 0.01 M metal nitrate solutions in waterbath at 80 ^{o}C for different S/L ratios. The sorption processes of metal-NaCLI systems considered throughout this study did not followed the first and pseudo-first order models however the high values of R^2 for the pseudo-second order kinetic model show the agreement of experimental data.

The external mass transfer coefficient (k_f) and effective diffusion coefficients (D_e) were calculated for all metal-NaCLI systems with different S/L ratios in waterbath at 80 ^{o}C are given in Table 6.29.

Table 6.29. External mass transfer coefficient *(kf)*, pore diffusion coefficient *(D_p)* and Biot Number for (Ag^+, Co^{2+} and Cu^{2+}) ¯NaCLI systems.

Solid/Liquid Ratio	k_f (m/sec)			D_p *(cm^2/sec)*		
	Ag^+	Co^{2+}	Cu^{2+}	Ag^+	Co^{2+}	Cu^{2+}
S/L=1/20	$1.2 \cdot 10^{-04}$	$1.5 \cdot 10^{-04}$	$4.5 \cdot 10^{-04}$	$2.1 \cdot 10^{-06}$	$1.6 \cdot 10^{-07}$	$3.9 \cdot 10^{-07}$
S/L=1/50	$1.3 \cdot 10^{-04}$	$6.2 \cdot 10^{-04}$	$7.2 \cdot 10^{-04}$	$2.1 \cdot 10^{-07}$	$9.8 \cdot 10^{-07}$	$3.1 \cdot 10^{-06}$
S/L=1/100	$5.5 \cdot 10^{-05}$	$5.7 \cdot 10^{-04}$	$2.0 \cdot 10^{-03}$	$2.0 \cdot 10^{-07}$	$1.2 \cdot 10^{-06}$	$9.1 \cdot 10^{-06}$
	Biot Number					
S/L=1/20	1.57		23.17		27.86	
S/L=1/50	17.16		16.00		5.92	
S/L=1/100	7.64		12.01		5.60	

Since rapid initial (up to 3 min) uptake was observed for all sorption processes, mass transport was assumed to be controlled by external-phase mass transfer at earlier stages and by pore-phase mass transfer at later stages. Based on this assumption, the external mass transfer coefficient (k_f) and pore diffusion coefficient (D_p) were calculated using Equation 3.19 and Equation 3.26 and are given in Table 6.29. The k_f and D_p values were found in the range of $10^{-5} – 10^{-3}$ cm^2/sec and $10^{-7} – 10^{-6}$ cm/sec, respectively. The upper limit of Biot number for external mass transfer rate-controlled processes was reported between 10 and 30 for different systems in literature (Ülkü et al., 1998 and Depaoli et al., 1996). The dimensionless Biot numbers for our systems were calculated

using Equation 3.28 indicates that the sorption processes are controlled mainly by external-phase mass transfer. Although the moderate Biot numbers might indicate the validity of both models, solute sorbed (q_t) versus square root of time $t^{1/2}$ did not yield a straight line passing through the origin as indicated in Figure 6.53 supporting the defined mechanism derived by means of Biot number. Thus, external-phase mass transfer mechanism has prominent effect on the sorption process compared to pore-phase mass transfer mechanism. The processes followed the pseudo-second-order model considered at all time intervals based on the sorption kinetics as given in Table 6.28. Therefore, for better evaluation of the dominating mass transport mechanism deeper investigation on the effect of process parameters like the agitation speed, concentration of the metal solutions, particle size of the adsorbent and etc is needed to be considered.

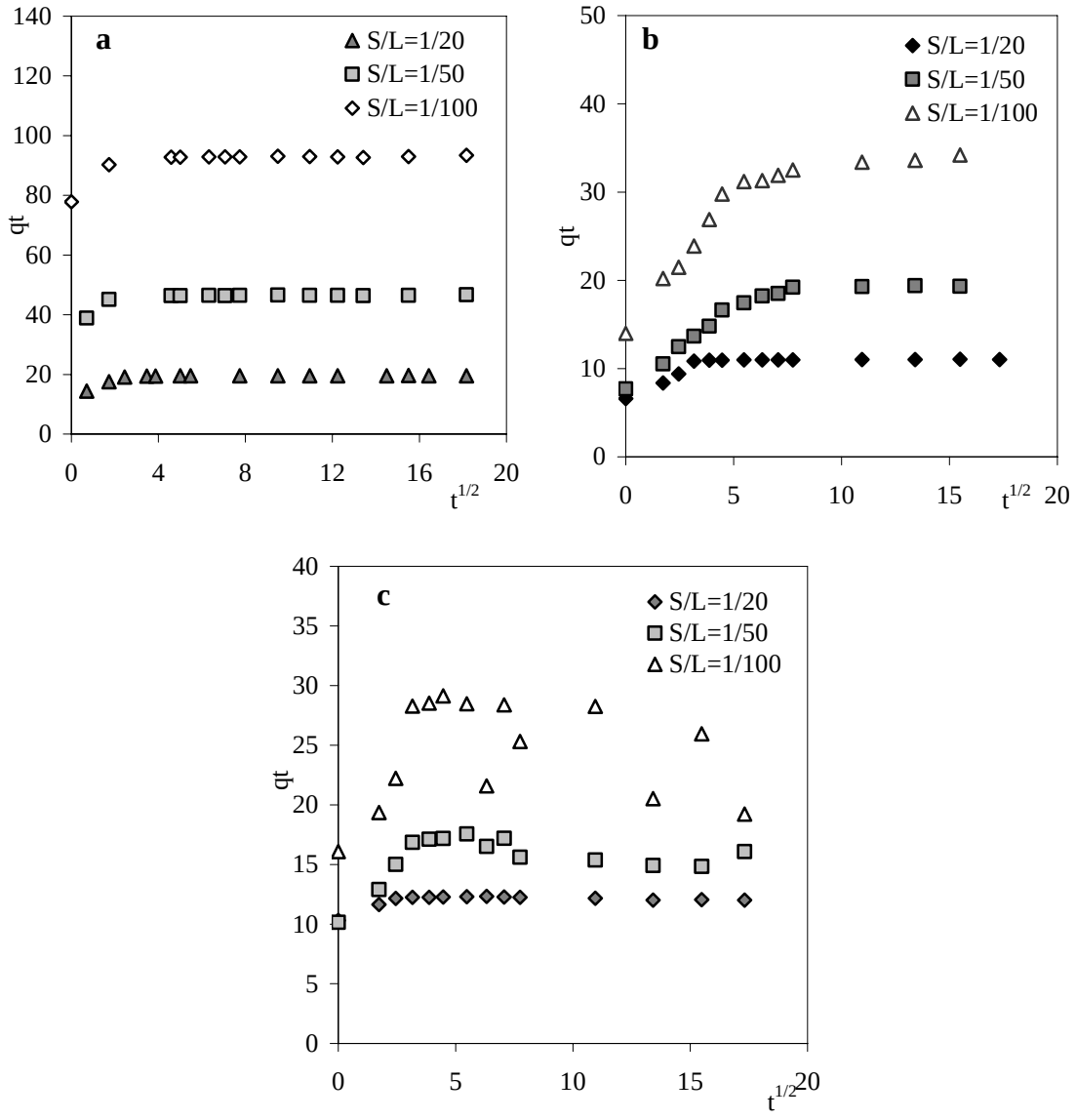

Figure 6.53. q_t versus √time for a) Ag^+ b) Co^{2+} c) Cu^{2+} sorption on NaCLI at 80 ^oC.

6.9. Equilibrium Study of Ag^{+}, Co^{2+} and Cu^{2+} exchange NaCLI

Several isotherm models are available to describe the equilibrium adsorption distribution in which in this study is Langmuir and Freundlich models were used to fit equilibrium data to experimental data. The sorption isotherms of Ag^{+} sorption on NaCLI at different temperatures are given in between Figure 6.54 and Figure 6.56.

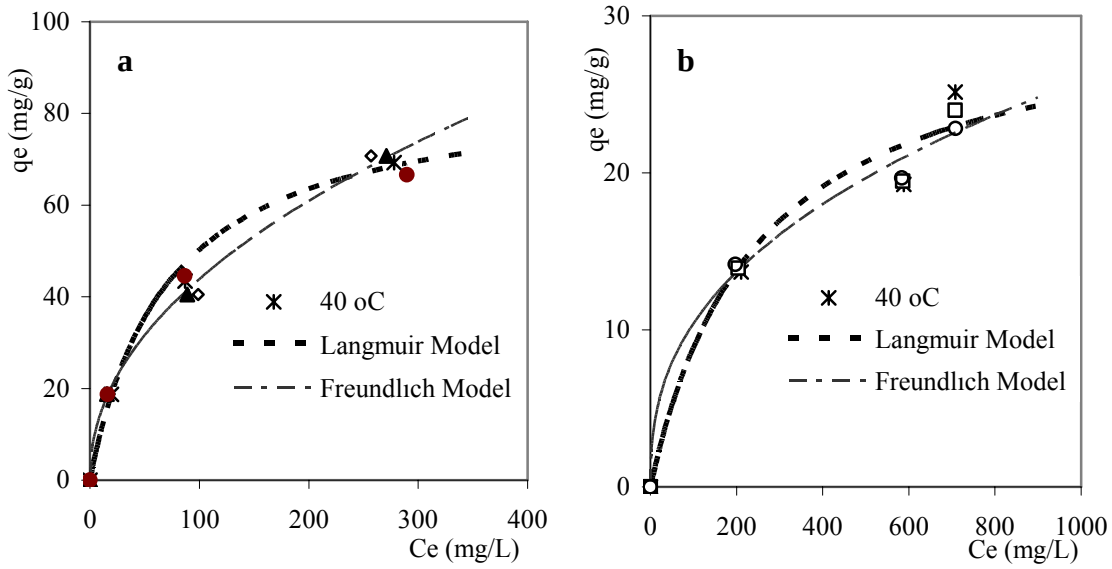

Figure 6.54. Equilibrium Isotherms for sorption of Ag^{+} on NaCLI at 40 ^{o}C a) waterbath b) microwave irradiation.

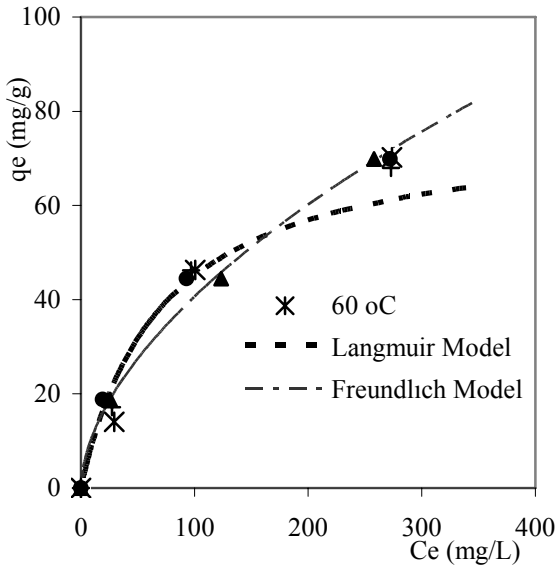

Figure 6.55. Equilibrium Isotherms for sorption of Ag^{+} on NaCLI at 60 ^{o}C (waterbath).

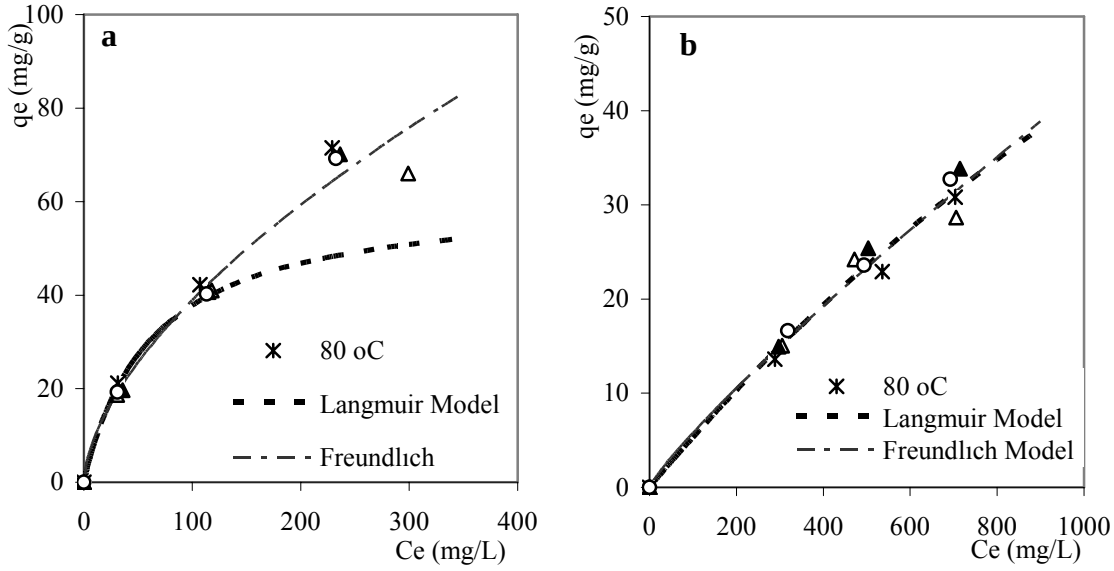

(a) (b)

Figure 6.56. Equilibrium Isotherms for sorption of Ag^{+} on NaCLI at 80 ^{o}C a) waterbath b) microwave irradiation.

The maximum capacity of the Ag^{+} sorption on NaCLI samples has not been reached yet thus higher concentrations should be considered for more accurate results and interpretations. The Langmuir and Freundlich model constant determined from the linearized forms of the model equations are given in Table 6.30 for sorption of Ag^{+} on NaCLI at 40, 60 and 80 ^{o}C.

Table 6.30. Equilibrium constants of for sorption of Ag^+ on NaCLI.

T (^oC)	Langmuir Model				Freundlich Model		
	Q_o	b	R^2	ΔG (kj/mol)	K_f	N	R^2
40′	86.21	0014	0.98	-6.806	4.96	0.21	0.99
60′	90.09	0.012	0.92	-6.458	3.00	1.77	0.95
80′	81.96	0.016	0.92	-7.213	2.40	1.65	0.98
40 ~	31.05	0.004	0.92	-3.404	2.53	1.68	0.94
60~	-	-	-	-	-	-	-
80~	169	0.0003	0.40	2.932	0.11	1.54	0.96

(′ corresponding to waterbath , ~corresponding to microwave irradiation)

As indicated from Table 6.30, the Ag^+ sorption by NaCLI exhibited a good fit to Langmuir model ($R^2 > 0.95$) however; a better fit to Freundlich model was concluded since greater R^2 values which are closer to unity was obtained. The adsorptive behaviors indicate that the sorption takes place on heterogeneous surface, which may be attributed to the various active sites on of NaCLI and it is dominated as a physical sorption process. The theoretical Q_o values calculated from Langmuir model equation are in good agreement with the experimental values determined from kinetic data.

The standard free energy (ΔG°), the enthalpy (ΔH°) and entropy (ΔS°) and their changes are associated with the sorption process therefore it is important to determine them in order to describe the process. van't hoff plots for sorption reaction of Ag^+ onto NaCLI in waterbath and microwave are given in Figure 6.57.

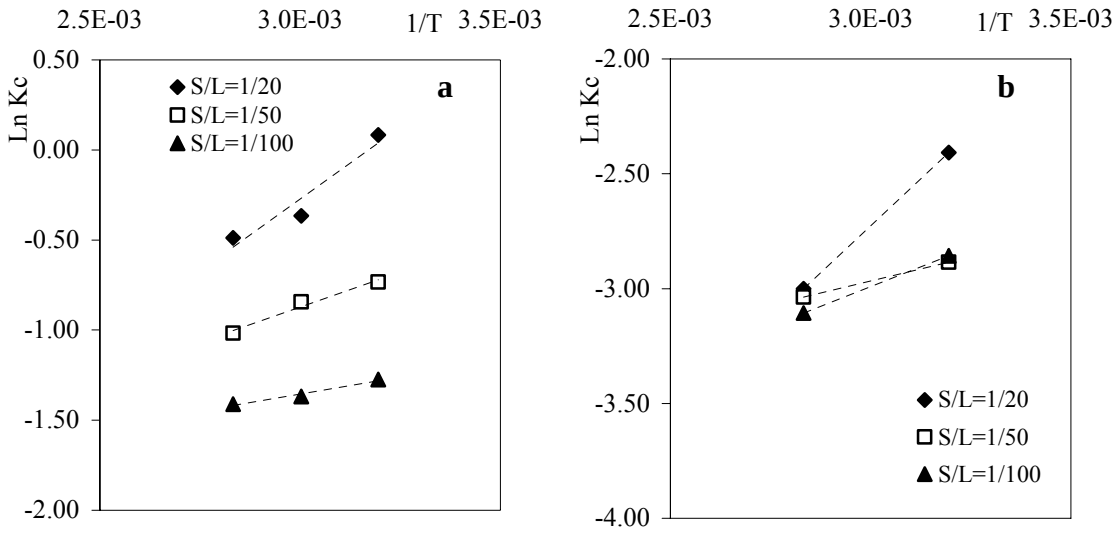

Figure 6.57. Ln K_C versus 1/T for sorption of Ag^+ on NaCLI at 80 ^oC a) waterbath b) microwave irradiation.

Thermodynamic parameters, ΔG°, ΔH^o and ΔS°, determined using von't Hoff plots given in Figure 6.56 for Ag^+ sorption process are given in Table 6.31.

Table 6.31. Thermodynamic properties of Ag^+ Sorption onto NaCLI.

Ag^+	Waterbath Exchange		Microwave Irradiated Exchange	
S/L Ratio	(ΔH°) (kJ /mol)	(ΔS°) (J/mol K)	(ΔH°) (kJ /mol)	(ΔS°) (J/mol K)
1/20	-13.260	-41.98	-13.61	-63.52
1/50	-6.484	-26.682	-3.48	-35.09
1/100	-3.136	-20.69	-5.72	-41.99

The apparent ΔG° is the fundamental criterion of spontaneity. It has been calculated from Langmuir relation (Han et.al, 2008). As indicated in Table 6.12, ΔG^o values are negative and reveals that the reaction occurs spontaneously. In other words, at given conditions system does not gain energy from external resource. ΔH^o value found as negative which is an evidence of exothermic sorption which controlled by physical processes. The negative calculated ΔS° values shows decrease in randomness at the solid-solution interface and no significant changes occur in the internal structure of the adsorbents through the sorption (Han et al., 2008).

The sorption isotherms of Co^{2+} and Cu^{2+} sorption on NaCLI at 80 ^{o}C are given in Figure 6.58 and Figure 6.59, respectively.

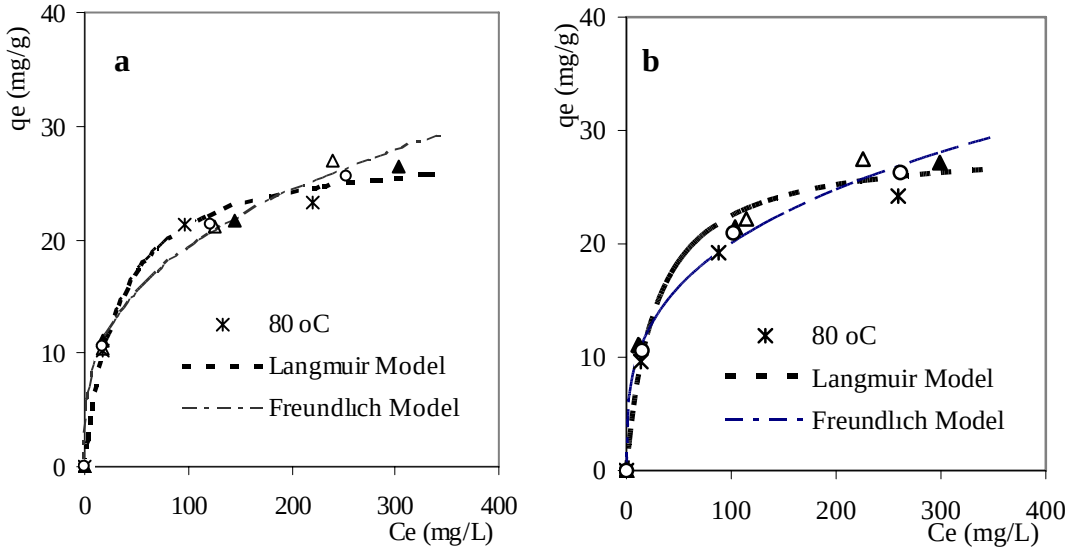

Figure 6.58. Equilibrium Isotherms for sorption of Co^{2+} on NaCLI at 80 ^{o}C a) waterbath b) microwave irradiation.

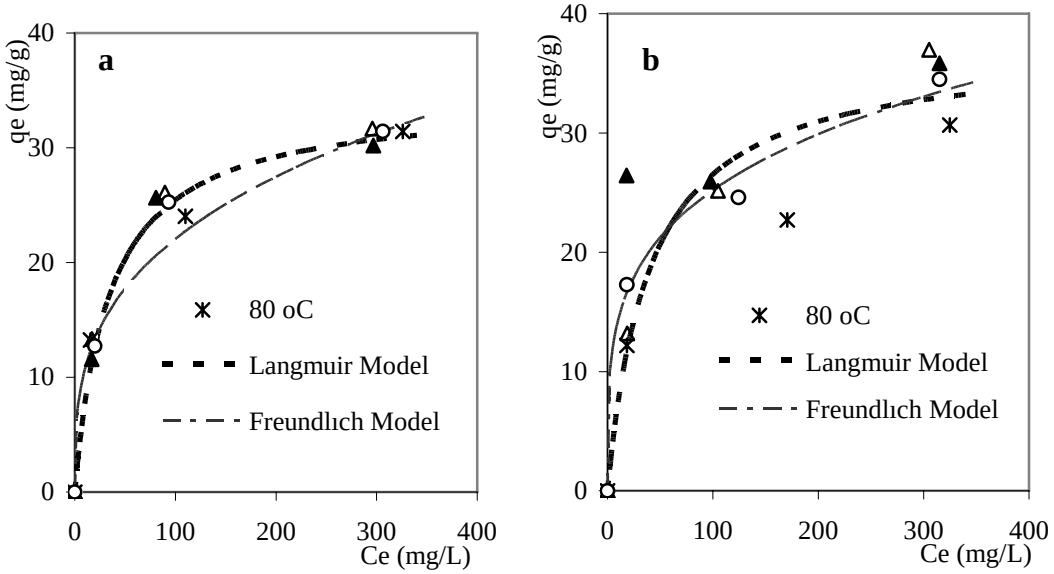

Figure 6.59. EquilibriumIsotherms for sorption of Cu^{2+} on NaCLI at 80 ^{o}C a) waterbath b) microwave irradiation.

The maximum capacity of the NaCLI samples has not been reached for Co^{2+} and Cu^{2+} cases alike the Ag^{+} case thus increasing concentartions should be considered for more accurate comments and interpretations.

Table 6.32. Langmuir and Freundlich constants of Co^{2+} and Cu^{2+} at 80 ^{o}C.

80 ^{o}C	Langmuir Model				Freundlich Model		
	Q_o	b	R^2	ΔG (kj/mol)	K_f	n	R^2
Waterbath *	28.02	0.030	0.99	-8.828	4.13	2.99	0.93
Microwave*	28.74	0.036	0.99	-9.310	4.88	3.26	0.97
Waterbath •	34.24	0.029	0.99	-8.423	5.42	3.16	0.94
Microwave•	34.14	0.025	0.95	-8.101	4.06	4.06	0.95

(* corresponding to Co^{2+} , • corresponding to Cu^{2++})

As indicated from Table 6.32, the Co^{2+} and Cu^{2+} sorption by NaCLI exhibited a good fit to Freundlich model ($R^2 > 0.95$) however; a better fit to Langmuir model was concluded since greater R^2 values which are closer to unity was obtained in contrast to Ag^{+} sorption on NaCLI. The theoretical Q_o values calculated from Langmuir model equation are also in good agreement with the experimental values determined from kinetic data. The adsorptive behaviors indicate that the sorption takes place on homogenous surface by monolayer sorption without interaction between sorbed molecules.

6.10. Antibacterial Test Results of Ag^{+}, Co^{2+} and Cu^{2+} Exchanged NaCLI

Antibacterial activities of the Ag^{+} , Co^{2+} and Cu^{2+} exchanged NaCLI for different set of experiments were determined by the disk diffusion method as discussed in Materials and Method chapter. The measured inhibition zone diameters in four directions

and averaged values for Ag^{+}, Co^{2+} and Cu^{2+} exchanged NaCLI are given in between Table 6.33 and Table 6.35.

Table 6.33. Inhibition Zone Diameters of Co^{2+} exchanged NaCLI (80 ^{o}C, 1hr).

Zone Diameter (mm) / Mineral Code		D1	D2	D3	D4	D_{avg}
S/L=1/20	waterbath	11.95	11.88	11.89	11.73	11.86
	microwave	11.43	11.44	11.48	11.44	11.45
S/L=1/50	waterbath	12.03	11.78	12.05	12.05	11.98
	microwave	11.40	11.39	11.35	11.45	11.40
S/L=1/100	waterbath	11.76	12.09	11.72	11.98	11.89
	microwave	11.39	11.34	11.31	11.42	11.36

Table 6.34. Inhibition Zone Diameters of Co^{2+} exchanged NaCLI (80 ^{o}C, 1hr).

Zone Diameter (mm) / Mineral Code		D1	D2	D3	D4	D_{avg}
S/L=1/20	waterbath	13.65	14.07	13.80	13.89	13.85
	microwave	13.42	13.78	14.24	13.61	13.76
S/L=1/50	waterbath	19.26	19.33	19.36	19.95	19.48
	microwave	19.13	19.14	19.56	19.11	19.24
S/L=1/100	waterbath	20.96	21.42	21.45	21.43	21.32
	microwave	21.90	22.13	21.45	21.76	21.81

Table 6.35. Inhibition Zone Diameters of Cu^{2+} exchanged NaCLI (80 ^{o}C, 1hr).

Zone Diameter (mm) / Mineral Code		D1	D2	D3	D4	D_{avg}
S/L=1/20	waterbath	11.97	12.63	12.23	12.08	12.23
	microwave	11.16	11.23	11.72	11.46	11.39
S/L=1/50	waterbath	14.01	13.97	14.70	14.57	14.31
	microwave	14.10	14.31	14.40	14.43	14.31
S/L=1/100	waterbath	15.98	16.63	16.67	16.01	16.32
	microwave	16.12	15.79	15.86	15.96	15.93

The NaCLI showed no antibacterial activity towards *E.Coli* whie the Ag^{+}, Co^{2+} and Cu^{2+} exchanged NaCLI exchanged samples showed considerable superiority against *E.Coli* in the order of Co^{2+}>Cu^{2+} >Ag^{+}. It is also observed that, the S/L ratio, exchange of time and temperature has slightly affected the inhibition zone diameter. The pictorial representation of NaCLI and Ag^{+} exchanged NaCLI in waterbath and microwave is given in Figure 6.60 in which the inhibition zones around the pellets were clearly detected.

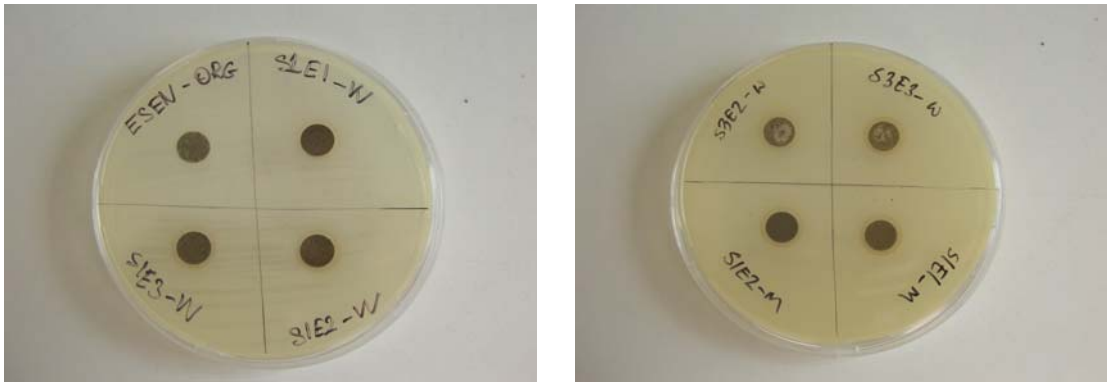

Figure 6.60. Inhibition Zones of NaCLI and Ag^{+} exchanged NaCLI in waterbath and microwave.

The measured inhibition zone diameters in four directions and averaged values for Ag^{+}, Co^{2+} and Cu^{2+} exchanged NaCLI for the utilized parameters are given in Appendix H.

CHAPTER 7

CONCLUSIONS

The main purpose of this study is describing the ion exchange process as a whole and the effect of microwave treatment on ion exchange process which also covers the theoretical background of zeolites, sorption process and microwaves. The effect of microwave irradiation on ion exchange process in zeolites as well as the zeolite properties owing to different cationic forms is important for their possible use in various applications. Therefore investigating the influence of microwave irradiation on ion exchange mechanism and structure of the natural zeolite has great importance and is the main purpose of this study.

The solid phase and liquid phase analysis is very important in determining the exchange mechanism in solid-solution systems therefore in this study both phases were analyzed. It has been concluded that no considerable changes within the solid were observed for the cations Fe^{3+}, Mg^{2+} and K^{+} whereas the changes for the cations Ca^{2+} and Na^{+} were evident for Ag^{+}, Co^{2+} and Cu^{2+} exchange on NaCLI. The higher extent of these cations exchange was explained by the structural location of Na^{+} and Ca^{2+} within the mineral and its lower hydrated radii compared to other cations. The ion exchange degree of Ag^{+}, Co^{2+} and Cu^{2+} on NaCLI for the utilized parameters was determined and concluded that S/L ratio has higher effect. For some parameters microwave treatment was found effective however on the whole it did not significantly increase the ion exchange degree compared to waterbath treatment.

The non-continuity of the microwave power supply of EDMS might have influenced the microwave irradiation efficiency on ion exchange. Besides, applied microwave power was not used with 100% continuous efficiency throughout the total exchange time for EDMS. Although in DMS microwave power was continuous, maximum 50 watts of microwave power was being able to be used for the system. It was claimed that microwave driven ion exchange, the concentration of the metal ion solution has an effect on the extent of ion exchange however for higher Ag^{+}, Co^{2+} and Cu^{2+} ion

concentrations the exchange degree did not increase for microwave as expected. The highest degree of exchange was observed for the Ag^{+} exchange compared to Co^{2+} and Cu^{2+} in both treatments for all cases. As well as the hydrated radii, hydration energies of ions have an influence on exchange degree.

There is a non-stoichiometry between the incoming and outgoing ions for all Ag^{+}, Co^{2+} and Cu^{2+} exchange on NaCLI. Both for waterbath and microwave treatments, the amount of amount of exchangeable cations [$\Sigma(Ca^{2+}+Na^{+}+K^{+}+Mg^{2+})$] release is higher than metal uptake for all Ag^{+}, Co^{2+} and Cu^{2+}-NaCLI systems. This may be due to the hydrolysis of the exchangeable cations with -OH groups in the solution and forming metal-hydroxyl complexes. For the systems considered, ion exchange is assumed to be blocked with the formation of inner-sphere complexes and surface precipitation. Ag^{+}, Co^{2+} and Cu^{2+} exchange on NaCLI is mainly due to ion exchange whereas limited inner-sphere complex formation, dissolution and surface precipitation thought to be existed for the systems considered.

FTIR spectra of metal exchanged forms of NaCLI indicated that no framework dealumination within structure occurred due to the unchanged position of the most intense bands. Introducing the cations into the structure of NaCLI did not distinctly change the peak intensities at 609 cm^{-1} whereas slight changes might due to NaCLI being a natural mineral. Peak intensities of the metal exchanged forms of NaCLI at 3628 cm^{-1}, did not change distinctly. X-Ray patterns of Ag^{+}, Co^{2+} and Cu^{2+} exchanged NaCLI showed no transition of clinoptilolite-heulandite phase and no shifts in characteristic peaks positions of NaCLI. Similarly, SEM micrographs of Ag^{+}, Co^{2+} and Cu^{2+} exchanged NaCLI did not show any structural changes such as shape of clinoptilolite crystals with waterbath and microwave treatments. The Ag^{+}, Co^{2+}, Cu^{2+} exchanged NaCLI showed Type 4 isotherm corresponding to mesoporous structure of Na-LI. The decrease of volume adsorbed determined for Ag^{+}, Co^{2+} and Cu^{2+} exchanged NaCLI was probably due to clogging effect of impurities and framework cations present within the structure.

Desorption of water for the metal exchanged forms of NaCLI started at same temperature but they had been completed at different temperatures. This is related to different cation content of different metal exchanged forms of NaCLI. In addition to TGA, DTA concluded thermal behavior of Co^{2+} and Cu^{2+} exchanged NaCLI showed no significance change in their thermal stability compared to NaCLI however, due to

possible oxidation reaction occurrence in the case of Ag^+ exchanged NaCLI mineral it showed different thermal behavior toward heating upto 1000 ^oC.

It has been concluded from kinetic studies that very short times, almost an hour, is enough for the completion of the process. It has been determined that amount of metal sorbed per gram of NaCLI increased with the decrease of S/L ratio due to increase in solute–solution interaction. The dimensionless Biot number was found in between 2 and 28 for sorption processes thus it has been concluded that mainly external (film) mass-transfer was the controlling mechanism. The processes followed the pseudo-second-order model considered at all time intervals based on the sorption kinetics. For better evaluation of the transport mechanism the process parameters like the agitation speed, concentration of the metal solutions, particle size of the adsorbent and etc is needed to be considered. Equilibrium studies which described by adsorption isotherms showed that Ag^+ sorption on NaCLI fitted to Langmuir model ($R^2 > 0.95$) however; a better fit to Freundlich model was concluded since greater R^2 values which are closer to unity was obtained whereas reverse situation is obtained for Co^{2+} and Cu^{2+} -NaCLI system. The standard free energy (ΔG°), the enthalpy (ΔH°) and entropy (ΔS°) and their changes are associated with the sorption process therefore it is important to determine them in order to describe the process. For the ion exchange process of all cases, the ΔG^o values were determined as negative which showed that reactions were occurred spontaneously. The negative values of ΔH^o and ΔS° were determined for all cases.

It has been concluded from Kirby–Bauer antibacterial tests that NaCLI had no antibacterial activity towards *E.Coli* while the Ag^+, Co^{2+} and Cu^{2+} exchanged NaCLI samples showed considerable superiority against *E.Coli* with following the order determined as; Co^{2+}>Cu^{2+} >Ag^+. Additionally, insignificant effects of S/L ratio, exchange of time and temperature on inhibition zone diameter were found.

Consequently, the microwave irradiation can be proposed as an alternative and reliable method that can be used to prepare an ion-exchanged mineral for different purposes. Higher exchange rates of different cations on clinoptilolite rich mineral could be obtained with higher and continuous microwave power. Microwave interaction with matter is also characterized by a penetration depth, DP, but its effect has not been clearly understood. In that respect, more variations of solid and solution amounts providing different dielectric properties for the system might be considered to explain the DP for the Ag^+, Co^{2+} and Cu^{2+} -NaCLI systems in microwave irradiated process.

REFERENCES

Afzal, M.; G. Yasmeen, M.; Saleem, P.;K.Butt, A. K.; Khattak, J.A. TG and DTA Study of Thermal Dehydration of Metal Exchanged Zeolite 4A Samples. *Journal of Thermal Analysis and Calorimetry*. **2000**, *62*, 721-727.

Akdeniz, Y.; and Ülkü, S.; Microwave Effect on Ion-Exchange And Structure of Clinoptilolite. *Journal of Porous Materials*. **2007,** *14*, 55-60.

Akdeniz, Y. Cation Exchange in Zeolites, Structure Modification by Using a Microwave. MSc. Thesis, İYTE,1999.

Arcoya, A; Gonzalez, J.A.; Llabel, G.; Seona, X.L.; and Travieso, N.; Role of Exchange Cations on The Molecular Sieve Properties of A Clinoptilolite. *Microporous Materials.* **1996,** *7*, 1-13.

Argun, M.E. Use of Clinoptilolite For The Removal of Nickel Ions From Water: Kinetics and Thermodynamics. *Journal of Hazardous Materials*. **2008,** *150*, 587–595.

Autie´,C. G.; Guerra, E.M.; Autie´, P. M.; Moreno-Tost, R.; Rodrı´guez-Castello´, E. Jime´nez-Lo´pez, A. Adsorption Properties of Natural And Cu(II); Zn(II); Ag(I) Exchanged Cuban Mordenites. *Microporous and Mesoporous Materials.* **2008**,*108*, 325–332.

Banik, S.; Bandyopadhyay, S.; Ganguly, S. Bioeffects of Microwave-A Brief Review. *Biosource Technology.* **2003,** *87*, 155-159.

Bekkum, H. V..; Flanigen, E.M.; Jansen, J.C. In *Introduction to Zeolite Science and Practice;* Elsevier Science Publishing Company Inc. Newyork; NY 10010: USA; 1991.

Bektaş, N.; Kara, S. Removal of Lead From Aqueous Solutions By Natural Clinoptilolite: Equilibrium And Kinetic Studies. *Separation and Purification Technology*. **2004**, *39*, 189–200.

Benaliouche, F.; Boucheffa, Y.; Ayrault, P.; Mignard, S.; Magnoux P. NH_3-TPD and FTIR Spectroscopy of Pyridine Adsorption Studies for Characterization of Ag- and Cu-Exchanged X Zeolites. *Microporous and Mesoporous Materials.* **2008**, *111*, 80-88.

Bish, D.L. Effects of Composition on The Dehydration Behavior of Clinoptilolite And Heulandite. In *Natural Zeolites Occurrence; Properties and Use*. Pergamon Press: 1978.

Blanchard, G.; Maunaye, M.; Martin, G. Removal of Heavy Metals from Wastewater by Means of Natural Zeolites. *Water Research*. **1984***, 18*, 1501-1507

Breck, D.W. *Zeolite_Molecular Sieve; Structure; Chemistry and Use*; by John Wiley and Sons; Newyork: 1974.

DePaoli S.M.; Perona J.J. Model for Sr-Cs-Ca-Mg-Na Ion Exchange Uptake Kinetics on Chabazite. AIChE. **1996,** 42 (12), 3434-3441.

Dyer, A.; White, K.J. Cation Diffusion In The Natural Zeolite Clinoptilolite. *Thermochimica acta.***1999**, *340*; 341-348.

Can, Ö. Ion Exchnage In Natural Zeolite Packed Column. MSc. Thesis, İYTE, 2003.

Cansever, B. Treatment of Domestic Wastewater With Natural Zeolite. MSc. Thesis, İYTE, 2003.

Castaldi, P.; Santona, L.; Enzo, S.; Melis, P. Sorption Processes And XRD Analysis of a Natural Zeolite Exchanged With Pb^{2+}; Cd^{2+} And Zn^{2+} Cations. *Journal of Hazardous Materials.* **2005**, 734, 99-105.

Castaldi, P.; Santona, L.; Cozza, C.; Giuliano, V.; Abbruzzese, C.; Nastro V.; Melis, P. Thermal And Spectroscopic Studies of Zeolites Exchanged with Metal Cations. *Journal of Molecular Structure,* **2008**, *156*, 428-434.

Chiang H.L.; Tsai H.J.; Chang G.M.; HsuY.H. Adsorption Kinetic Characteristics of H_2S on Activated Carbon, *Adsorption*, **2002**, 8, 325–340.

Chitrakar, R.; Kanoh, H.; Miyai, Y.; Oi, K. Rapid Communication: Synthesis of 0-$LiMnO_2$ by Microwave Irradiation and Study Its Heat Treatment and Lithium Exchange. *Journal of Solid State Chemistry*; **2002**, *163*; 1-4.

Christidis, G.E.; Moraetis, D.K.; Akhalbedashvilli, M.; Kekelidze, N.; Gevorkyan, R.; Yeritsyan, H.; Sargsyan, H. Chemical And Thermal Modification of Natural HEU-Type Zeolitic Materials From Armenia; Georgia and Greece. *Applied Clay Science.*; **2003**, *24*, 79-91.

Colic, M. Natural zeolite Clinoptilolite: New Adjuvant in Anticancer Therapy. *Journal Mol. Medical*. **2001,** *78*; 708-720.

Cruciani, G. Zeolites upon heating: Factors Governing Their Thermal Stability and Structural Changes. *Journal of Physics and Chemistry of Solids*. **2006**, *67*, 1973-1194.

Cullity, B.D.In *Elements of X-ray Diffraction*, 2nd Ed. Addison-Wesley:1978.

Çağın, V. Use of Clinoptilolite for Copper and Nickel Removal from Aqueous Solutıons; MSc. Thesis, METU, 2006.

Dyer A.; In *Introduction to Molecular Sieves.* John Wiley and Sons; Newyork, 1988.

Dyer, A.; White, K.J. Cation Diffusion in The Natural Zeolite Clinoptilolite. *Thermochimica Acta*; **1999,** *340,* 341-348.

Doretea M.S.; Pivac, H. The Effect of Natural Clinoptilolite on the Serotonergic Receptors in The Brain of Mice With Mammary Carcinoma. *Life Sciences*; **2003**, *73*, 2059-2069.

Doula, M.; Ioannou, A.; Dimirkou, A. Copper Adsorption and Si; Al; Ca; Mg and Na Release from Clinoptilolite. *Journal of Colloid and Interfaces Science.* **2002,** *245*, 237-250.

Doula, M.; Ioannou, A. The Effect of Electrolyte Anion on Cu Adsorption–Desorption by Clinoptilolite. *Microporous and Mesoporous Materials*. **2003**, *58*, 115-130.

Duvarcı, Ç.Ö.; Akdeniz, Y.; Özmıhçı, F.; Ülkü, S.; Balköse, D.; Çiftçioğlu, M. Thermal Behaviour of a Zeolitic Tuff. *Ceramics International.**2007***, *33*; 795-801.

Elaiopoulos, K.; Perraki, T.; Grigoropoulou, E. Mineralogical Study and Porosimetry Measurments of Zeolites From Scaloma Area, Thrace; Greece. *Microporous and Mesoporous Materials*; **2008** , *112*; 441-449.

Englert, A.H.; Rubio, J. Characterization And Environmental Application of a Chilean Natural Zeolite. *International Journal of Mineral Processing. **2005*** , *75*; 21-29.

Erdem, E.; Karapınar, N.; Donat, R. The Removal of Heavy Metal Cations by Natural Zeolites. *Journal of Colloid and Interface Science;* **2004**, *280*. 309-314.

Ersoy, B.; Çelik, M.S. Electromagnetic Properties of Clinoptilolite With Mono-and Multivalent Electrolytes. *Microporous and Mesoporous Materials* **2002**, *55*; 305-312.

Esenli, F.; Kumbasar, I. Thermal Behaviour of Heulandites and Clinoptilolites of Western Anatolia. *Zeolites and Related Microporous Materials: State of the Art.* **1994,** *84*, 645-651.

Godelitsas, A.; Armbuster,T. HEU-Type Zeolites Modified by Transition Elements and Lead. *Microporous and Mesaporus Materails.* **2003**, *61*, 3-24.

Gottardi, G.; Galli, E. In *Minerals Rocks, Natural Zeolites*. Goresy and Heidelberg Springer-Verlag; Berlin,1985.

Göktaş, S. A Novel Drug Carrier System Using Clinoptilolite For Ginkgo Biloba Leaf Extract; MSc. Thesis, İYTE, 2003.

Grce, M.; Kresimir, P. Antiviral Properties of Clinoptilolite. *Microporous and Mesaporus Materails.* **2005,** *79,* 165-169.

Gruner, J.E.; Ming, D.W.; Henderson, K.E.; Galindo, C.J. Common Ion Effects in Zeoponic Substrates: Wheat Plant Growth Experiment. *Microporous and Mesoporous Materials.* **2003,** *61*, 223-230.

Han, Y.; Ma, H.; Qui, S.; Xiao, F.S. Preparation of Zeolite A Membranes by Microwave Heating. *Microporous and Mesoporous Materials.* **1999,** *30*, 321-326.

Haque, K.E. Microwave Energy for Mineral Treatment Processes-A Brief Review. *International Journal of Mineral Processing*. **1999**, *57*, 1-24.

Higgins F.M.; Leeuw N.H. and Parker S.C. Modeling ohe Effect of Water on Cation Exchange in Zeolite A; *Journal of Materials Chemsitry.* **2002,** 12, 124-131.

Inglezakis, V.J.; Loizidou, M.D.; Grigoropoulou, H.P. Effect of Pore Clogging on Kinetics of Lead Uptake by Clinoptilolite. *Journal of Colloid and Interface Science*. **1999,** *215,* 54-57.

Inglezakis, V.J.; Loizidou, M.D.; Grigoropoulou, H.P. Equilibrium and Kinetic Ion Exchange Studies of Pb^{2+}; Cr^{3+};Fe^{3+} and Cu^{2+} on Natural Clinoptilolite. *Water Research*. **2002,** *36*, 2784-2792.

Inglezakis, V.J.; Loizidou, M.D.; Grigoropoulou, H.P. Ion Exchange Studies on Natural and Modified Zeolites And The Concept of Exchange Site Accessibility. *Journal of Colloid and Interface Science*. **2004**, *275;* 570-576.

Jha, K.M; Matsuda, M.; Miyake, M. Sorption Properties of The Activated Carbon-Zeolite Composite Prepared From Coal Fly Ash for Ni^{2+}; Cu^{2+}; Cd^{2+} and Pb^{2+}. *Journal of Hazardous Materials.* **2008,** 160, 148–153.

Joshi, U.D.; Joshi, P.N. ; Tamhankar, S.S.; Jıoshi, V.P.; Idage, B.B.; Joshi, V.V.; Shiralkar, V.P. Influence of The Size of The Framework Monovalnet Cations In X- Type Zeolite on Their Thermal Behaviour. *Thermoactica Acta.* **2002,** 387, 121-130.

Kaçmaz, H.; Köktürk, U. Geochemistry and Mineralogy of Zeolitic Tuffs From the Alaçatı (Çeşme) Area; Turkey; *Clays and Clay Minerals.* **2004**, *52*, 705–713.

Karadağ, D.; Koç, Y.; Turan, M.; Armağan, B. Removal of Ammonium Ion from Aqueous Solution Using Natural Turkish Clinoptilolite. *Journal of Hazardous Materials.* **2006,** *136*, 604–609.

Karger, J.; Ruthven, D. M. *Diffusion in Zeolites and Other Microporous Solids;* John Wiley and Sons: New York, 1992.

Katsuki, H.; Furuta, S. Microwave Versus Conventional Hydrothermal Synthesis of Nay Zeolite. *Journal of Porous Materials.* **2001**, 8, 5-12.

Knowlton, G.D.; White, T.R. Thermal Study of Types of Water Associated with Clinoptilolite. *Clays and Clay Minerals*. **1981,** *29*, 404-411.

Kingston, Howard M. *Microwave-Enhanced Chemistry*; H.M.Kingst: 1997

Korkuna, O.; Leboda, R.; Skubiszewska-Zieba, J.; Vrublevs'ka, T.; Gun'ko ,V.M.; Ryckowski J. Structural And Physicaochemical Properties of Natural Zeolites: Clinoptilolite And Mordenite. *Microporous and Mesaporous Materials.* **2005,** *87*, 243-254.

Kuroda, Y; Okamoto, T; Kumashiro, R; Yoshikawa, Y; Nagaoi M. Microwave-Assisted Simple Ion-Exchange of ZSM-5-Type Zeolites With Copper Ions and Their Specific Adsorption Properties For N_2 Molecules at Room Temperature. *Chemical Communications.* **2002,** 1758-1759.

Lam, A; Sierra, L.R.; Rojaz, G.; Rivera, A.; Rodriguez-Fuentes, G.; Montero, L.A. Theoretical Study of Physical Adsorption of Aspirin on Natural Clinoptilolite. *Microporous and Mesaporous Materials.* **1998,** *23*; 247-252.

Langella, A.; Pansini, M.; Cerri, G ; Cappellett, P. ; De'gennaro, M. Thermal Behavior of Natural And Cation Exchanged of Clinoptilolite from Sardina (Italy). *Clays and Clay Minerals,* **2003,** *51*,625-633.

Loizidan, M.; Townsend, P. Ion Exchanges Properties of Natural Clinoptilolite; Ferrite And Mordenite Part 2. Lead-Sodium and Lead-Ammonium Equilibria. *Zeolites*. **1987,** 153-157.

Lopes, J.M.; Serralha, F.N.; Costa, C.; Lemos, F.; Ribeiro, R. Preparation of Hnay Zeolite by Ion Exchange under Microwave Treatment. A Preliminary Study. *Catalysis Letters*.**1998,** *53*, 103-106.

Misshra, D. I. X-Ray and Thermal Studies on Zeolite-13X And Its Mn(II) and Zn(II) Exchange and Adsorbed Derivatives; *Studies Surface Science And Catalysis.* **2004,** *154*, 1693-1699.

Monsef-Mirzai, P; Kavanagh, DM; Bodman, S; Lange, S; McWhinnie, WR. Microwave Enhanced Ion Exchange of Cationic and Anionic Clays. *Journal of Microwave Power Electromagnetic Energy.* **1999,** *34*, 216-201.

Mozgawa, W. The Influence of Some Heavy Metals Cations on the FTIR Spectra of Zeolites. *Journal of Molecular Structure*. **2000,** *555*; 299-304.

Mumpton, F.A. Natural Zeolites; Where Have We Been; Where Are We Going.*'4th FEZA Euroworkhop on Zeolites. Natural Zeolites: Occurance, Properties* and *Use.* Italy. **1997**.

Mumpton, F.A. Uses of Natural Zeolites in Agriculture and Industry *Proceedings of the National Academy of Sciences of the United States of America***. 1999,** *96*, 3463-3470.

Mumpton, F.A. *Natural Zeolites; Occurrence; Properties and Use*. Pergamon Press; 1978.

Narin G. Chromatographic Study of Carbon Monoxide Adsorption in Clinoptilolite. MSc. Theis, İYTE, 2001.

Negiş, F. Zeolite Based Composites in Energy Storage. MSc. Thesis, İYTE, 1999.

O'Connor, J.F.; Rodney, P.; Townsend J. Exchange of Lead (II) Ions in Synthetic Faujasitic Zeolites: Th Effect of Framework Charge. *Zeolites;* **1985,** *5*, 158-205.

Ohgushi, T.; Komarneni, S.; Bhalla A.S. Mechanism of Microwave Heating of Zeolite A. *Journal of Porous Materials* .**2001,** *8*, 23-35.

Ohgushi, T.; Numata, T. Importance of Site III Cation of Zeoite A in Microwave Heating. *Journal of Porous Materials*. **2003**, *10*, 207-211.

Ozmıhçı, F. Polypropylene-Natural Zeolite Composite Films. MSc. Thesis, İYTE, 1999.

Palaban, T.R. Thermodynamics of Ion Exchange Between Clinoptilolite and Aqueous Solutions of Na^{+}/K^{+} And Na^{+}/Ca^{2+}. *Geochimica et Cosmochimica Acta.* **1994,** *58*; 4573-4590.

Pavelic, K.; Hadzija, M.; Bedrica, L.; Pavelic, J; Dikic, I.; Katic, M.; Kralj, M.; Bosnar, MH.; Kapitanovic, S.; Poljak-Blazi, M.; Krizanac, S.; Stojkovic, R.; Jurin, M.; Subotic, Perić, J.; Trgo, M.; Medvidović, N.V. Removal of Zinc; Copper and Lead by Natural Zeolite-A Comparision of Adsorption Isotherms. *Water Research.* **2004,** *38,* 1893-1899.

Perraki, T.; Orfanaudaki, A. Mineralogical Study of Zeolites from Pentalofos Area; Thace; Greece. *Applied Clay Science.* **2004,** *25*, 9-16.

Pilter, Z.; Szabo, S.; Hasznos-Nezdei, M.; Pallai-Varsayni, E. X-Ray Diffraction Study of the Effect of Microwave Treatment of Zeolite NaX. *Microporous and Mesoporous Materials.* **2000,** *40*, 257-262.

Papaionnou, D.S.; Kyriakis, C.S.; Alexopoulos, C.; Tzika, E.D.; Polizopoulou, Z.S.; Kyriakis, S.C. A Field Study on The Dietry Use of Clinoptilolite-Rich Tuff; Alone or in Combination with Certain Antimicrobials; on the Health Status and Performance of Weaned; Growing and Finishing Pigs; *Research in Veterinary Science*; **2003,** *76*; 19-29.

Rivera-Garza, M.; Olguin, M.T.; Garcia-Sosa, I.; Alcantara, D.; Rodriguez-Fuentes G. Silver Supported on Natural Mexican Zeolite as an Antimicrobial Material. *Microporous and Mesoporous Materials.* **2000,** *39*, 431-444.

Rodriguez-Fuentes, G.; Barrios, M.A.; Iraizoz, A.; Perdomo, I.; Cedre, B. Enterex : Anti-Diarrheic Drug Based on Purified Natural Clinoptilolite. *Zeolites*; **1997,** *19*, 441-448.

Rodriguez-Fuentes, G.; Ruiz-Salvador, A.R.; Mir, M.; Picazo, O.; Quintana, G.; Delgado, M. Thermal And Cation Influence on IR Vibrations of Modified Natural Clinoptilolite. *Microporous and Mesoporous Materials.* **1998**, *20*, 269-281.

Romero, M.D.; Ovejero, G.; Uguina, M.A.; Rodriguez, A.; Gomez, J.M. Fast Removal of the Acid Properties in the NaX Zeolite by Ion Exchange under Microwave Heating. *Catalysis Communications.* **2004,** *5*, 157-160.

Ruthven; D. *Principles of Adsorption and Adsorption Processes*; John Wiley and Sons, Newyork, 1984.

Sari, A.; Tuzen, M; Citak, D.; Soylak, M. Equilibrium; Kinetic and Thermodynamic Studies of Adsorption of Pb (II) from Aqueous Solution onto Turkish Kaolinite Clay. *Journal of Hazardous Materials*. **2007,** *149,* 283-291.

Semmens, M.J.; Seyfarth, M. The Selectivity of Clinoptilolite for Certain Heavy Metals. *Environmental Science and Technology.* **1975**, *11*, 517-526.

Šljivić, M.; Smičiklas, I.; Pejanović, S.; Plećaš, I. Comparative Study of Cu^{2+} Adsorption on a Zeolite; A Clay And a Diatomite From Serbia. *Applied Clay Science*., **2009,** *43*, 33-44.

Stout S.; Komarneni S. A Microwave-Assisted Method for the Rapid Removal of K from Phlogopite. *Clays and Clay Minerals.* **2002,** *50*, 248-253.

Stumm, W.; James, J. Aquatic Chemical Kinetics. In *Reaction Rates of Processes in Natural Waters Environmental Science and Technology*. Wiley-Inter Science Series of Texts and Monographs, 1990.

Tomasevic-Canovic, M.; Dakovic, A.; Markovic, V.; Stojsic, D. The Effect of Exchangeable Cations in Clinoptilolite and Montmorillonite Non The Adsorption of Aflatoxin B1. *J.Serb. Chem. Soc*. **2001,** *66*, 555-561.

Tomasevic-Canovic, M. Purification of Natural Zeolite-Clinoptilolite for Medical Application-Extraction of Lead. *Journal of Serbian Chemical Society.* **2005***, 70,* 1335-1345.

Top, A.; Ülkü , S. Silver; Zinc And Copper Exchange in A Na-Clinoptilolite and Resulting Effect on Antimicrobial Activity. *Applied Clay Science.* **2004,** *27*, 13-19.

Top, A. Cation-Exchange (Ag;Cu;Zn) Behavior of Natural Zeolites. MSc. Thesis, İYTE, 2001.

Trgo, M.; Peric, J. Interaction of the Zeolitic Tuff With Zn-Containing Simulated Pollutant Solution. *Journal of Colloidal Science and Interface Science*. **2003,** *260*, 166-175.

Trgo, M.; Peri´c, J.; Vukojevi´c, M.N. A Comparative Study of Ion Exchange Kinetics in Zinc/Lead—Modified Zeolite-Clinoptilolite Systems. *Journal of Hazardous Materials*. **2006**, *316*, 938-945.

Tsitsishvilli, G.V.; Andronikashhvilli, T.G; Filizova, L.D.; Kırov, G.N. *Natural Zeolites*: Ellis Horwood Limited, England, 1992.

Türkmen, M. Removal of Heavy Metals from Wastewaters by Use of Natural Zeolites. MSc. Thesis, İYTE, 2001.

Ülkü, S. Application of Natural Zeolites in Water Treatment. Çevre ‘84-Umwelli ’84; V. Deutch- Turkisches Symposium fur Unweltingenieurwesen.

Ülkü, S.; Balköse, D.; Çağa, T., Özkan, F.; Ulutan, S. A Study of Adsorption of Water Vapour on Wool under Static and Dynamic Conditions, *Adsorption*, **1998,** 4, 63–73.

Vimonses, V; Lei, S.; Jin, B.; Chow, C.W.K.; Saint, C. Kinetic Study And Equilibrium Isotherm Analysis of Congo Red Adsorption by Clay Materials. *Chemical Engineering Journal.* **2009,** *148*, 454-464.

Vujakoviæ, A**.**D.; Djurièiæ, M.A.; Tomaeviæ-Èanoviæ, M.R. Thermal Study of Surfactant and Anion Adsorption on Clinoptilolite. *Journal of Thermal Analysis and Calorimetry*. **2001,** *63*, 161-172.

Wang, X.S.; Huang, J.; Hu, H.O.; Wang, J.; Qin Y. Determination of Kinetic and Equilibrium Parameters of the Batch Adsorption of Ni(II) from Aqeous Solutions by Na-Mordenite. *Journal of Hazardous Materials.* **2007,** *141*, 468-476.

Wathey, B.; Tierney, J.; Lidstrom, P.; Westman, J. The Impact of Microwave-Assisted Organic Chemistry on Drug Discovery. *Research Focus* **2002**, *7*, 373-380.

Whittington, B.J.; Milestone, N.B. The Microwave Heating of Zeolites. *Zeolites*. **1992**, 815-818.

Woods, R-M.; Gunter, M.E. Na-And Cs-Exchange in a Clinoptilolite: Analysis of the Outgoing Cations in Solution. *American Mineralogist*. **2001**, *86*, 424-430.

Xu, X.; Yang, W; Liu, J.; Lin, L. Synthesis of Naa Zeolite Membrane by Microwave Heating. *Separation and Purification Technology*. **2002,** *25*, 41–249.

Xu, R.; Pang, W.; Yu, P.; Hup, Q; Chen. J. Chemistry of Zeolites and Related Porous Materials: Synthesis and Structıure; Wiley, 2007.

Yin, D.; Yin, D. The Dispersion and Solid State Ion Exchange of $ZnCl_2$ onto the Surface of NaX Zeolite Using Microwave Irradiation. *Microporous and Mesoporous Materials*. **1998,** *24*, 123-126.

APPENDIX A

SOLID PHASE ICP RESULTS

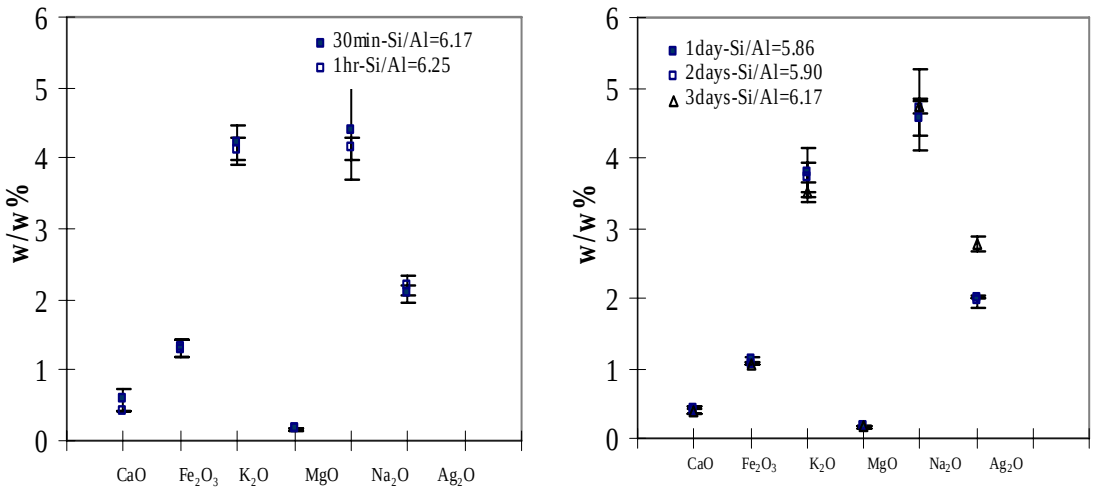

Figure A.1. Solid phase ICP results (0.01 M $AgNO_3$, 40 ^oC, S/L=1/20, waterbath).

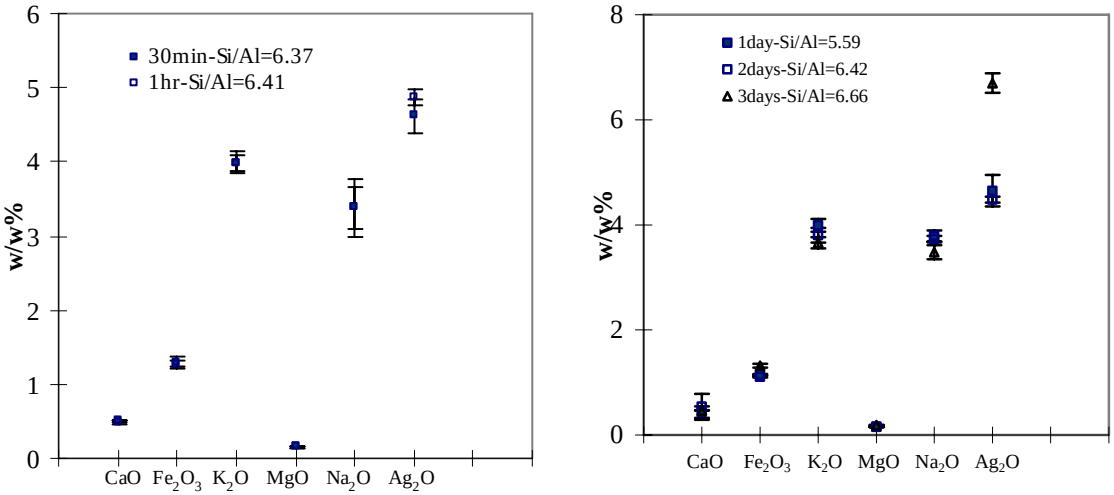

Figure A.2. Solid phase ICP results (0.01 M $AgNO_3$, 40 ^oC, S/L=1/50, waterbath).

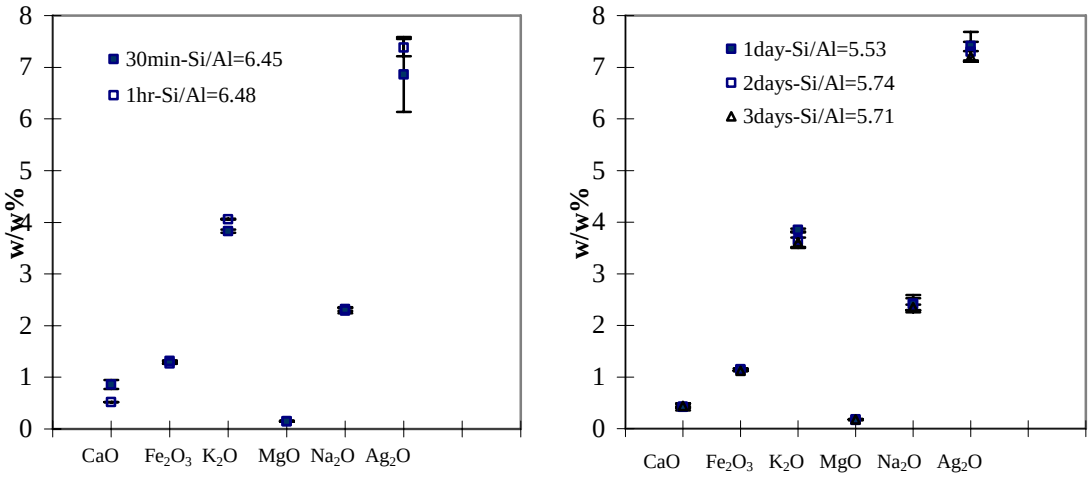

Figure A.3. Solid phase ICP results (0.01 M $AgNO_3$, 40 ^oC, S/L=1/100, waterbath).

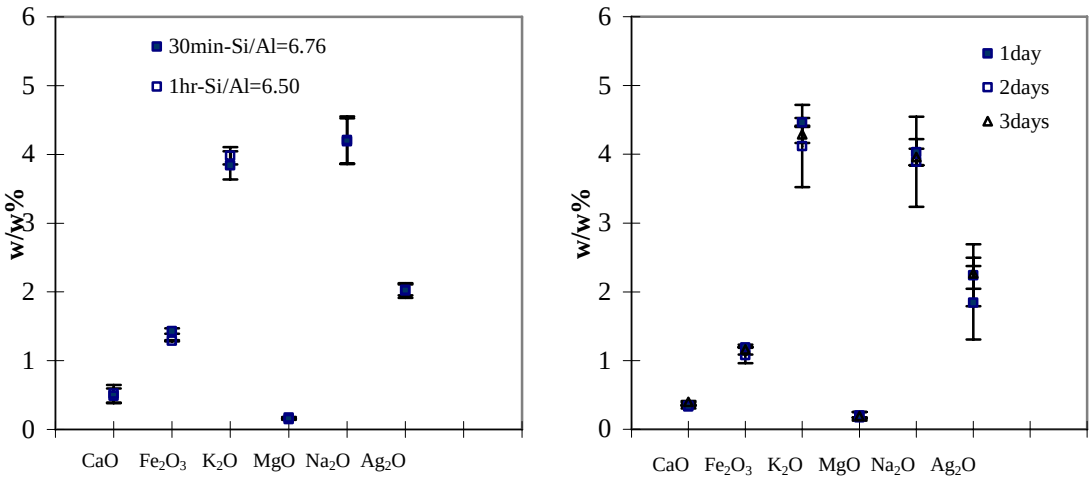

Figure A.4. Solid phase ICP results (0.01 M $AgNO_3$, 60 ^oC, S/L=1/20, waterbath).

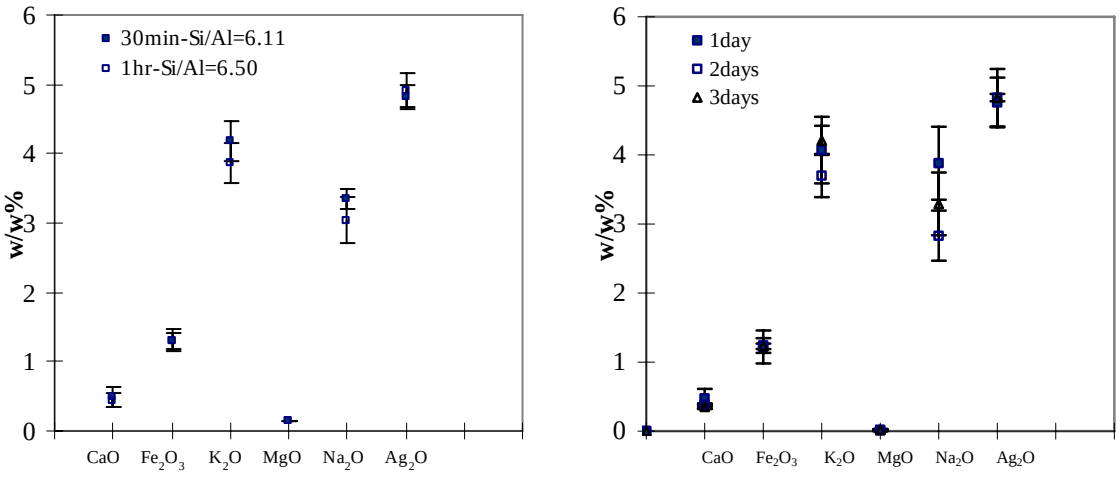

Figure A.5. Solid phase ICP results (0.01 M $AgNO_3$, 60 ^oC, S/L=1/50, waterbath).

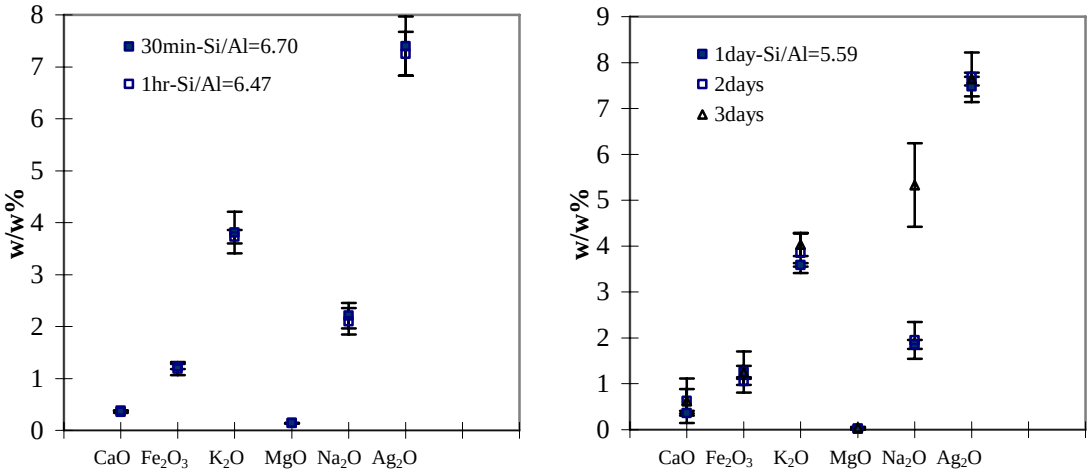

Figure A.6. Solid phase ICP results (0.01 M $AgNO_3$, 60 ^oC, S/L=1/50, waterbath).

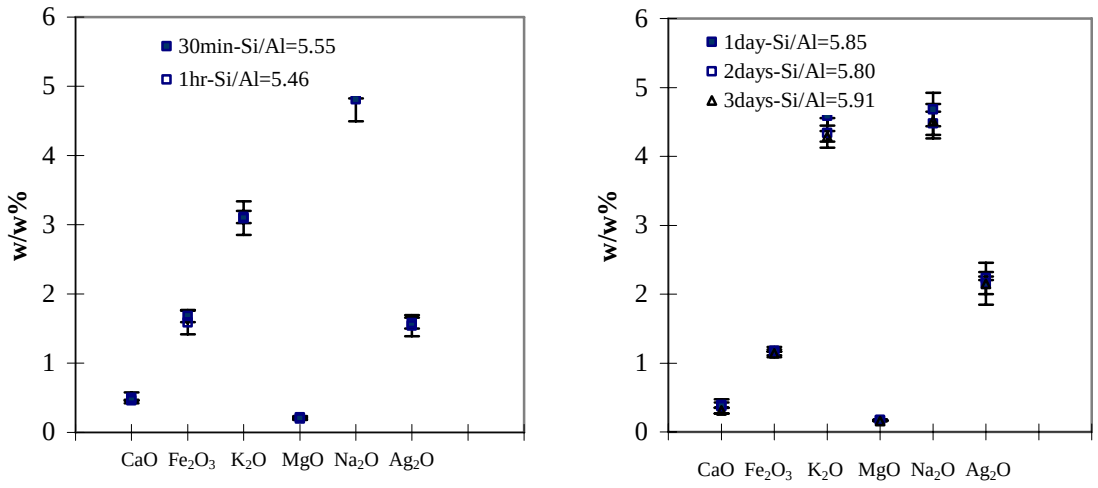

Figure A.7. Solid phase ICP results (0.01 M $AgNO_3$, 80 ^oC, S/L=1/20, waterbath).

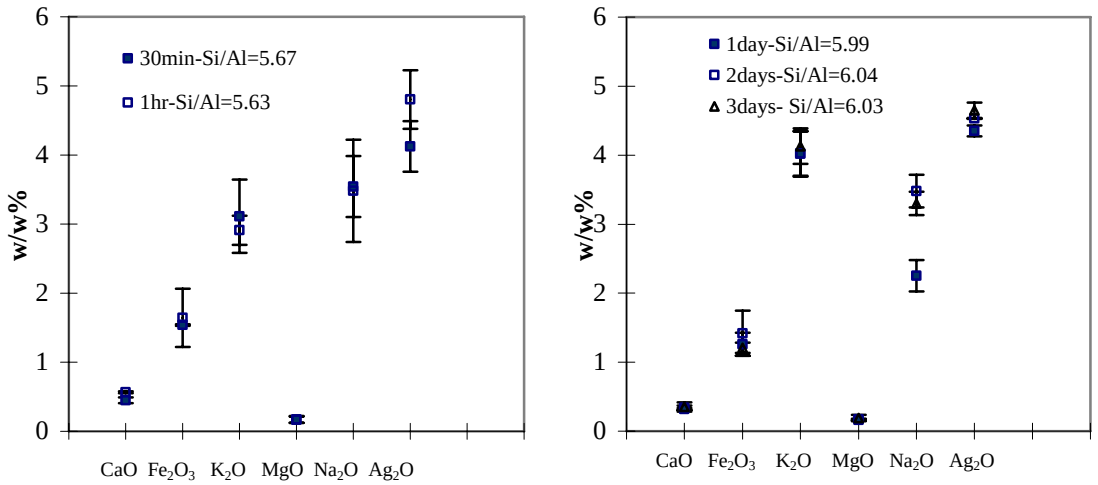

Figure A.8. Solid phase ICP results (0.01 M $AgNO_3$, 80 ^oC, S/L=1/50, waterbath).

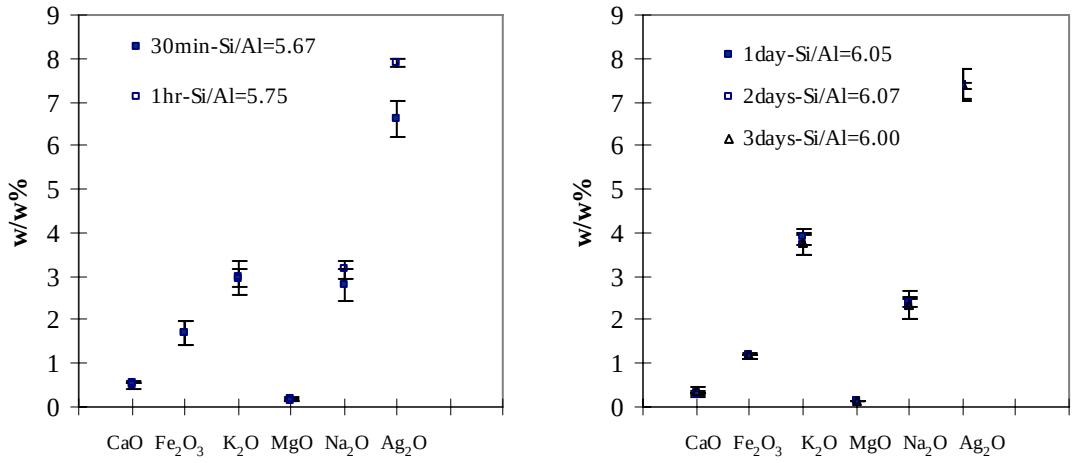

Figure A.9. Solid phase ICP results (0.01 M $AgNO_3$, 80 ^oC, S/L=1/100, waterbath).

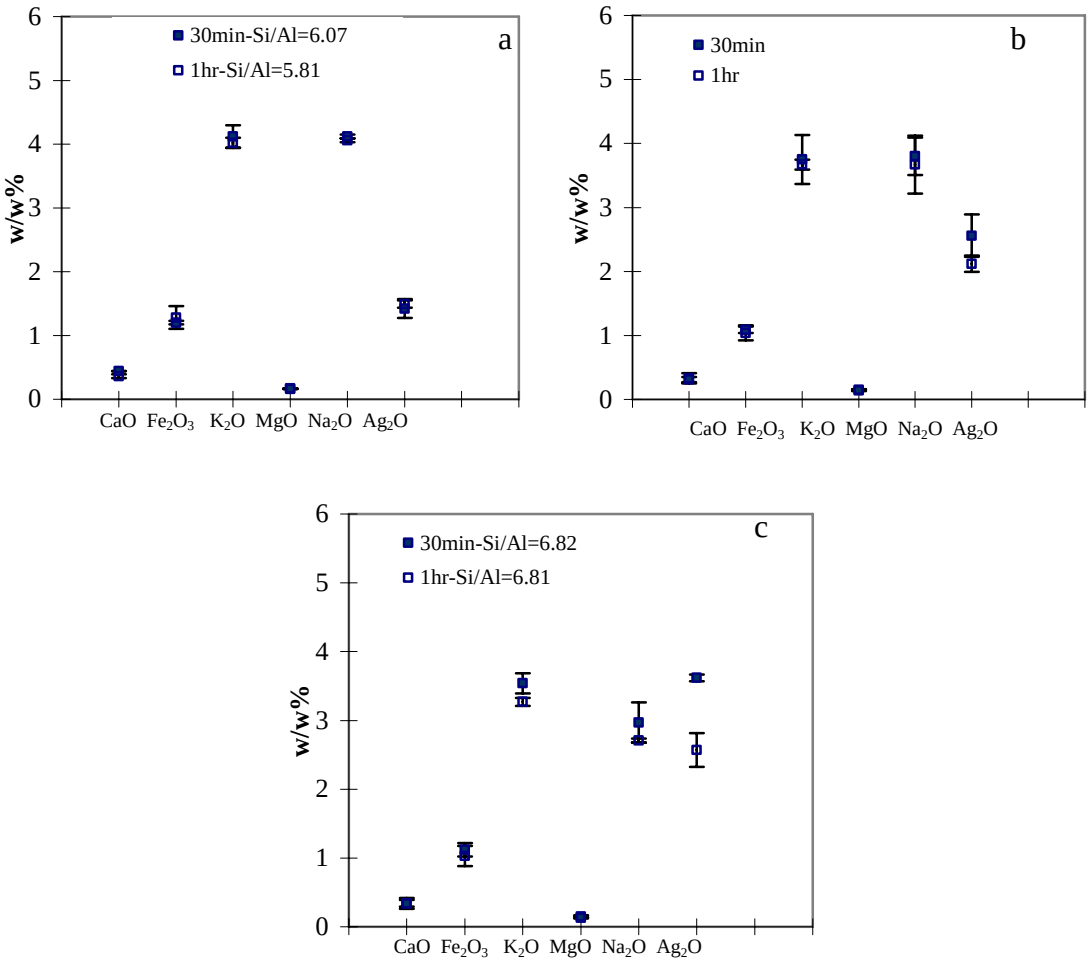

Figure A.10. Solid phase ICP results a) S/L= 1/20 b) S/L=1/50 c) S/L=1/100 (0.01 M $AgNO_3$, 40 ^oC, microwave irradiation, SR=0).

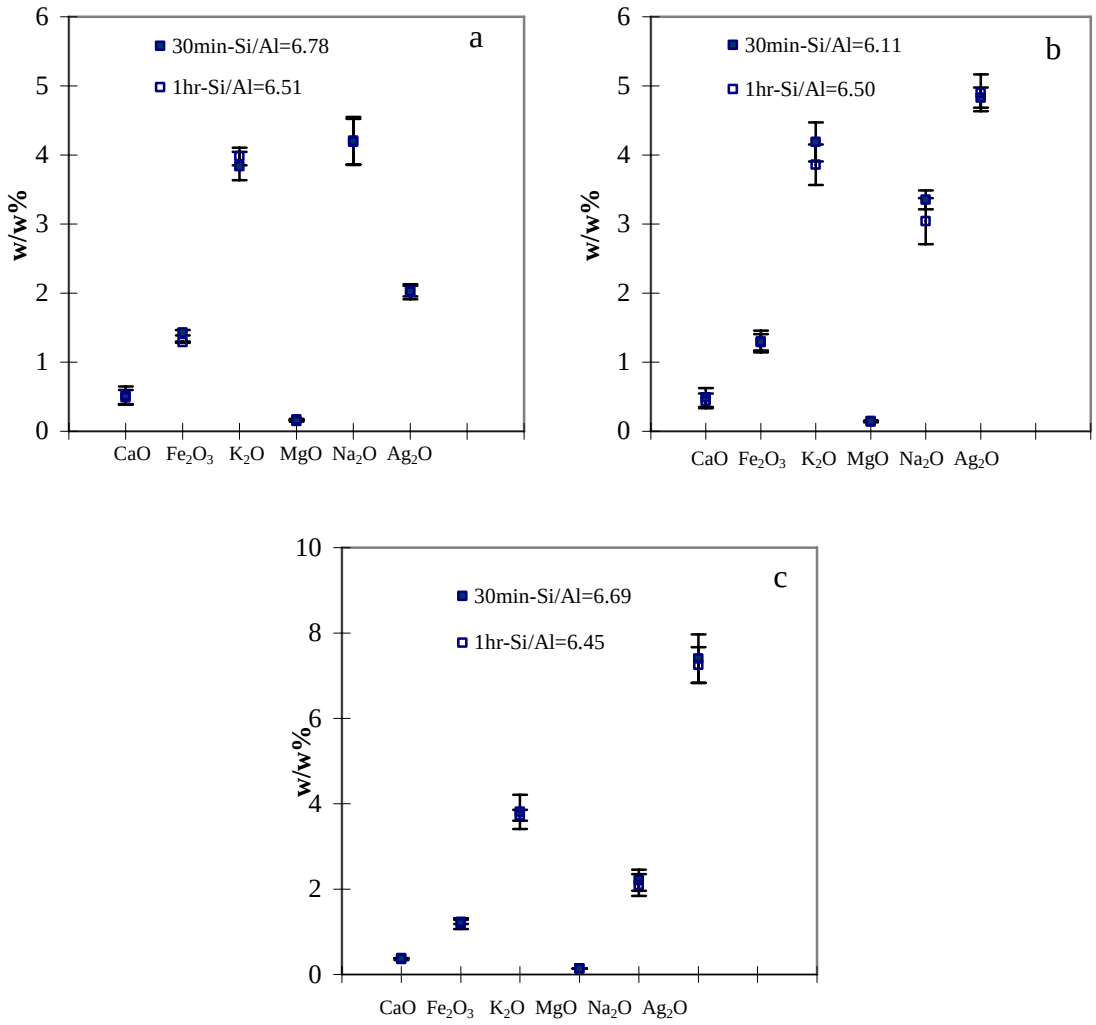

Figure A.11. Solid phase ICP results a) S/L= 1/20 b) S/L=1/50 c) S/L=1/100 (0.01 M $AgNO_3$, 60 ^oC, microwave irradiation, SR=3).

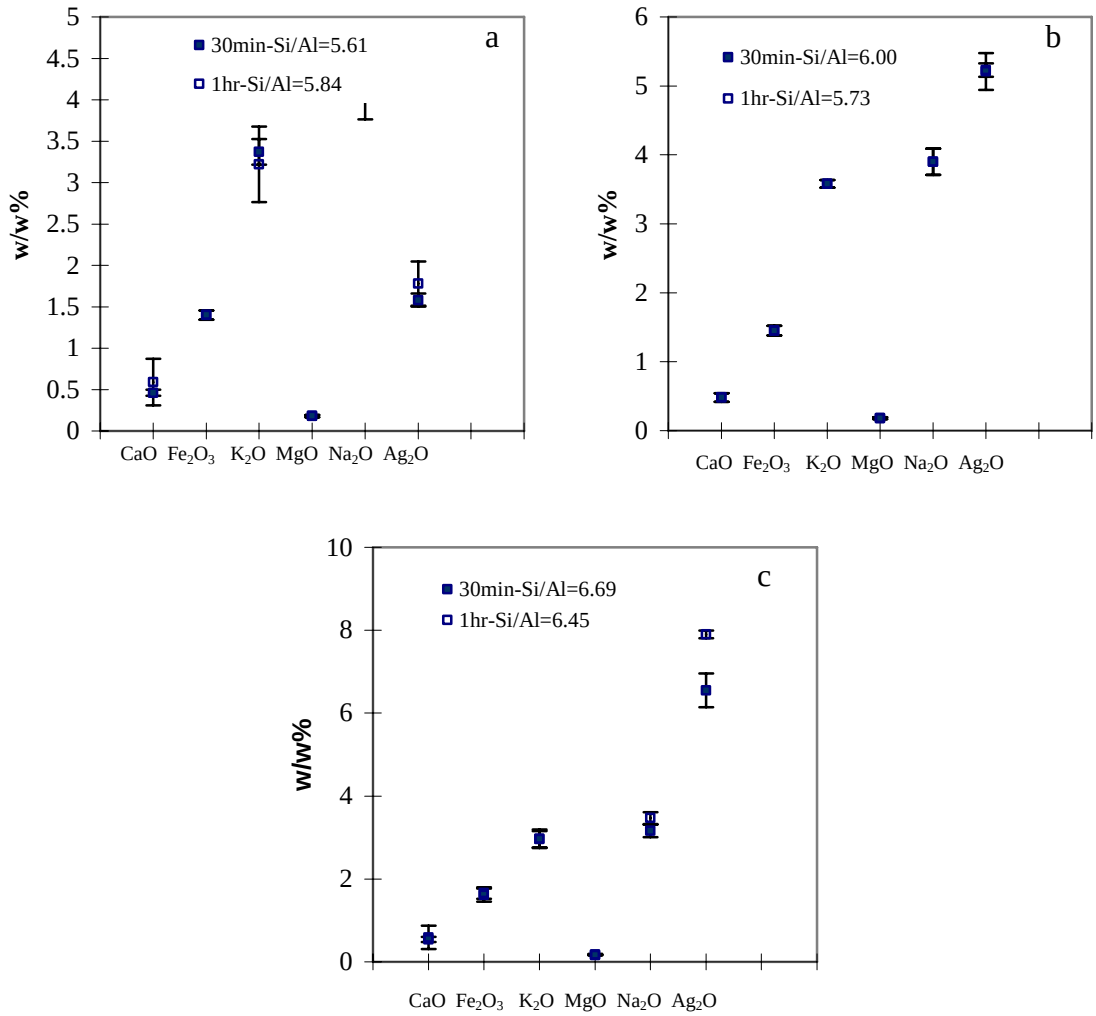

Figure A.12. Solid phase ICP results a) S/L= 1/20 b) S/L=1/50 c) S/L=1/100 (0.01 M $AgNO_3$, 80 ^oC, microwave irradiation, SR=3).

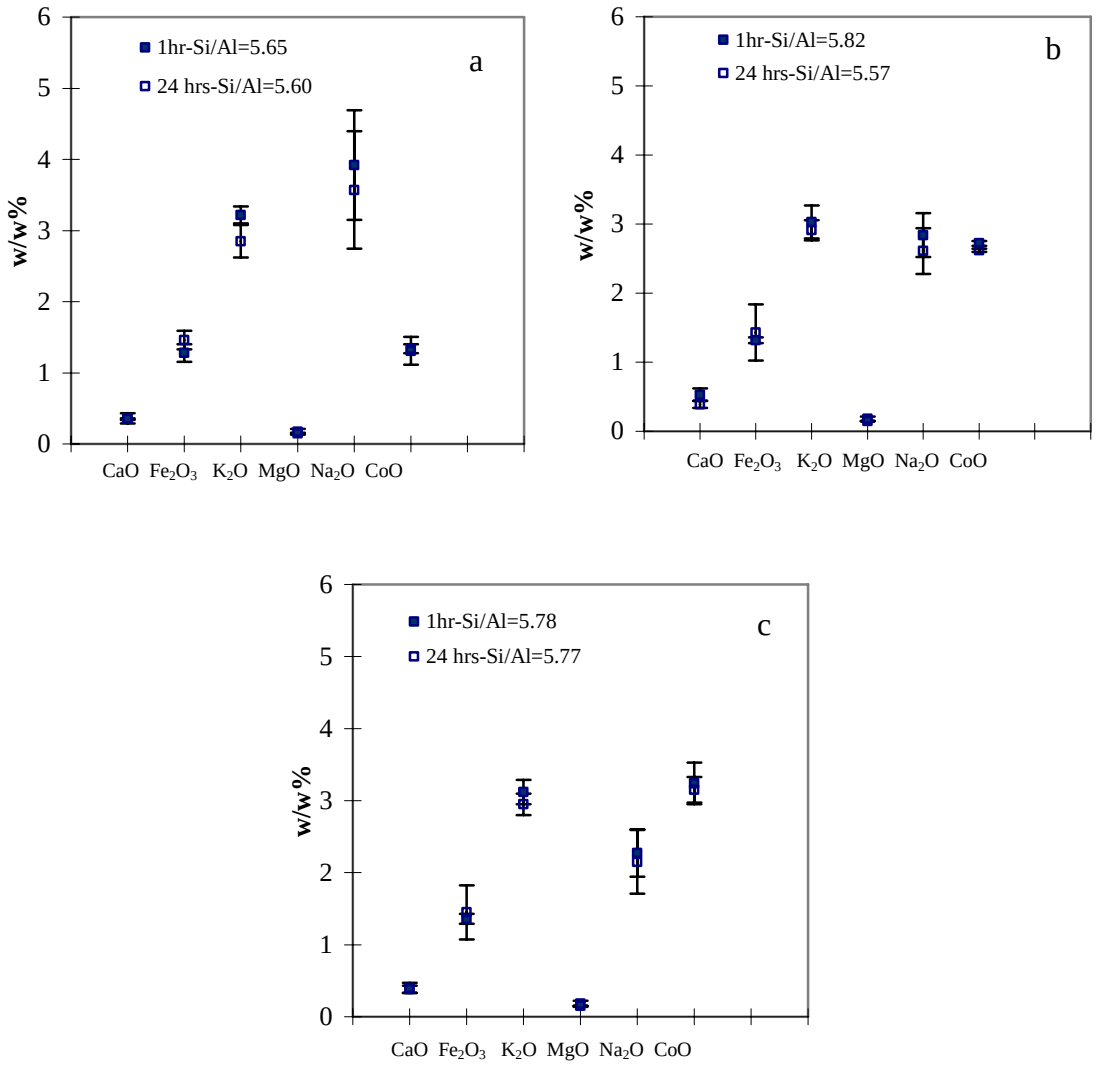

Figure A.13. Solid phase ICP results a) S/L= 1/20 b) S/L=1/50 c) S/L=1/100 (0.01 M $Co(NO_3)_2 6H_2O$ 80 ^oC, waterbath).

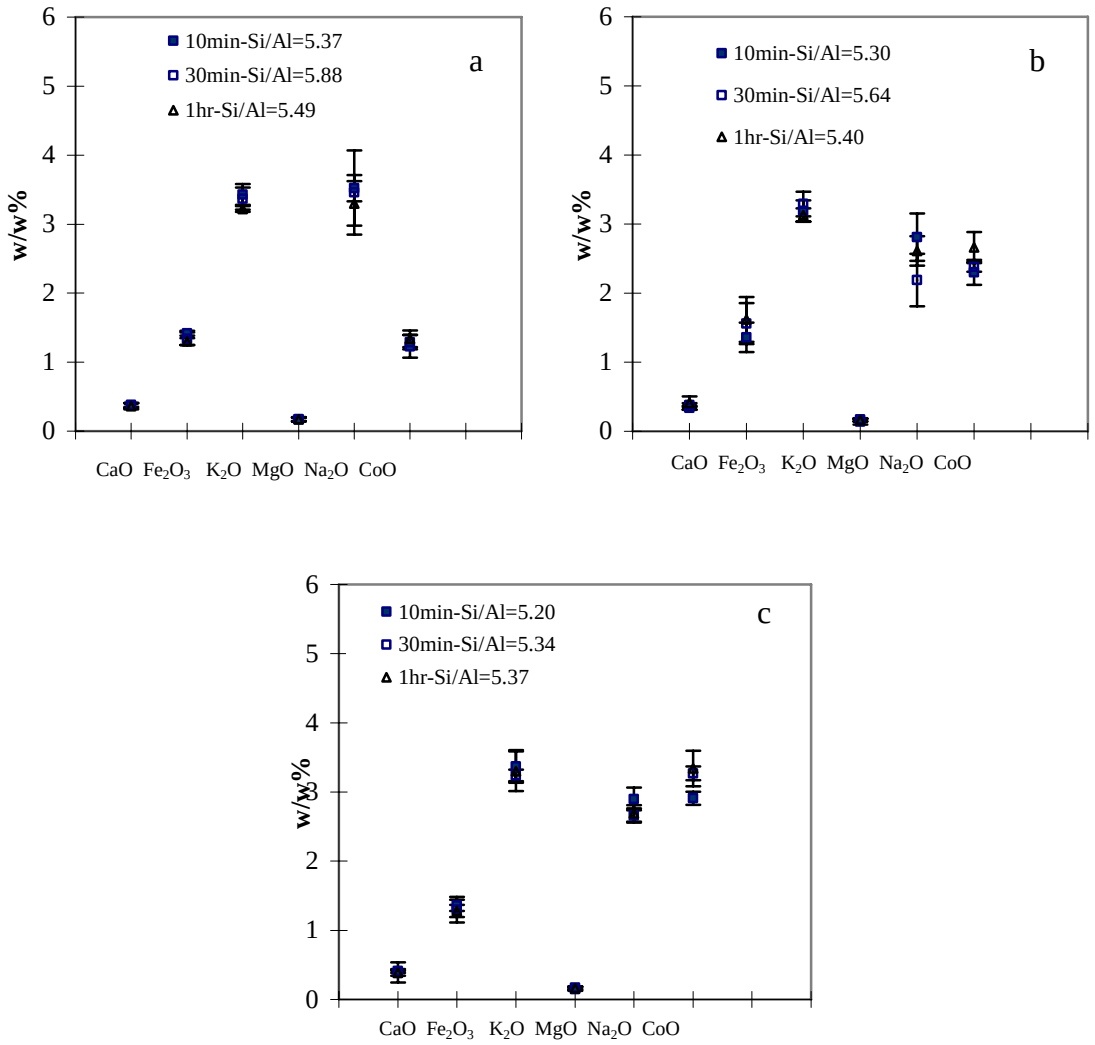

Figure A.14. Solid phase ICP results a) S/L= 1/20 b) S/L=1/50 c) S/L=1/100 (0.01 M $Co(NO_3)_2 \cdot 6H_2O$ 80 ^oC, microwave irradiation).

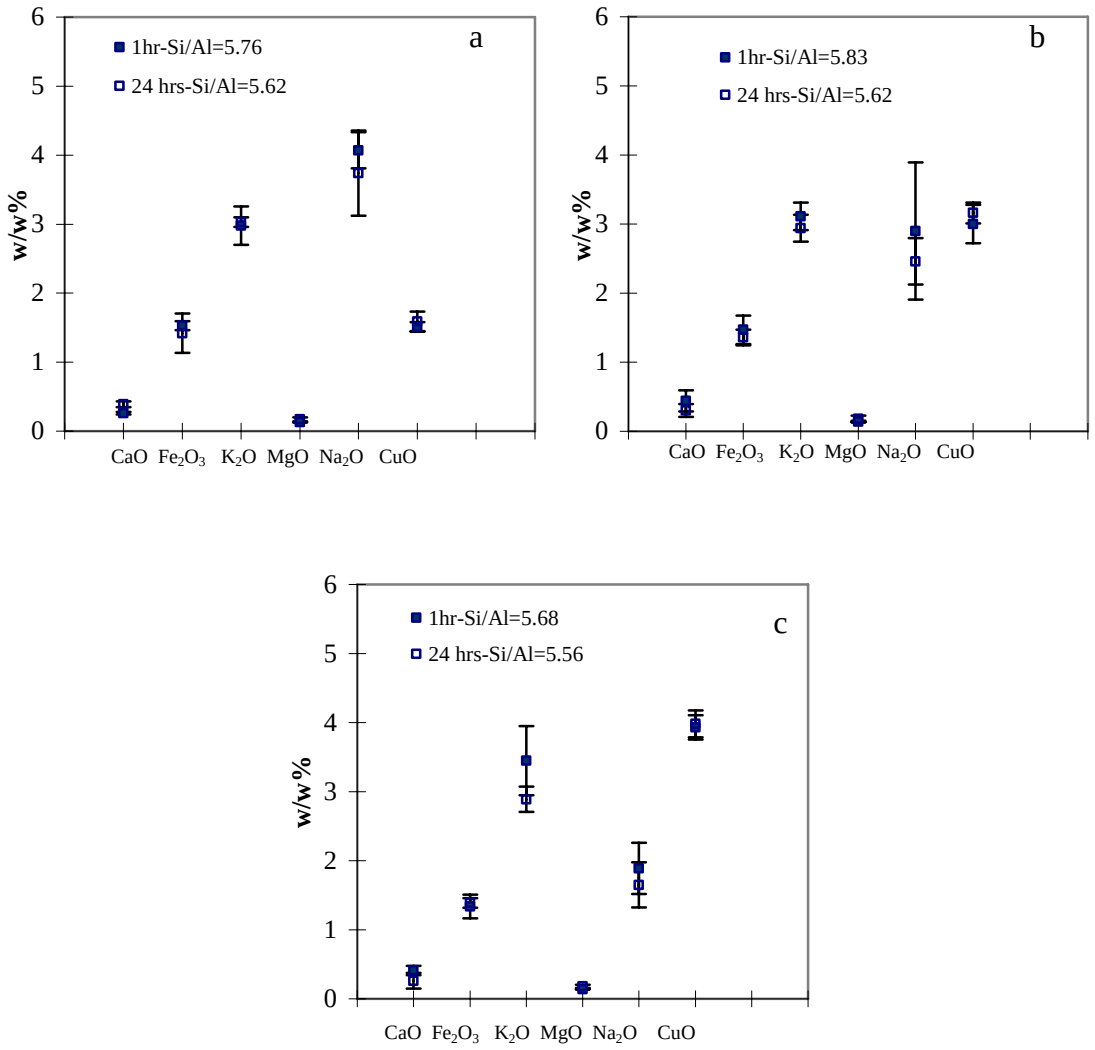

Figure A.15. Solid phase ICP results a) S/L= 1/20 b) S/L=1/50 c) S/L=1/100 (0.01 M $Cu(NO_3)_2 \cdot 5/2H_2O$ 80 ^oC, waterbath).

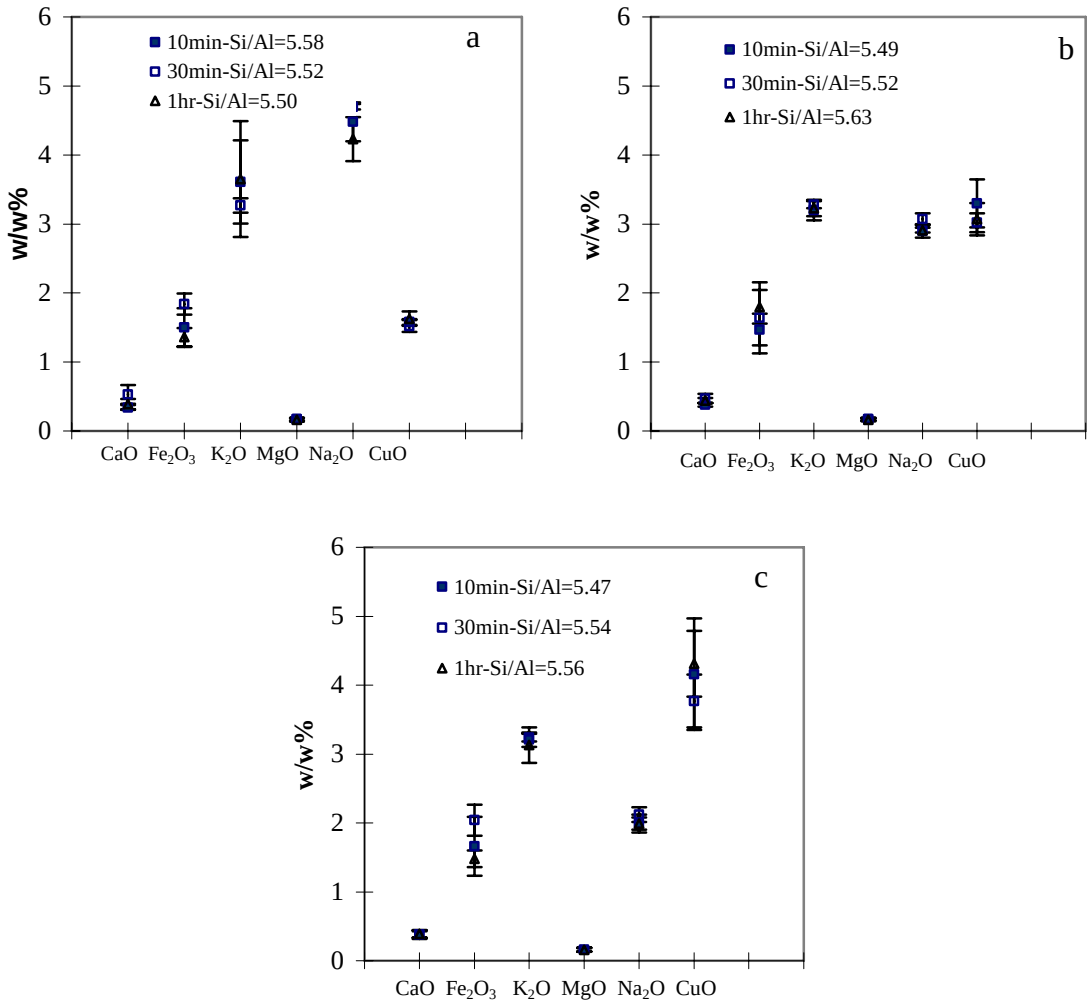

Figure A.16. Solid phase ICP results a) S/L= 1/20 b) S/L=1/50 c) S/L=1/100 (0.01 M $Cu(NO_3)_2 5/2H_2O$ 80 ^oC, microwave irradiation).

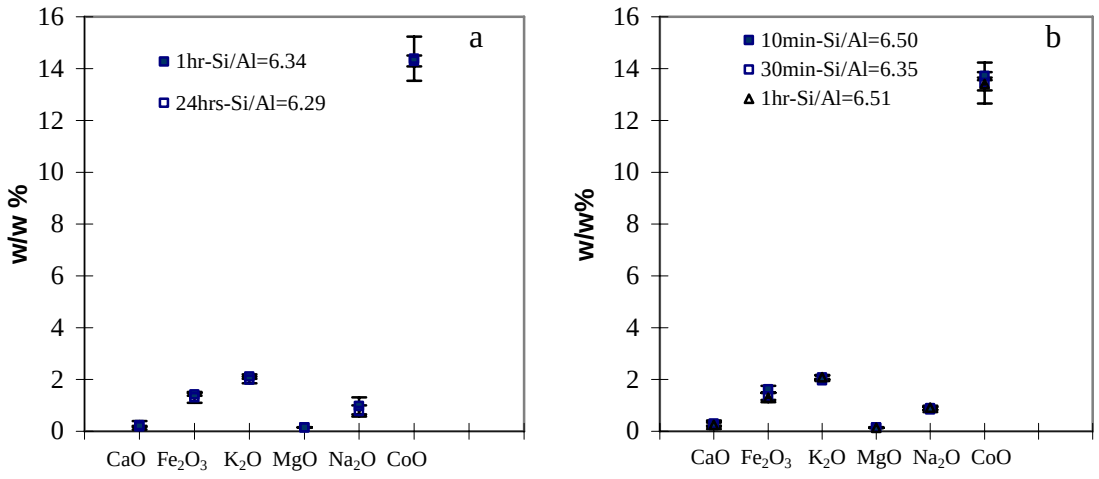

Figure A.17. Solid phase ICP results a) waterbath b) microwave irradiation (0.1 M $AgNO_3$,80 ^oC, S/L=1/100).

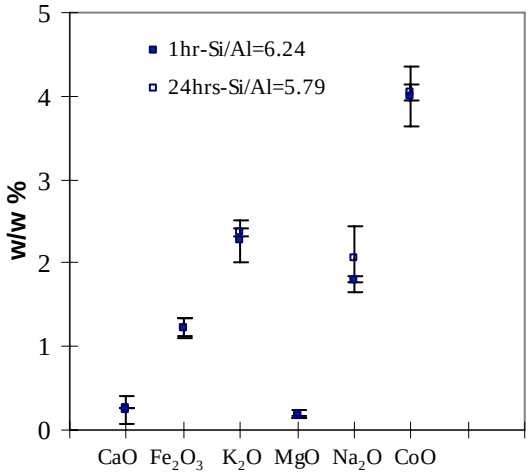

Figure A.18. Solid phase ICP results (0.1 M $Co{\cdot}(NO_3)_2{\cdot}6H_2O$,80 ^oC,S/L=1/100, waterbath).

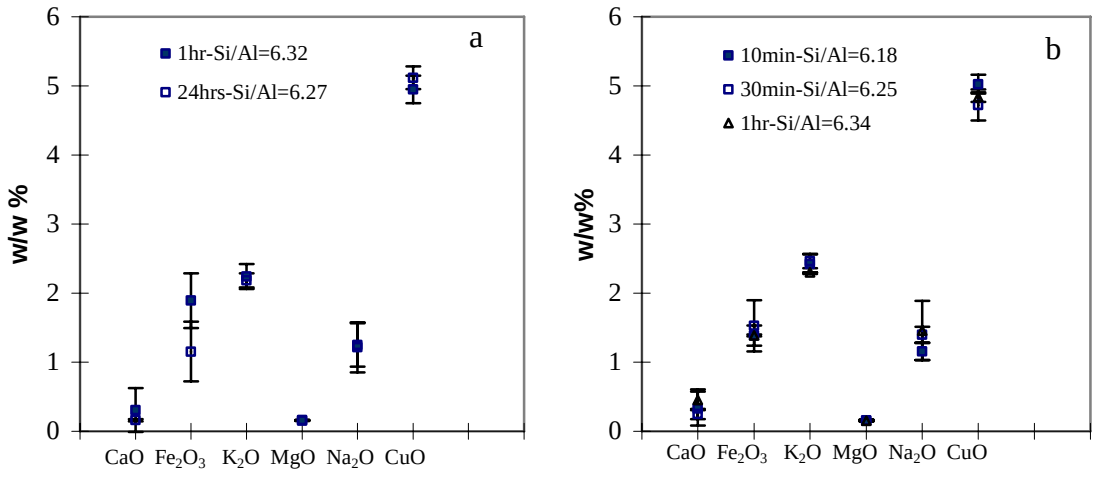

Figure A.19. Solid phase ICP results a) watrebath b) microwave irradiation (0.1 M $Cu(NO_3)_2 \cdot 5/2H_2O$,80 ^oC,S/L=1/100).

APPENDIX B

LIQUID PHASE ICP RESULTS

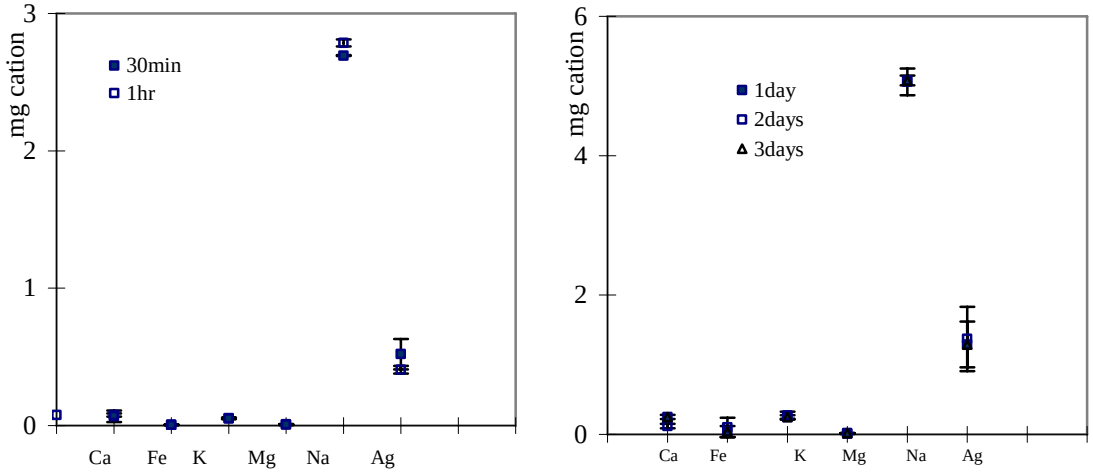

Figure B.1. Liquid phase ICP results (0.01 M $AgNO_3$, 40 ^oC, S/L=1/20, waterbath).

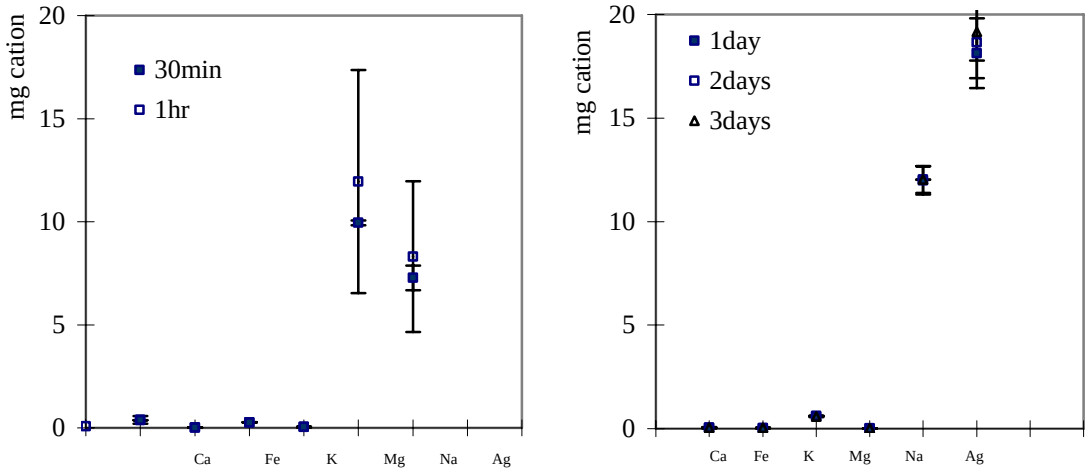

Figure B.2. Liquid phase ICP results (0.01 M $AgNO_3$, 40 ^oC, S/L=1/50, waterbath).

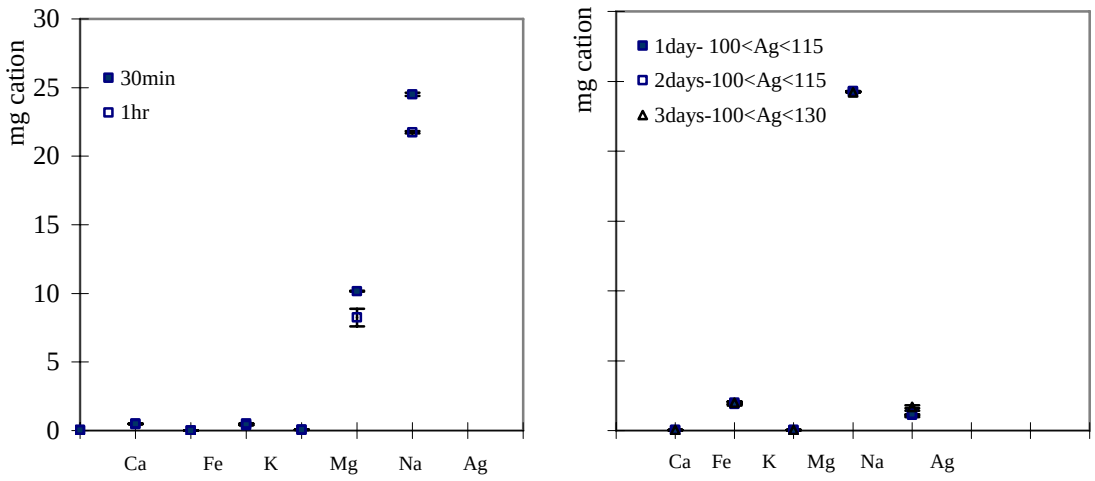

Figure B.3. Liquid phase ICP results (0.01 M $AgNO_3$, 40 ^oC, S/L=1/100, waterbath).

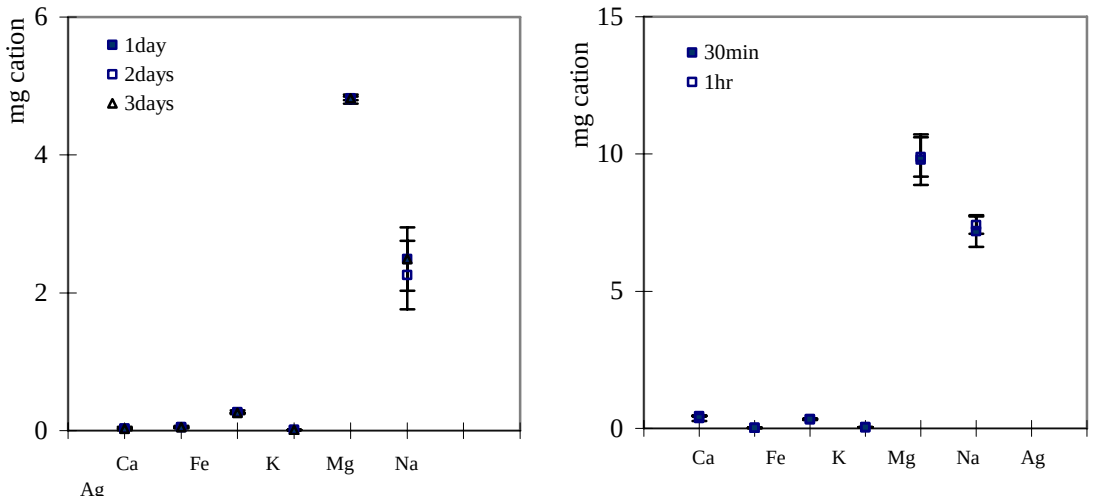

Figure B.4. Liquid phase ICP results (0.01 M $AgNO_3$, 60 ^oC, S/L=1/20, waterbath).

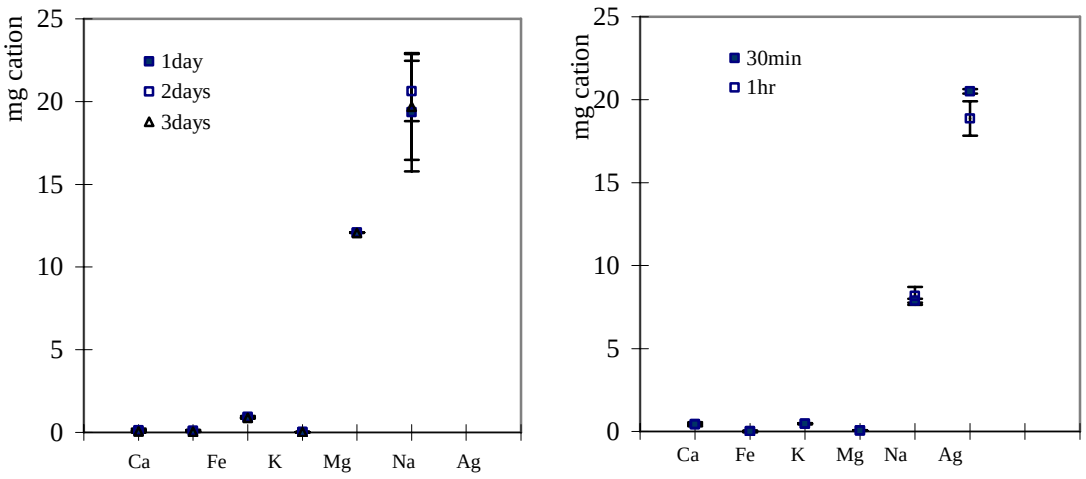

Figure B.5. Liquid phase ICP results (0.01 M $AgNO_3$, 60 ^oC, S/L=1/50, waterbath).

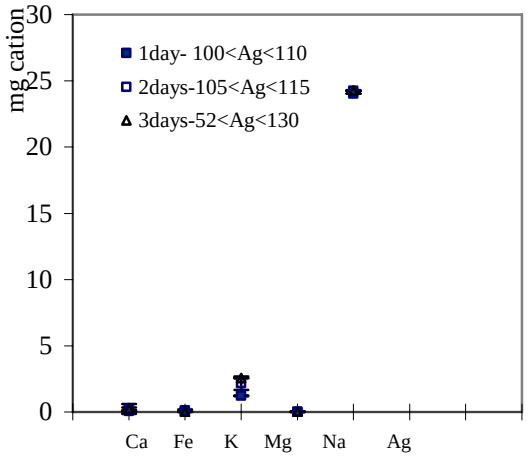

Figure B.6. Liquid phase ICP results (0.01 M $AgNO_3$, 60 ^oC, S/L=1/100, waterbath).

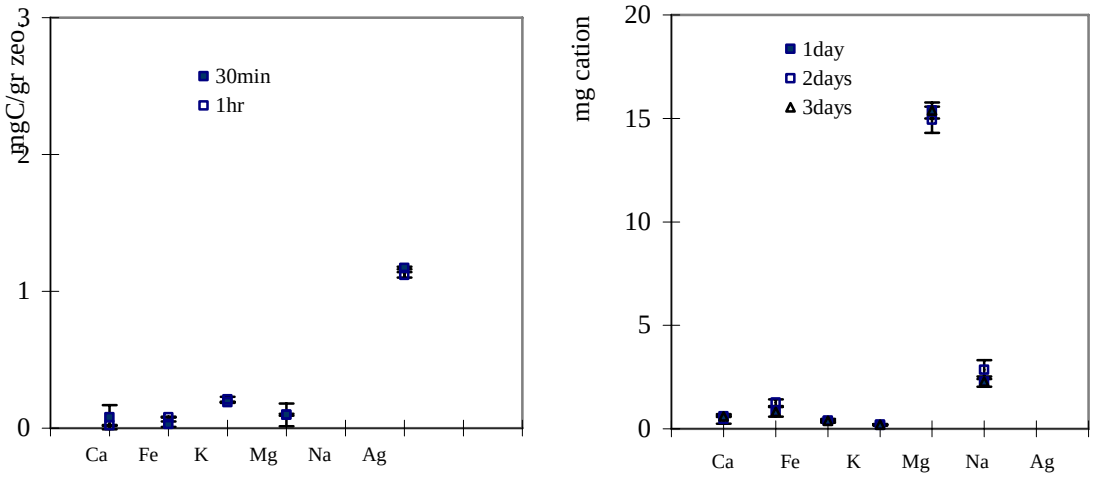

Figure B.7. Liquid phase ICP results (0.01 M $AgNO_3$, 80 ^oC, S/L=1/20, waterbath).

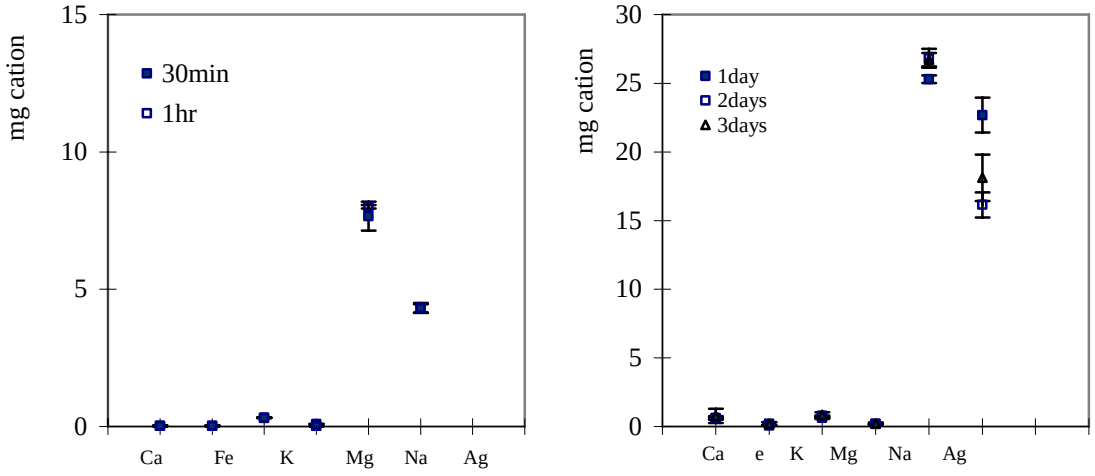

B.8. Liquid phase ICP results (0.01 M $AgNO_3$, 80 ^oC, S/L=1/50, waterbath).

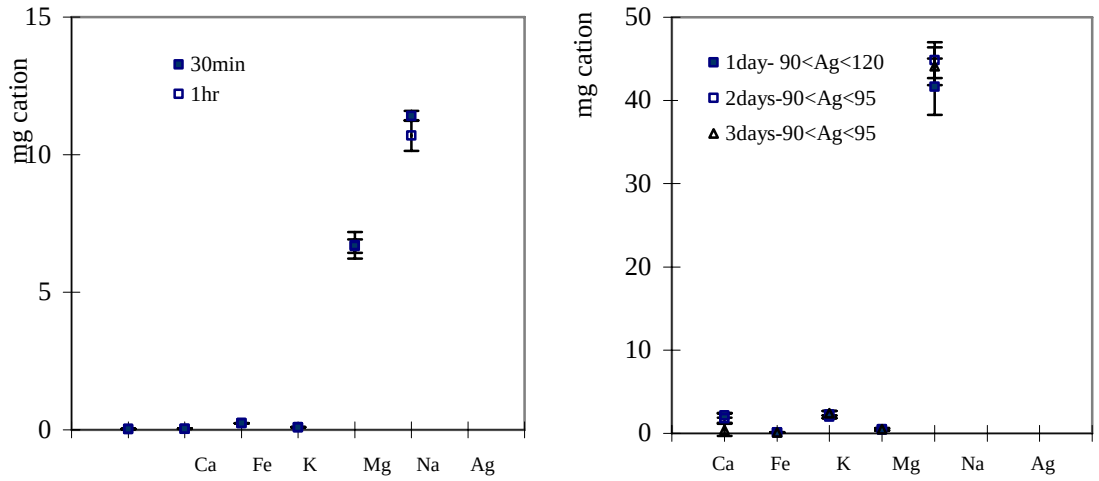

Figure B.9. Liquid Phase ICP Results (mg); 0.01 M Ag^{+} exchanged NaCLI at 80 ^{o}C, S/L=1/100, waterbath

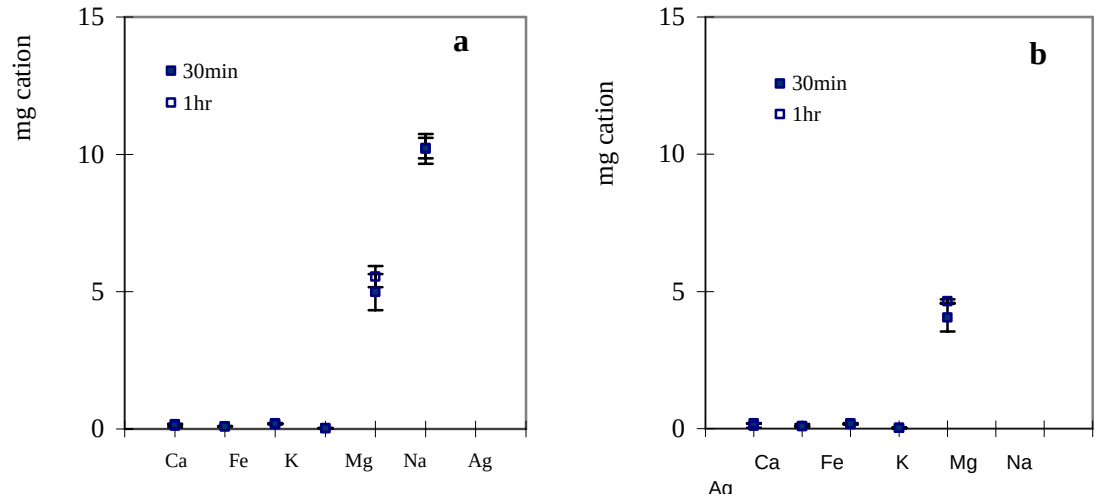

Figure B.10. Liquid phase ICP results a) S/L=1/20 b) S/L=1/50 (0.01 M $AgNO_3$, 40 ^{o}C, microwave irradiation SR=0).

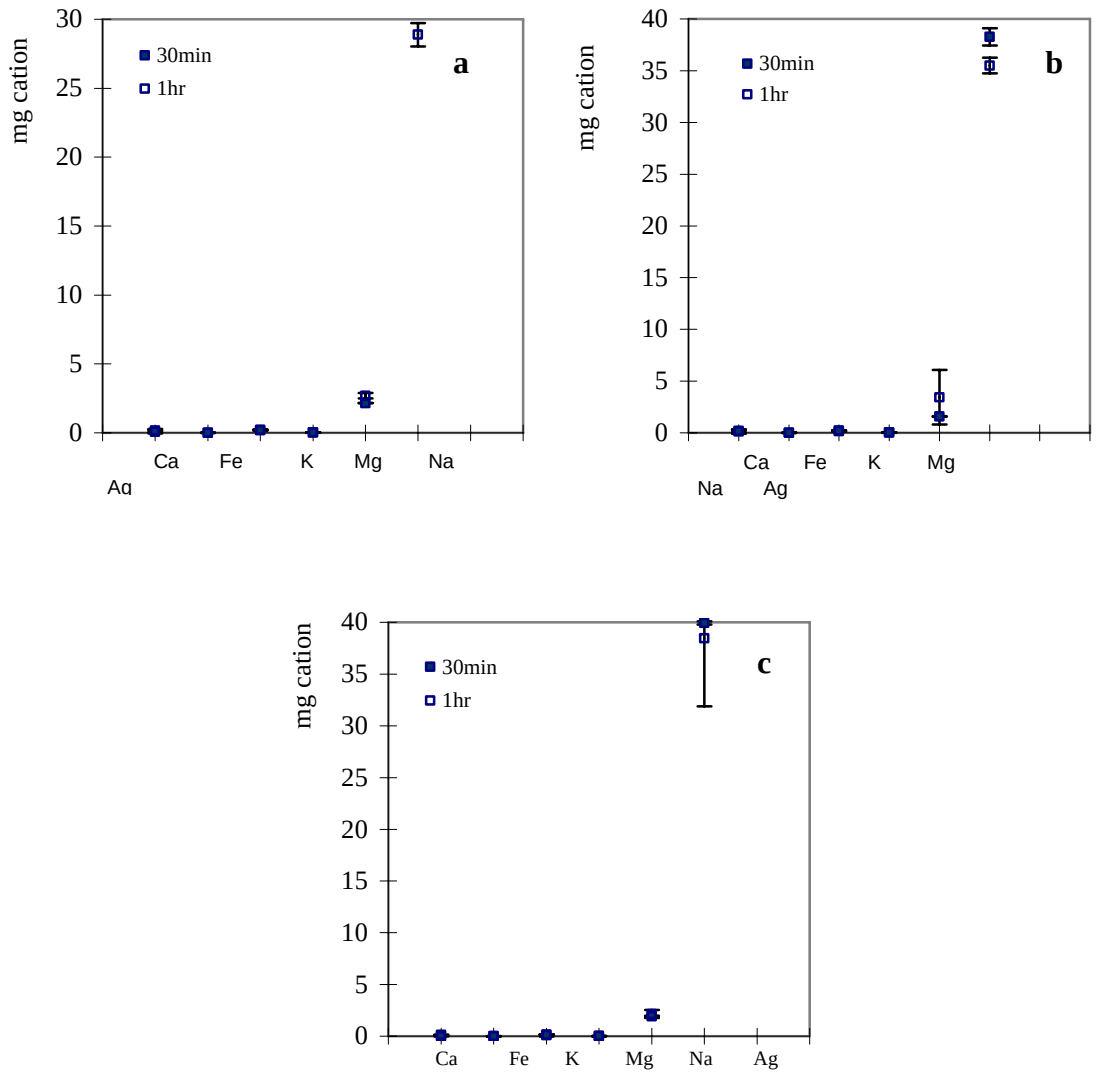

Figure B.11. Liquid phase ICP results a) S/L=1/20 b) S/L=1/50 c) S/L=1/100 (0.01 M $AgNO_3$, 60 ^oC, microwave irradiation SR=3).

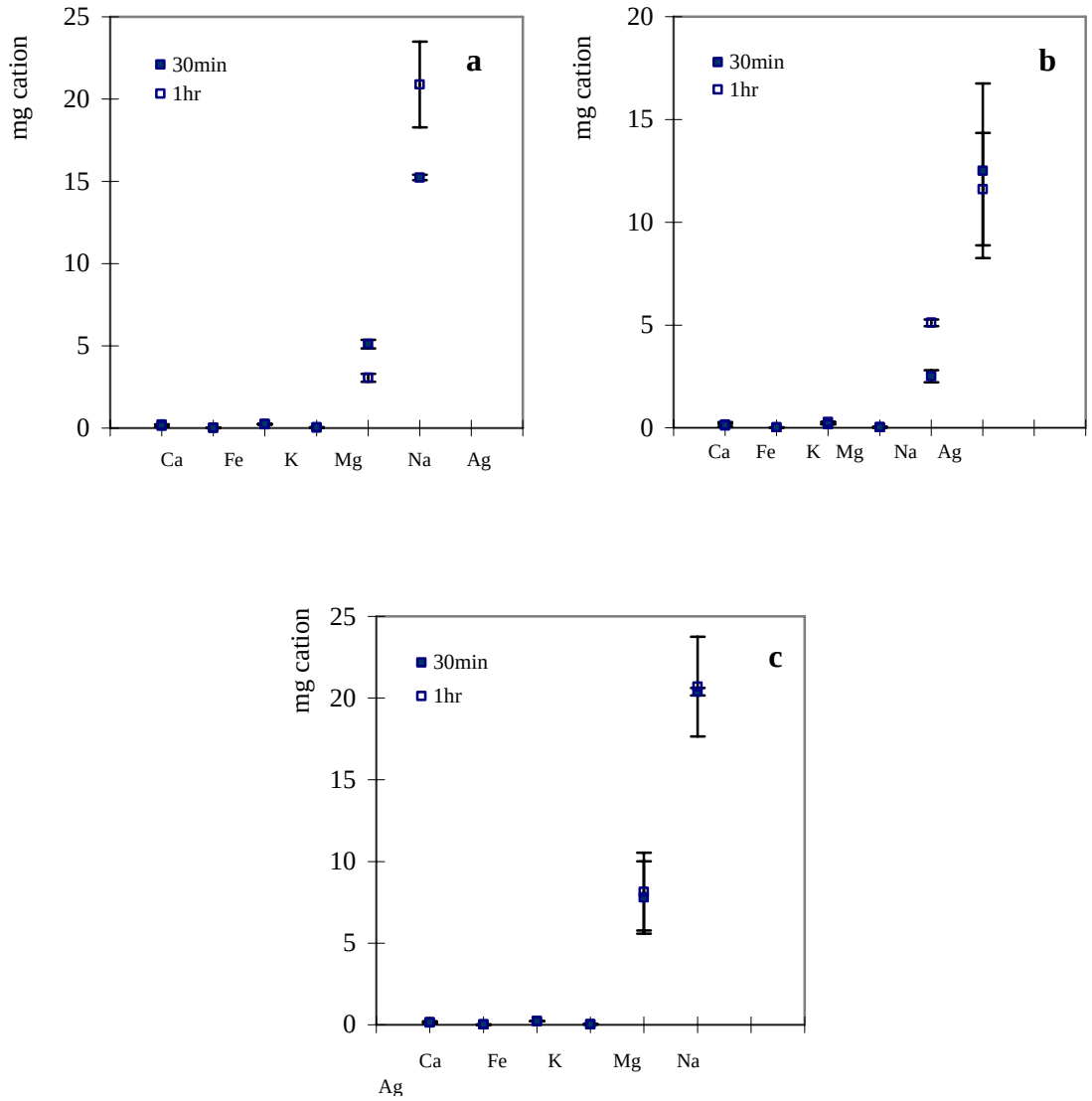

Figure B.12. Liquid phase ICP results a) S/L=1/20 b) S/L=1/50 c) S/L=1/100 (0.01 M $AgNO_3$, 80 ^oC, microwave irradiation SR=3).

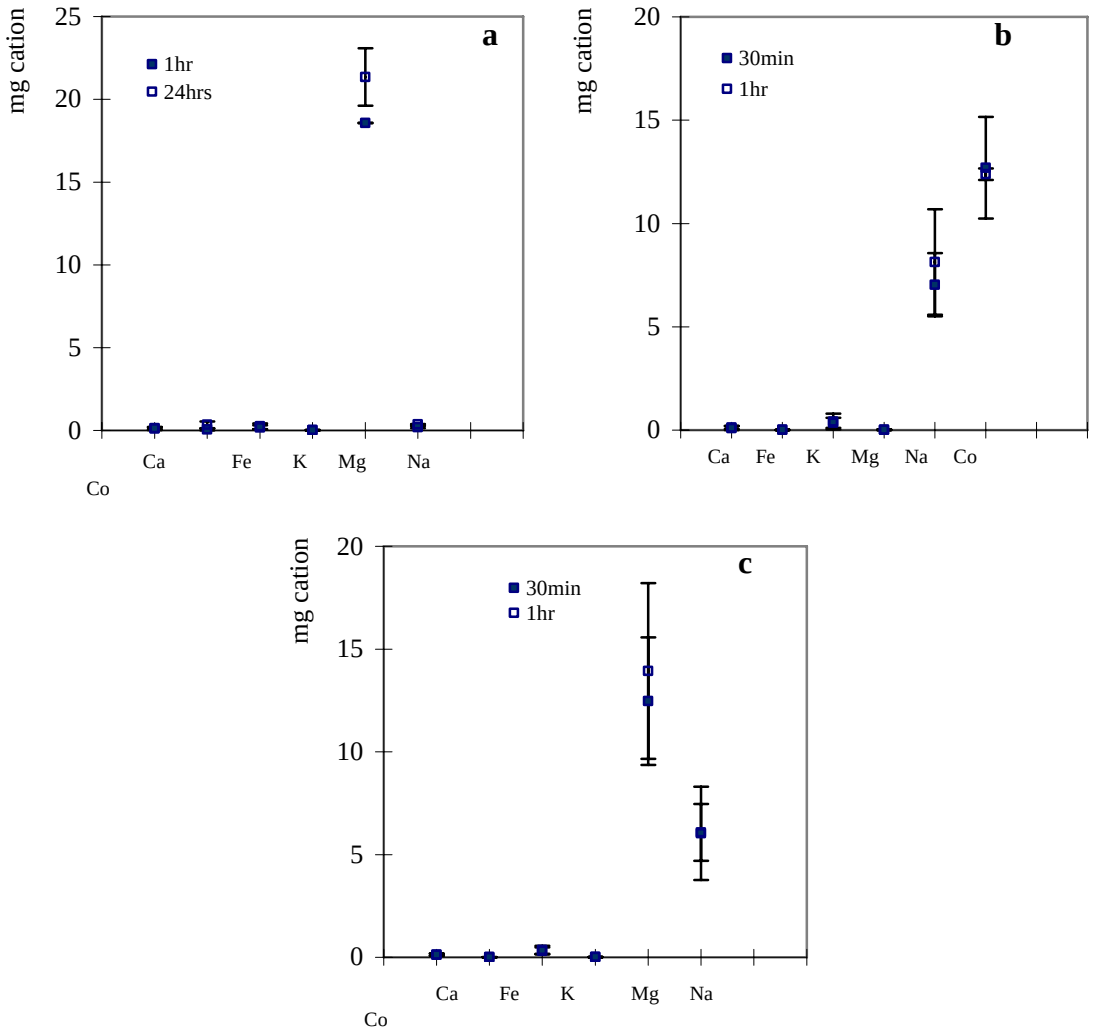

Figure B.13. Liquid phase ICP results a) S/L=1/20 b) S/L=1/50 c) S/L=1/100 (0.01 M $Co{\cdot}(NO_3)_2{\cdot}6H_2O$, 80 ^oC,, waterbath).

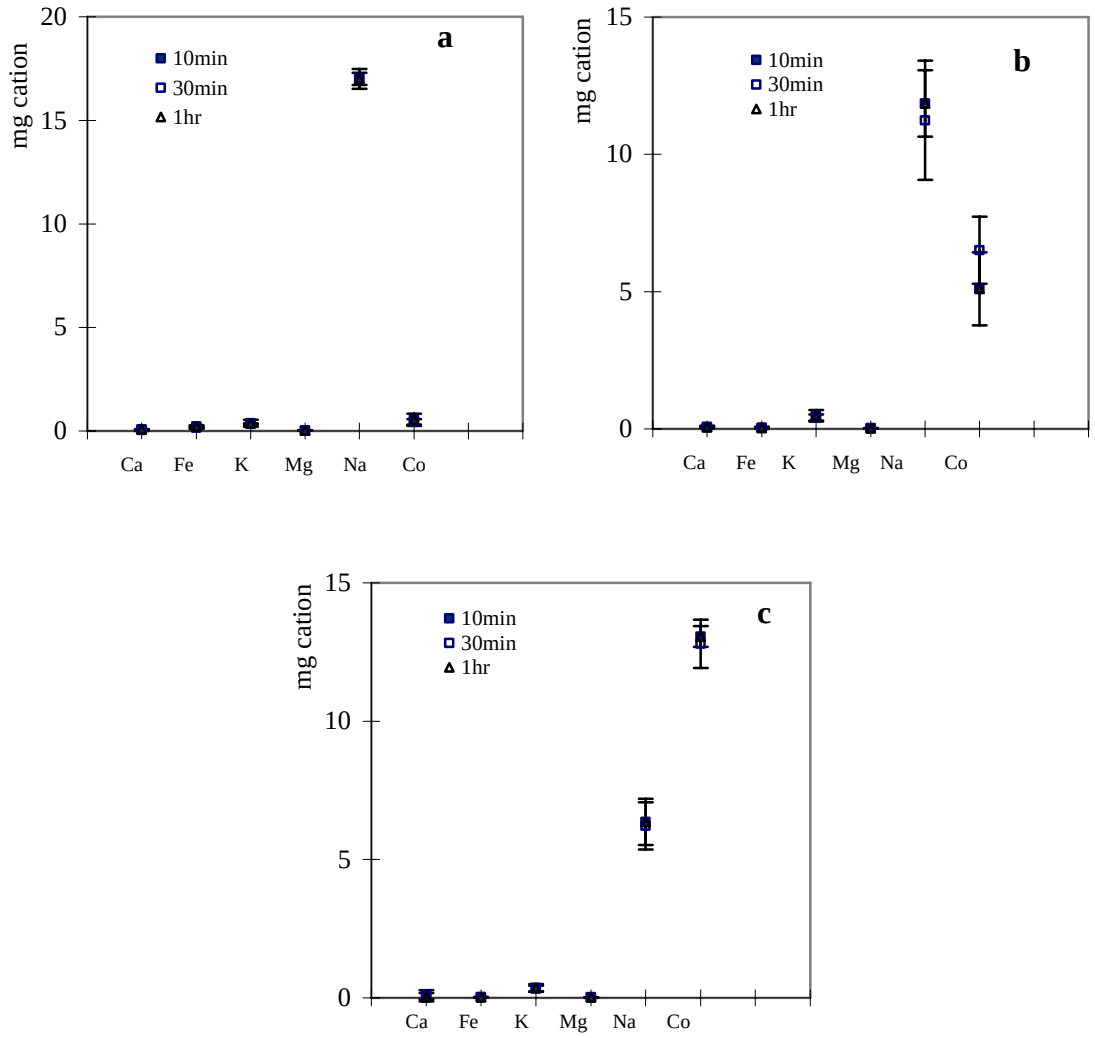

Figure 14. Liquid phase ICP results a) S/L=1/20 b) S/L=1/50 c) S/L=1/100 (0.01 M $Co(NO_3)_2 \cdot 6H_2O$, 80 ^oC, microwave irradiation SR=3).

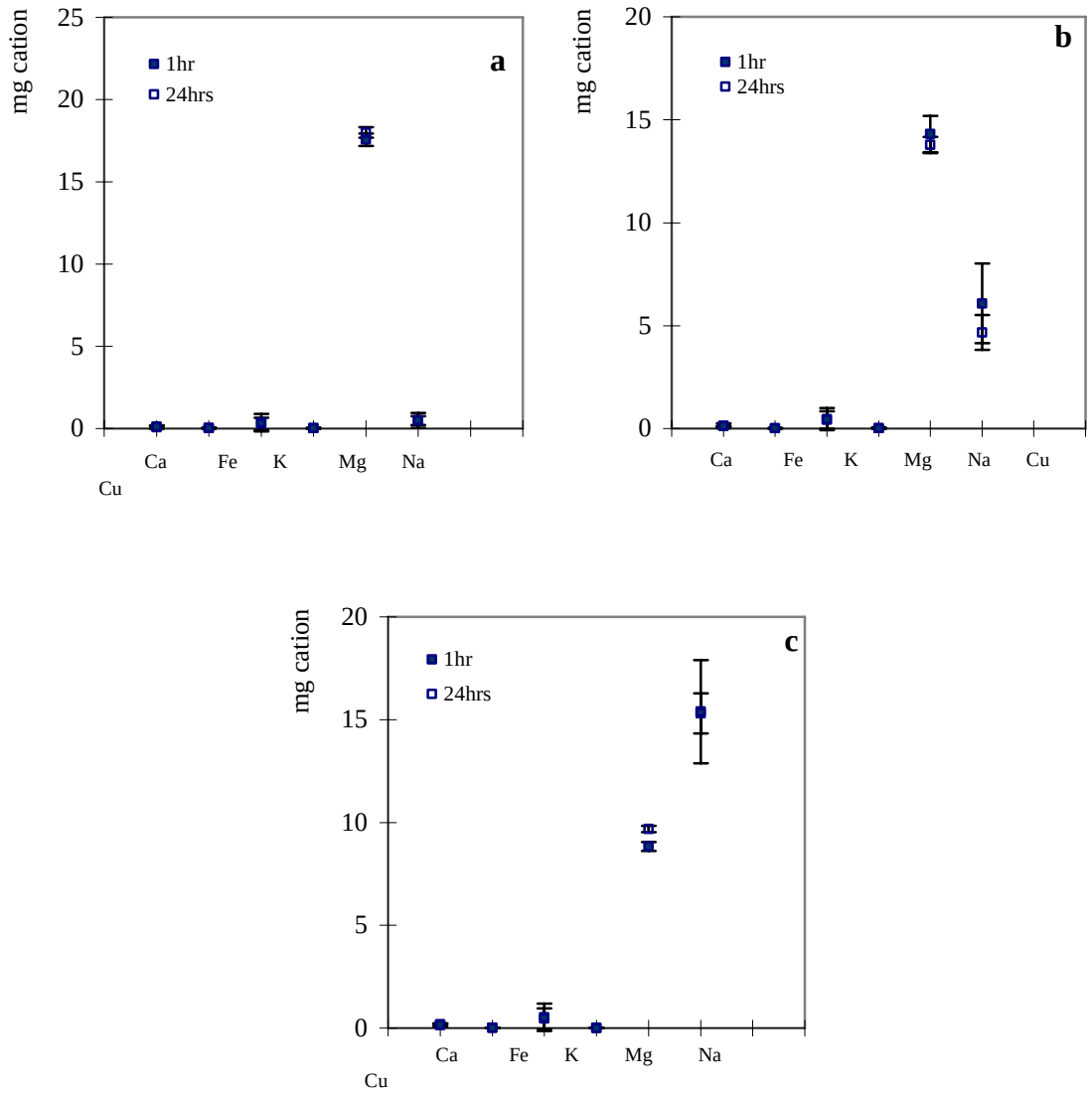

Figure B.15. Liquid phase ICP results a) S/L=1/20 b) S/L=1/50 c) S/L=1/100 (0.01 M $Cu(NO_3)_2 \cdot 5/2H_2O$, 80 ^oC waterbath).

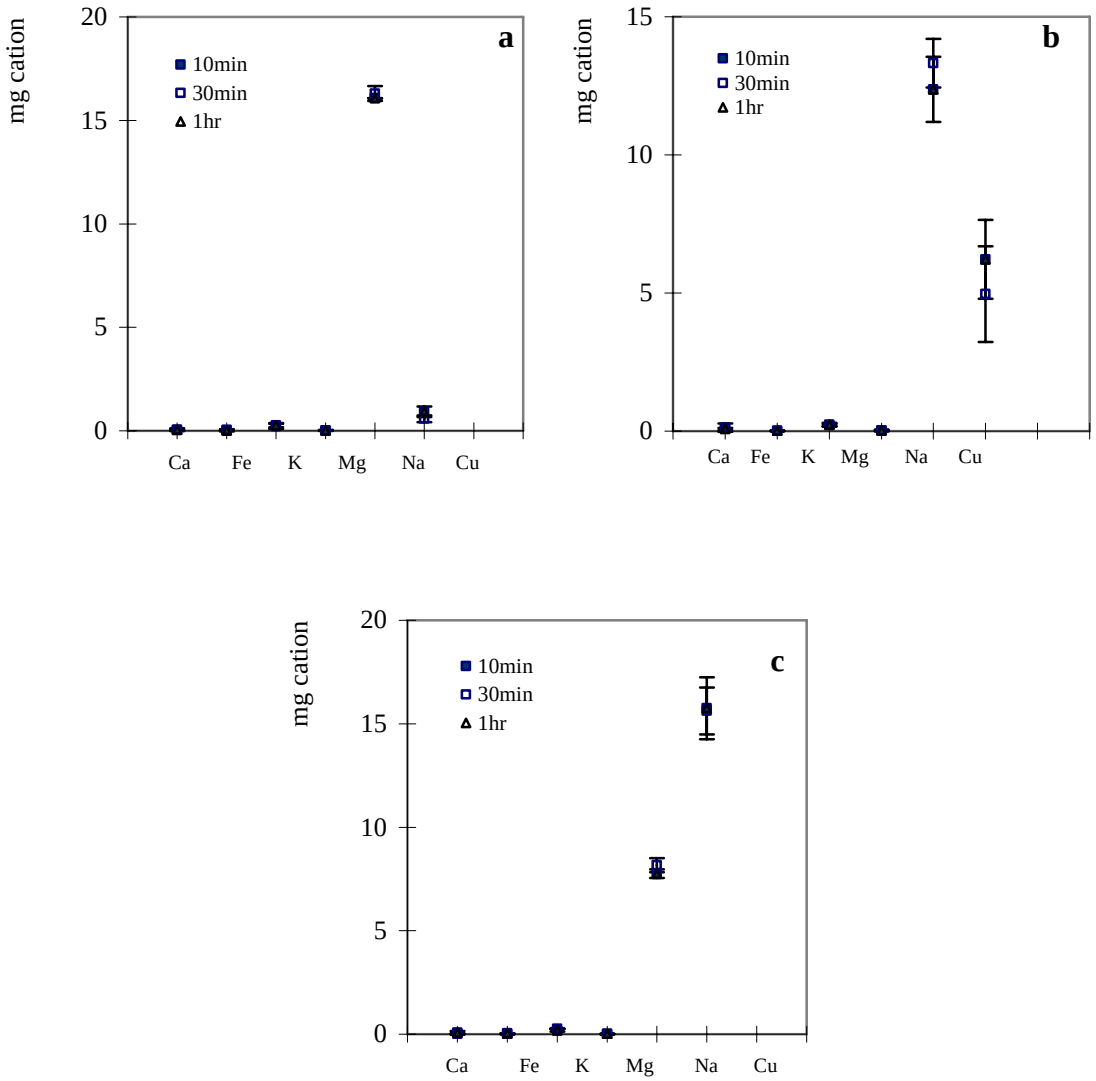

Figure B.16. Liquid phase ICP results a) S/L=1/20 b) S/L=1/50 c) S/L=1/100 (0.01 M $Cu(NO_3)_2 \cdot 5/2H_2O$, 80 ^oC, microwave irradiation).

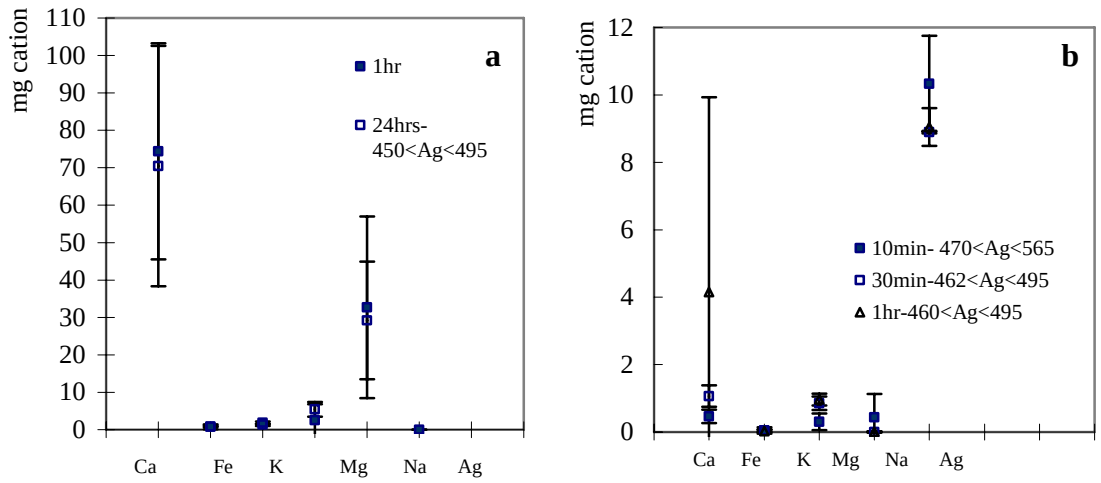

Figure B.17. Liquid phase ICP results a) waterbath b) microwave irradiation (0.1 M $AgNO_3$, 80 ^oC, S/L=1/100).

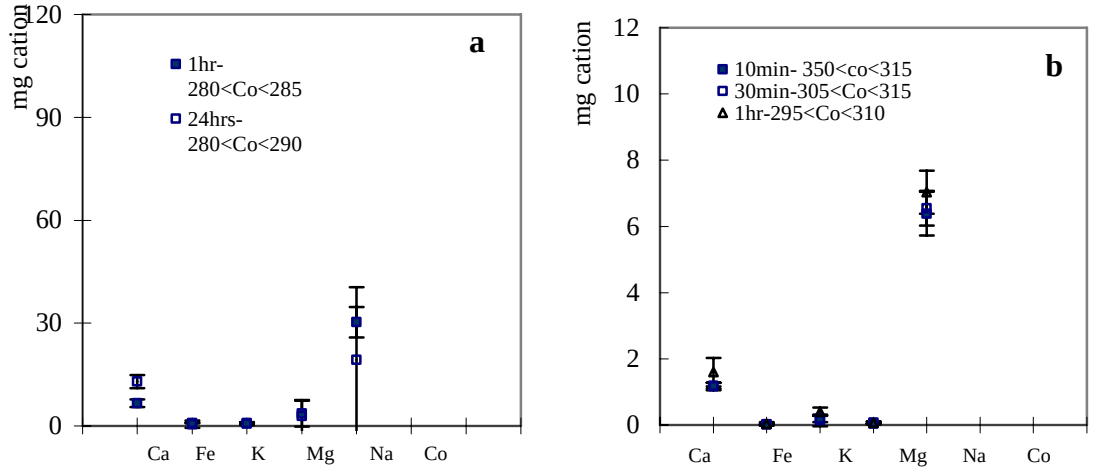

Figure B.18. Liquid phase ICP results a) waterbath b) microwave irradiation (0.1 M $Co(NO_3)_2 6H_2$, 80 ^oC, S/L=1/100)

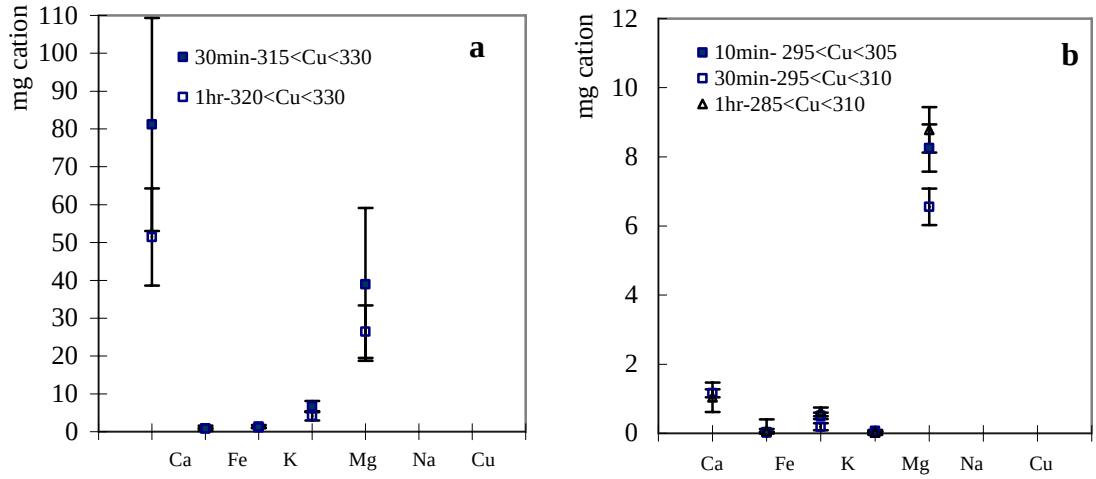

Figure B.19. Liquid phase ICP results a) waterbath b) microwave irradiation (0.1 M $Cu(NO_3)_2 \cdot 5/2H_2O$, 80 ^oC, S/L=1/100).

APPENDIX C

SOLID AND LIQUID PHASE COMPOSITIONS

Table C.1. Solid and liquid phase compositions (0.01 M $AgNO_3$, 40 ^oC, 30 min, S/L=1/20, waterbath).

	SOLID (meq/gr zeolite)		LIQUID (meq/gr zeolite)	
Elements	Initial	Final	Initial	Final
Ca	0.31	0.21	0	0.004
Fe	0.44	0.49	0	0
K	0.83	0.90	0	0.001
Mg	0.09	0.08	0	0.001
Na	1.81	1.41	0	0.117
Ag	0.00	0.18	0.200	0.004
(meq/gr zeolite)	$\sum(Ca^{2+}+Na^{+}+K^{+}+Mg^{2+})$		Ag^{+}	
	0.58		*0.20*	

Table C.2. Solid and liquid phase compositions (0.01 M $AgNO_3$, 40 ^oC, 1 hr, S/L=1/20, waterbath).

	SOLID (meq/gr zeolite)		LIQUID (meq/gr zeolite)	
Elements	Initial	Final	Initial	Final
Ca	0.31	0.15	0	0.000
Fe	0.44	0.49	0	0.001
K	0.83	0.87	0	0.001
Mg	0.09	0.08	0	0.109
Na	1.81	1.33	0	0.004
Ag	0.00	0.19	0.200	0.000
(meq/gr zeolite)	$\sum(Ca^{2+}+Na^{+}+K^{+}+Mg^{2+})$		Ag^{+}	
	0.69		*0.20*	

Table C.3. Solid and liquid phase compositions (0.01 M $AgNO_3$, 40 ^oC, 1 day, S/L=1/20, waterbath).

	SOLID (meq/gr zeolite)		LIQUID (meq/gr zeolite)	
Elements	Initial	Final	Initial	Final
Ca	0.31	0.14	0	0.001
Fe	0.44	0.42	0	0.001
K	0.83	0.81	0	0.002
Mg	0.09	0.08	0	0.000
Na	1.81	1.47	0	0.055
Ag	0.00	0.17	0.200	0.004
(meq/gr zeolite)	$\sum(Ca^{2+}+Na^{+}+K^{+}+Mg^{2+})$		Ag^{+}	
	0.55		*0.20*	

Table C.4. Solid and liquid phase compositions (0.01 M $AgNO_3$, 40 ^oC, 2 days, S/L=1/20, waterbath).

	SOLID (meq/gr zeolite)		LIQUID (meq/gr zeolite)	
Elements	Initial	Final	Initial	Final
Ca	0.31	0.14	0	0.001
Fe	0.44	0.40	0	0.001
K	0.83	0.79	0	0.002
Mg	0.09	0.08	0	0.000
Na	1.81	1.52	0	0.055
Ag	0.00	0.17	0.200	0.003
(meq/gr zeolite)	$\sum(Ca^{2+}+Na^{+}+K^{+}+Mg^{2+})$		Ag^{+}	
	0.52		*0.20*	

Table C.5. Solid and liquid phase compositions (0.01 M $AgNO_3$, 40 ^oC, 3 days, S/L=1/20, waterbath).

	SOLID (meq/gr zeolite)		LIQUID (meq/gr zeolite)	
Elements	Initial	Final	Initial	Final
Ca	0.31	0.14	0	0.003
Fe	0.44	0.40	0	0.001
K	0.83	0.75	0	0.002
Mg	0.09	0.08	0	0.000
Na	1.81	1.53	0	0.055
Ag	0.00	0.16	0.200	0.003
(meq/gr zeolite)	$\sum(Ca^{2+}+Na^{+}+K^{+}+Mg^{2+})$		Ag^{+}	
	0.55		*0.20*	

Table C.6. Solid and liquid phase compositions (0.01 M $AgNO_3$, 40 ^oC, 30 min, S/L=1/50, waterbath).

	SOLID (meq/gr zeolite)		LIQUID (meq/gr zeolite)	
Elements	Initial	Final	Initial	Final
Ca	0.31	0.18	0	0.001
Fe	0.44	0.48	0	0.017
K	0.83	0.85	0	**0.012**
Mg	0.09	0.08	0	0.000
Na	1.81	1.09	0	0.004
Ag	0.00	0.40	0.200	0.002
(meq/gr zeolite)	$\Sigma(Ca^{2+}+Na^{+}+K^{+}+Mg^{2+})$		Ag^{+}	
	0.88		*0.46*	

Table C.7. Solid and liquid phase compositions (0.01 M $AgNO_3$, 40 ^oC, 1 hr, S/L=1/50, waterbath).

	SOLID (meq/gr zeolite)		LIQUID (meq/gr zeolite)	
Elements	Initial	Final	Initial	Final
Ca	6.47	-0.33	0	0.012
Fe	0.31	0.17	0	0.000
K	0.44	0.48	0	0.004
Mg	0.83	0.86	0	0.002
Na	0.09	0.08	0	0.325
Ag	1.81	1.04	0.500	0.048
(meq/gr zeolite)	$\Sigma(Ca^{2+}+Na^{+}+K^{+}+Mg^{2+})$		Ag^{+}	
	0.95		*0.45*	

Table C.8. Solid and liquid phase compositions (0.01 M $AgNO_3$, 40 ^oC, 1 day, S/L=1/50, waterbath).

	SOLID (meq/gr zeolite)		LIQUID (meq/gr zeolite)	
Elements	Initial	Final	Initial	Final
Ca	0.31	0.16	0	0.001
Fe	0.44	0.42	0	0.000
K	0.83	0.85	0	0.004
Mg	0.09	0.07	0	0.000
Na	1.81	1.22	0	0.131
Ag	0.00	0.40	0.500	0.040
(meq/gr zeolite)	$\Sigma(Ca^{2+}+Na^{+}+K^{+}+Mg^{2+})$		Ag^{+}	
	0.78		*0.46*	

Table C.9. Solid and liquid phase compositions (0.01 M $AgNO_3$, 40 ^oC, 2 days, S/L=1/50, waterbath).

	SOLID (meq/gr zeolite)		LIQUID (meq/gr zeolite)	
Elements	Initial	Final	Initial	Final
Ca	0.31	0.19	0	0.001
Fe	0.44	0.43	0	0.000
K	0.83	0.81	0	0.004
Mg	0.09	0.08	0	0.000
Na	1.81	1.20	0	0.130
Ag	0.00	0.39	0.500	0.045
(meq/gr zeolite)	$\sum(Ca^{2+}+Na^{+}+K^{+}+Mg^{2+})$		Ag^{+}	
	0.76		*0.46*	

Table C.10. Solid and liquid phase compositions (0.01 M $AgNO_3$, 40 ^oC, 3 days, S/L=1/50, waterbath).

	SOLID (meq/gr zeolite)		LIQUID (meq/gr zeolite)	
Elements	Initial	Final	Initial	Final
Ca	0.31	0.17	0	0.001
Fe	0.44	0.49	0	0.001
K	0.83	0.78	0	0.004
Mg	0.09	0.09	0	0.000
Na	1.81	1.12	0	0.131
Ag	0.00	0.39	0.500	0.043
(meq/gr zeolite)	$\sum(Ca^{2+}+Na^{+}+K^{+}+Mg^{2+})$		Ag^{+}	
	0.88		*0.46*	

Table C.11. Solid and liquid phase compositions (0.01 M $AgNO_3$, 40 ^oC, 30 min, S/L=1/100, waterbath)..

	SOLID (meq/gr zeolite)		LIQUID (meq/gr zeolite)	
Elements	Initial	Final	Initial	Final
Ca	0.31	0.30	0	**0.026**
Fe	0.44	0.49	0	0.000
K	0.83	0.81	0	0.013
Mg	0.09	0.08	0	0.006
Na	1.81	0.75	0	0.444
Ag	0.00	0.59	1.000	0.228
(meq/gr zeolite)	$\sum(Ca^{2+}+Na^{+}+K^{+}+Mg^{2+})$		Ag^{+}	
	1.10		*0.77*	

Table C.12. Solid and liquid phase compositions (0.01 M $AgNO_3$, 40 ^oC, 1 hr, S/L=1/100, waterbath).

	SOLID (meq/gr zeolite)		LIQUID (meq/gr zeolite)	
Elements	Initial	Final	Initial	Final
Ca	0.31	0.19	0	0.029
Fe	0.44	0.48	0	0.000
K	0.83	0.86	0	0.013
Mg	0.09	0.07	0	0.005
Na	1.81	0.74	0	0.448
Ag	0.00	0.64	1.000	0.252
(meq/gr zeolite)	$\sum(Ca^{2+}+Na^{+}+K^{+}+Mg^{2+})$		Ag^{+}	
	1.25		*0.75*	

Table C.13. Solid and liquid phase compositions (0.01 M $AgNO_3$, 40 ^oC, 1 day, S/L=1/100, waterbath).

	SOLID (meq/gr zeolite)		LIQUID (meq/gr zeolite)	
Elements	Initial	Final	Initial	Final
Ca	0.31	0.15	0	0.004
Fe	0.44	0.43	0	0.000
K	0.83	0.82	0	0.013
Mg	0.09	0.08	0	0.001
Na	1.81	0.78	0	0.264
Ag	0.00	0.64	1.000	0.258
(meq/gr zeolite)	$\sum(Ca^{2+}+Na^{+}+K^{+}+Mg^{2+})$		Ag^{+}	
	1.22		*0.74*	

Table C.14. Solid and liquid phase compositions (0.01 M $AgNO_3$, 40 ^oC, 2 days, S/L=1/100, waterbath).

	SOLID (meq/gr zeolite)		LIQUID (meq/gr zeolite)	
Elements	Initial	Final	Initial	Final
Ca	0.31	0.14	0	0.003
Fe	0.44	0.43	0	0.000
K	0.83	0.79	0	0.012
Mg	0.09	0.09	0	0.001
Na	1.81	0.79	0	0.264
Ag	0.00	0.64	1.000	0.250
(meq/gr zeolite)	$\sum(Ca^{2+}+Na^{+}+K^{+}+Mg^{2+})$		Ag^{+}	
	1.24		*0.75*	

Table C.15. Solid and liquid phase compositions (0.01 M $AgNO_3$, 40 ^oC, 3 day, S/L=1/100, waterbath).

	SOLID (meq/gr zeolite)		LIQUID (meq/gr zeolite)	
Elements	Initial	Final	Initial	Final
Ca	0.31	0.15	0	0.002
Fe	0.44	0.42	0	0.000
K	0.83	0.77	0	0.013
Mg	0.09	0.09	0	0.001
Na	1.81	0.75	0	0.263
Ag	0.00	0.63	1.000	0.268
(meq/gr zeolite)	$\sum(Ca^{2+}+Na^{+}+K^{+}+Mg^{2+})$		Ag^{+}	
	1.29		*0.73*	

Table C.16. Solid and liquid phase compositions (0.01 M $AgNO_3$, 60 ^oC, 30 min, S/L=1/20, waterbath).

	SOLID (meq/gr zeolite)		LIQUID (meq/gr zeolite)	
Elements	Initial	Final	Initial	Final
Ca	0.31	0.18	0	0.005
Fe	0.44	0.54	0	0.000
K	0.83	0.81	0	0.002
Mg	0.09	0.08	0	0.001
Na	1.81	1.35	0	0.117
Ag	0.00	0.18	0.200	0.005
(meq/gr zeolite)	$\sum(Ca^{2+}+Na^{+}+K^{+}+Mg^{2+})$		Ag^{+}	
	0.63		*0.20*	

Table C.17. Solid and liquid phase compositions (0.01 M $AgNO_3$, 60 ^oC, 1 hr, S/L=1/20, waterbath).

	SOLID (meq/gr zeolite)		LIQUID (meq/gr zeolite)	
Elements	Initial	Final	Initial	Final
Ca	0.31	0.19	0	0.006
Fe	0.44	0.48	0	0.001
K	0.83	0.85	0	0.002
Mg	0.09	0.08	0	0.001
Na	1.81	1.36	0	0.118
Ag	0.00	0.17	0.200	0.004
(meq/gr zeolite)	$\sum(Ca^{2+}+Na^{+}+K^{+}+Mg^{2+})$		Ag^{+}	
	0.60		*0.20*	

Table C.18. Solid and liquid phase compositions (0.01 M $AgNO_3$, 60 ^oC, 1 day, S/L=1/20, waterbath).

	SOLID (meq/gr zeolite)		LIQUID (meq/gr zeolite)	
Elements	Initial	Final	Initial	Final
Ca	0.31	0.12	0	0.000
Fe	0.44	0.45	0	0.001
K	0.83	0.95	0	0.002
Mg	0.09	0.09	0	0.000
Na	1.81	1.30	0	0.052
Ag	0.00	0.16	0.200	0.005
(meq/gr zeolite)	$\sum(Ca^{2+}+Na^{+}+K^{+}+Mg^{2+})$		Ag^{+}	
	0.82		*0.20*	

Table C.19. Solid and liquid phase compositions (0.01 M $AgNO_3$, 60 ^oC, 2 day, S/L=1/20, waterbath).

	SOLID (meq/gr zeolite)		LIQUID (meq/gr zeolite)	
Elements	Initial	Final	Initial	Final
Ca	0.31	0.12	0	0.000
Fe	0.44	0.41	0	0.001
K	0.83	0.88	0	0.002
Mg	0.09	0.10	0	0.000
Na	1.81	1.26	0	0.052
Ag	0.00	0.19	0.200	0.006
(meq/gr zeolite)	$\sum(Ca^{2+}+Na^{+}+K^{+}+Mg^{2+})$		Ag^{+}	
	0.80		*0.19*	

Table C.20. Solid and liquid phase compositions (0.01 M $AgNO_3$, 60 ^oC, 3 days, S/L=1/20, waterbath).

	SOLID (meq/gr zeolite)		LIQUID (meq/gr zeolite)	
Elements	Initial	Final	Initial	Final
Ca	0.31	0.14	0	0.000
Fe	0.44	0.44	0	0.001
K	0.83	0.91	0	0.002
Mg	0.09	0.10	0	0.000
Na	1.81	1.28	0	0.052
Ag	0.00	0.20	0.200	0.004
(meq/gr zeolite)	$\sum(Ca^{2+}+Na^{+}+K^{+}+Mg^{2+})$		Ag^{+}	
	0.78		*0.20*	

Table C.21. Solid and liquid phase compositions (0.01 M $AgNO_3$, 60 ^oC, 30 min, S/L=1/50, waterbath).

	SOLID (meq/gr zeolite)		LIQUID (meq/gr zeolite)	
Elements	Initial	Final	Initial	Final
Ca	0.31	0.18	0	**0.012**
Fe	0.44	0.49	0	0.000
K	0.83	0.89	0	0.005
Mg	0.09	0.07	0	0.002
Na	1.81	1.08	0	0.266
Ag	0.00	0.42	0.500	0.042
(meq/gr zeolite)	$\sum(Ca^{2+}+Na^{+}+K^{+}+Mg^{2+})$		Ag^{+}	
	0.91		*0.46*	

Table C.22. Solid and liquid phase compositions (0.01 M $AgNO_3$, 60 ^oC, 1 hr, S/L=1/50, waterbath).

	SOLID (meq/gr zeolite)		LIQUID (meq/gr zeolite)	
Elements	Initial	Final	Initial	Final
Ca	0.31	0.16	0	0.04
Fe	0.44	0.48	0	0.001
K	0.83	0.82	0	0.005
Mg	0.09	0.07	0	0.003
Na	1.81	0.98	0	0.269
Ag	0.00	0.42	0.500	0.043
(meq/gr zeolite)	$\sum(Ca^{2+}+Na^{+}+K^{+}+Mg^{2+})$		Ag^{+}	
	1.01		*0.46*	

Table C.23. Solid and liquid phase compositions (0.01 M $AgNO_3$, 60 ^oC, 1 day, S/L=1/50, waterbath).

	SOLID (meq/gr zeolite)		LIQUID (meq/gr zeolite)	
Elements	Initial	Final	Initial	Final
Ca	0.31	0.17	0	0.002
Fe	0.44	0.46	0	0.001
K	0.83	0.92	0	0.006
Mg	0.09	0.01	0	0.000
Na	1.81	1.57	0	0.131
Ag	0.00	0.41	0.500	0.045
(meq/gr zeolite)	$\sum(Ca^{2+}+Na^{+}+K^{+}+Mg^{2+})$		Ag^{+}	
	0.55		*0.46*	

Table C.24. Solid and liquid phase compositions (0.01 M $AgNO_3$, 60 ^oC, 2 days, S/L=1/50, waterbath).

	SOLID (meq/gr zeolite)		LIQUID (meq/gr zeolite)	
Elements	Initial	Final	Initial	Final
Ca	0.31	0.13	0	0.001
Fe	0.44	0.50	0	0.001
K	0.83	0.79	0	0.006
Mg	0.09	0.01	0	0.000
Na	1.81	0.91	0	0.131
Ag	0.00	0.40	0.500	0.048
(meq/gr zeolite)	$\sum(Ca^{2+}+Na^{+}+K^{+}+Mg^{2+})$		Ag^{+}	
	1.21		*0.46*	

Table C.25. Solid and liquid phase compositions (0.01 M $AgNO_3$, 60 ^oC, 3 days, S/L=1/50, waterbath).

	SOLID (meq/gr zeolite)		LIQUID (meq/gr zeolite)	
Elements	Initial	Final	Initial	Final
Ca	0.31	0.12	0	0.001
Fe	0.44	0.46	0	0.001
K	0.83	0.90	0	0.006
Mg	0.09	0.01	0	0.000
Na	1.81	1.60	0	0.131
Ag	0.00	0.42	0.500	0.046
(meq/gr zeolite)	$\sum(Ca^{2+}+Na^{+}+K^{+}+Mg^{2+})$		Ag^{+}	
	0.54		*0.46*	

Table C.26. Solid and liquid phase compositions (0.01 M $AgNO_3$, 60 ^oC, 30 min, S/L=1/100, waterbath).

	SOLID (meq/gr zeolite)		LIQUID (meq/gr zeolite)	
Elements	Initial	Final	Initial	Final
Ca	0.31	0.13	0	**0.026**
Fe	0.44	0.46	0	0.000
K	0.83	0.81	0	0.015
Mg	0.09	0.07	0	0.005
Na	1.81	0.71	0	0.429
Ag	0.00	0.64	1.000	0.238
(meq/gr zeolite)	$\sum(Ca^{2+}+Na^{+}+K^{+}+Mg^{2+})$		Ag^{+}	
	1.32		*0.76*	

Table C.27. Solid and liquid phase compositions (0.01 M $AgNO_3$, 60 ^oC, 1 hr, S/L=1/100, waterbath).

	SOLID (meq/gr zeolite)		LIQUID (meq/gr zeolite)	
Elements	Initial	Final	Initial	Final
Ca	0.31	0.13	0	0.027
Fe	0.44	0.45	0	0.000
K	0.83	0.79	0	0.015
Mg	0.09	0.07	0	0.005
Na	1.81	0.68	0	0.444
Ag	0.00	0.63	1.000	0.219
(meq/gr zeolite)	$\sum(Ca^{2+}+Na^{+}+K^{+}+Mg^{2+})$		Ag^{+}	
	1.38		*0.78*	

Table C.28. Solid and liquid phase compositions (0.01 M $AgNO_3$, 60 ^oC, 1 day, S/L=1/100, waterbath).

	SOLID (meq/gr zeolite)		LIQUID (meq/gr zeolite)	
Elements	Initial	Final	Initial	Final
Ca	0.31	0.13	0	0.001
Fe	0.44	0.55	0	0.001
K	0.83	0.76	0	0.008
Mg	0.09	0.01	0	0.000
Na	1.81	0.60	0	0.262
Ag	0.00	0.65	1.000	0.236
(meq/gr zeolite)	$\sum(Ca^{2+}+Na^{+}+K^{+}+Mg^{2+})$		Ag^{+}	
	1.54		*0.76*	

Table C.29. Solid and liquid phase compositions (0.01 M $AgNO_3$, 60 ^oC, 2 day, S/L=1/100, waterbath).

	SOLID (meq/gr zeolite)		LIQUID (meq/gr zeolite)	
Elements	Initial	Final	Initial	Final
Ca	0.31	0.17	0	0.003
Fe	0.44	0.43	0	0.000
K	0.83	0.84	0	0.014
Mg	0.09	0.02	0	0.001
Na	1.81	0.57	0	0.264
Ag	0.00	0.67	1.000	0.253
(meq/gr zeolite)	$\sum(Ca^{2+}+Na^{+}+K^{+}+Mg^{2+})$		Ag^{+}	
	1.47		*0.75*	

Table C.30. Solid and liquid phase compositions (0.01 M $AgNO_3$, 60 ^oC, 3 days, S/L=1/50, waterbath).

	SOLID (meq/gr zeolite)		LIQUID (meq/gr zeolite)	
Elements	Initial	Final	Initial	Final
Ca	0.31	0.22	0	0.003
Fe	0.44	0.47	0	0.000
K	0.83	0.85	0	0.016
Mg	0.09	0.02	0	0.000
Na	1.81	1.72	0	0.264
Ag	0.00	0.66	1.000	0.256
(meq/gr zeolite)	$\sum(Ca^{2+}+Na^{+}+K^{+}+Mg^{2+})$		Ag^{+}	
	1.27		*0.74*	

Table C.31. Solid and liquid phase compositions (0.01 M $AgNO_3$, 80 ^oC, 30 min, S/L=1/20, waterbath).

	SOLID (meq/gr zeolite)		LIQUID (meq/gr zeolite)	
Elements	Initial	Final	Initial	Final
Ca	0.31	0.17	0	0.001
Fe	0.44	0.60	0	0.000
K	0.83	0.65	0	0.001
Mg	0.09	0.09	0	0.000
Na	1.81	1.46	0	0.090
Ag	0.00	0.14	0.200	0.003
(meq/gr zeolite)	$\sum(Ca^{2+}+Na^{+}+K^{+}+Mg^{2+})$		Ag^{+}	
	0.68		*0.20*	

Table C.32. Solid and liquid phase compositions (0.01 M $AgNO_3$, 80 ^oC, 1 hr, S/L=1/20, waterbath).

	SOLID (meq/gr zeolite)		LIQUID (meq/gr zeolite)	
Elements	Initial	Final	Initial	Final
Ca	0.31	0.21	0	0.000
Fe	0.44	0.61	0	0.001
K	0.83	0.65	0	0.001
Mg	0.09	0.09	0	0.000
Na	1.81	1.52	0	0.088
Ag	0.00	0.15	0.200	0.003
(meq/gr zeolite)	$\sum(Ca^{2+}+Na^{+}+K^{+}+Mg^{2+})$		Ag^{+}	
	0.58		*0.20*	

Table C.33. Solid and liquid phase compositions (0.01 M $AgNO_3$, 80 ^oC, 1 day, S/L=1/20, waterbath).

	SOLID (meq/gr zeolite)		LIQUID (meq/gr zeolite)	
Elements	Initial	Final	Initial	Final
Ca	0.31	0.14	0	0.007
Fe	0.44	0.44	0	0.012
K	0.83	0.98	0	0.002
Mg	0.09	0.08	0	0.004
Na	1.81	1.51	0	0.177
Ag	0.00	0.18	0.200	0.006
(meq/gr zeolite)	$\Sigma(Ca^{2+}+Na^{+}+K^{+}+Mg^{2+})$		Ag^{+}	
	0.63		*0.20*	

Table C.34. Solid and liquid phase compositions (0.01 M $AgNO_3$, 80 ^oC, 2 days, S/L=1/20, waterbath).

	SOLID (meq/gr zeolite)		LIQUID (meq/gr zeolite)	
Elements	Initial	Final	Initial	Final
Ca	0.31	0.13	0	0.006
Fe	0.44	0.44	0	0.017
K	0.83	0.94	0	0.002
Mg	0.09	0.08	0	0.004
Na	1.81	1.46	0	0.159
Ag	0.00	0.19	0.200	0.006
(meq/gr zeolite)	$\Sigma(Ca^{2+}+Na^{+}+K^{+}+Mg^{2+})$		Ag^{+}	
	0.65		*0.19*	

Table C.35. Solid and liquid phase compositions (0.01 M $AgNO_3$, 80 ^oC, 2 days, S/L=1/20, waterbath).

	SOLID (meq/gr zeolite)		LIQUID (meq/gr zeolite)	
Elements	Initial	Final	Initial	Final
Ca	0.31	0.11	0	0.008
Fe	0.44	0.42	0	0.011
K	0.83	0.91	0	0.002
Mg	0.09	0.08	0	0.004
Na	1.81	1.45	0	0.171
Ag	0.00	0.17	0.200	0.005
(meq/gr zeolite)	$\Sigma(Ca^{2+}+Na^{+}+K^{+}+Mg^{2+})$		Ag^{+}	
	0.65		*0.20*	

Table C.36. Solid and liquid phase compositions (0.01 M $AgNO_3$, 80 ^oC, 1 day, S/L=1/50, waterbath).

	SOLID (meq/gr zeolite)		LIQUID (meq/gr zeolite)	
Elements	Initial	Final	Initial	Final
Ca	0.31	0.10	0	0.008
Fe	0.44	0.38	0	0.001
K	0.83	0.74	0	0.005
Mg	0.09	0.07	0	0.004
Na	1.81	0.89	0	0.275
Ag	0.00	0.28	0.500	0.053
(meq/gr zeolite)	$\sum(Ca^{2+}+Na^{+}+K^{+}+Mg^{2+})$		Ag^{+}	
	1.25		*0.45*	

Table C.37. Solid and liquid phase compositions (0.01 M $AgNO_3$, 80 ^oC, 2 days, S/L=1/50, waterbath).

	SOLID (meq/gr zeolite)		LIQUID (meq/gr zeolite)	
Elements	Initial	Final	Initial	Final
Ca	0.31	0.08	0	0.008
Fe	0.44	0.33	0	0.003
K	0.83	0.58	0	0.004
Mg	0.09	0.05	0	0.004
Na	1.81	0.75	0	0.292
Ag	0.00	0.39	0.500	0.037
(meq/gr zeolite)	$\sum(Ca^{2+}+Na^{+}+K^{+}+Mg^{2+})$		Ag^{+}	
	1.59		*0.46*	

Table C.38. Solid and liquid phase compositions (0.01 M $AgNO_3$, 80 ^oC, 3 days, S/L=1/50, waterbath).

	SOLID (meq/gr zeolite)		LIQUID (meq/gr zeolite)	
Elements	Initial	Final	Initial	Final
Ca	0.31	0.13	0	0.010
Fe	0.44	0.46	0	0.003
K	0.83	0.88	0	0.005
Mg	0.09	0.09	0	0.004
Na	1.81	1.09	0	0.291
Ag	0.00	0.41	0.500	0.042
(meq/gr zeolite)	$\sum(Ca^{2+}+Na^{+}+K^{+}+Mg^{2+})$		Ag^{+}	
	0.95		*0.46*	

Table C.39. Solid and liquid phase compositions (0.01 M $AgNO_3$, 80 ^oC, 30 min, S/L=1/50, waterbath).

	SOLID (meq/gr zeolite)		LIQUID (meq/gr zeolite)	
Elements	Initial	Final	Initial	Final
Ca	0.31	0.17	0	**0.001**
Fe	0.44	0.58	0	0.000
K	0.83	0.64	0	0.005
Mg	0.09	0.08	0	0.000
Na	1.81	1.13	0	0.208
Ag	0.00	0.37	0.500	0.025
(meq/gr zeolite)	$\sum(Ca^{2+}+Na^{+}+K^{+}+Mg^{2+})$		Ag^{+}	
	1.03		*0.48*	

Table C.40. Solid and liquid phase compositions (0.01 M $AgNO_3$, 80 ^oC, 1 hr, S/L=1/50, waterbath).

	SOLID (meq/gr zeolite)		LIQUID (meq/gr zeolite)	
Elements	Initial	Final	Initial	Final
Ca	0.31	0.20	0	0.000
Fe	0.44	0.78	0	0.001
K	0.83	0.62	0	0.005
Mg	0.09	0.08	0	0.000
Na	1.81	1.07	0	0.218
Ag	0.00	0.42	0.500	0.025
(meq/gr zeolite)	$\sum(Ca^{2+}+Na^{+}+K^{+}+Mg^{2+})$		Ag^{+}	
	1.08		*0.48*	

Table C.41. Solid and liquid phase compositions (0.01 M $AgNO_3$, 80 ^oC, 30 min, S/L=1/100, waterbath).

	SOLID (meq/gr zeolite)		LIQUID (meq/gr zeolite)	
Elements	Initial	Final	Initial	Final
Ca	0.31	0.19	0	**0.001**
Fe	0.44	0.73	0	0.002
K	0.83	0.67	0	0.008
Mg	0.09	0.11	0	0.000
Na	1.81	1.00	0	0.363
Ag	0.00	0.54	1.000	0.132
(meq/gr zeolite)	$\sum(Ca^{2+}+Na^{+}+K^{+}+Mg^{2+})$		Ag^{+}	
	1.11		*0.87*	

Table C.42. Solid and liquid phase compositions (0.01 M $AgNO_3$, 80 ^oC, 1 hr, S/L=1/100, waterbath).

	SOLID (meq/gr zeolite)		LIQUID (meq/gr zeolite)	
Elements	Initial	Final	Initial	Final
Ca	0.31	0.15	0	0.003
Fe	0.44	0.72	0	0.003
K	0.83	0.70	0	0.008
Mg	0.09	0.10	0	0.000
Na	1.81	0.96	0	0.365
Ag	0.00	0.68	1.000	0.124
(meq/gr zeolite)	$\Sigma(Ca^{2+}+Na^{+}+K^{+}+Mg^{2+})$		Ag^{+}	
	1.15		*0.88*	

Table C.43. Solid and liquid phase compositions (0.01 M $AgNO_3$, 80 ^oC, 1 day, S/L=1/100, waterbath).

	SOLID (meq/gr zeolite)		LIQUID (meq/gr zeolite)	
Elements	Initial	Final	Initial	Final
Ca	0.31	0.12	0	0.027
Fe	0.44	0.44	0	0.001
K	0.83	0.83	0	0.013
Mg	0.09	0.08	0	0.010
Na	1.81	0.77	0	0.453
Ag	0.00	0.64	1.000	0.216
(meq/gr zeolite)	$\Sigma(Ca^{2+}+Na^{+}+K^{+}+Mg^{2+})$		Ag^{+}	
	1.25		*0.78*	

Table C.44. Solid and liquid phase compositions (0.01 M $AgNO_3$, 80 ^oC, 2 days, S/L=1/100, waterbath).

	SOLID (meq/gr zeolite)		LIQUID (meq/gr zeolite)	
Elements	Initial	Final	Initial	Final
Ca	0.31	0.10	0	0.023
Fe	0.44	0.43	0	0.002
K	0.83	0.80	0	0.015
Mg	0.09	0.08	0	0.009
Na	1.81	0.74	0	0.488
Ag	0.00	0.64	1.000	0.213
(meq/gr zeolite)	$\Sigma(Ca^{2+}+Na^{+}+K^{+}+Mg^{2+})$		Ag^{+}	
	1.34		*0.79*	

Table C.45. Solid and liquid phase compositions (0.01 M $AgNO_3$, 80 ^oC, 3 days, S/L=1/100, waterbath).

	SOLID (meq/gr zeolite)		LIQUID (meq/gr zeolite)	
Elements	Initial	Final	Initial	Final
Ca	0.31	0.11	0	0.001
Fe	0.44	0.44	0	0.032
K	0.83	0.80	0	0.003
Mg	0.09	0.07	0	0.908
Na	1.81	0.75	0	0.985
Ag	0.00	0.64	0.500	0.268
(meq/gr zeolite)	$\sum(Ca^{2+}+Na^{+}+K^{+}+Mg^{2+})$		Ag^{+}	
	1.31		*0.73*	

Table C.46. Solid and liquid phase compositions (0.01 M $AgNO_3$, 40 ^oC, 30 min, S/L=1/20, microwave irradiation).

	SOLID (meq/gr zeolite)		LIQUID (meq/gr zeolite)	
Elements	Initial	Final	Initial	Final
Ca	0.31	0.16	0	0.003
Fe	0.44	0.45	0	0.000
K	0.83	0.88	0	0.002
Mg	0.09	0.08	0	0.001
Na	1.81	1.33	0	0.090
Ag	0.00	0.12	0.200	0.039
(meq/gr zeolite)	$\sum(Ca^{2+}+Na^{+}+K^{+}+Mg^{2+})$		Ag^{+}	
	0.69		*0.16*	

Table C.47. Solid and liquid phase compositions (0.01 M $AgNO_3$, 40 ^oC, 1 hr, S/L=1/20, microwave irradiation).

	SOLID (meq/gr zeolite)		LIQUID (meq/gr zeolite)	
Elements	Initial	Final	Initial	Final
Ca	0.31	0.13	0	0.003
Fe	0.44	0.48	0	0.000
K	0.83	0.85	0	0.002
Mg	0.09	0.08	0	0.001
Na	1.81	1.31	0	0.086
Ag	0.00	0.13	0.200	0.038
(meq/gr zeolite)	$\sum(Ca^{2+}+Na^{+}+K^{+}+Mg^{2+})$		Ag^{+}	
	0.71		*0.16*	

Table C.48. Solid and liquid phase compositions (0.01 M $AgNO_3$, 40 ^oC, 30min, S/L=1/50, microwave irradiation).

	SOLID (meq/gr zeolite)		LIQUID (meq/gr zeolite)	
Elements	Initial	Final	Initial	Final
Ca	0.31	0.12	0	**0.010**
Fe	0.44	0.41	0	0.000
K	0.83	0.80	0	0.004
Mg	0.09	0.07	0	0.002
Na	1.81	1.23	0	0.176
Ag	0.00	0.22	0.500	0.256
(meq/gr zeolite)	$\sum(Ca^{2+}+Na^{+}+K^{+}+Mg^{2+})$		Ag^{+}	
	0.83		*0.24*	

Table C.49. Solid and liquid phase compositions (0.01 M $AgNO_3$, 40 ^oC, 1 hr, S/L=1/50, microwave irradiation).

	SOLID (meq/gr zeolite)		LIQUID (meq/gr zeolite)	
Elements	Initial	Final	Initial	Final
Ca	0.31	0.11	0	0.006
Fe	0.44	0.39	0	0.000
K	0.83	0.78	0	0.005
Mg	0.09	0.07	0	0.002
Na	1.81	1.09	0	0.183
Ag	0.00	0.18	0.500	0.272
(meq/gr zeolite)	$\sum(Ca^{2+}+Na^{+}+K^{+}+Mg^{2+})$		Ag^{+}	
	1.00		*0.23*	

Table C.50. Solid and liquid phase compositions (0.01 M $AgNO_3$, 40 ^oC, 30min, S/L=1/100, microwave irradiation).

	SOLID (meq/gr zeolite)		LIQUID (meq/gr zeolite)	
Elements	Initial	Final	Initial	Final
Ca	0.31	0.12	0	**0.02**
Fe	0.44	0.42	0	0.00
K	0.83	0.75	0	0.01
Mg	0.09	0.08	0	0.01
Na	1.81	0.96	0	0.24
Ag	0.00	0.31	1.000	0.66
(meq/gr zeolite)	$\sum(Ca^{2+}+Na^{+}+K^{+}+Mg^{2+})$		Ag^{+}	
	1.14		*0.34*	

Table C.51. Solid and liquid phase compositions (0.01 M $AgNO_3$, 40 ^oC, 1 hr S/L=1/100, microwave irradiation).

	SOLID (meq/gr zeolite)		LIQUID (meq/gr zeolite)	
Elements	Initial	Final	Initial	Final
Ca	0.31	0.12	0	0.02
Fe	0.44	0.39	0	0.00
K	0.83	0.69	0	0.01
Mg	0.09	0.07	0	0.01
Na	1.81	0.88	0	0.19
Ag	0.00	0.22	1.000	0.66
(meq/gr zeolite)	$\sum(Ca^{2+}+Na^{+}+K^{+}+Mg^{2+})$		Ag^{+}	
	1.29		*0.34*	

Table C.52. Solid and liquid phase compositions (0.01 M $AgNO_3$, 60 ^oC, 30 min, S/L=1/20, microwave irradiation).

	SOLID (meq/gr zeolite)		LIQUID (meq/gr zeolite)	
Elements	Initial	Final	Initial	Final
Ca	0.31	0.20	0	0.001
Fe	0.44	0.54	0	0.000
K	0.83	0.81	0	0.002
Mg	0.09	0.08	0	0.001
Na	1.81	1.35	0	0.038
Ag	0.00	0.18	0.200	0.065
(meq/gr zeolite)	$\sum(Ca^{2+}+Na^{+}+K^{+}+Mg^{2+})$		Ag^{+}	
	0.61		*0.14*	

Table C.53. Solid and liquid phase compositions (0.01 M $AgNO_3$, 60 ^oC, 1 hr, S/L=1/20, microwave irradiation).

	SOLID (meq/gr zeolite)		LIQUID (meq/gr zeolite)	
Elements	Initial	Final	Initial	Final
Ca	0.31	0.19	0	0.003
Fe	0.44	0.48	0	0.000
K	0.83	0.85	0	0.002
Mg	0.09	0.08	0	0.001
Na	1.81	1.36	0	0.047
Ag	0.00	0.17	0.200	0.070
(meq/gr zeolite)	$\sum(Ca^{2+}+Na^{+}+K^{+}+Mg^{2+})$		Ag^{+}	
	0.60		*0.13*	

Table C.54. Solid and liquid phase compositions (0.01 M $AgNO_3$, 60 ^oC, 30 min, S/L=1/50, microwave irradiation).

	SOLID (meq/gr zeolite)		LIQUID (meq/gr zeolite)	
Elements	Initial	Final	Initial	Final
Ca	0.31	0.17	0	**0.010**
Fe	0.44	0.49	0	0.000
K	0.83	0.89	0	0.004
Mg	0.09	0.07	0	0.002
Na	1.81	1.17	0	0.176
Ag	0.00	0.42	0.500	0.169
(meq/gr zeolite)	$\sum(Ca^{2+}+Na^{+}+K^{+}+Mg^{2+})$		Ag^{+}	
	0.86		*0.33*	

Table C.55. Solid and liquid phase compositions (0.01 M $AgNO_3$, 60 ^oC, 1hr, S/L=1/20, microwave irradiation).

	SOLID (meq/gr zeolite)		LIQUID (meq/gr zeolite)	
Elements	Initial	Final	Initial	Final
Ca	0.31	0.16	0	0.006
Fe	0.44	0.48	0	0.000
K	0.83	0.82	0	0.006
Mg	0.09	0.07	0	0.002
Na	1.81	0.98	0	0.150
Ag	0.00	0.42	0.500	0.144
(meq/gr zeolite)	$\sum(Ca^{2+}+Na^{+}+K^{+}+Mg^{2+})$		Ag^{+}	
	1.01		*0.36*	

Table C.56. Solid and liquid phase compositions (0.01 M $AgNO_3$, 60 ^oC, 30 min, S/L=1/100, microwave irradiation).

	SOLID (meq/gr zeolite)		LIQUID (meq/gr zeolite)	
Elements	Initial	Final	Initial	Final
Ca	0.31	0.14	0	**0.012**
Fe	0.44	0.46	0	0.000
K	0.83	0.81	0	0.009
Mg	0.09	0.07	0	0.004
Na	1.81	0.71	0	0.165
Ag	0.00	0.64	1.000	0.406
(meq/gr zeolite)	$\sum(Ca^{2+}+Na^{+}+K^{+}+Mg^{2+})$		Ag^{+}	
	1.32		*0.59*	

Table C.57. Solid and liquid phase compositions (0.01 M $AgNO_3$, 60 ^oC, 1 hr, S/L=1/100, microwave irradiation).

	SOLID		LIQUID	
Elements	Initial	Final	Initial	Final
Ca	0.31	0.13	0	0.000
Fe	0.44	0.45	0	0.000
K	0.83	0.79	0	0.004
Mg	0.09	0.07	0	0.000
Na	1.81	0.68	0	0.186
Ag	0.00	0.63	1.000	0.388
(meq/gr zeolite)	$\sum(Ca^{2+}+Na^{+}+K^{+}+Mg^{2+})$		Ag^{+}	
	1.39		*0.61*	

Table C.58. Solid and liquid phase compositions (0.01 M $AgNO_3$, 80 ^oC, 30 min, S/L=1/20, microwave irradiation).

	SOLID (meq/gr zeolite)		LIQUID (meq/gr zeolite)	
Elements	Initial	Final	Initial	Final
Ca	0.31	0.17	0	0.004
Fe	0.44	0.51	0	0.000
K	0.83	0.68	0	0.003
Mg	0.09	0.10	0	0.001
Na	1.81	1.33	0	0.093
Ag	0.00	0.14	0.200	0.059
(meq/gr zeolite)	$\sum(Ca^{2+}+Na^{+}+K^{+}+Mg^{2+})$		Ag^{+}	
	0.78		*0.14*	

Table C.59. Solid and liquid phase compositions (0.01 M $AgNO_3$, 80 ^oC, 1 hr, S/L=1/20, microwave irradiation).

	SOLID (meq/gr zeolite)		LIQUID (meq/gr zeolite)	
Elements	Initial	Final	Initial	Final
Ca	0.31	0.31	0	0.004
Fe	0.44	0.51	0	0.000
K	0.83	0.59	0	0.002
Mg	0.09	0.10	0	0.001
Na	1.81	1.33	0	0.051
Ag	0.00	0.17	0.200	0.073
(meq/gr zeolite)	$\sum(Ca^{2+}+Na^{+}+K^{+}+Mg^{2+})$		Ag^{+}	
	0.73		*0.13*	

Table C.60. Solid and liquid phase compositions (0.01 M $AgNO_3$, 80 ^oC, 30 min, S/L=1/50, microwave irradiation).

	SOLID (meq/gr zeolite)		LIQUID (meq/gr zeolite)	
Elements	Initial	Final	Initial	Final
Ca	0.31	0.17	0	**0.008**
Fe	0.44	0.55	0	0.000
K	0.83	0.76	0	0.004
Mg	0.09	0.09	0	0.002
Na	1.81	1.26	0	0.109
Ag	0.00	0.45	0.500	0.116
(meq/gr zeolite)	$\Sigma(Ca^{2+}+Na^{+}+K^{+}+Mg^{2+})$		Ag^{+}	
	0.77		*0.38*	

Table C.61. Solid and liquid phase compositions (0.01 M $AgNO_3$, 80 ^oC, 1 hr, S/L=1/50, microwave irradiation).

	SOLID (meq/gr zeolite)		LIQUID (meq/gr zeolite)	
Elements	Initial	Final	Initial	Final
Ca	0.31	0.19	0	0.005
Fe	0.44	0.54	0	0.000
K	0.83	0.75	0	0.007
Mg	0.09	0.10	0	0.002
Na	1.81	1.28	0	0.222
Ag	0.00	0.46	0.500	0.108
(meq/gr zeolite)	$\Sigma(Ca^{2+}+Na^{+}+K^{+}+Mg^{2+})$		Ag^{+}	
	0.75		*0.39*	

Table C.62. Solid and liquid phase compositions (0.01 M $AgNO_3$, 80 ^oC, 30 min, S/L=1/100, microwave irradiation).

	SOLID (meq/gr zeolite)		LIQUID (meq/gr zeolite)	
Elements	Initial	Final	Initial	Final
Ca	0.31	0.19	0	**0.01**
Fe	0.44	0.62	0	0.00
K	0.83	0.63	0	0.01
Mg	0.09	0.09	0	0.00
Na	1.81	1.02	0	0.68
Ag	0.00	0.57	1.000	0.38
(meq/gr zeolite)	$\Sigma(Ca^{2+}+Na^{+}+K^{+}+Mg^{2+})$		Ag^{+}	
	1.11		*0.62*	

Table C.63. Solid and liquid phase compositions (0.01 M $AgNO_3$, 80 ^oC, 1 hr, S/L=1/20, microwave irradiation).

	SOLID (meq/gr zeolite)		LIQUID (meq/gr zeolite)	
Elements	Initial	Final	Initial	Final
Ca	0.31	0.21	0	0.02
Fe	0.44	0.60	0	0.00
K	0.83	0.63	0	0.01
Mg	0.09	0.08	0	0.00
Na	1.81	1.12	0	0.71
Ag	0.00	0.68	0.500	0.38
(meq/gr zeolite)	$\sum(Ca^{2+}+Na^{+}+K^{+}+Mg^{2+})$		Ag^{+}	
	1.01		*0.62*	

Table C.64. Solid and liquid phase compositions (0.01 M $Co\cdot(NO_3)_2\cdot 6H_2O$, 80 ^oC, 1hr S/L=1/20,waterbath).

	SOLID (meq/gr zeolite)		LIQUID (meq/gr zeolite)	
Elements	Initial	Final	Initial	Final
Ca	0.09	0.06	0	0.001
Fe	0.31	0.24	0	0.001
K	0.36	0.34	0	0.001
Mg	0.04	0.04	0	0.000
Na	0.92	0.63	0	0.144
Co	0.01	0.18	0.200	0.001
(meq/gr zeolite)	$\sum(Ca^{2+}+Na^{+}+K^{+}+Mg^{2+})$		Co^{2+}	
	0.34		*0.20*	

Table C.65. Solid and liquid phase compositions (0.01 M $Co\cdot(NO_3)_2\cdot 6H_2O$, 80 ^oC, 24 hrs, S/L=1/20,waterbath).

	SOLID (meq/gr zeolite)		LIQUID (meq/gr zeolite)	
Elements	Initial	Final	Initial	Final
Ca	0.09	0.06	0	0.001
Fe	0.31	0.27	0	0.004
K	0.36	0.30	0	0.001
Mg	0.04	0.04	0	0.000
Na	0.92	0.58	0	0.160
Co	0.01	0.17	0.200	0.002
(meq/gr zeolite)	$\sum(Ca^{2+}+Na^{+}+K^{+}+Mg^{2+})$		Co^{2+}	
	0.44		*0.20*	

Table C.66. Solid and liquid phase compositions (0.01 M $Co{\cdot}(NO_3)_2{\cdot}6H_2O$, 80 ^oC, 1hr S/L=1/50,waterbath).

	SOLID (meq/gr zeolite)		LIQUID (meq/gr zeolite)	
Elements	Initial	Final	Initial	Final
Ca	0.09	0.09	0	**0.001**
Fe	0.31	0.25	0	0.000
K	0.36	0.32	0	0.005
Mg	0.04	0.04	0	0.000
Na	0.92	0.46	0	0.208
Co	0.01	0.36	0.500	0.102
(meq/gr zeolite)	$\sum(Ca^{2+}+Na^{+}+K^{+}+Mg^{2+})$		Co^{2+}	
	0.50		*0.40*	

Table C.67. Solid and liquid phase compositions (0.01 M $Co{\cdot}(NO_3)_2{\cdot}6H_2O$, 80 ^oC, 24 hrs, S/L=1/50,waterbath).

	SOLID (meq/gr zeolite)		LIQUID (meq/gr zeolite)	
Elements	Initial	Final	Initial	Final
Ca	0.09	0.07	0	0.000
Fe	0.31	0.27	0	0.001
K	0.36	0.31	0	0.005
Mg	0.04	0.05	0	0.000
Na	0.92	0.42	0	0.218
Co	0.01	0.35	0.500	0.103
(meq/gr zeolite)	$\sum(Ca^{2+}+Na^{+}+K^{+}+Mg^{2+})$		Co^{2+}	
	0.58		*0.40*	

Table C.68. Solid and liquid phase compositions (0.01 M $Co{\cdot}(NO_3)_2{\cdot}6H_2O$, 80 ^oC, 1 hr, S/L=1/100,waterbath).

	SOLID (meq/gr zeolite)		LIQUID (meq/gr zeolite)	
Elements	Initial	Final	Initial	Final
Ca	0.09	0.07	0	**0.00**
Fe	0.31	0.26	0	0.00
K	0.36	0.33	0	0.01
Mg	0.04	0.04	0	0.00
Na	0.92	0.37	0	0.31
Co	0.01	0.43	1.000	0.43
(meq/gr zeolite)	$\sum(Ca^{2+}+Na^{+}+K^{+}+Mg^{2+})$		Co^{2+}	
	0.61		*0.57*	

Table C.69. Solid and liquid phase compositions (0.01 M $Co(NO_3)_2 \cdot 6H_2O$, 80 ^oC, 24 hrs, S/L=1/100,waterbath).

	SOLID (meq/gr zeolite)		LIQUID (meq/gr zeolite)	
Elements	Initial	Final	Initial	Final
Ca	0.09	0.07	0	0.00
Fe	0.31	0.27	0	0.00
K	0.36	0.31	0	0.01
Mg	0.04	0.04	0	0.00
Na	0.92	0.35	0	0.36
Co	0.01	0.42	1.000	0.26
(meq/gr zeolite)	$\sum(Ca^{2+}+Na^{+}+K^{+}+Mg^{2+})$		Co^{2+}	
	0.65		*0.74*	

Table C.70. Solid and liquid phase compositions (0.01 M $Co(NO_3)_2 \cdot 6H_2O$, 80 ^oC, 10 min, S/L=1/20, microwave irradiation).

	SOLID (meq/gr zeolite)		LIQUID (meq/gr zeolite)	
Elements	Initial	Final	Initial	Final
Ca	0.09	0.07	0	0.000
Fe	0.31	0.27	0	0.000
K	0.36	0.37	0	0.001
Mg	0.04	0.04	0	0.000
Na	0.92	0.57	0	0.145
Co	0.01	0.16	0.500	0.004
(meq/gr zeolite)	$\sum(Ca^{2+}+Na^{+}+K^{+}+Mg^{2+})$		Co^{2+}	
	0.40		*0.20*	

Table C.71. Solid and liquid phase compositions (0.01 M $Co(NO_3)_2 \cdot 6H_2O$, 80 ^oC, 30 min, S/L=1/20, microwave irradiation).

	SOLID (meq/gr zeolite)		LIQUID (meq/gr zeolite)	
Elements	Initial	Final	Initial	Final
Ca	0.09	0.07	0	0.000
Fe	0.31	0.25	0	0.002
K	0.36	0.36	0	0.002
Mg	0.04	0.04	0	0.000
Na	0.92	0.56	0	0.148
Co	0.01	0.17	0.200	0.003
(meq/gr zeolite)	$\sum(Ca^{2+}+Na^{+}+K^{+}+Mg^{2+})$		Co^{2+}	
	0.40		*0.20*	

Table C.72. Solid and liquid phase compositions (0.01 M $Co(NO_3)_2 \cdot 6H_2O$, 80 ^oC, 1hr, S/L=1/20, microwave irradiation).

	SOLID (meq/gr zeolite)		LIQUID (meq/gr zeolite)	
Elements	Initial	Final	Initial	Final
Ca	0.09	0.06	0	0.001
Fe	0.31	0.24	0	0.002
K	0.36	0.34	0	0.002
Mg	0.04	0.04	0	0.000
Na	0.92	0.53	0	0.148
Co	0.01	0.18	0.200	0.004
(meq/gr zeolite)	$\sum(Ca^{2+}+Na^{+}+K^{+}+Mg^{2+})$		Co^{2+}	
	0.44		*0.20*	

Table C.73. Solid and liquid phase compositions (0.01 M $Co(NO_3)_2 \cdot 6H_2O$, 80 ^oC, 10 min, S/L=1/50, microwave irradiation).

	SOLID (meq/gr zeolite)		LIQUID (meq/gr zeolite)	
Elements	Initial	Final	Initial	Final
Ca	0.09	0.07	0	**0.001**
Fe	0.31	0.26	0	0.000
K	0.36	0.34	0	0.004
Mg	0.04	0.04	0	0.000
Na	0.92	0.45	0	0.158
Co	0.01	0.31	0.500	0.130
(meq/gr zeolite)	$\sum(Ca^{2+}+Na^{+}+K^{+}+Mg^{2+})$		Co^{2+}	
	0.52		*0.37*	

Table C.74. Solid and liquid phase compositions (0.01 M $Co(NO_3)_2 \cdot 6H_2O$, 80 ^oC, 30 min, S/L=1/20, microwave irradiation).

	SOLID (meq/gr zeolite)		LIQUID (meq/gr zeolite)	
Elements	Initial	Final	Initial	Final
Ca	0.09	0.06	0	0.002
Fe	0.31	0.29	0	0.001
K	0.36	0.35	0	0.005
Mg	0.04	0.03	0	0.001
Na	0.92	0.35	0	0.244
Co	0.01	0.32	0.500	0.111
(meq/gr zeolite)	$\sum(Ca^{2+}+Na^{+}+K^{+}+Mg^{2+})$		Co^{2+}	
	0.62		*0.39*	

Table C.75. Solid and liquid phase compositions (0.01 M $Co{\cdot}(NO_3)_2{\cdot}6H_2O$, 80 ^oC, 1 hr, S/L=1/50, microwave irradiation).

	SOLID (meq/gr zeolite)		LIQUID (meq/gr zeolite)	
Elements	Initial	Final	Initial	Final
Ca	0.09	0.07	0	0.00
Fe	0.31	0.30	0	0.00
K	0.36	0.33	0	0.01
Mg	0.04	0.04	0	0.00
Na	0.92	0.42	0	0.26
Co	0.01	0.36	0.500	0.09
(meq/gr zeolite)	$\Sigma(Ca^{2+}+Na^{+}+K^{+}+Mg^{2+})$		Co^{2+}	
	0.55		*0.41*	

Table C.76. Solid and liquid phase compositions (0.01 M $Co{\cdot}(NO_3)_2{\cdot}6H_2O$, 80 ^oC, 10 min, S/L=1/100, microwave irradiation).

	SOLID (meq/gr zeolite)		LIQUID (meq/gr zeolite)	
Elements	Initial	Final	Initial	Final
Ca	0.09	0.09	0	**0.007**
Fe	0.31	0.24	0	0.000
K	0.36	0.86	0	0.006
Mg	0.04	0.07	0	0.001
Na	0.92	1.26	0	0.266
Co	0.01	0.49	1.000	0.438
(meq/gr zeolite)	$\Sigma(Ca^{2+}+Na^{+}+K^{+}+Mg^{2+})$		Co^{2+}	
	0.88		*0.56*	

Table C.77. Solid and liquid phase compositions (0.01 M $Co{\cdot}(NO_3)_2{\cdot}6H_2O$, 80 ^oC, 30 min, S/L=1/100, microwave irradiation).

	SOLID (meq/gr zeolite)		LIQUID (meq/gr zeolite)	
Elements	Initial	Final	Initial	Final
Ca	0.09	0.10	0	0.005
Fe	0.31	0.23	0	0.001
K	0.36	0.83	0	0.008
Mg	0.04	0.06	0	0.001
Na	0.92	1.16	0	0.271
Co	0.01	0.55	1.000	0.434
(meq/gr zeolite)	$\Sigma(Ca^{2+}+Na^{+}+K^{+}+Mg^{2+})$		Co^{2+}	
	0.74		*0.57*	

Table C.78. Solid and liquid phase compositions0.01 M Co^{2+} exchanged Na-CLI at 80 ^{o}C, S/L=1/100, 30min., microwave irradiation).

	SOLID (meq/gr zeolite)		LIQUID (meq/gr zeolite)	
Elements	Initial	Final	Initial	Final
Ca	0.09	0.07	0	-
Fe	0.31	0.24	0	-
K	0.36	0.35	0	-
Mg	0.04	0.04	0	-
Na	0.92	0.43	0	-
Co	0.01	0.45	0.500	-
(meq/gr zeolite)	$\sum(Ca^{2+}+Na^{+}+K^{+}+Mg^{2+})$		Co^{2+}	
	0.52		-	

Table C.79. Solid and liquid phase compositions (0.01 M $Co{\cdot}(NO_3)_2{\cdot}6H_2O$, 80 ^{o}C, 1hr, S/L=1/100, microwave irradiation).

	SOLID (meq/gr zeolite)		LIQUID (meq/gr zeolite)	
Elements	Initial	Final	Initial	Final
Ca	0.09	0.05	0	0.001
Fe	0.31	0.29	0	0.000
K	0.36	0.32	0	0.001
Mg	0.04	0.03	0	0.000
Na	0.92	0.66	0	0.153
Cu	0.01	0.19	0.200	0.003
(meq/gr zeolite)	$\sum(Ca^{2+}+Na^{+}+K^{+}+Mg^{2+})$		Cu^{2+}	
	0.36		*0.20*	

Table C.80. Solid and liquid phase compositions (0.01 M $Cu{\cdot}(NO_3)_2{\cdot}5/2H_2O$, 80 ^{o}C, 24 hrs, S/L=1/20, waterbath).

	SOLID (meq/gr zeolite)		LIQUID (meq/gr zeolite)	
Elements	Initial	Final	Initial	Final
Ca	0.09	0.07	0	0.001
Fe	0.31	0.27	0	0.000
K	0.36	0.32	0	0.002
Mg	0.04	0.04	0	0.000
Na	0.92	0.60	0	0.157
Cu	0.01	0.20	0.200	0.003
(meq/gr zeolite)	$\sum(Ca^{2+}+Na^{+}+K^{+}+Mg^{2+})$		Cu^{2+}	
	0.38		*0.20*	

Table C.81. Solid and liquid phase compositions (0.01 M $Cu{\cdot}(NO_3)_2{\cdot}5/2H_2O$, 80 ^oC,1 hr, S/L=1/50, waterbath).

	SOLID (meq/gr zeolite)		LIQUID (meq/gr zeolite)	
Elements	Initial	Final	Initial	Final
Ca	0.09	0.08	0	**0.003**
Fe	0.31	0.28	0	0.000
K	0.36	0.33	0	0.006
Mg	0.04	0.03	0	0.001
Na	0.92	0.47	0	0.311
Cu	0.01	0.38	0.500	0.103
(meq/gr zeolite)	$\sum(Ca^{2+}+Na^{+}+K^{+}+Mg^{2+})$		Cu^{2+}	
	0.50		*0.40*	

Table C.82. Solid and liquid phase compositions (0.01 M $Cu{\cdot}(NO_3)_2{\cdot}5/2H_2O$, 80 ^oC, 24 hrs, S/L=1/50, waterbath).

	SOLID (meq/gr zeolite)		LIQUID (meq/gr zeolite)	
Elements	Initial	Final	Initial	Final
Ca	0.09	0.05	0	0.003
Fe	0.31	0.25	0	0.000
K	0.36	0.31	0	0.005
Mg	0.04	0.04	0	0.000
Na	0.92	0.40	0	0.300
Cu	0.01	0.40	0.500	0.079
(meq/gr zeolite)	$\sum(Ca^{2+}+Na^{+}+K^{+}+Mg^{2+})$		Cu^{2+}	
	0.62		*0.42*	

Table C.83. Solid and liquid phase compositions (0.01 M $Cu{\cdot}(NO_3)_2{\cdot}5/2H_2O$, 80 ^oC, 24 hrs, S/L=1/100, waterbath).

	SOLID (meq/gr zeolite)		LIQUID (meq/gr zeolite)	
Elements	Initial	Final	Initial	Final
Ca	0.09	0.05	0	0.009
Fe	0.31	0.26	0	0.000
K	0.36	0.31	0	0.013
Mg	0.04	0.05	0	0.001
Na	0.92	0.27	0	0.421
Cu	0.01	0.50	1.000	0.520
(meq/gr zeolite)	$\sum(Ca^{2+}+Na^{+}+K^{+}+Mg^{2+})$		Cu^{2+}	
	0.76		*0.48*	

Table C.84. Solid and liquid phase compositions (0.01 M $Cu(NO_3)_2 \cdot 5/2H_2O$, 80 ^oC, 10 min, S/L=1/20, microwave irradiation).

	SOLID (meq/gr zeolite)		LIQUID (meq/gr zeolite)	
Elements	Initial	Final	Initial	Final
Ca	0.09	0.06	0	0.000
Fe	0.31	0.28	0	0.000
K	0.36	0.38	0	0.001
Mg	0.04	0.04	0	0.000
Na	0.92	0.72	0	0.145
Cu	0.01	0.20	0.200	0.005
(meq/gr zeolite)	$\sum(Ca^{2+}+Na^{+}+K^{+}+Mg^{2+})$		Cu^{2+}	
	0.27		*0.20*	

Table C.85. Solid and liquid phase compositions (0.01 M $Cu(NO_3)_2 \cdot 5/2H_2O$, 80 ^oC, 30 min, S/L=1/20, microwave irradiation).

	SOLID (meq/gr zeolite)		LIQUID (meq/gr zeolite)	
Elements	Initial	Final	Initial	Final
Ca	0.09	0.09	0	0.000
Fe	0.31	0.35	0	0.000
K	0.36	0.35	0	0.001
Mg	0.04	0.04	0	0.000
Na	0.92	0.76	0	0.142
Cu	0.01	0.19	0.200	0.004
(meq/gr zeolite)	$\sum(Ca^{2+}+Na^{+}+K^{+}+Mg^{2+})$		Cu^{2+}	
	0.45		*0.20*	

Table C.86. Solid and liquid phase compositions (0.01 M $Cu(NO_3)_2 \cdot 5/2H_2O$,80 ^oC, 1 hr, S/L=1/20, microwave irradiation).

	SOLID (meq/gr zeolite)		LIQUID (meq/gr zeolite)	
Elements	Initial	Final	Initial	Final
Ca	0.09	0.07	0	0.000
Fe	0.31	0.26	0	0.000
K	0.36	0.39	0	0.001
Mg	0.04	0.04	0	0.000
Na	0.92	0.68	0	0.140
Cu	0.01	0.20	0.200	0.006
(meq/gr zeolite)	$\sum(Ca^{2+}+Na^{+}+K^{+}+Mg^{2+})$		Cu^{2+}	
	0.30		*0.20*	

Table C.87. Solid and liquid phase compositions (0.01 M $Cu{\cdot}(NO_3)_2{\cdot}5/2H_2O$, 80 ^oC, 10 min, S/L=1/50, microwave irradiation).

	SOLID (meq/gr zeolite)		LIQUID (meq/gr zeolite)	
Elements	Initial	Final	Initial	Final
Ca	0.09	0.07	0	**0.001**
Fe	0.31	0.28	0	0.000
K	0.36	0.34	0	0.003
Mg	0.04	0.04	0	0.000
Na	0.92	0.47	0	0.283
Cu	0.01	0.42	0.500	0.092
(meq/gr zeolite)	$\sum(Ca^{2+}+Na^{+}+K^{+}+Mg^{2+})$		Cu^{2+}	
	0.50		*0.41*	

Table C.88. Solid and liquid phase compositions (0.01 M $Cu{\cdot}(NO_3)_2{\cdot}5/2H_2O$, 80 ^oC, 30 min, S/L=1/50, microwave irradiation).

	SOLID (meq/gr zeolite)		LIQUID (meq/gr zeolite)	
Elements	Initial	Final	Initial	Final
Ca	0.09	0.10	0	0.003
Fe	0.31	0.23	0	0.000
K	0.36	0.83	0	0.003
Mg	0.04	0.06	0	0.001
Na	0.92	-	0	0.290
Cu	0.01	0.51	0.500	0.083
(meq/gr zeolite)	$\sum(Ca^{2+}+Na^{+}+K^{+}+Mg^{2+})$		Cu^{2+}	
	0.51		*0.42*	

Table C.89. Solid and liquid phase compositions (0.01 M $Cu{\cdot}(NO_3)_2{\cdot}5/2H_2O$, 80 ^oC, 1 hr S/L=1/50, microwave irradiation).

	SOLID (meq/gr zeolite)		LIQUID (meq/gr zeolite)	
Elements	Initial	Final	Initial	Final
Ca	0.09	0.08	0	0.00
Fe	0.31	0.34	0	0.00
K	0.36	0.34	0	0.00
Mg	0.04	0.04	0	0.00
Na	0.92	0.47	0	0.27
Cu	0.01	0.39	0.500	0.10
(meq/gr zeolite)	$\sum(Ca^{2+}+Na^{+}+K^{+}+Mg^{2+})$		Cu^{2+}	
	0.48		*0.40*	

Table C.90. Solid and liquid phase compositions (0.01 M $Cu{\cdot}(NO_3)_2{\cdot}5/2H_2O$, 80 ^oC, 10 min, S/L=1/100, microwave irradiation).

	SOLID (meq/gr zeolite)		LIQUID (meq/gr zeolite)	
Elements	Initial	Final	Initial	Final
Ca	0.09	0.07	0	**0.00**
Fe	0.31	0.31	0	0.00
K	0.36	0.34	0	0.01
Mg	0.04	0.04	0	0.00
Na	0.92	0.32	0	0.34
Cu	0.01	0.52	1.000	0.49
(meq/gr zeolite)	$\sum(Ca^{2+}+Na^{+}+K^{+}+Mg^{2+})$		Cu^{2+}	
	0.65		*0.51*	

Table C.91. Solid and liquid phase compositions (0.01 M $Cu{\cdot}(NO_3)_2{\cdot}5/2H_2O$, 80 ^oC, 30 min, S/L=1/100, microwave irradiation).

	SOLID (meq/gr zeolite)		LIQUID (meq/gr zeolite)	
Elements	Initial	Final	Initial	Final
Ca	0.09	0.07	0	0.00
Fe	0.31	0.38	0	0.00
K	0.36	0.34	0	0.01
Mg	0.04	0.04	0	0.00
Na	0.92	0.34	0	0.36
Cu	0.01	0.47	1.000	0.49
(meq/gr zeolite)	$\sum(Ca^{2+}+Na^{+}+K^{+}+Mg^{2+})$		Cu^{2+}	
	0.62		*0.51*	

Table C.92. Solid and liquid phase compositions (0.01 M $Cu{\cdot}(NO_3)_2{\cdot}5/2H_2O$, 80 ^oC, 1hr S/L=1/100, microwave irradiation).

	SOLID (meq/gr zeolite)		LIQUID (meq/gr zeolite)	
Elements	Initial	Final	Initial	Final
Ca	0.09	0.07	0	0.00
Fe	0.31	0.28	0	0.00
K	0.36	0.33	0	0.00
Mg	0.04	0.04	0	0.00
Na	0.92	0.32	0	0.34
Cu	0.01	0.54	1.000	0.50
(meq/gr zeolite)	$\sum(Ca^{2+}+Na^{+}+K^{+}+Mg^{2+})$		Cu^{2+}	
	0.65		*0.50*	

Table C.93. Solid and liquid phase compositions (0.1 M AgNO3, 80 ^{o}C, 1hr S/L=1/100,waterbath).

	SOLID (meq/gr zeolite)		LIQUID (meq/gr zeolite)	
Elements	Initial	Final	Initial	Final
Ca	0.10	0.07	0	9.419
Fe	0.52	0.55	0	0.096
K	0.58	0.44	0	0.096
Mg	0.09	0.07	0	0.991
Na	1.66	0.30	0	2.844
Ag	0.00	1.24	10.000	nd
(meq/gr zeolite)	$\sum(Ca^{2+}+Na^{+}+K^{+}+Mg^{2+})$		Ag^{+}	
	1.54		*nd*	

Table C.94. Solid and liquid phase compositions (0.1 M AgNO3, 80 ^{o}C, 24 hr S/L=1/100,waterbath).

	SOLID (meq/gr zeolite)		LIQUID (meq/gr zeolite)	
Elements	Initial	Final	Initial	Final
Ca	0.10	0.08	0	7.031
Fe	0.52	0.49	0	0.084
K	0.58	0.42	0	0.068
Mg	0.09	0.07	0	0.905
Na	1.66	0.25	0	2.627
Ag	0.00	1.25	10.000	8.457
(meq/gr zeolite)	$\sum(Ca^{2+}+Na^{+}+K^{+}+Mg^{2+})$		Ag^{+}	
	1.60		*1.54*	

Table C.95. Solid and liquid phase compositions (0.1 M AgNO3, 80 ^{o}C,10 min S/L=1/100,microwave irradiation).

	SOLID (meq/gr zeolite)		LIQUID (meq/gr zeolite)	
Elements	Initial	Final	Initial	Final
Ca	0.10	0.10	0	-0.047
Fe	0.52	0.58	0	0.005
K	0.58	0.42	0	0.015
Mg	0.09	0.07	0	0.071
Na	1.66	0.28	0	0.899
Ag	0.00	1.20	10.000	8.674
(meq/gr zeolite)	$\sum(Ca^{2+}+Na^{+}+K^{+}+Mg^{2+})$		Ag^{+}	
	1.56		*1.32*	

Table C.96. Solid and liquid phase compositions (0.1 M AgNO3, 80 ^{o}C,30 min S/L=1/100,microwave irradiation).

	SOLID (meq/gr zeolite)		LIQUID (meq/gr zeolite)	
Elements	Initial	Final	Initial	Final
Ca	0.10	0.09	0	-0.106
Fe	0.52	0.54	0	0.005
K	0.58	0.44	0	0.044
Mg	0.09	0.07	0	0.000
Na	1.66	0.27	0	0.774
Ag	0.00	1.17	10.000	8.642
(meq/gr zeolite)	$\sum(Ca^{2+}+Na^{+}+K^{+}+Mg^{2+})$		Ag^{+}	
	1.56		*1.36*	

Table C.97. Solid and liquid phase compositions (0.1 M AgNO3, 80 ^{o}C, 1hr S/L=1/100,microwave irradiation).

	SOLID (meq/gr zeolite)		LIQUID (meq/gr zeolite)	
Elements	Initial	Final	Initial	Final
Ca	0.10	0.09	0	-0.414
Fe	0.52	0.48	0	0.003
K	0.58	0.44	0	0.049
Mg	0.09	0.06	0	0.002
Na	1.66	0.29	0	0.787
Ag	0.00	1.16	10.000	8.688
(meq/gr zeolite)	$\sum(Ca^{2+}+Na^{+}+K^{+}+Mg^{2+})$		Ag^{+}	
	1.54		*1.31*	

Table C.98. Solid and liquid phase compositions (0.1 M $Co{\cdot}(NO_3)_2{\cdot}6H_2O$, 80 ^{o}C, 1hr S/L=1/100, waterbath).

	SOLID (meq/gr zeolite)		LIQUID (meq/gr zeolite)	
Elements	Initial	Final	Initial	Final
Ca	0.05	0.04	0	**0.331**
Fe	0.26	0.23	0	0.048
K	0.29	0.24	0	0.021
Mg	0.04	0.04	0	0.298
Na	0.83	0.27	0	1.318
Co	0.00	0.53	10.340	9.743
(meq/gr zeolite)	$\sum(Ca^{2+}+Na^{+}+K^{+}+Mg^{2+})$		Co^{2+}	
	0.62		*0.60*	

Table C.99. Solid and liquid phase compositions (0.1 M $Co{\cdot}(NO_3)_2{\cdot}6H_2O$, 80 ^oC, 24 hr S/L=1/100, waterbath).

	SOLID (meq/gr zeolite)		LIQUID (meq/gr zeolite)	
Elements	Initial	Final	Initial	Final
Ca	0.05	0.09	0	1.687
Fe	0.26	0.22	0	0.026
K	0.29	0.25	0	0.016
Mg	0.04	0.04	0	0.235
Na	0.83	0.30	0	0.841
Co	0.00	0.55	10.340	9.743
(meq/gr zeolite)	$\Sigma(Ca^{2+}+Na^{+}+K^{+}+Mg^{2+})$		Co^{2+}	
	0.60		*0.60*	

Table C.100. Solid and liquid phase compositions (0.1 M $Co{\cdot}(NO_3)_2{\cdot}6H_2O$,80 ^oC,10min, S/L=1/100, microwave irradiation).

	SOLID (meq/gr zeolite)		LIQUID (meq/gr zeolite)	
Elements	Initial	Final	Initial	Final
Ca	0.05	0.04	0	**-0.059**
Fe	0.26	0.27	0	0.001
K	0.29	0.26	0	0.004
Mg	0.04	0.04	0	0.003
Na	0.83	0.32	0	0.278
Co	0.00	0.44	10.870	10.487
(meq/gr zeolite)	$\Sigma(Ca^{2+}+Na^{+}+K^{+}+Mg^{2+})$		Co^{2+}	
	0.56		*0.39*	

Table C.101. Solid and liquid phase compositions (0.1 M $Co{\cdot}(NO_3)_2{\cdot}6H_2O$,80 ^oC,30min, S/L=1/100, irradiation).

	SOLID (meq/gr zeolite)		LIQUID (meq/gr zeolite)	
Elements	Initial	Final	Initial	Final
Ca	0.05	0.04	0	-0.058
Fe	0.26	0.27	0	0.001
K	0.29	0.26	0	0.005
Mg	0.04	0.04	0	0.006
Na	0.83	0.30	0	0.285
Co	0.00	0.45	10.870	10.462
(meq/gr zeolite)	$\Sigma(Ca^{2+}+Na^{+}+K^{+}+Mg^{2+})$		Co^{2+}	
	0.58		*0.40*	

Table C.102. Solid and liquid phase compositions (0.1 M $Co{\cdot}(NO_3)_2{\cdot}6H_2O$,80 ^oC,1 hr, S/L=1/100, microwave irradiation)

	SOLID (meq/gr zeolite)		LIQUID (meq/gr zeolite)	
Elements	Initial	Final	Initial	Final
Ca	0.05	0.04	0	-0.030
Fe	0.26	0.59	0	0.002
K	0.29	0.25	0	0.010
Mg	0.04	0.03	0	0.005
Na	0.83	0.28	0	0.306
Co	0.00	0.48	10.870	10.337
(meq/gr zeolite)	$\Sigma(Ca^{2+}+Na^{+}+K^{+}+Mg^{2+})$		Co^{2+}	
	0.61		*0.53*	

Table C.103. Solid and liquid phase compositions (0.1 M $Cu{\cdot}(NO_3)_2{\cdot}5/2H_2O$,80 ^oC,1 hr, S/L=1/100, waterbath)

	SOLID (meq/gr zeolite)		LIQUID (meq/gr zeolite)	
Elements	Initial	Final	Initial	Final
Ca	0.05	0.05	0	**4.052**
Fe	0.26	0.36	0	0.046
K	0.29	0.24	0	0.035
Mg	0.04	0.04	0	0.547
Na	0.83	0.20	0	1.694
Cu	0.00	0.68	11.673	10.906
(meq/gr zeolite)	$\Sigma(Ca^{2+}+Na^{+}+K^{+}+Mg^{2+})$		Cu^{2+}	
	0.70		*0.76*	

Table C.104. Solid and liquid phase compositions(0.1 M $Cu{\cdot}(NO_3)_2{\cdot}5/2H_2O$,80 ^oC,24 hr, S/L=1/100, waterbath)

	SOLID (meq/gr zeolite)		LIQUID (meq/gr zeolite)	
Elements	Initial	Final	Initial	Final
Ca	0.05	0.03	0	2.568
Fe	0.26	0.22	0	0.045
K	0.29	0.23	0	0.028
Mg	0.04	0.04	0	0.343
Na	0.83	0.20	0	1.151
Cu	0.00	0.69	11.673	11.010
(meq/gr zeolite)	$\Sigma(Ca^{2+}+Na^{+}+K^{+}+Mg^{2+})$		Cu^{2+}	
	0.72		*0.48*	

Table C.105. Solid and liquid phase compositions (0.1 M $Cu(NO_3)_2 5/2H_2O$,80 ^oC, 10 min, S/L=1/100, microwave irradiation).

	SOLID (meq/gr zeolite)		LIQUID (meq/gr zeolite)	
Elements	Initial	Final	Initial	Final
Ca	0.05	0.06	0	**-0.029**
Fe	0.26	0.37	0	0.002
K	0.29	0.26	0	0.013
Mg	0.04	0.04	0	0.000
Na	0.83	0.19	0	0.359
Cu	0.00	0.67	10.650	9.795
(meq/gr zeolite)	$\sum(Ca^{2+}+Na^{+}+K^{+}+Mg^{2+})$		Cu^{2+}	
	0.69		*0.86*	

Table C.106. Solid and liquid phase compositions (0.1 M $Cu(NO_3)_2 5/2H_2O$,80 ^oC, 30 min, S/L=1/100, microwave irradiation).

	SOLID (meq/gr zeolite)		LIQUID (meq/gr zeolite)	
Elements	Initial	Final	Initial	Final
Ca	0.09	0.07	0	-0.058
Fe	0.31	0.28	0	0.001
K	0.36	0.33	0	0.005
Mg	0.04	0.04	0	0.006
Na	0.92	0.32	0	0.285
Cu	0.01	0.54	10.650	10.162
(meq/gr zeolite)	$\sum(Ca^{2+}+Na^{+}+K^{+}+Mg^{2+})$		Cu^{2+}	
	0.64		*0.50*	

Table C.107. Solid and liquid phase compositions (0.1 M $Cu(NO_3)_2 5/2H_2O$,80 ^oC,1 hr S/L=1/100, microwave irradiation).

	SOLID (meq/gr zeolite)		LIQUID (meq/gr zeolite)	
Elements	Initial	Final	Initial	Final
Ca	0.05	0.07	0	-0.052
Fe	0.26	0.46	0	0.004
K	0.29	0.24	0	0.016
Mg	0.04	0.04	0	0.002
Na	0.83	0.25	0	0.382
Cu	0.00	0.64	10.650	10.128
(meq/gr zeolite)	$\sum(Ca^{2+}+Na^{+}+K^{+}+Mg^{2+})$		Cu^{2+}	
	0.65		*0.53*	

APPENDIX D

WATERBATH AND MICROWAVE IRRADIATION

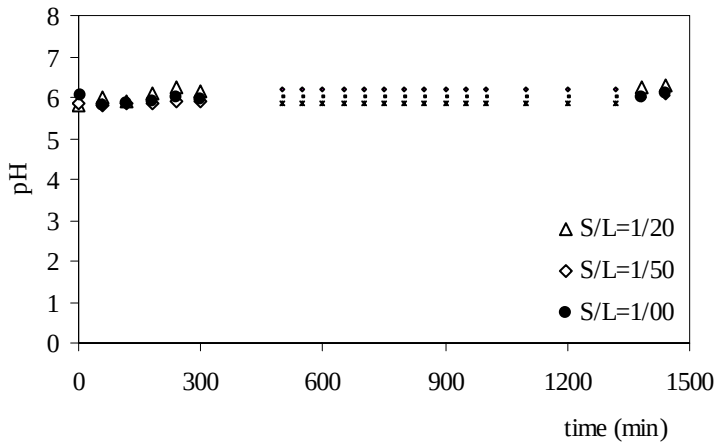

Figure D.1. pH versus time for Ag^{+} – Na-CLI system (60 ^{o}C, waterbath).

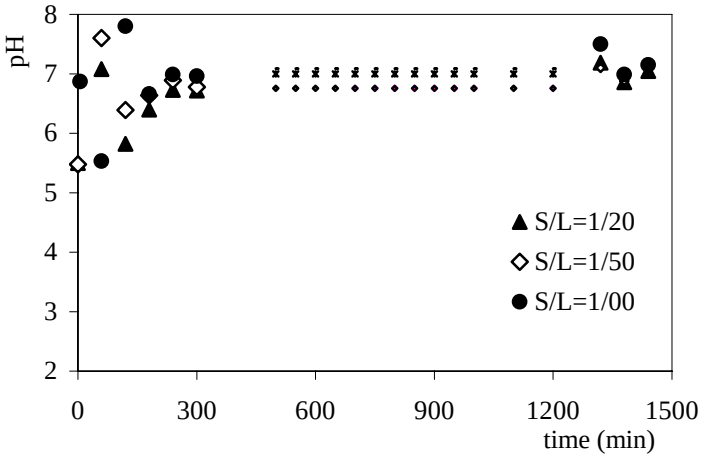

Figure D.2. pH versus time for ultrapure water–Na-CLI system (60 ^{o}C, waterbath).

.

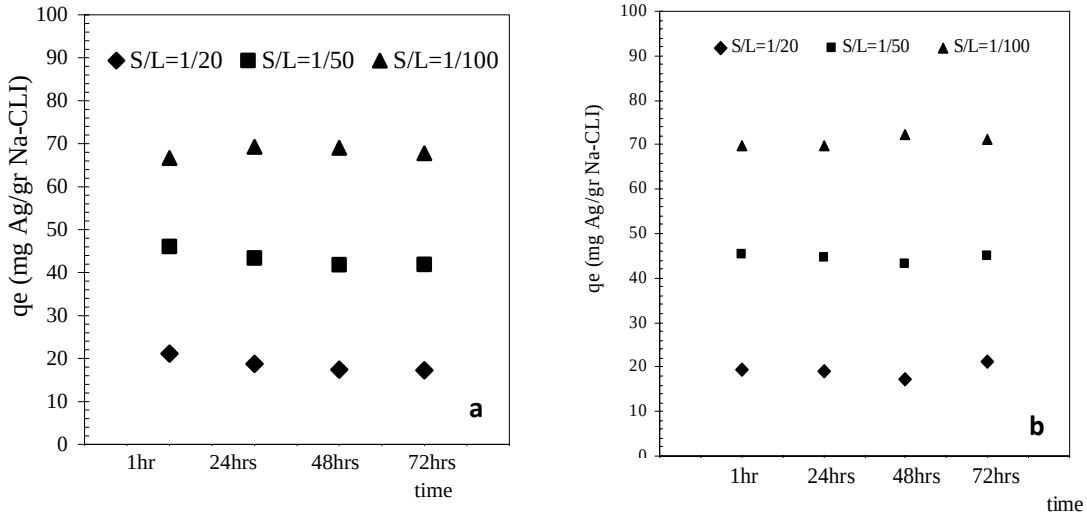

Figure D.3. Effect of S/L ratio and time on Ag^{+} exchange 40 ^{o}C b) 60 ^{o}C (NaCLI, waterbath).

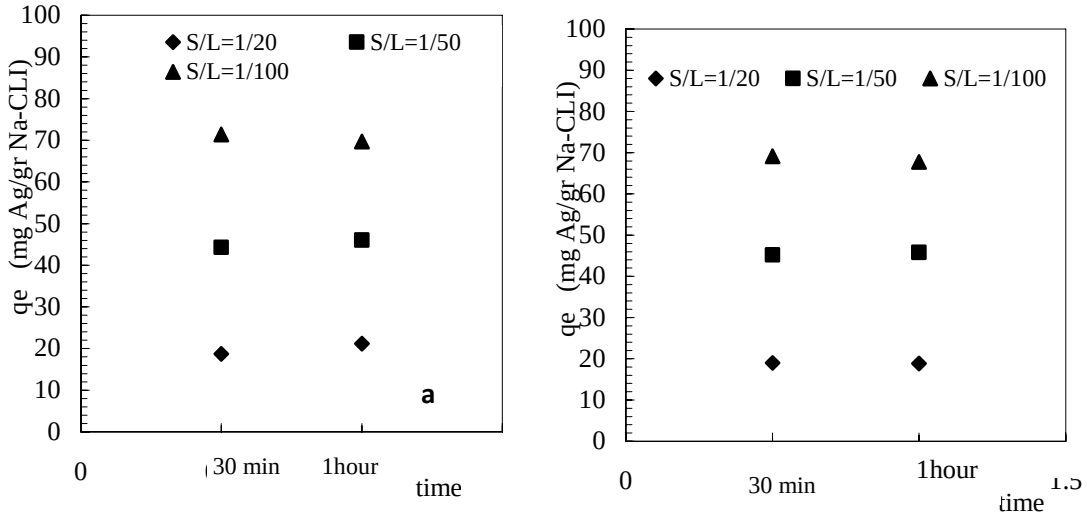

Figure D.4. Effect of S/L ratio and time on Ag^{+} exchange 40 ^{o}C b) 60 ^{o}C (NaCLI, microwave irradiation).

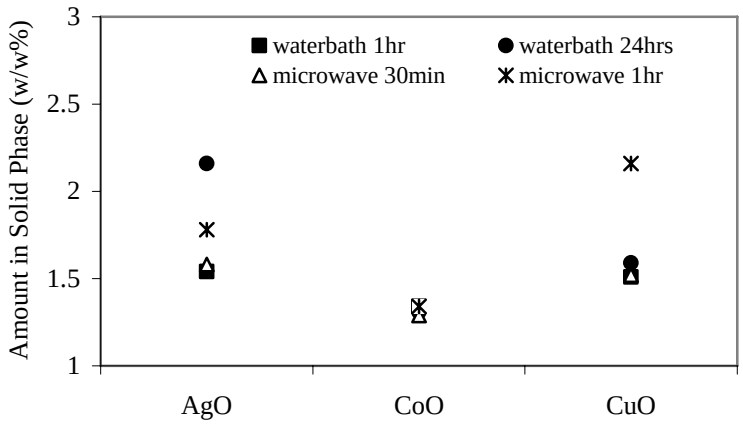

Figure D.5. Microwave versus Waterbath (S/L=1/20, 80 ^{o}C, 0.01M Metal Solution).

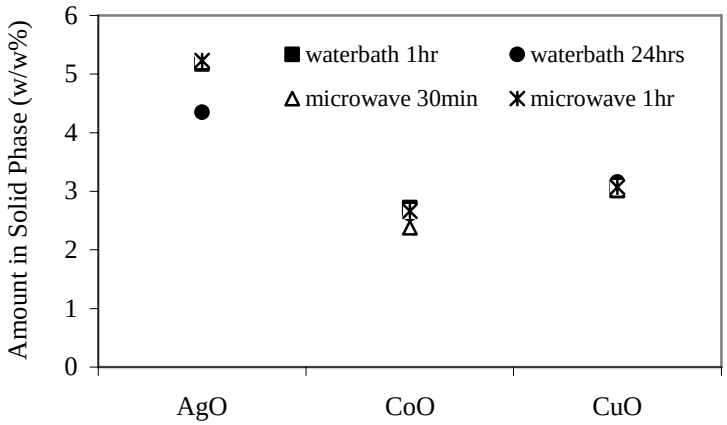

Figure D.6. Microwave versus Waterbath (S/L=1/50, 80 ^{o}C, 0.01M Metal Solution).

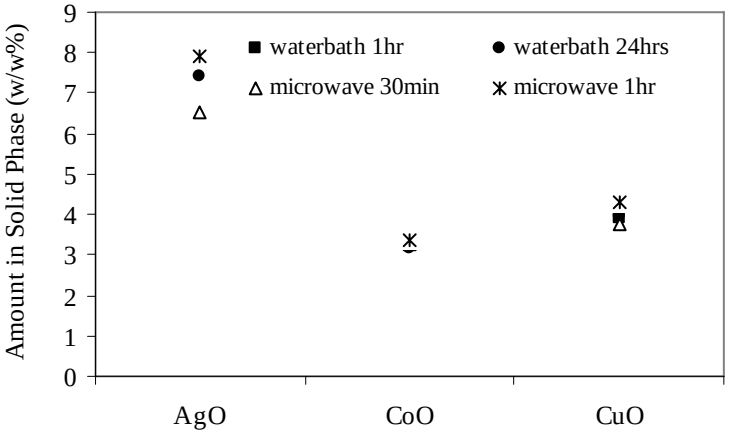

Figure D.7. Microwave versus Waterbath (S/L=1/10, 80 ^{o}C, 0.01M Metal Solution).

APPENDIX E

XRD PATTERNS

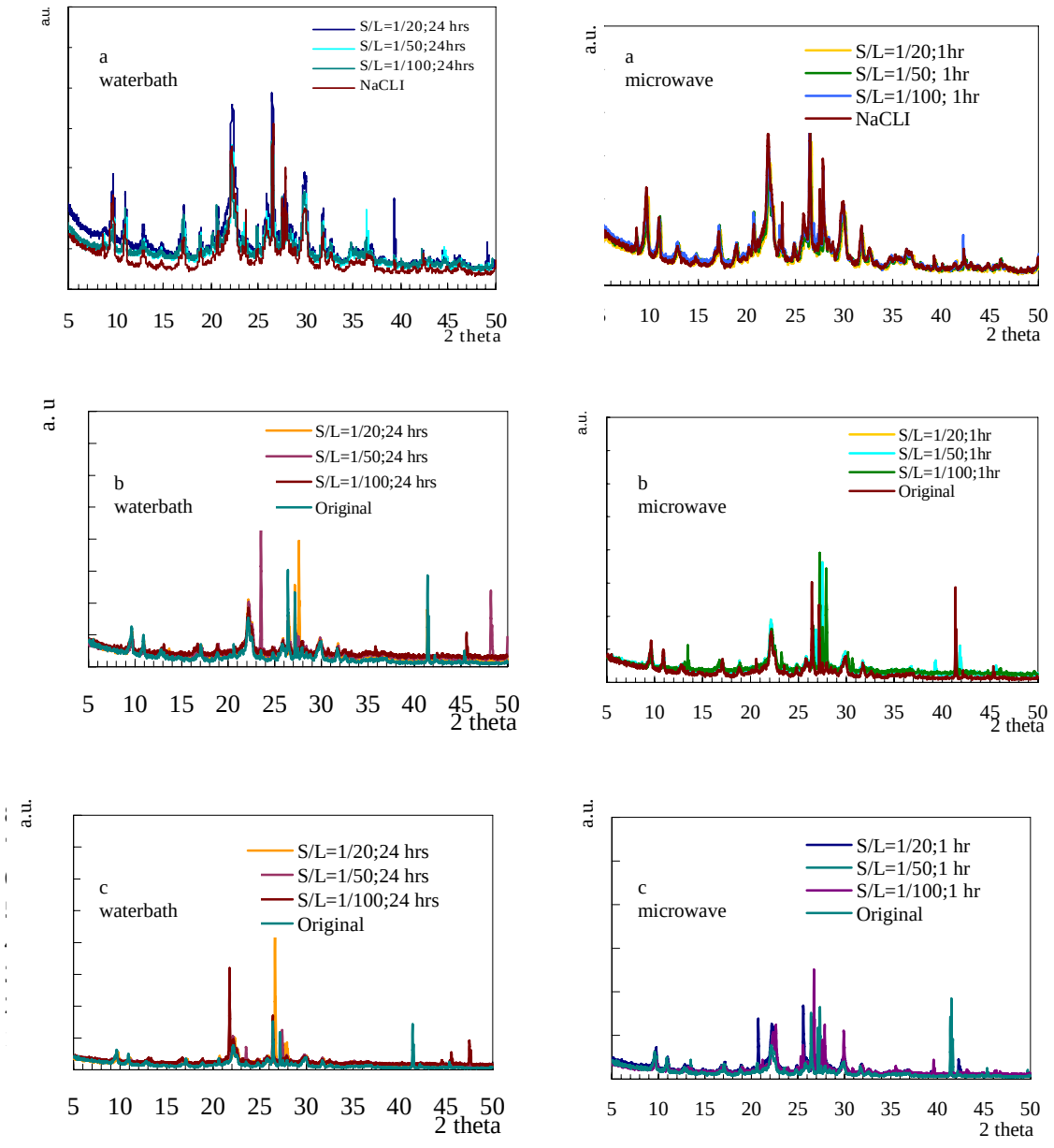

Figure E.1. XRD pattern of a) Ag^{+} b) Co^{2+} c) Cu^{2+} exchanged Na-CLI (24hrs, waterbath, 1hr microwave irradiation, 80 ^{o}C).

APPENDIX F

FTIR SPECTRA

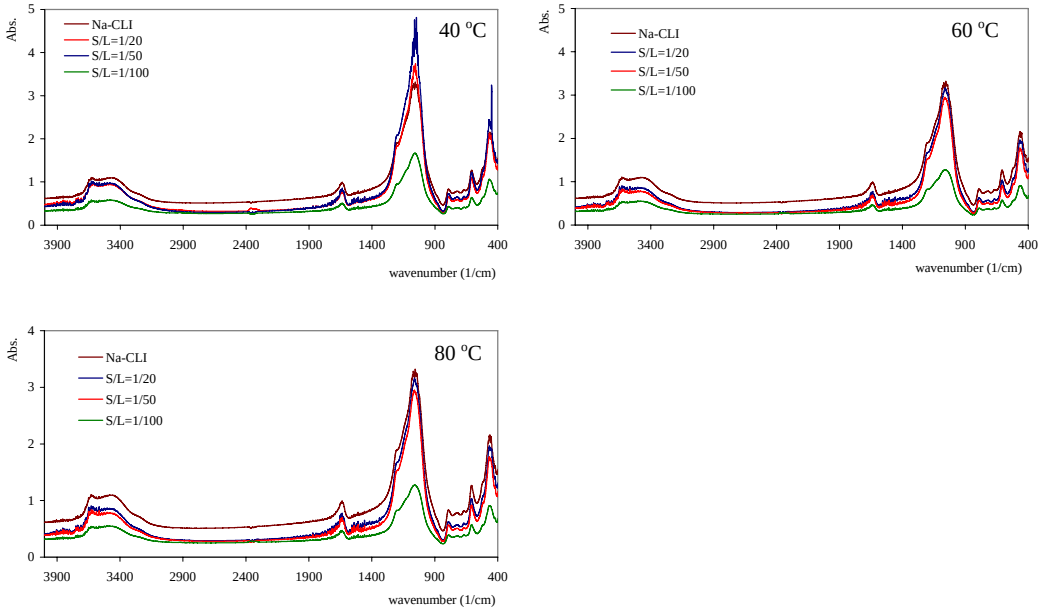

Figure F.1. FTIR Spectra of Ag^{+} exchanged Na-CLI (waterbath).

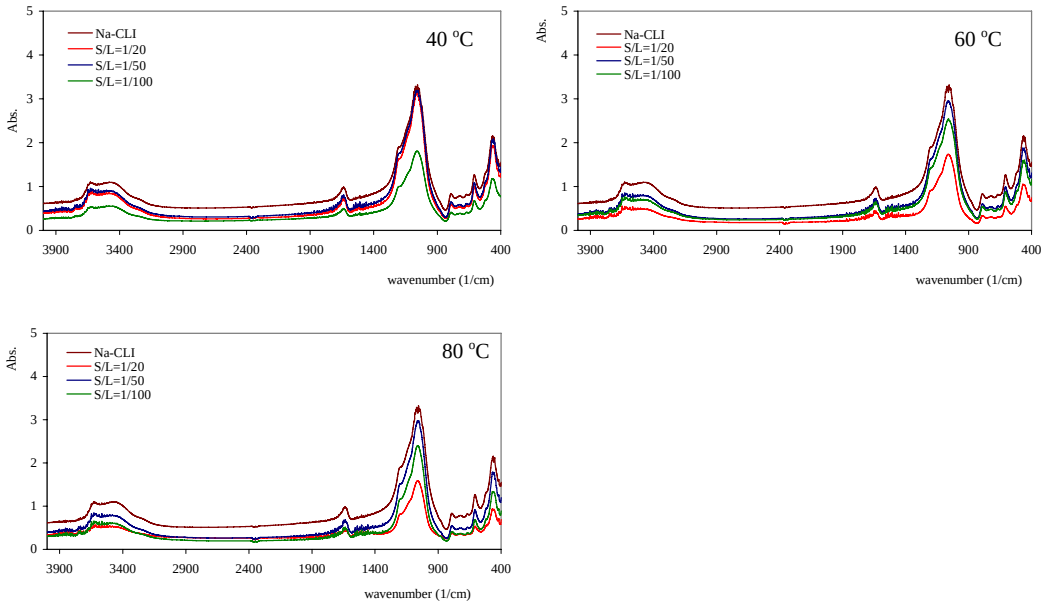

Figure F.2. FTIR Spectra of Ag^{+} exchanged Na-CLI (microwave irradiation).

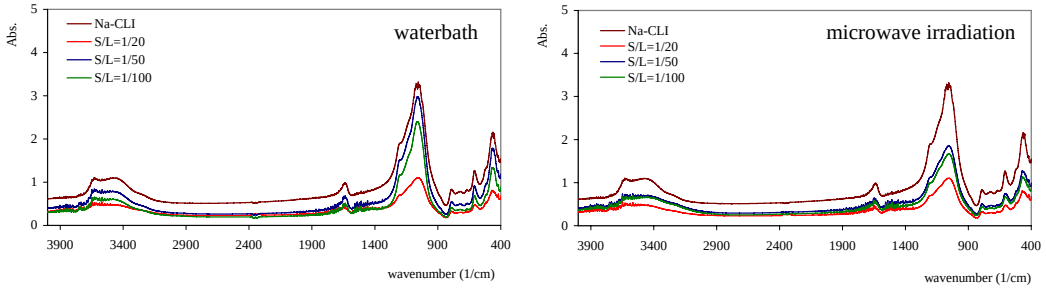

Figure F.3. FTIR Spectra of Co^{2+} exchanged Na-CLI at 80 °C.

.

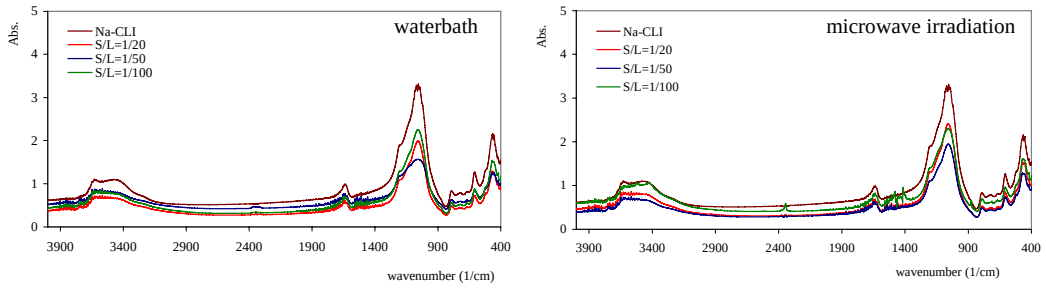

Figure F.4. FTIR Spectra of Cu^{2+} exchanged Na-CLI at 80 °C.

APPENDIX G

SEM MICROGRAPHS

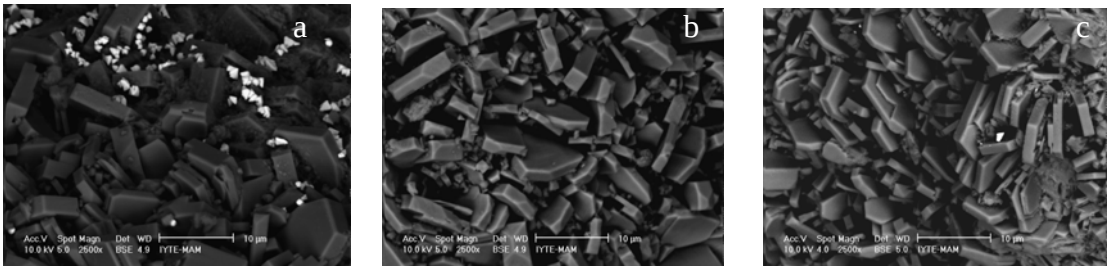

Figure G.1. SEM micrograph of Ag^{+} exchanged Na-CLI (3 day, waterbath) a) S/L=1/50 40 ^{o}C b) S/L= 1/100, 60 ^{o}C c) S/L=1/50, 80 ^{o}C.

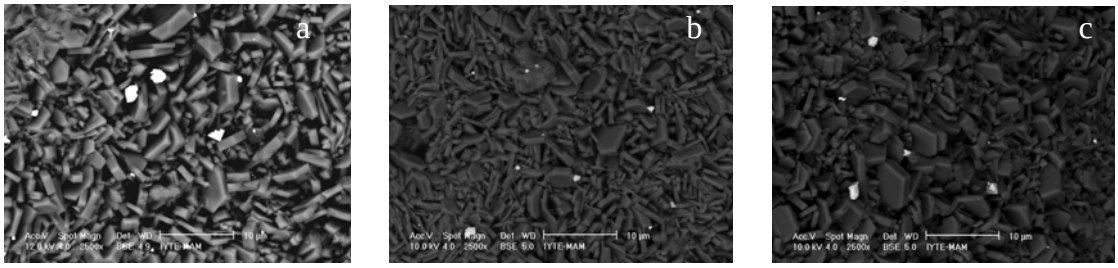

Figure G.2. SEM micrograph of Ag^{+} exchanged Na-CLI (1 hr, microwave irradiation) a) S/L=1/20, 40 ^{o}C b) S/L= 1/50, 60 ^{o}C c) S/L=1/50, 80 ^{o}C.

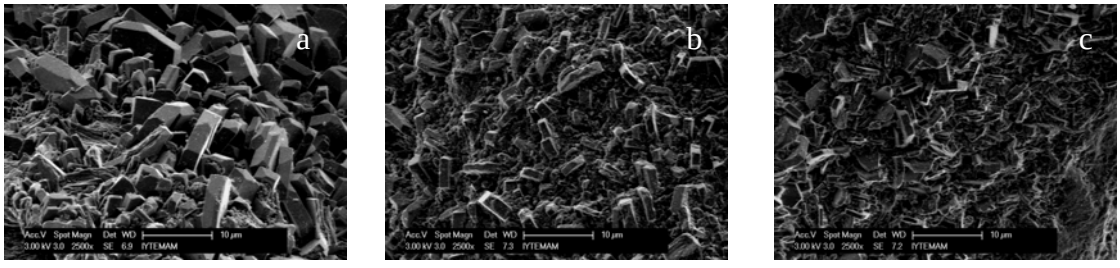

Figure G.3. SEM micrograph of Co^{2+} exchanged Na-CLI (24 hr, 80 ^{o}C, waterbath) a)S/L=1/20 b) S/L=1/50 c) S/L=1/100.

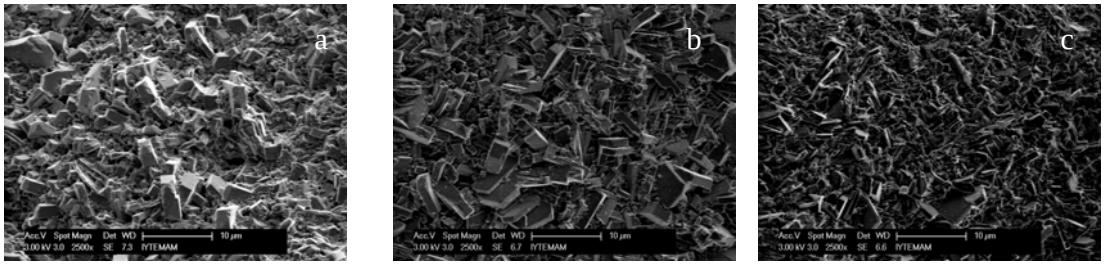

Figure G.4. SEM micrograph of Co^{2+} exchanged Na-CLI (24 hr, 80 ^{o}C, microwave irradiation) a) S/L=1/20 b) S/L= 1/50 c) S/L=1/100.

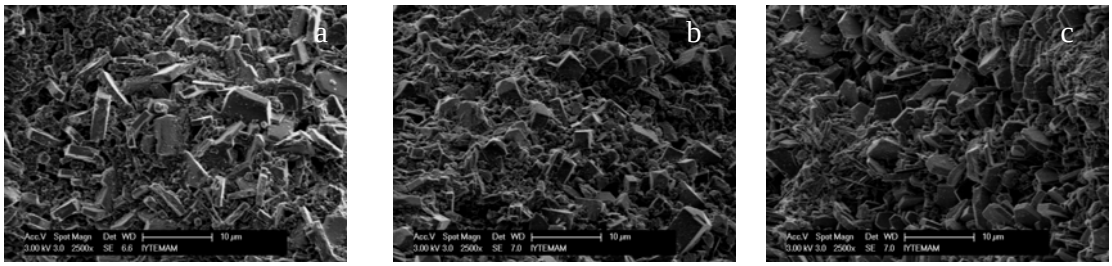

Figure G.5. SEM micrograph of Cu^{2+} exchanged Na-CLI (24 hr, 80 ^{o}C, waterbath) a)S/L=1/20 b) S/L=1/50 c) S/L=1/100.

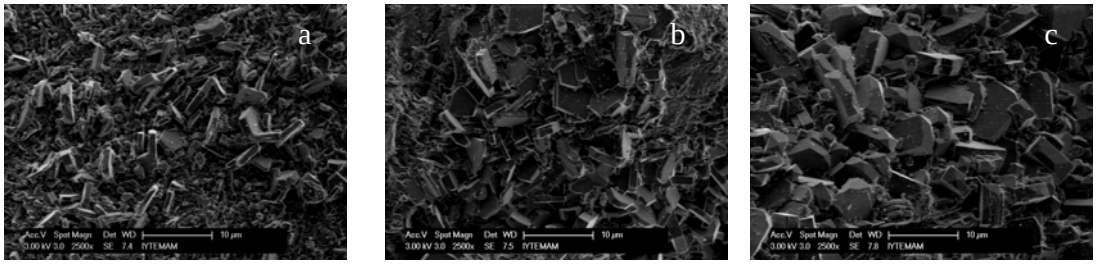

Figure G.6. SEM micrograph of Cu^{2+} exchanged Na-CLI (24 hr, 80 ^{o}C, microwave irradiation) a) S/L=1/20 b) S/L= 1/50 c) S/L=1/100.

APPENDIX H

SORPTION ISOTHERMS

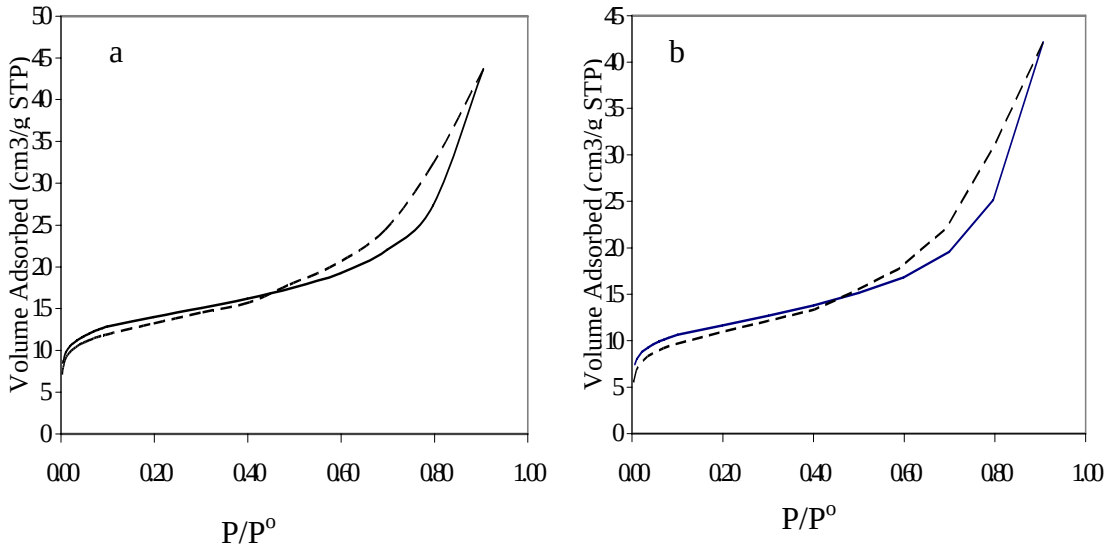

Figure H.1. Sorption Isotherm of a) CLI b) NaCLI.

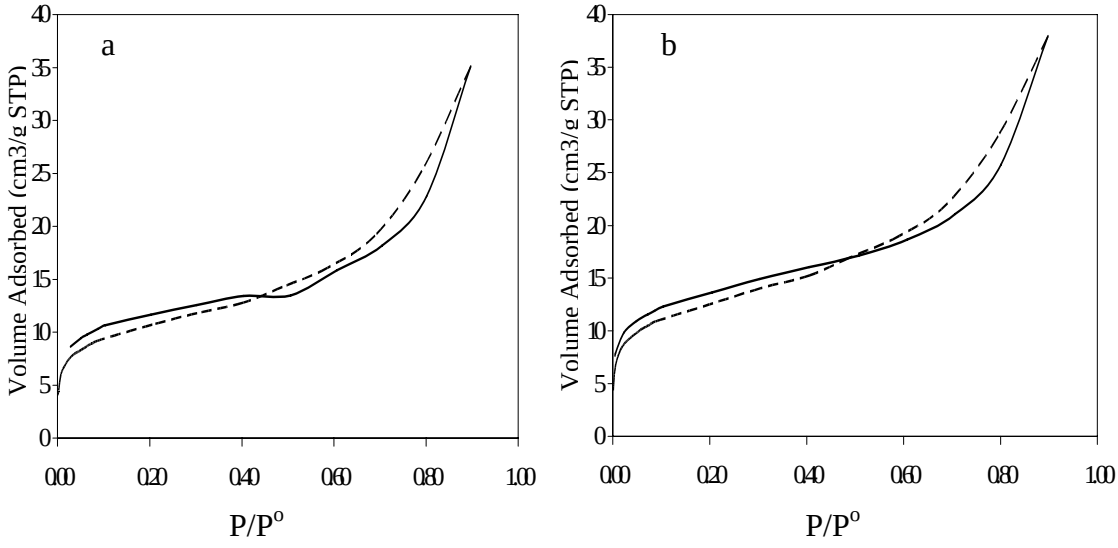

Figure H.2. Sorption Isotherm of Ag^{+} exchanged Na-CLI a) S/L=1/100, 80 ^{o}C, waterbath, 24hrs b) S/L=1/100 at 80 ^{o}C , microwave irradiation, 1hr.

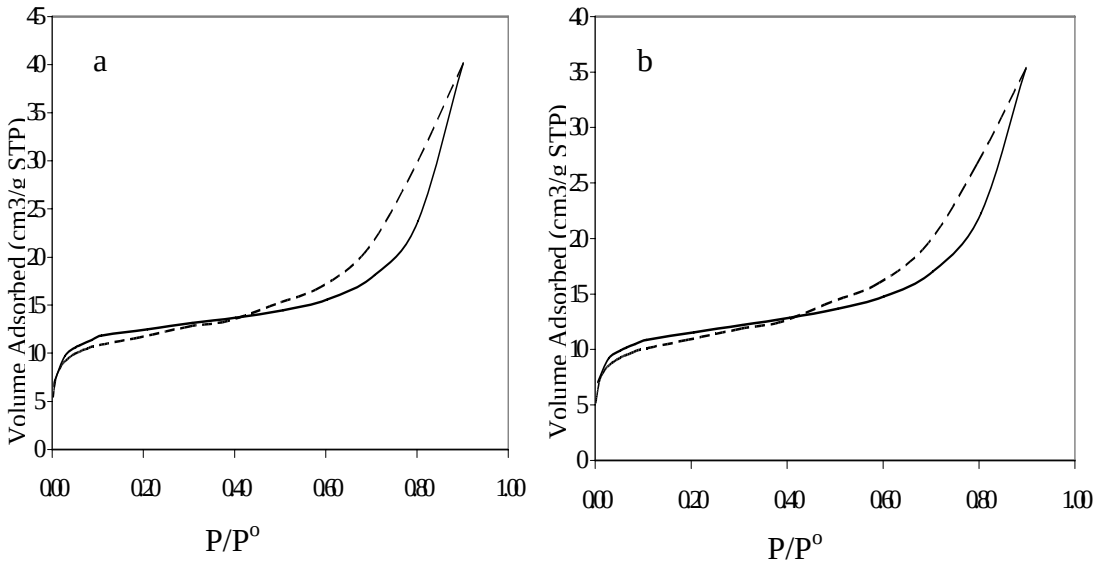

Figure H.3. Sorption Isotherm of Co^{2+} exchanged Na-CLI a) S/L=1/100, 80 °C, waterbath, 24hrs b) S/L=1/100 at 80 °C , microwave irradiation, 1hr.

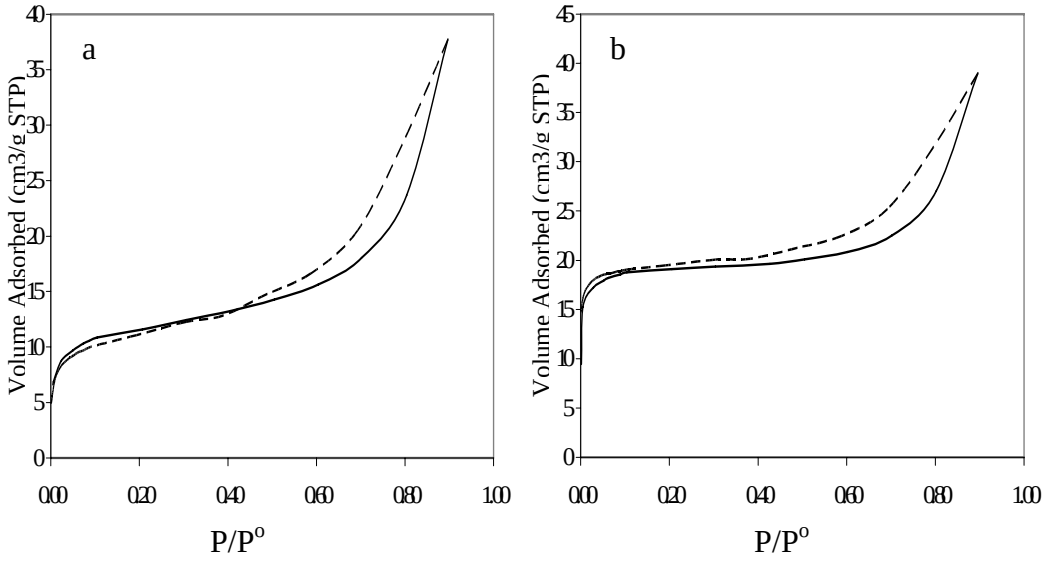

Figure H.4. Sorption Isotherm of Cu^{2+} exchanged Na-CLI a) S/L=1/100, 80 °C, waterbath, 24hrs b) S/L=1/100 at 80 °C , microwave irradiation, 1hr.

APPENDIX I

ANTIBACTERIAL TESTS

Table I.1. Inhibition Zone Diameters of Ag^{+} exchanged NaCLI (waterbath,40 ^{o}C).

Zone Diameter (mm) / Mineral Code		1	2	3	4	Average
S/L=1/20	1 day	11.28	11.33	11.33	11.31	**11.32**
	2 days	11.21	11.21	11.13	11.30	**11.23**
	3 days	11.14	11.20	11.16	11.09	**11.15**
S/L=1/50	1 day	11.30	11.18	11.25	11.35	**11.27**
	2 days	11.32	11.35	11.23	11.21	**11.28**
	3 days	11.22	11.15	11.13	11.25	**11.19**
S/L=1/100	1 day	11.24	11.18	10.96	11.16	**11.14**
	2 days	11.22	11.40	11.17	11.16	**11.24**
	3 days	11.08	10.88	11.04	10.92	**10.98**

Table I.2. Inhibition Zone Diameters of Ag^{+} exchanged NaCLI (waterbath,60 ^{o}C).

Zone Diameter (mm) / Mineral Code		1	2	3	4	Average
S/L=1/20	1 day	11.27	11.43	11.26	11.28	**11.31**
	2 days	11.43	11.38	11.18	11.26	**11.31**
	3 days	11.15	11.19	11.18	11.26	**11.20**
S/L=1/50	1 day	11.23	11.21	11.16	11.24	**11.21**
	2 days	11.22	11.22	11.08	11.21	**11.23**
	3 days	11.23	11.15	11.20	11.19	**11.19**
S/L=1/100	1 day	10.98	11.10	10.92	11.11	**11.03**
	2 days	11.09	11.01	11.11	11.09	**11.08**
	3 days	11.06	11.11	11.08	11.05	**11.08**

Table I.3. Inhibition Zone Diameters of Ag^+ exchanged NaCLI (waterbath ,80 ^oC).

Zone Diameter (mm) / Mineral Code		1	2	3	4	Average
S/L=1/20	1 day	11.22	11.18	11.19	11.26	**11.22**
	2 days	11.21	11.19	11.30	11.10	**11.20**
	3 days	11.31	10.97	11.16	11.16	**11.28**
S/L=1/50	1 day	11.35	11.12	11.13	11.19	**11.20**
	2 days	11.30	11.20	11.26	11.38	**11.24**
	3 days	11.43	11.32	11.59	11.56	**11.48**
S/L=1/100	1 day	11.46	11.26	11.62	11.98	**11.58**
	2 days	11.85	11.91	11.42	11.29	**11.62**
	3 days	11.54	11.38	11.48	11.96	**11.59**

Table I.4. Inhibition Zone Diameters of Ag^+ exchanged NaCLI (waterbath ,40 ^oC).

Zone Diameter (mm) / Mineral Code		1	2	3	4	Average
S/L=1/20	1hour	11.33	11.23	11.38	11.03	11.24
	24 hour	11.59	11.60	11.61	11.69	11.62
S/L=1/50	1hour	11.55	11.68	11.51	11.58	11.58
	24 hour	11.47	11.66	11.76	11.89	11.70
S/L=1/100	1hour	11.76	11.92	11.58	11.62	11.72
	24 hour	11.98	11.52	11.22	11.70	11.61

Table I.5. Inhibition Zone Diameters of Ag^+ exchanged NaCLI (microwave irradiation, 40°C).

Zone Diameter (mm) / Mineral Code		1	2	3	4	Average
S/L=1/20	**30 min**	12.39	12.25	12.31	12.23	**12.29**
	1 hour	11.53	11.43	11.37	11.59	**11.48**
S/L=1/50	**30 min**	11.34	11.38	11.49	11.31	**11.38**
	1 hour	11.92	11.85	11.60	11.32	**11.67**
S/L=1/100	**30 min**	11.93	12.25	12.40	12.26	**12.21**
	1 hour	11.50	11.66	11.73	11.31	**11.55**

Table I.6. Inhibition Zone Diameters of Ag^+ exchanged NaCLI (waterbath ,60 °C).

Zone Diameter (mm) / Mineral Code		1	2	3	4	Average
S/L=1/20	**1hour**	11.08	11.48	11.37	11.45	11.35
	24 hour	11.46	11.19	11.35	11.08	11.27
S/L=1/50	**1hour**	11.13	11.59	11.37	11.68	11.44
	24 hour	11.36	11.76	11.72	11.22	11.52
S/L=1/100	**1hour**	11.47	11.31	11.35	11.23	11.34
	24 hour	11.74	11.66	11.36	11.40	11.54

Table I.7. Inhibition Zone Diameters of Ag^+ exchanged NaCLI (microwave irradiation, 60°C).

Zone Diameter (mm) / Mineral Code		1	2	3	4	Average
S/L=1/20	**30 min**	11.70	11.49	11.64	11.57	**11.60**
	1 hour	11.74	11.53	11.53	11.63	**11.61**
S/L=1/50	**30 min**	11.44	11.49	11.59	11.40	**11.48**
	1 hour	11.62	11.36	11.36	11.36	**11.42**
S/L=1/100	**30 min**	11.34	11.50	11.60	11.58	**11.50**
	1 hour	11.59	11.39	11.38	11.38	**11.43**

Table I.8. Inhibition Zone Diameters of Ag^{+} exchanged NaCLI (waterbath at 80 ^{o}C).

Zone Diameter (mm) / Mineral Code		1	2	3	4	Average
S/L=1/20	1hour	11.95	11.88	11.89	11.73	11.86
	24 hour	12.01	11.98	11.94	11.95	11.97
S/L=1/50	1hour	12.03	11.78	12.05	12.05	11.98
	24 hour	11.75	11.79	11.65	11.98	11.79
S/L=1/100	1hour	11.76	12.09	11.72	11.98	11.89
	24 hour	11.77	12.02	11.91	11.95	11.91

Table I.9. Inhibition Zone Diameters of Ag^{+} exchanged NaCLI (microwave irradiation, 80^{o}C).

Zone Diameter (mm) / Mineral Code		1	2	3	4	Average
S/L=1/20	30 min	11.22	11.35	11.28	11.32	11.29
	1 hour	11.43	11.44	11.48	11.44	11.45
S/L=1/50	30 min	11.31	11.33	11.26	11.28	11.29
	1 hour	11.40	11.39	11.35	11.45	11.40
S/L=1/100	30 min	11.38	11.38	11.55	11.42	11.43
	1 hour	11.39	11.34	11.31	11.42	11.36

Table I.10. Inhibition Zone Diameters of Co^{2+} exchanged NaCLI (waterbath at 80 ^{o}C).

Zone Diameter (mm) / Mineral Code		1	2	3	4	Average
S/L=1/20	1hour	13.65	14.07	13.80	13.89	13.85
	24 hour	13.66	14.02	14.03	14.36	14.02
S/L=1/50	1hour	19.26	19.33	19.36	19.95	19.48
	24 hour	19.33	19.38	19.21	19.25	19.29
S/L=1/100	1hour	20.96	21.42	21.45	21.43	21.32
	24 hour	21.14	21.66	21.40	21.70	21.48

Table I.11. Inhibition Zone Diameters of Co^{2+} exchanged NaCLI (microwave irradiation, 80°C).

Zone Diameter (mm) / Mineral Code		**1**	**2**	**3**	**4**	**Average**
S/L=1/20	**30 min**	14.00	13.26	13.76	13.42	13.61
	1 hour	13.42	13.78	14.24	13.61	13.76
S/L=1/50	**30 min**	18.77	19.06	18.78	18.91	18.88
	1 hour	19.13	19.14	19.56	19.11	19.24
S/L=1/100	**30 min**	20.93	20.43	20.89	20.90	20.79
	1 hour	21.90	22.13	21.45	21.76	21.81

Table I.12. Inhibition Zone Diameters of Cu^{2+} exchanged NaCLI (waterbath at 80 °C).

Zone Diameter (mm) / Mineral Code		1	2	3	4	Average
S/L=1/20	1hour	11.97	12.63	12.23	12.08	12.23
	24 hour	12.04	11.70	11.78	12.21	11.93
S/L=1/50	1hour	14.01	13.97	14.70	14.57	14.31
	24 hour	13.38	13.45	13.42	13.67	13.48
S/L=1/100	1hour	15.98	16.63	16.67	16.01	16.32
	24 hour	14.78	14.88	14.83	14.85	14.84

Table I.13. Inhibition Zone Diameters of Cu^{2+} exchanged NaCLI (microwave irradiation, 80°C).

Zone Diameter (mm) / Mineral Code		1	2	3	4	Average
S/L=1/20	30 min	11.36	11.76	11.65	11.83	11.65
	1 hour	11.16	11.23	11.72	11.46	11.39
S/L=1/50	30 min	14.28	14.19	14.21	14.22	14.23
	1 hour	14.10	14.31	14.40	14.43	14.31
S/L=1/100	30 min	16.08	15.92	16.16	16.26	16.11

YELDA AKDENİZ

Date of Birth: September 09, 1974

Place of Birth: İzmir/Turkey

Citizenship: Turkish

EDUCATION

[1992-1996] B.Sc. (Chemical Engineering)

Ege University

Department of Chemical Engineering, İzmir, Turkey

[1996-1999] M.Sc. (Material Science and Engineering Programme)

İzmir Institute of Technology

Department of Material Science and Engineering, İzmir, Turkey

Dissertation: Cation Exchange in Zeolites, Structure Modification by Using a Microwave.

Advisor: Prof.Dr.Semra Ülkü

İzmir Institute of Technology

[2002-2009] Ph.D. (Chemical Engineering)

Department of Chemical Engineering, İzmir,Turkey

Dissertation: The Effect of Microwave on Ion Exchange in Zeolites

Advisor: Prof.Dr. Semra Ülkü

PUBLICATIONS

Akdeniz, Y., and Ülkü, S. (2008) "Thermal Stability of Ag-exchanged clinoptilolite rich mineral" *Journal of Thermal Analysis and Calorimetry*, Vol. 94(3), 703-710.

Akdeniz, Y., and Ülkü, S. (2007) "Microwave effect on ion-exchange and structure of clinoptilolite" *Journal of Porous Materials,* Vol.14, 55-60.

Duvarci, Ö.Ç., Akdeniz, Y., Özmıhçı, F., Ülkü, S., Balköse, D., Çiftçioğlu, M. (2007 "Thermal behaviour of a zeolitic tuff" *Ceramic International*, Vol. 33 (5) 795-801

Akdeniz Y., Özmıhçı F., Çağlar Ö., Balköse D., Ülkü S. (2004) Kırka Tinkal Mineralinden Elde Edilen Kilin Karakterizasyonu, XI. Ulusal Kil Sempozyumu, Bildiri Kitapçığı.